Traffic control in large-scale urban networks

Liudmila Tumash

UNIVERSITÉ GRENOBLE ALPES

THÈSE

pour obtenir le grade de

DOCTEUR DE L'UNIVERSITÉ GRENOBLE ALPES

Spécialité : **Automatique - productique**

Arrêté ministériel : 25 mai 2016

Présentée par
Liudmila TUMASH

Thèse dirigée par **Carlos CANUDAS DE WIT** et
codirigée par **Maria Laura DELLE MONACHE**

préparée au sein du
laboratoire Grenoble Images Parole Signal Automatique (GIPSA)
dans **L'École Doctorale Électronique, Électrotechnique, Automatique, Traitement du Signal (EEATS)**

Traffic control in large-scale urban networks

Thèse soutenue publiquement le **07 septembre 2021**,
devant le jury composé de:

Christophe PRIEUR
Directeur de recherche, GIPSA-Lab, Grenoble INP, Président du jury
Nikolaos BEKIARIS-LIBERIS
Professeur assistant, Technical University of Crete, Rapporteur
Christian CLAUDEL
Professeur associé, University of Texas at Austin, Rapporteur
Ludovic LECLERCQ
Directeur de recherche, Université Gustave Eiffel, Examinateur
Benedetto PICCOLI
Professeur des Universités, Rutgers University-Camden, Examinateur

UNIVERSITÉ DE GRENOBLE ALPES

ÉCOLE DOCTORALE EEATS

Électronique, Électrotechnique, Automatique, Traitement du Signal

T H È S E

pour obtenir le titre de

docteur en sciences

de l'Université de Grenoble

Mention : AUTOMATIQUE

Présentée et soutenue par

Liudmila TUMASH

Traffic control in large-scale urban networks

Thèse dirigée par Carlos CANUDAS-DE-WIT et
codirigée par Maria Laura DELLE MONACHE

préparée au laboratoire Grenoble Images Parole Signal Automatique (GIPSA-Lab)

soutenue le 07/09/2021

Jury :

Rapporteurs :	Nikolaos BEKIARIS-LIBERIS	-	Technical University of Crete
	Christian CLAUDEL	-	University of Texas at Austin
Président :	Christophe PRIEUR	-	GIPSA-Lab, Grenoble INP
Examinateurs :	Ludovic LECLERCQ	-	Université Gustave Eiffel
	Benedetto PICCOLI	-	Rutgers University-Camden

Résumé — Ce travail du doctorat est effectué dans le cadre du projet European Research Council's (ERC) Advanced Grant Scale-FreeBack. L'objectif du projet Scale-FreeBack est de développer une approche holistique de contrôle sans échelle des systèmes complexes, et de poser de nouvelles bases pour une théorie traitant des réseaux physiques complexes avec une dimension arbitraire. Un cas particulier est celui des systèmes de transport intelligents capables d'empêcher l'apparition de congestions aux heures de pointe. Les contributions de cette thèse du doctorat sont principalement liées à la conception du contrôle aux limites et à la modélisation du trafic sur les réseaux urbains à grande échelle. Le trafic est consideré du point de vue macroscopique, c'est-à-dire on le décrit en termes des variables agrégées telles que le flux et la densité de véhicules. L'équation dynamique correspond à l'équation différentielle partielle (EDP) hyperbolique du premier ordre. On propose des techniques du contrôle qui reposent entièrement sur les propriétés intrinsèques du modèle du trafic. Tout d'abord, problèmes du contrôle aux limites sont resolus sur des routes uniques (1D). L'état du trafic est entraîné vers une trajectoire souhaitée dépendant de l'espace et du temps qui admet la commutation des régimes du trafic. Une telle conception du contrôle est loin d'être triviale en raison des non-linéarités de l'équation d'état. Ensuite, le problème est étendu aux réseaux urbains de taille arbitraire, dont la dynamique est décrite par un modèle de loi de conservation bidimensionnel (2D). Les paramètres du modèle sont définis partout dans le plan du continu à partir de ses valeurs sur les routes physiques qui sont ensuite interpolées. La direction du flux est déterminée par la géométrie du réseau et les paramètres d'infrastructure. Ce modèle 2D est applicable dans les réseaux avec une direction de mouvement préférée. Pour ce cas, nous élaborons une méthode unique qui simplifie considérablement la conception de contrôle. En particulier, nous présentons une transformation de coordonnées curvilignes qui traduit le modèle continu en 2D en un ensemble paramétré de systèmes 1D. Cela permet une élaboration explicite de stratégies pour diverses tâches du contrôle à résoudre: on calcule des états stables, conceve un contrôle aux limites pour la densité 2D, applique un contrôle de limite de vitesse variable pour conduire le trafic vers n'importe quel équilibre. Enfin, un nouveau modèle de trafic continu bidimensionnel multidirectionnel est présenté. Il s'appelle le modèle NEWS, car il se compose de quatre EPD qui décrivent l'évolution de la densité des véhicules par rapport aux directions cardinales: Nord, Est, Ouest et Sud (North-East-West-South - NEWS). La direction du flux est déterminée par les rapports de braquage aux intersections. Pour ce modèle, on conceve un contrôle aux limites qui conduit le trafic congestionné à l'équilibre souhaité. L'efficacité de ces contributions a été testée à l'aide de données simulées et réelles. Dans le premier cas, les résultats sont vérifiés en utilisant le célèbre logiciel du trafic Aimsun, qui produit des microsimulations de trajectoires de véhicules dans un réseau modélisé. Dans le second cas, les données réelles sont obtenues à partir de capteurs situés en centre-ville de Grenoble et collectées à l'aide du Grenoble Traffic Lab (GTL).

Mots clés : Contrôle aux limites, réseaux de trafic à grande échelle, Hamilton-Jacobi, équations aux dérivées partielles.

Abstract — This research is done in the context of European Research Council's (ERC) Advanced Grant project Scale-FreeBack. The aim of Scale-FreeBack project is to develop a holistic scale-free control approach to complex systems, and to set new foundations for a theory dealing with complex physical networks with arbitrary dimension. One particular case is intelligent transportation systems that are capable to prevent the occurrence of congestions in rush hours. The contributions of the present PhD work are mainly related to boundary control design and modeling of traffic on large-scale urban networks. We consider traffic from a macroscopic viewpoint describing it in terms of aggregated variables such as flow and density of vehicles. The corresponding dynamic equation corresponds to a first-order hyperbolic partial differential equation (PDE). Within this PhD thesis, we propose control design techniques that rely on the intrinsic properties of the model. First of all, we solve one-dimensional (1D) boundary control problems, i.e., for traffic evolving on single roads. Thereby, the traffic state is driven to a space- and time-dependent desired trajectory that admits traffic regimes switching. Such control design is far from being trivial due to nonlinearities of the state equation. Then, the problem is extended to urban networks of arbitrary size. Large-scale traffic dynamics are described by a two-dimensional (2D) conservation law model. Model parameters are defined everywhere in a continuum domain from their values on physical roads that are further interpolated. Traffic flow direction is determined by network geometry and infrastructure parameters. This 2D model is applicable to any urban area with a preferred direction of motion. For this case, we elaborate a unique method that considerably simplifies control design for urban traffic systems. We present a curvilinear coordinate transformation that translates a 2D continuous traffic model into a parametrized set of 1D systems. This enables an explicit elaboration of strategies for various control tasks to solve on large-scale networks: calculation of steady states, boundary control design for a mixed regime traffic, apply variable speed limit control to drive traffic to any space-dependent equilibrium. Finally, a new multi-directional 2D continuous traffic model is presented. This model is formally derived from the demand-supply concept at one intersection. It is called the NEWS model, since it consists of four PDEs that describe the evolution of vehicle density with respect to cardinal directions: North, East, West and South. The traffic flow direction is determined by turning ratios at intersections. We then design a boundary control that drives multi-directional congested traffic to a desired equilibrium. The effectiveness of our contributions were tested using simulated and real data. In the first case, the results are verified by using the well-known commercial traffic Aimsun, which produces microsimulations of vehicles' trajectories in a modeled network. In the second case, the real data are obtained from sensors located in the downtown area of the city of Grenoble and collected using the Grenoble Traffic Lab (GTL).

Keywords: Boundary control, large-scale traffic networks, Hamilton-Jacobi, partial differential equations.

Grenoble Images Parole Signal Automatique (GIPSA-Lab)
11 Rue des Mathématiques, 38400 Saint-Martin-d'Hères

Acknowledgements

I would like to express the deepest appreciation to my supervisors, Carlos Canudas-de-Wit and Maria Laura Delle Monache. From them I have learned a lot of valuable lessons that considerably enhanced my abilities as a researcher. Without their guidance and persistent help this PhD thesis would not have been possible.

I would like to thank my jury members Christophe Prieur, Nikolaos Bekiaris-Liberis, Christian Claudel, Ludovic Leclerq and Benedetto Piccoli for their valuable comments and questions asked during my PhD presentation. This allowed me to look at my results from different perspectives.

I would also like to express my thanks to the guys in our group whom I got to know during my PhD: Martin Rodriguez Vega, Ujjwal Pratap, Umar Niazi, Stéphane Mollier, Nicolas Martin, Vadim Bertrand and Leo Senique. Drinking coffee, playing board games and sharing all ups and downs of a PhD life in general could have been nicer. The time that we have spent together will always make part of my beautiful memories.

A huge thank you goes to family, my mother Iryna and my stepfather Jean-Marc, for their constant patience and care. They have always supportive during this period in all aspects.

A special thanks goes to my husband Denis Nikitin, with whom I also shared the office during my PhD. We had long and deep discussions on all possible scientific or irrelevant topics, which was often so inpiring and enjoyable. Our common trips all over Southern Europe will always be one of the most beautiful highlights of my PhD time.

This thesis was mainly funded by the European Research Council (ERC) under the European Union's Horizon 2020 research and innovation programme (ERCAdG no. 694209, Scale-FreeBack, website: http://scale-freeback.eu/).

Résumé

L'urbanisation continue de la planète contribue à une augmentation de la demande de transport, ce qui entraîne la formation de graves congestions. Cela a un impact négatif sur la vie quotidienne. Par conséquent, des solutions efficaces pour la gestion intelligente des transports sont d'une grande importance.

Dans ce travail de thèse, on traite principalement du contrôle et de la modélisation du trafic sur des réseaux urbains de dimension arbitraire avec une application à la ville de Grenoble. Le trafic est considéré d'un point de vue macroscopique. Son état est prédit par une équation différentielle partielle (EDP) qui décrit le trafic en termes du flux et de la densité des véhicules dans une zone donnée. Dans cette approche de modélisation, on suppose qu'il existe une relation concave entre le flux et la densité, connue sous le nom de diagramme fondamental (Fundamental Diagram - FD). Ainsi, en fonction de la densité des véhicules, on distingue deux régimes du trafic: le régime du flux libre (la densité est inférieure à la valeur critique) et le régime de la congestion (la densité est supérieure à la valeur critique).

On propose des techniques de la conception du contrôle qui reposent sur les propriétés intrinsèques des modèles du trafic macroscopiques. Tout d'abord, nous résolvons des problèmes du contrôle aux limites unidimensionnelles (1D) pour le trafic évoluant sur des routes simples. Ensuite, divers problèmes du contrôle sont posés et résolus pour le trafic sur des réseaux urbains de la taille arbitraire. La dynamique du trafic est alors décrite par un modèle bidimensionnel (2D) de loi de conservation. Ce modèle 2D est évolutif, c'est-à-dire qu'il décrit le trafic urbain par une seule EDP. Cependant, il n'est applicable qu'aux zones urbaines ayant une direction de mouvement préférée. Enfin, nous présentons un nouveau modèle du trafic continu en 2D qui peut capturer la véritable multidirectionnalité du trafic. Ce modèle est formellement dérivé du concept d'offre et de demande à une intersection. Il se compose de quatre EDP qui décrivent l'évolution de la densité des véhicules par rapport aux directions cardinales: Nord, Est, Ouest et Sud (North-East-West-South - NEWS). Les performances du modèle NEWS ont été testées en utilisant des données simulées et réelles (provenant des capteurs installés dans la ville de Grenoble).

Les principaux résultats de cette thèse sont résumés ci-dessous.

Contrôle du trafic sur les routes

Dans ce chapitre, l'évolution de la dynamique du trafic est étudié sur une route unique de la longueur finie en utilisant le modèle de Lighthill-Whitham-Richards (LWR). Ce modèle est une EDP hyperbolique non linéaire du premier ordre qui représente une loi de conservation, le nombre de véhicules étant la quantité conservée. Deux problèmes du contrôle aux limites sont posés pour suivre une densité désirée qui est une trajectoire dépendante de l'espace et du temps. Ces dépendances sont capables de capturer des nombreuses situations réalistes lorsque

les conditions du trafic changent rapidement. Par exemple, il est courant qu'une route ait des valeurs du flux entrant différentes au cours d'une même journée (il peut y avoir plus de véhicules à 9 heures du matin lorsque les gens vont au bureau et moins de voitures la nuit). En outre, un état d'équilibre souhaité ne représente qu'un profil général variant dans l'espace et dans le temps. Cependant, un tel profil cible général entraîne une dynamique d'erreur non triviale.

Tout d'abord, nous considérons que le trafic est uniquement en régime congestionné. Cela simplifie le modèle LWR qui devient une EDP linéaire. Ce modèle est cependant inhomogène, puisque nous ajoutons également une fonction de perturbation générale dans le domaine dépendant de l'espace. Cette fonction incorpore une éventuelle inadéquation entre le modèle et la réalité. Par exemple, il peut y avoir un flux non mesuré de véhicules provenant de routes secondaires ou de véhicules en stationnement. Pour ce système linéaire inhomogène, nous formulons des problèmes d'atténuation des perturbations tout en atteignant le profil souhaité en termes de normes spatiales L_2 et L_∞. La trajectoire souhaitée est également restreinte au régime congestionné pour des raisons de simplicité, c'est-à-dire qu'elle est régie par le système linéaire homogène LWR. On traite la fonction de perturbation inconnue en utilisant la méthode des caractéristiques qui permet d'exprimer la fonction de perturbation par des variables connues (mesurées) telles que la densité des véhicules et les actions du contrôle appliquées au cours des étapes temporelles précédentes. Le contrôle conçu se compose d'une partie à action directe et d'une partie à rétroaction.

En outre, on considére également un problème plus complexe dans le cas où l'état et la trajectoire souhaitée sont régis par des modèles non linéaires LWR comme dans sa formulation originale (et sans la perturbation). Le principal défi est alors lié aux chocs (discontinuités), qui apparaissent dans de tels systèmes même pour des données initiales régulaires en temps fini. Cela rend l'analyse explicite fastidieuse, puisqu'il n'existe pas de solutions classiques, et nous ne devons les considérer que dans un sens faible et suivre la dynamique des chocs. Un autre défi est lié aux conditions aux limites faibles, ce qui implique qu'aucune action de contrôle ne peut être imposée aux limites (on doit prendre en compte l'état actuel du système). Pour traiter ces deux problèmes, nous traduisons LWR en EDP de Hamilton-Jacobi (H-J) qui représente sa forme intégrale. La solution de l'EDP H-J est exempte de discontinuités et, dans le pire des cas, elle peut seulement devenir non-différenciable. Son état correspond au nombre cumulé de véhicules qui peut être obtenu en intégrant la densité des véhicules. Le système H-J peut être vu comme un problème de contrôle optimal, et sa solution est obtenue de manière semi-explicite comme le minimum de tous les chemins valides. Dans le cas d'un FD triangulaire, la solution est obtenue comme le minimum sur seulement trois chemins valides, chacun associé à la condition initiale ou aux conditions limites, respectivement. Pour analyser le comportement du système en temps asymptotique, on estime le temps minimal auquel il est garanti que les conditions initiales n'affectent plus la solution H-J. La solution est alors formulée comme un minimum de seulement deux chemins valides associés aux conditions aux limites. La formulation intégrale du système de la circulation de Hamilton-Jacobi ainsi que la possibilité d'exprimer exactement sa solution, nous permettent d'analyser explicitement les périodes du temps, lorsque les limites sont restreintes pour accepter des actions du contrôle en fonction de l'état réel de la circulation. Ces fonctions dites de restriction du contrôle

permettent de diviser la dynamique d'erreur en trois régimes différents en fonction des limites qui peuvent actuellement accepter des actions du contrôle. Nous montrons que même lorsque les limites sont parfois incapables d'accepter les contrôles proposés, le système converge vers la trajectoire souhaitée de manière exponentielle. Les résultats sont validés numériquement pour différents gains de contrôle.

Trafic unidirectionnel sur les réseaux

Ce chapitre est consacré au contrôle du trafic sur les réseaux urbains de toute taille. Sa dynamique est décrite par le modèle LWR en 2D (2D LWR) qui représente une loi de conservation en deux dimensions. Le trafic est traité comme un fluide qui se propage maintenant sur un plan 2D continu.

Le modèle 2D LWR est inspiré de la modélisation de la foule, la seule différence étant la restriction pour les véhicules de se déplacer sur des routes physiques. Ainsi, le modèle nécessite de supposer que le réseau urbain est suffisamment dense pour être considéré comme un domaine continu. Pour modéliser le trafic, il faut disposer d'informations sur la géométrie et l'infrastructure du réseau urbain, c'est-à-dire l'emplacement des routes et des intersections, le nombre de voies de chaque route et ses limites de vitesse. Ces informations sont utilisées pour définir la densité et les capacités maximales partout dans le domaine du continuum. En particulier, on applique la pondération inverse à la distance pour attribuer des valeurs aux variables partout en fonction de la distance aux routes. Tous ces paramètres étant spécifiques aux différents réseaux urbains sont incorporés dans un FD qui devient explicitement dépendant de l'espace. Une analyse directe d'un tel modèle est une tâche compliquée en raison de la dérivée seconde de l'espace. Il n'est pas non plus évident de savoir quel point limite doit être actionné pour affecter un point ou une zone spécifique du domaine.

On trouve une approche pour analyser ce modèle de telle sorte que l'on puisse suivre les trajectoires du flux dans la zone urbaine. Ceci est possible, car la structure du modèle 2D LWR limite son applicabilité uniquement pour les réseaux constitués de routes unidirectionnelles. Le champ de direction ne dépend que de la géométrie du réseau et non de l'état. S'il n'y a pas de boucles dans un réseau, on peut définir une transformation de coordonnées curviligne. Cette transformation de coordonnées traduit le système de trafic 2D en un ensemble paramétré de systèmes 1D avec un FD dépendant de l'espace, ce qui est beaucoup plus facile à analyser. Mathématiquement, cela signifie qu'au lieu de deux dérivées partielles par rapport à l'espace, le système modifié n'en a qu'une. Bien que cette transformation des coordonnées ait pu être définie en raison des restrictions spécifiques de 2D LWR, ce modèle peut néanmoins être utilisé pour prédire l'évolution du trafic dans plusieurs situations fréquentes, par exemple lorsque, à l'heure de pointe du matin, tous les véhicules se dirigent vers le centre-ville où se trouvent la plupart des bureaux.

En outre, nous présentons plusieurs résultats obtenus en analysant 2D LWR en coordonnées curvilignes. Nous élaborons une technique permettant d'obtenir une distribution de véhicules dans un état d'équilibre uniquement en connaissant les données du flux entrant et du flux

sortant d'une zone urbaine. Cette capacité d'analyser l'équation en 2D pour obtenir des équilibres admissibles est un résultat essentiel qui permet de formuler des tâches de contrôle pour la stabilisation du trafic urbain. En outre, nous concevons un contrôleur de frontière pour atténuer les congestions dans une zone urbaine. Ainsi, pour simplifier, le trafic est limité au régime de la congestion.

Ensuite, un problème de contrôle aux limites visant à approximer la trajectoire désirée du véhicule est posé pour un régime de trafic mixte en temps asymptotique. Pour cela, le modèle 2D LWR en coordonnées curvilignes est ensuite considéré dans le formalisme de Hamilton-Jacobi qui facilite la gestion des discontinuités pour la conception du contrôle aux limites. Le problème du contrôle aux limites est résolu de la même manière que pour le cas 1D. La difficulté supplémentaire est introduite par la dépendance spatiale explicite dans le diagramme fondamental, de sorte que la formule classique de Lax-Hopf ne peut être appliquée. Au lieu de cela, on applique la théorie de la viabilité élaborée pour le cas des hamiltoniens dépendants de l'espace. Pour un exemple numérique, nous prend la structure du centre-ville de Grenoble comme réseau urbain.

Enfin, le modèle 2D LWR est utilisé en coordonnées curvilignes pour concevoir un contrôleur de limite de vitesse variable (Variable Speed Limit - VSL). Le contrôleur VSL est utilisé pour affecter directement le flux de trafic en imposant des restrictions temporaires sur la vitesse autorisée, ce qui est souvent utilisé pour des situations spécifiques telles que les accidents, les mauvaises conditions météorologiques, etc. Il s'agit d'un contrôleur intra-domaine qui est appliqué d'une manière continue dans l'espace sur l'ensemble du domaine. Il agit comme une linéarisation par rétroaction de sorte que l'équation d'état perd sa structure de loi de conservation, ce qui facilite son analyse. Le contrôleur VSL peut être utilisé pour stabiliser le système 2D à n'importe quel équilibre souhaité variant dans l'espace. Si FD a une dépendance concave par rapport au contrôleur dans le régime de trafic congestionné et une dépendance linéaire dans le régime du flux libre, le contrôleur est différentiable presque partout dans l'espace. On conçoit également un état d'équilibre optimal qui correspond à la maximisation du flux obtenue pour le nombre maximal possible de voitures. Dans un exemple numérique, on utilise à nouveau la structure du centre-ville de Grenoble, puis on démontre comment le contrôleur VSL conçu fait converger la densité de véhicules vers l'équilibre souhaité.

Trafic multidirectionnel sur les réseaux

Dans ce chapitre, nous proposons notre propre méthode pour traiter le trafic multidirectionnel évoluant sur des réseaux urbains de taille arbitraire à un niveau macroscopique. Le trafic multidirectionnel est beaucoup plus proche de la représentation du trafic urbain dans des situations réalistes que le modèle 2D LWR. L'idée globale consiste à dériver un modèle EDP qui capture le comportement du trafic évoluant dans un réseau urbain dans n'importe quelle direction avec des croisements de flux.

On commence par considérer un modèle du flux du trafic à une intersection basé sur le

modèle classique de transmission cellulaire. Chaque intersection est caractérisée par un certain nombre de routes entrantes et sortantes qui peuvent être orientées arbitrairement dans l'espace. Ainsi, il y a un nombre différent de paramètres à régler pour chaque intersection individuelle. Comme un réseau peut être composé de milliers d'intersections, on trouve une approche unifiée pour décrire le trafic aux intersections indépendamment de leurs paramètres individuels. Ainsi, on suppose que la dynamique du trafic multidirectionnel peut être représentée par seulement 4 couches de direction: Nord, Est, Ouest et Sud (North-East-West-South - NEWS). Dans le formalism du NEWS, on déploie des matrices de projection basées sur la géométrie pour appliquer le flux de trafic le long de toute route dans les directions cardinales. Les poids de projection varient continuellement avec l'angle d'orientation de la route. Ensuite, le concept du flux partiels est introduit pour capturer divers modèles d'origine-destination aux intersections.

Ainsi, on obtiens un modèle du flux du trafic qui prédit le taux de changement de l'accumulation de véhicules à l'intersection d'une manière unifiée. Ensuite, la méthode de continuation est appliquée pour obtenir un modèle qui prédit l'évolution de la densité des véhicules à proximité d'une intersection. Cette méthode est utilisée pour transformer une EDO (modèle routier) en une EDP (modèle d'intersection), qui représente un modèle de continuum macroscopique pour une intersection. Comme chaque intersection a été décrite de la manière unifiée, pondération inverse à la distance est appliquée pour définir tous les paramètres d'intersection pour chaque point dans un plan continuum. La dérivation du modèle NEWS a été faite analytiquement en utilisant une seule hypothèse sur la structure du réseau. À savoir, les réseaux urbains doivent être bien conçus en termes de flux maximal, c'est-à-dire que si les véhicules se déplacent à un flux maximal avant une intersection, ils continuent à utiliser la capacité de la route au maximum après le virage.

En conséquence, on obtiens le modèle NEWS qui prédit l'évolution du trafic dans quatre directions cardinales. La propagation du flux du trafic dans chaque direction est pilotée par le concept d'offre et de demande qui s'appuie sur le diagramme fondamental. De plus, véhicules peuvent changer de couche de direction, c'est-à-dire qu'il existe un couplage entre différentes couches, ce qui est un aspect important en raison de son ubiquité physique.

Les propriétés mathématiques du modèle NEWS dérivé sont également analysées. Le système d'EDP est hyperbolique pour tout ensemble de paramètres. Le fait de pouvoir classer un modèle comme une EDP hyperbolique simplifie considérablement l'analyse pour les tâches futures, puisque de nombreux résultats analytiques ont déjà été élaborés pour ce type de systèmes. Il a également été démontré que le modèle représente une loi de conservation, la densité du trafic étant la quantité conservée. De plus, il a été démontré que son état est borné, ce qui est une hypothèse réaliste importante pour la modélisation du trafic.

Les résultats de la prédiction du modèle sont validés à l'aide de la microsimulateur Aimsun et de la plateforme expérimentale GTL Ville qui fournit des données en temps réel provenant d'un réseau des capteurs installés dans le centre-ville de Grenoble. Les résultats de validation révèlent que la distribution de la densité prédite par le modèle NEWS reste en bon accord avec la densité de référence, soit 90 % de similarité avec Aimsun et 80 % de similarité avec l'expérience réelle. La validation du modèle avec des données réelles est un projet open source, c'est-à-dire que les résultats sont reproductibles et peuvent être utilisés pour des études futures.

Enfin, le modèle NEWS est étudié du point de vue du contrôle, où on se limite au régime du trafic congestionné pour des raisons de simplicité. On analyse la classe d'équilibres admissibles souhaités qui doivent satisfaire un certain système d'EDP. On pose et résolve le problème de la recherche d'un état d'équilibre qui permet de minimiser la congestion dans un réseau urbain sous la contrainte que sa gamme de valeurs doit rester dans le régime de congestion. De plus, on prouve la convergence exponentielle d'un état congestionné contrôlé depuis un limite vers cet équilibre désiré en utilisant des méthodes de Lyapunov. Le réseau du centre-ville de Grenoble est à nouveau utilisé pour démontrer la performance du contrôleur aux limites dérivé à l'aide d'un exemple numérique. On montre que le contrôleur fait converger la densité du trafic vers l'équilibre optimal désiré en temps fini, ce qui est lié à la nature hyperbolique de l'EDP.

Perspectives et extensions

Sur la base des résultats de cette thèse de doctorat, je vois un grand nombre de directions intéressantes pour la recherche future. Les questions ouvertes suivantes semblent être les plus pertinentes:

- Dans cette thèse, le trafic a été décrit d'une manière assez simpliste, puisque LWR représente un modèle macroscopique le plus simple du trafic. En général, il est bien connu que l'approche de la modélisation LWR présente plusieurs inconvénients, car elle ne prend pas en compte de nombreux phénomènes importants tels que l'accélération limitée ou la baisse de capacité due à la transition d'un régime flux libre à un régime congestionné. En outre, une façon possible d'affiner la description du trafic est de prendre en compte différentes classes de conducteurs en fonction de leur vitesse (par exemple, rapide et lente). Ainsi, on pourrait étudier les problèmes du contrôle des limites à l'aide d'une approche de modélisation plus sophistiquée qui tient compte des limites du modèle LWR (modèles d'ordre supérieur et multi-classes).

- Le modèle 2D LWR est limité à la description du trafic sur les réseaux qui ont une direction de mouvement préférée, ce qui n'est pas réaliste pour le trafic général. Par conséquent, comme une extension prometteuse de la recherche sur la modélisation macroscopique du trafic urbain, on pourrait développer des algorithmes de partitionnement qui divisent un réseau urbain en zones ayant une direction de mouvement préférée.

- Les contrôleurs aux limites sont conçus pour un trafic évoluant sur un domaine rectangulaire continu qui se rapproche du réseau urbain sous-jacent. En conséquence, on a obtenu des lois de contrôle définies sur une ligne continue, ce qui n'est pas directement interprétable. Il serait donc intéressant d'étudier ce problème et de mettre au point une méthode permettant de transformer les contrôleurs aux limites définis sur des lignes continues en contrôleurs réglés sur des points ou des intervalles spécifiques sur des routes réelles.

- Le modèle NEWS est un système de seulement quatre EDP qui est capable de prédire l'évolution du trafic multidirectionnel sur les réseaux urbains de manière assez précise. Il est important pour les études futures de caractériser rigoureusement les propriétés mathématiques de ses solutions. De plus, il serait intéressant d'étudier ce modèle pour concevoir un contrôle des limites pour le trafic à régime mixte.

Contents

List of Figures

List of Tables

List of acronyms

1D	one-dimensional
2D	two-dimensional
CTM	Cell Transmission Model
FD	Fundamental Diagram
H-J	Hamilton-Jacobi
IBVP	Initial Boundary Value Problem
IDW	Inverse Distance Weighting
GTL	Grenoble Traffic Lab
CFL	Courant-Friedrichs-Lewy (condition)
KDE	Kernel Density Estimation
LWR	Lighthill-Whitham-Richards (model)
MF	Moskowitz Function
MFD	Macroscopic Fundamental Diagram
NEWS	North-East-West-South (model)
ODE	Ordinary Differential Equation
PDE	Partial Differential Equation
SR	Supply Ratio
SSIM	Structural Similarity Measure
TR	Turning Ratio
VSL	Variable Speed Limit

Chapter 1

Introduction

1.1 Traffic on roads

Traffic models have been developed and studied in order to describe traffic dynamics and predict the appearance of congestions since the beginning of the twentieth century. The origin of the traffic flow theory takes us back to the thirties, when Greenshields [59] collected data from a highway road on the car headway distance (average distance of two consequative vehicles) and their average velocity. One year later, in [58] he proposed a fundamental relation connecting the average car velocity with the vehicle density. This empirically established law became very famous later in the traffic engineering community, and nowadays it is known as the Greenshields fundamental diagram. It can also be represented in terms of vehicle density ρ (average number of vehicles per unit length) and flow ϕ (average number of vehicles per time unit), which yields a concave relation $\Phi(\rho)$:

$$\phi = \Phi(\rho) = v_{max}\left(1 - \frac{\rho}{\rho_{max}}\right)\rho,$$

where ρ_{max} is the vehicle density at the traffic jam, and $v_{max} = \Phi'(0)$ is the maximal average density of vehicles on a freeway. Afterwards, many other possible shapes of fundamental diagrams have been proposed, see [91] for a detailed overview on flow-density curves. Nowadays, the most simplistic flow-density relation that is widely used for analysis of traffic is the triangular (bilinear) fundamental diagram proposed by Daganzo in 1994 [38].

1.1.1 Origins of traffic modeling

The discovery of fundamental diagram plays an essential role in the history of traffic flow modeling. It was the first evidence that traffic can be described and analyzed in terms of dynamic systems rather than considering it as a collection of independent vehicles. Thus, the ability to formulate a fundamental diagram gave rise to appearance of different traffic flow models, see [140] for a detailed review. In general, these can be categorized as microscopic and macroscopic traffic models depending on the level of description detail. Microscopic models trace the behaviour of each individual vehicle. The main assumption of these models is that drivers adapt their behaviour to that of the leading vehicle, i.e., car-following models, see for example [116, 80]. On the other hand, traffic can be alternatively described from the macroscopic point of view. In this case, traffic state is given in terms of aggregated variables

such as average density and average flow, while individual vehicles are not modeled. In this thesis, we describe traffic in terms of macroscopic variables. This enables to analyze traffic on some aggregated level that is a useful approach when it comes to large-scale transportation networks.

Macroscopic traffic models are often compared to fluid, since they describe traffic flow as if it were a continuum. In the fifties, the kinematic wave theory for traffic has been formulated by Lighthill and Whitham [96] and, independently, Richards [118]. This so-called LWR model is a fluido-dynamic model that prescribes the conservation of the number of vehicles. It describes the spatio-temporal evolution of vehicle density on an infinite highway road as the following first-order scalar hyperbolic partial differential equation (PDE):

$$\partial_t \rho(x,t) + \partial_x \Phi(\rho) = 0, \qquad \forall (x,t) \in \mathbb{R} \times \mathbb{R}^+.$$

Its key assumption is the existence of a concave flow-density relation (fundamental diagram), which allows to consider this conservation law equation as a model for traffic.

The LWR model was the first macroscopic model in the history of traffic modeling, and it has some physical limitations. For instance, according to the LWR model vehicles reach the new equilibrium velocity immediately after a change in the traffic state, which implies infinite acceleration. This problem was addressed in [84, 88], where the LWR model was extended to take the bounded acceleration into account. Another drawback of the LWR model is that the transition from the free-flow to the congested traffic regime occurs at the same density and without capacity drop. This was addressed by [41, 75] by introducing lane changing. However, even despite the appearance of more sophisticated first-order [35, 144, 18] or even higher-order models [12, 57] capable of covering more realistic traffic behaviour, the LWR model remains the most used one to study due to its simplicity and ability to reproduce the most essential traffic phenomena such as wave formation and propagation. LWR model was also shown to be consistent with car-following behaviors at the aggregated level [109].

Although being the most simple continuous traffic model, the explicit analysis of the LWR equation is a tedious task. In general, such partial differential equations are solved using the method of characteristics [46]. However, the nonlinearity of the fundamental diagram introduces nonlinearities in the characteristic fields. Therefore, even with a smooth initial datum characteristic lines may intersect, which leads to discontinuities at intersection points. This triggers a shock or a rarefaction wave depending on the state at the moment of intersection (Riemann problem). Then, the conservation law solution is not defined in the classical sense, and therefore needs to be considered in its weak formulation. This formulation yields multiple solutions, among which the entropy solution [8] is recognized to be the physically reasonable one. Mathematical properties of hyperbolic conservation laws have been extensively studied, and an interested reader is referred to [21, 70, 83].

There is however a way to study the kinematic waves of traffic without any need to deal with shocks in the solution. In [106, 107, 108] Newell proposed an alternative way to consider traffic on a macroscopic scale by numbering vehicles at the highway entry and following the evolution of vehicle numbers at every location and time. Thus, the traffic state can be described

in terms of cumulative number of vehicles M that evolves as

$$\partial_t M(x,t) + \Phi(\partial_x M) = 0, \qquad \forall (x,t) \in \mathbb{R} \times \mathbb{R}^+.$$

This equation has the structure of a Hamilton-Jacobi PDE, which represents an integral form of the LWR PDE. Its solution is a Lipschitz continuous function that is free of shocks (in the worst case it is only non-differentiable), and it can obtained by solving a simple minimization problem.

A variational formulation of kinematic waves was studied in [36, 37], who showed that every well-posed traffic problem with a concave flow-density relation can be solved as a set of shortest paths. In general, the explicit solution of Hamilton-Jacobi PDE can be obtained using the viability framework, which was first shown for the case of convex conservation laws in [76, 77]. The viability framework is based on using Lax-Hopf formula that exploits the structure of a dynamic programming problem, and the solution is obtained as the minimum of all valid paths, see also [28]. Several computational algorithms have been developped to obtain solutions of H-J PDE for some special cases in the context of traffic modeling. Thus, [27] presented a computational method for any piecewise affine initial condition. The Lax-Hopf algorithm to compute the solution on a single link for any concave fundamental diagram has been suggested by [100]. Its improved version with a lower computational time has been proposed in [127].

In some cases, the exact solution to LWR PDE can be obtained using the wave-front tracking method [65, 99, 145]. This method can also be used to prove the existence of solutions to conservation laws, see for example [30]. The solution of a LWR PDE can also be numerically approximated using computational methods such as the Godunov scheme [56], or the Lax-Friedrichs method [89]. These are both finite difference methods. The Godunov scheme deals with Riemann problems at each cell, and the Lax-Friedrichs method requires adding artificial viscosity.

In the nineties, a time-discrete approximation of the LWR equation was introduced in [38, 39], which is now known as the cell transmission model (CTM). This model can be viewed as a Godunov-type discretization of LWR, and it is based on approximating links (roads) by cells. The amount of flux that is transmitted between cells is based on their current occupancy (the demand-supply concept). Nowadays, CTM is the most popular model in the traffic community due to its simplicity and the ability of a straightforward extension to networks.

1.1.2 Road control

Continuing urbanization caused by ever-growing population of the planet implies a growing demand for transportation. This entails formation of severe congestions that cost people hundreds of hours per year and that also have a significant negative impact on the environment. For instance, the Urban Mobility Report [125] summarized the major daily life problems caused by traffic congestions in USA in 2017. According to this report, urban American drivers experience the following losses per year on average: 8.8 billion hours of time delay,

3.3 billion gallons of wasted fuel and an equivalent monetary cost of 179 billion dollars. This requires the development of efficient solutions for intelligent transportation management.

There are several common techniques to control traffic. One of the most widely used techniques is a suitable application of a variable speed limit (VSL) along a highway road. It is applied such that the maximal allowed speed is decreased, which mitigates risk of accidents, as well as it results into a lower fuel consumption and reduced emissions. Previous works [2, 95, 150] confirmed that the VSL control enhances traffic safety and has a positive environmental impact. Reduced travel time is another positive effect of VSL controllers reported by [105, 49]. The effect of VSL on the shape of the fundamental diagram was studied in [23, 113]. However, the improvement of travel time achieved with VSL control revealed inconsistencies in microscopic simulations and field tests [79, 124]. These inconsistencies are related to the fact that it is hard to precisely predict traffic conditions at some localized congested bottleneck via the macroscopic modeling. Moreover, not every human driver adapts his/her velocity to numbers displayed on electronic traffic signs.

Alternatively, traffic can be regulated from the boundary, that is either from entry or exit of the corresponding highway road, e.g., by actuating on- and off-ramps. By managing on-ramp traffic inflows, the application of meters also reduces the travel time, harmful emissions and improves highway safety [90]. Moreover, [148] reported that ramp metering helps reducing the average freeway delay.

However, in most of the cases, control for a traffic road is designed using the discretized version of the corresponding traffic model. According to [89], such discretizations are known to alter essential phenomena predicted by the original macroscopic traffic models and may lead to inconsistent discrete versions. Recall that from the mathematical viewpoint, macroscopic traffic models such as LWR mostly represent conservation laws with dynamics governed by hyperbolic partial differential equations. The theory on the exact controllability and exact observability was completely developed in [122, 98] for linear and in [92] for 1D quasilinear hyperbolic PDEs. The results on exact controllability for nonlinear scalar conservation laws with a strictly convex flux function were discussed in [115]. Classical techniques widely used for control of hyperbolic conservation laws are backstepping [31], Lyapunov-based [19, 32] and optimal control methods using adjoint-based calculus [139, 60, 72, 15]. Optimal control tasks for traffic are considered to solve the most common problems of traffic regulation, i.e., minimization of total travel time and fuel consumption, or throughput maximization.

However, the classical control methods mentioned above are not always well suited to handle shocks, since they require the knowledge on the internal shock dynamics. Tracking dynamics of shocks was done, e.g., in [20], where the weak formulation and the Rankine-Hugoniot relation were used to stabilize solution of the Burgers equation to a constant equilibrium. In a recent work [14] the problem of boundary control of solutions with jump discontinuities has been considered. In both [20, 14], the desired state was stationary and the Lyapunov methods were applied. In [43] the exact controllability of solutions to conservation laws to space- and time-dependent trajectories has been studied. Nevertheless, the problem of stabilizing a state with shocks to space- and time-dependent trajectories that may also contain shocks has never been considered before. We address this problem in Chapter 2.

1.2 Traffic on urban networks

In its original formulation, the LWR-model is applicable only to single roads of infinite length. Extension to urban networks required developing a methodology for intersection modeling within the LWR framework. This was first done at the end of the last century by [69], who considered a network of uni-directional roads. Later on, this formulation was refined to capture multi-directional traffic, e.g., see [29]. The CTM has also been extended to networks in [39], who considered networks as directed graphs consisting of links (roads) and nodes (junctions). The general theory of traffic flow on networks is presented in [50]. The Cauchy problem for complex networks (with more than two incoming and outgoing roads at junctions) was considered in [51].

The most common way to control traffic on a urban level is to optimize the time intervals of green signal at signalized intersections, see [26, 52]. There exist also other control techniques applied in transportation networks, such as routing of traffic [60], ramp metering [111], variable speed limits [113, 141], see also [112] for a general review of traffic control strategies. The main challenge in this link-level (discrete) representation of traffic networks is the large computational time. For instance, if we consider large urban networks consisting of thousands of links, the need to use much of traffic data considerably exaggerates validation of control performance [152].

Another way to model traffic on urban areas is again to consider continuous macroscopic models. They describe traffic as a two-dimensional fluid moving on a continuum plane that corresponds to a dense urban network. This approach has various advantages, e.g., the problem size does not depend on the number of roads, as well as less data are required for the model setup. Early works on continuous urban traffic modeling [128, 131, 66] presented static models with the focus on determining equilibria states in urban networks. However, due to the lack of any knowledge of a flow-density relation on a city level, these models failed in capturing traffic dynamics during rush hours, see [68] for a general review of such models.

The first demonstration of existing macroscopic relation between density and flow should be recognized to [142], who used data from microsimulations. Later this relation was also observed during an experiment conducted in the congested region of Yokohama, Japan [53], and was then generalized in [40]. This functional relation has the same physical meaning as the fundamental diagram for highway roads, but it was shown to exist also on urban areas.

The discovery of macroscopic fundamental diagram (MFD) plays an essential role in the development of traffic models for urban areas. The empirical evidence of MFD led to appearance of reservoir models, which are also called accumulation models. These models predict the rate of change of the vehicle accumulation in some urban area (reservoir) that is determined by the difference between its inflow and outflow, see [5] for a review on several MFD-based models. The network's MFD can be defined by collecting real traffic data [53] or by running numerical simulations [62]. In [82] it has also been shown that the MFD can be well approximated by a function of only two parameters: the density of traffic lights and the mean red to green ratio across the network.

The MFD-based approach is intuitive and easy in use, which makes it popular for traffic control design such as perimeter control [54, 3], robust control [61], etc. It is important to note that only homogeneously congested areas may have a well-defined MFD, see [55] for properties of well-defined MFDs. In general, there must exist only one flow value for a given number of vehicles. This feature is preserved only in regions that consist of links characterized by similar congestion levels, while this causes problems in case of regions with heterogeneous links. In this case, one can apply partitioning algorithms that divide a problematic area into multiple smaller areas each having a well-defined MFD for given traffic conditions [63, 87]. For the case of rapidly changing traffic conditions (e.g., accident on a road), a dynamic clustering algorithm has been proposed by [123]. The main drawback of MFD-based modeling is that it assigns only one value to characterize traffic on some urban area being the current number of cars in this area. Thus, the level of precision to describe traffic behaviour on a global level depends on the number of defined clusters, i.e., in some sense it acts like CTM in 2D. This leads to the loss of information during the process of congestion formation and dissolution in a transportation network.

Another way to describe the evolution of traffic in urban areas is to use dynamic two-dimensional continuum models. These share a lot of features with pedestrian models [71]. The main difference is that crowds evolve in an open space, while vehicles are restricted to move on roads. In [121] authors considered a model including a diffusion term and a drift term that depends on the density. The direction of the drift vector is determined by the shape of the network. Other works [74, 45, 73] define the flux function by solving Eikonal equations such that the flow follows the path of the lowest cost. For a review of 2D continuum models the reader is referred to [5]. A recent work [103] introduced a direct extension of LWR model in two dimensions:

$$\frac{\partial \rho(x,y,t)}{\partial t} + \nabla \cdot \vec{\Phi}(x,y,\rho) = 0, \qquad \forall (x,y,t) \in \mathbb{R}^2 \times \mathbb{R}^+.$$

Thereby, the flux function became a vector. Its direction is retrieved from the geometry of the underlying urban network, while the flux magnitude depends on network infrastructure parameters that are incorporated into the space-dependency of the fundamental diagram. In Chapter 3 we investigate this model to design boundary and in-domain control for mixed-regime urban traffic that admits shocks.

The aforementioned references however consider traffic flow that has only one direction of motion. Several years ago a dynamic continuum model for multi-directional pedestrian flows was presented in [67]. This model represents an extesion of CTM to pedestrian dynamics, which however does not take urban network geometry into account. The first attempt to include multiple directions in 2D continuum models for vehicular traffic has been made also only a few years ago by [97] who deployed dynamic user-optimal principle for the path choice. The drawback of this model is that the traffic density may become unbounded (it is not based on a fundamental diagram). There exist also other works [102, 4] proposing 2D multi-layer models with bounded densities. However, these models do not include mixing between different direction layers, i.e., vehicles can not change their direction of motion. Then, these models are also not necessarily hyperbolic, i.e., their equation type varies with parameters, which exaggerates its analysis and numerical simulation. Hyperbolicity for all parameters implies

that it can be analysed like many other conservation law based models for traffic. We fix both of these aspects in Chapter 4 by elaborating a novel multi-directional model. Subsequently, this model is used for boundary control design of multi-directional urban traffic.

1.3 Problem statements and contributions

This thesis is devoted to control of urban traffic evolving on large-scale transportation networks. Traffic is described in terms of flow and density of vehicles, i.e., from the macroscopic point of view. The dynamic equation that predicts the spatio-temporal evolution of traffic corresponds to a PDE that has a structure of a conservation law. Thus, traffic can be seen as a 2D fluid that propagates along a continuum 2D plane with a total surface determined by the size of the underlying urban network. To manage urban traffic, we use a purely model-based control design. This means that control is designed by analysing the intrinsic properties of the model. Therefore, the obtained controller is scalable and adaptive to changing traffic conditions, as well as it is applicable to any urban network of arbitrary size.

- In Chapter 2, we consider traffic evolving along a single road of finite length with dynamics governed by the LWR PDE. Our main goal thereby is to derive a boundary control law such that the traffic state tracks some desired space- and time-varying trajectory. First, we consider a linear system with disturbance for congested traffic, which can be solved using the characteristics method. The desired trajectory is achieved by actuating the downstream boundary of the road (published in [137]). Then, we extend this problem to a mixed-regime traffic governed by a full LWR PDE, for which no classical solutions exist. We solve the problem by analysing the system in its Hamilton-Jacobi formulation. Thus, the main contribution of Chapter 2 is the *boundary control design for a mixed-regime traffic with solution shocks that tracks the desired trajectory that also admits solution shocks for asymptotic time*. This result can be seen as a general solution to any control problem that can be posed for LWR traffic on finite roads, and it was published in [133].

- Chapter 3 is devoted to control design for traffic on urban networks. Thereby, traffic dynamics are described by the LWR model that contains an additional space dimension. It considers traffic as a fluid moving on a 2D plane that represents a continuous approximation of the urban area under consideration. The network infrastructure parameters are embedded as an explicit space-dependency of the fundamental diagram. The direction of movement is determined by the network geometry. The main limitation of this model is that it is designed to describe traffic on networks with uni-directional roads. Our main contribution in this chapter is to propose a *holistic approach to solve any possible control task for uni-directional 2D traffic*, which was sent for a publication [132]. This is done by proposing a curvilinear coordinate transformation that allows to rewrite the 2D model such that it can be treated as a parametrized 1D problem, which can be explicitly analyzed. By analyzing this traffic model in new coordinates, we solve a variety of control problems. First, we present a method to analytically estimate a steady-state

knowing only network structure and inflow data (published in [135]). Then, this result is used for a boundary control design such that congested traffic achieves the best equilibrium corresponding to the throughput maximization (published in [138]). Moreover, we also use this 2D model in curvilinear coordinates to solve a trajectory tracking task for traffic in a mixed regime in a similar way as in Chapter 2 but handling additional technical issues. Finally, we also analyze the system to design a variable speed limit control. These results on mixed-regime traffic control were sent to a journal [132].

- In Chapter 4, we deal with the main limitation of the preceding chapter that considered only uni-directional urban networks. The main contribution of Chapter 4 is to *propose a novel macroscopic model for multi-directional traffic*. The model is rigorously derived from the CTM at one intersection by solely relying on the demand-supply concept. As a result, we obtain a system of four PDEs each describing the propagation of vehicle density in North, East, South and West direction, respectively. This model is applicable to any urban networks with arbitrarily oriented roads. It includes interactions between different direction layers, i.e., direction is determined by turning ratios at intersections. Our model is validated using real data provided by Grenoble Traffic Lab, which is an experimental platform that collects data from a network of real sensors installed in Grenoble downtown. The model design and validation results have been sent to a publication [136]. Finally, the new model was analyzed for a boundary control design that can mitigate congestions in multi-directional traffic networks (the result was accepted for a publication [134]).

This thesis is organized as follows. In Chapter 2, we introduce the LWR model and discuss its properties and solutions, as well as the Hamilton-Jacobi theory and the Godunov scheme are presented. Then, we present the control results obtained for traffic on a single road. In Chapter 3, we give details on the 2D LWR model and how it can be used to describe the dynamics of urban traffic, which is then also compared to an MFD-based model. Afterwards, we introduce the curvilinear coordinate transformation for the 2D LWR and solve a variety of control tasks for uni-directional urban traffic. In Chapter 4, a new model for traffic with multiple directions is derived. We also discuss its properties and validate it with synthetic and real data. Each chapter is divided into sections and is concluded with the summary of the main results. In turn, each section starts with its main contributions and concludes with the discussion of the results. All contributions and perspectives are summarized and discussed in Conclusions and Perspectives. Finally, lists of symbols used throughout the thesis are given in Appendix A, and technical proofs of some theorems and lemmas used in the main body of this work are given in Appendix B.

1.4 Publications

- Journal publications:

  1. L. Tumash, C. Canudas-de-Wit, M. L. Delle Monache; **Multi-Directional Continuous Traffic Model For Large-Scale Urban Networks.** Submitted to

Transportation Research Part B: Methodological, 2021. Accessible at: https://hal.archives-ouvertes.fr/hal-03236552

2. L. Tumash, C. Canudas-de-Wit, M. L. Delle Monache; **Boundary and VSL Control for Large-Scale Urban Traffic Networks.** Submitted to IEEE Transactions on Automatic Control, 2020. Preprint: https://hal.archives-ouvertes.fr/hal-03167733
3. L. Tumash, C. Canudas-de-Wit, M. L. Delle Monache; **Boundary Control Design for Traffic with Nonlinear Dynamics.** Published in: IEEE Transactions on Automatic Control (early access), doi: 10.1109/TAC.2021.3069394. Accessible at: https://hal.archives-ouvertes.fr/hal-02955853
4. M. U. B. Niazi, C. Canudas-de-Wit, A. Y. Kibangou, D. Nikitin, L. Tumash, P.-A. Bliman; **Modeling and control of COVID-19 epidemic through testing policies.** Submitted to Annual Reviews in Control, 2020. Preprint: https://hal.archives-ouvertes.fr/hal-02986566

- Conference publications:

5. L. Tumash, C. Canudas-de-Wit, M. L. Delle Monache; **Boundary Control for Multi-Directional Traffic on Urban Networks.** Accepted to 2021 IEEE 60th Conference on Decision and Control (CDC), December 2021, Austin, Texas, USA. Preprint: https://hal.archives-ouvertes.fr/hal-03182546
6. L. Tumash, C. Canudas-de-Wit, M. L. Delle Monache; **Topology-based control design for congested areas in urban networks.** 2020 IEEE 23rd International Conference on Intelligent Transportation Systems (ITSC), September 2020, Rhodes, Greece, doi: 10.1109/ITSC45102.2020.9294280. Accessible: https://hal.archives-ouvertes.fr/hal-02860455v2
7. L. Tumash, C. Canudas-de-Wit, M. L. Delle Monache; **Equlibrium manifolds in 2D fluid traffic models.** IFAC 2020 – 21st IFAC World Congress 2020, July 2020, Berlin, Germany. Preprint: https://hal.archives-ouvertes.fr/hal-02513273
8. L. Tumash, C. Canudas-de-Wit, M. L. Delle Monache; **Robust tracking control design for fluid traffic dynamics.** 2019 IEEE 58th Conference on Decision and Control (CDC), December 2019, Nice, France, doi: 10.1109/CDC40024.2019.9029559. Accessible at: https://hal.archives-ouvertes.fr/hal-02331493
9. M. U. B. Niazi, C. Canudas-de-Wit, A. Y. Kibangou, D. Nikitin, L. Tumash, P.-A. Bliman; **Testing policies for epidemic control.** Submitted to Submitted to 2021 IEEE 60th Conference on Decision and Control (CDC), December 2021, Austin, Texas, USA. Preprint: https://hal.archives-ouvertes.fr/hal-03185142v1

The material contained in publications 3 and 8 is presented in Chapter 2. The material from publications 2, 7 and 6 constitutes Chapter 3. Finally, the material from publications 1 and 5 is presented in Chapter 4.

1.5 Notations

Here we explain several notations used throughout this thesis. Let us start with notations used in Chapter 2 devoted to 1D traffic problems:

- We introduce the following norms with respect to the space variable x. For a function $\rho(x,t) \in [0,L] \times \mathbb{R}^+$ the L_1, L_2 and L_∞ norms are defined $\forall t \in \mathbb{R}^+$ as

$$\|\rho(\cdot,t)\|_1 := \int_0^L |\rho(x,t)|dx, \tag{1.1}$$

$$\|\rho(\cdot,t)\|_2 := \sqrt{\int_0^L \rho^2(x,t)dx}, \tag{1.2}$$

$$\|\rho(\cdot,t)\|_\infty := \sup_{x\in[0,L]} |\rho(x,t)|, \tag{1.3}$$

  where sup (inf) indicates the essential supremum (infimum).

- The deviation of the state from the desired vehicle density trajectory is defined $\forall (x,t) \in [0,L] \times \mathbb{R}^+$ as

$$\tilde{\rho}(x,t) = \rho(x,t) - \rho_d(x,t). \tag{1.4}$$

- The cumulative deviation from the desired vehicle density trajectory along a road of length L (integral error term, or error in the number of vehicles) is defined $\forall t \in \mathbb{R}^+$ as

$$e(t) = \int_0^L (\rho(s,t) - \rho_d(s,t))\, ds. \tag{1.5}$$

Now let us also explain the notations used in Chapters 3 and 4 devoted to 2D traffic problems:

- We introduce the L_1, L_2 and L_∞ spatial norms for a function in 2D $\rho(x,y,t) \in \Omega \times \mathbb{R}^+$, where $\Omega \in \mathbb{R}^2 : [x_{min}, x_{max}] \times [y_{min}, y_{max}]$, as

$$\|\rho(\cdot,t)\|_1 = \int_{x_{min}}^{x_{max}} \int_{y_{min}}^{y_{max}} |\rho(x,y,t)|\, dxdy. \tag{1.6}$$

$$\|\rho(\cdot,t)\|_2 := \sqrt{\int_{x_{min}}^{x_{max}} \int_{y_{min}}^{y_{max}} \rho^2(x,y,t)\, dx\, dy}, \quad \forall t \in \mathbb{R}^+, \tag{1.7}$$

  and

$$\|\rho(\cdot,t)\|_\infty := \sup_{(x,y)\in\Omega} |\rho(x,y,t)|. \tag{1.8}$$

- The deviation from a 2D space-varying desired equilibrium (constant in time) is defined $\forall (x, y, t) \in [x_{min}, x_{max}] \times [y_{min}, y_{max}] \times \mathbb{R}^+$ as

$$\tilde{\rho}(x, y, t) = \rho(x, y, t) - \rho_d(x, y). \tag{1.9}$$

- The deviation from a 2D time- and space-varying desired trajectory is defined $\forall (x, y, t) \in [x_{min}, x_{max}] \times [y_{min}, y_{max}] \times \mathbb{R}^+$ as

$$\tilde{\rho}(x, y, t) = \rho(x, y, t) - \rho_d(x, y, t). \tag{1.10}$$

Chapter 2

Traffic Control on Roads

This chapter is devoted to traffic control problems on single roads of finite length. We consider traffic within the macroscopic modeling approach that incorporates the kinematic wave theory for traffic that applies principles from fluid dynamics to predict traffic. Using intrisic properties of the model, we design a boundary control law to track a desired vehicle trajectory. Section 2.1 contains preliminaries that include explanation of LWR model and its mathematical properties (weak solutions, boundary conditions, etc.), the basic numerical scheme to approximate LWR, as well as an equivalent approach to describe traffic in terms of Hamilton-Jacobi equation. In Section 2.2, we first consider traffic being only in the congested regime with some in-domain disturbance, i.e., the state is driven by an inhomogeneous linear PDE system. The desired trajectory is also restricted to congested traffic regime for simplicity. In Section 2.3, we consider traffic state and desired trajectory both not being restricted to any particular traffic regime, i.e., boundary control design is performed for a nonlinear system, which is mathematically quite challenging to handle due to shocks that arise in a full LWR system.

2.1 Preliminaries

The kinematic wave theory for traffic was formulated in the fifties by Lighthill, Whitham and Richards, and it is now known as the LWR model [96, 118]. Its main assumption is the existence of a concave relation between the vehicle density and its flow. This model remains the most popular macroscopic model for traffic due to its simplicity, while it is still able to capture the most essential traffic phenomena. In this section, we present the LWR framework in more details, as well as discuss its solution, boundary conditions, the numerical scheme and its integral formulation.

2.1.1 Lighthill-Whitham-Richards model

The LWR model is a scalar conservation law, where the conserved quantity is the number of vehicles in some area. This conservation law model corresponds to a first-order hyperbolic PDE, which also implies that the information propagates at a finite speed. This model predicts

the spatio-temporal evolution of traffic $\forall(x,t) \in \mathbb{R} \times \mathbb{R}^+$ as follows

$$\begin{cases} \dfrac{\partial \rho(x,t)}{\partial t} + \dfrac{\partial \Phi(\rho(x,t))}{\partial x} = 0, \\ \rho(x,0) = \rho_0(x), \end{cases} \tag{2.1}$$

where $\rho : \mathbb{R} \times \mathbb{R}^+ \to \mathbb{R}^+$ is the vehicle density with $\rho_0(x)$ being the initial data, and $\Phi(\rho) : [0, \rho_{max}] \to \mathbb{R}^+$ is the flux function that relates vehicle flow $\phi(x,t)$ with vehicle density $\rho(x,t)$. This relation is an empirically established law [58] known as **fundamental diagram** (FD). Mathematically speaking, the flux function $\Phi(\rho(x,t))$ is a Lipschitz continuous and concave function that admits a unique maximum ϕ_{max} (**capacity**) attained at ρ_c (**critical density**), while its minimum value is achieved in two cases: either if there are no vehicles, i.e., $\Phi(0) = 0$, or if traffic is fully congested, i.e., $\Phi(\rho_{max}) = 0$, where ρ_{max} is the **traffic jam density**.

2.1.2 Fundamental diagram

The most simple flow-density relation corresponds to the triangular (bilinear) fundamental diagram proposed in [38], see Figure 2.1a):

$$\Phi(\rho) = \begin{cases} v\rho, & \rho \in [0, \rho_c], \\ -\omega(\rho - \rho_{max}), & \rho \in (\rho_c, \rho_{max}], \end{cases} \tag{2.2}$$

where v and ω are kinematic wave speeds in the free-flow regime (wave moving forwards) and in the congested regime (wave moving backwards), respectively. Notice that kinematic wave speeds are not related to velocities of individual vehicles that are determined on average as the flow divided by the density. For instance, in the traffic jam (when $\rho = \rho_{max}$) velocities of vehicles are zero, while the kinematic wave propagates backwards with $-\omega$.

Thus, the triangular FD has only two slopes, since kinematic waves can take only two values (v and ω). The critical density ρ_c and the capacity ϕ_{max} are defined as

$$\rho_c = \frac{\omega}{v + \omega}\rho_{max}, \qquad \phi_{max} = v\rho_c. \tag{2.3}$$

In this thesis, we will also use the Greenshields FD that was the first flow-density relation proposed in 1935 in [58], see Figure 2.1b). This relation is given by the following smooth concave function

$$\Phi(\rho) = v_{max}\left(1 - \frac{\rho}{\rho_{max}}\right)\rho, \tag{2.4}$$

with the critical density ρ_c and capacity ϕ_{max} given as

$$\rho_c = \frac{\rho_{max}}{2}, \qquad \phi_{max} = \frac{v_{max}\rho_{max}}{4}, \tag{2.5}$$

and $v_{max} = \Phi'(0)$ is the maximal kinematic wave (free-flow) speed determined by the speed of a vehicle moving along a freeway with $\rho = 0$.

Throughout this thesis, we will use $\rho_c = 1/3\rho_{max}$ for all cases when a triangular FD is assumed, and $\rho_c = 1/2\rho_{max}$ for the case of Greenshields FD.

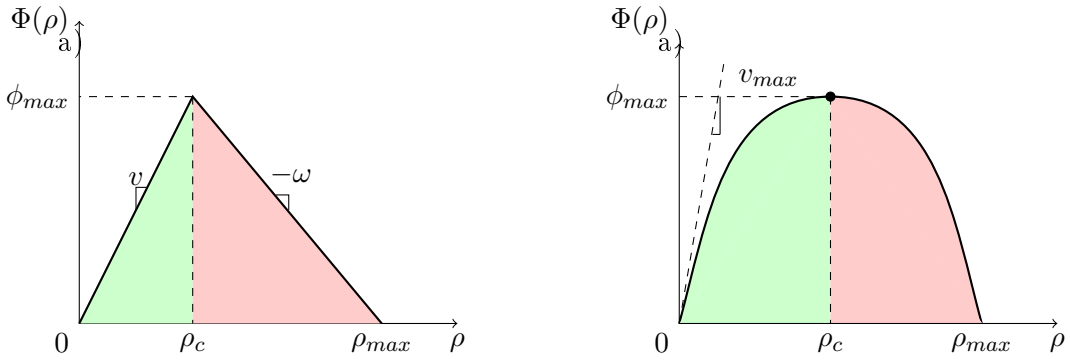

Figure 2.1: Fundamental diagrams: a) triangular, b) Greenshields. Free-flow and congested traffic regimes correspond to green and red areas, respectively.

Although in this work only triangular and Greenshields FDs are used to model the flow-density relation, there exist also many other types of FDs, see [91] for a review. Del Castillo [25] formulated properties that must hold for realistic fundamental diagrams:

1. The velocity range should be $v \in [0, v_{max}]$.
2. The vehicle density should be $\rho \in [0, \rho_{max}]$.
3. Cars stop moving when the traffic jam density is reached: $v(\rho_{max}) = 0$.
4. There is no traffic flow if there are no cars (zero density), or if cars are stuck in a traffic jam: $\Phi(0) = \Phi(\rho_{max}) = 0$.
5. Maximum velocity and congestion wave speed are the slopes of the fundamental relation at $\rho = 0$ and $\rho = \rho_{max}$, respectively.
6. Flux is a concave function of density.

2.1.3 Unique solution

Let us discuss the Cauchy problem (2.1). It has a structure of a first-order hyperbolic PDE that can be solved using the method of characteristics that yields lines along which the state remains constant (see [46] and Appendix B.1 for details). Thus, the characteristics of (2.1) are straight lines:

$$x - x_0 = \Phi'(\rho_0(x_0))t, \qquad x_0 \in \mathbb{R}^+, \tag{2.6}$$

where x_0 is a point in space, from which the characteristic line originates. The density is constant along each of these lines, that is for all (x, t) satisfying (2.6) we obtain

$$\rho(x, t) = \rho_0(x_0).$$

It can however happen that these lines intersect proposing two different values of ρ at the intersection point x_s, i.e., a discontinuity arises in the solution ρ. Hence, in general no classical solution exists for (2.1), and one needs to consider its solution in the weak sense.

A function $\rho : \mathbb{R} \times \mathbb{R}^+ \to \mathbb{R}^+$ is a weak solution of the Cauchy problem (2.1) if for any test function ψ (which is a C^1 function with compact support in $\mathbb{R}^2$) the following equation holds:

$$\int_0^{+\infty} \int_{-\infty}^{+\infty} (\rho\psi_t + \Phi(\rho)\psi_x)\, dx\, dt + \int_{-\infty}^{+\infty} \rho_0(x)\psi(x,0)\, dx = 0. \tag{2.7}$$

and the map $t \to \rho(\cdot, t)$ is continuous from $\mathbb{R}^+$ into L^1_{loc} (set of locally integrable functions).

Given that ρ is smooth around the point of discontinuity, we can integrate (2.7) to obtain the speed of discontinuity $\dot{x}_s$ known as the Rankine-Hugoniot relation [126]:

$$\dot{x}_s = \frac{\Phi(\rho_r) - \Phi(\rho_l)}{\rho_r - \rho_l}, \tag{2.8}$$

where ρ_r and ρ_l are values of the right and of the left limit of ρ at the point of discontinuity.

It is important to note that the Cauchy problem (2.1) can have an infinite number of weak solutions. Hence, the weak solution (2.7) must be completed by a uniqueness condition:

$$\Phi'(\rho_r) \leq \dot{x}_s \leq \Phi'(\rho_l), \tag{2.9}$$

where $\Phi'(\rho_r)$ and $\Phi'(\rho_l)$ are the characteristic speeds to the right and to the left of the discontinuity, correspondingly. In the theory of hyperbolic conservation laws, equation (2.9) is known as the *Lax admissibility condition* [83]. It selects the unique solution out of a set of weak solutions. The Lax condition has a simple geometrical interpretation. Namely, the unique solution is the particular weak solution for which the characteristics run into the shock: all characteristics must end at the discontinuity as illustrated in Figure 2.2.

Ansorge [8] was the first to consider this uniqueness condition (2.9) in the context of traffic. He interpreted it as driver's ride impulse, i.e., one starts driving when a traffic light switches from red to green. Thus, a weak solution of (2.1) satisfying (2.9) is the physically relevant one. It is also known as the **entropy solution**.

In particular, considering piecewise-constant initial state $\rho_0(x) = \rho_l$ for $x < x_s$ and $\rho_0(x) = \rho_r$ for $x > x_s$ (known also as a **Riemann problem**), entropy solutions can be of the two following types:

1. If $\rho_l < \rho_r$, *shock* arises. The entropy solution remains piecewise-constant, and shock wave propagates through space with velocity determined by (2.8): $\rho(x,t) = \rho_l$ for $x < x_s(t)$ and $\rho(x,t) = \rho_r$ for $x > x_s(t)$.

2. If $\rho_l > \rho_r$, the entropy solution becomes continuous and propagates in a form of a *rarefaction wave*. For any straight line starting from $(x_s, 0)$ the solution is constant and is determined only by $(x - x_s)/t$:

$$\rho(x,t) = \begin{cases} \rho_l, & \text{if } (x - x_s)/t < \Phi'(\rho_l), \\ \Phi^{-1}((x - x_s)/t), & \text{if } (x - x_s)/t \in [\Phi'(\rho_l), \Phi'(\rho_r)], \\ \rho_r, & \text{if } (x - x_s)/t > \Phi'(\rho_r). \end{cases}$$

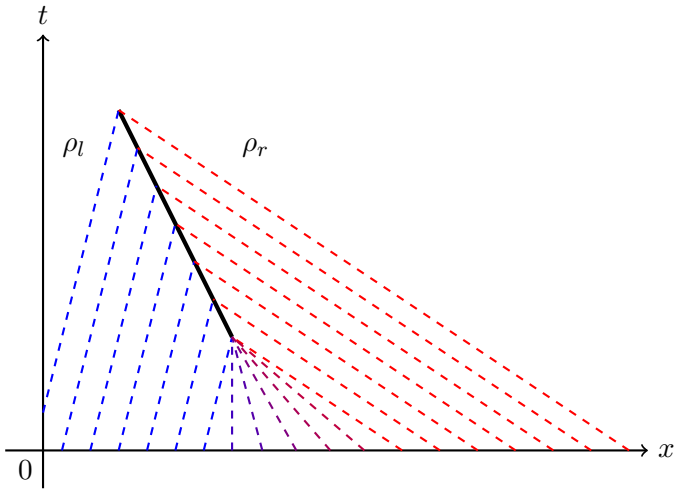

Figure 2.2: Geometrical interpretation of Lax admissibility condition. Thick black line: shock curve.

2.1.4 Boundary conditions

In its original formulation, the LWR model (2.1) describes traffic for infinitely long highways without any on-ramps or off-ramps, which is a serious physical limitation. Thus, one needs to include the boundary conditions for (2.1) in order to be able to include ramps and in general to consider roads of finite length (bounded domains).

Let us consider a road of length L. The conservation principle states that the evolution of each aggregated conserved quantity in some domain $[0, L]$ depends only on the flows at its boundaries and exogenous flows. Thus, for a complete model describing traffic evolution along some road, we need to specify boundary conditions ρ_{in} and ρ_{out} that are all assumed to be functions of bounded variation (as well as the initial condition ρ_0). Then, the initial-boundary value problem (IBVP) reads $\forall (x,t) \in [0,L] \times \mathbb{R}^+$

$$\begin{cases} \dfrac{\partial \rho(x,t)}{\partial t} + \dfrac{\partial \Phi(\rho(x,t))}{\partial x} = 0, \\ \rho(x,0) = \rho_0(x), \\ \rho(0,t) = \rho_{in}(t), \quad \rho(L,t) = \rho_{out}(t). \end{cases} \tag{2.10}$$

The main feature of the boundary conditions in conservation laws is that they can not be applied strongly for all time, see [13]. Thus, the boundary conditions should be viewed only as proposed signals.

In general, boundary conditions may only be prescribed for the boundary where the characteristics are incoming. Hence, if traffic is in the free-flow regime at road's entry for some t, then the kinematic wave propagates forward and we can write $\rho(0,t) = \rho_{in}(t)$, or if traffic is congested at the road exit, then $\rho(L,t) = \rho_{out}(t)$. However, this behaviour is not guaranteed

for general nonlinear conservation law systems such as (2.10). In order to guarantee that the weak solution $\rho(x,t)$ is the entropy one $\forall (x,t) \in [0,L] \times \mathbb{R}^+$, one needs to consider *weak boundary conditions*. See Section 2.1.3 for the physical sense of entropy solution.

In [129] the weak boundary conditions were considered for the case of concave flux function. Thus, for a weak formulation of the boundary conditions of system (2.10), one of the following conditions must hold for the upstream boundary:

$$\begin{aligned} &\rho(0,t) = \rho_{in}(t), \quad \text{or} \\ &\Phi'(\rho(0,t)) \leq 0 \ \text{ and } \ \Phi'(\rho_{in}(t)) \leq 0, \quad \text{or} \\ &\Phi'(\rho(0,t)) \leq 0 \ \text{ and } \ \Phi'(\rho_{in}(t)) \geq 0 \ \text{ and } \ \Phi(\rho(0,t)) \leq \Phi(\rho_{in}(t)), \end{aligned} \tag{2.11}$$

and similarly for the downstream boundary:

$$\begin{aligned} &\rho(L,t) = \rho_{out}(t), \quad \text{or} \\ &\Phi'(\rho(L,t)) \geq 0 \ \text{ and } \ \Phi'(\rho_{out}(t)) \geq 0, \quad \text{or} \\ &\Phi'(\rho(L,t)) \geq 0 \ \text{ and } \ \Phi'(\rho_{out}(t)) \leq 0 \ \text{ and } \ \Phi(\rho(L,t)) \geq \Phi(\rho_{out}(t)). \end{aligned} \tag{2.12}$$

2.1.5 The demand-supply concept

In some works [86, 85], the weak boundary conditions are modeled using the *demand-supply concept*. According to this concept, in case of concave flow-density function $\Phi(\rho)$ (e.g., triangular or Greenshields FD), the proposed traffic flow at the upstream boundary is given by the *demand function*

$$D(\rho_{in}) = \begin{cases} \Phi(\rho_{in}), & \text{if} \quad 0 \leq \rho_{in} \leq \rho_c, \\ \phi_{max}, & \text{if} \quad \rho_c < \rho_{in} \leq \rho_{max}, \end{cases} \tag{2.13}$$

and the proposed flow at the downstream boundary is given by the *supply function*

$$S(\rho_{out}) = \begin{cases} \phi_{max}, & \text{if} \quad 0 \leq \rho_{out} \leq \rho_c, \\ \Phi(\rho_{out}), & \text{if} \quad \rho_c < \rho_{out} \leq \rho_{max}. \end{cases} \tag{2.14}$$

The boundary Riemann problem for the upstream boundary flow is then given $\forall t \in \mathbb{R}^+$ by

$$\phi_{in}(t) = \min\left\{D(\rho_{in}(t)), S(\rho(0,t))\right\}, \tag{2.15}$$

whereas the downstream boundary flow is defined as

$$\phi_{out}(t) = \min\left\{D(\rho(L,t)), S(\rho_{out}(t))\right\}. \tag{2.16}$$

Notice that (2.15) and (2.16) are consistent with (2.11) and (2.12), i.e., these are weak boundary conditions in terms of flows. Thus, the amount of flow that can enter the domain ϕ_{in} is constrained by the supply at road's entry, while the traffic flow leaving the domain ϕ_{out} is constrained by the demand at road's exit. This means that incoming cars can be blocked by congested traffic at the entry of the road, as well as the outflow control may not be imposed if there are only a few cars at the exit.

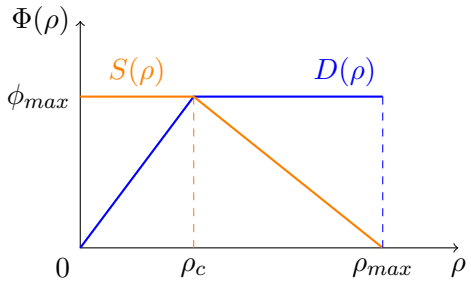

Figure 2.3: Demand $D(\rho)$ (in blue) and supply $S(\rho)$ functions (in orange) for triangular FD.

In case of triangular fundamental diagram, the demand an supply functions are given by

$$\begin{aligned} D(\rho(t)) &= \min\{v\rho(t), \phi_{max}\}, \\ S(\rho(t)) &= \min\{\omega(\rho_{max} - \rho(t)), \phi_{max}\}. \end{aligned} \tag{2.17}$$

Figure 2.3 illustrates the demand and the supply functions for the case of triangular FD.

The demand-supply concept is equivalent to the weak boundary conditions formulation introduced above in terms of densities (2.11)-(2.12), though being much simpler. This concept has important practical implications when dealing with numerical schemes to simulate the LWR model, as we are going to show later in this thesis.

2.1.6 The Godunov scheme

Now let us describe the most basic numerical method for approximating conservation laws such as the LWR model. The **Godunov scheme** proposed in [56] is a first-order numerical method based on solutions to Riemann problems. The global idea of the Godunov scheme is to approximate the initial datum by a piecewise linear function, then to compute solutions to Riemann problems and then to piece these solutions together.

We start by defining a numerical grid in $[0, L] \times \mathbb{R}^+$ by setting

- n to be number of cells,
- $\Delta x = L/n$ to be the space cell size,
- Δt to be the time cell size,
- $(i\Delta x, k\Delta t)$ for $i \in \{1, \ldots, n\}$ and $k \in \mathbb{Z}^+$ to be the grid points.

The mesh sizes Δx and Δt are chosen such that they satisfy the Courant-Friedrichs-Lewy (CFL) condition [33]:

$$\Delta t \max_{\rho} |\Phi'(\rho)| \leq \frac{\Delta x}{2},$$

where $\max_\rho |\Phi'(\rho)|$ corresponds to the maximal kinematic wave speed in the free-flow regime, e.g., v (v_{max}) in case of triangular (Greenshields) FD. This condition needs to be satisfied, since it provides the non-interaction of waves generated by different Riemann problems.

The discrete density is then $\rho_i(k)$, and according to the Godunov scheme, we update it as follows $\forall (i,k) \in \{1,\dots,n\} \times \mathbb{Z}^+$:

$$\begin{cases} \rho_1(k+1) = \rho_1(k) + \dfrac{\Delta t}{\Delta x}\left(\varphi_{in}(k) - \varphi_2(k)\right), \\ \rho_i(k+1) = \rho_i(k) + \dfrac{\Delta t}{\Delta x}\left(\varphi_i(k) - \varphi_{i+1}(k)\right), \\ \rho_n(k+1) = \rho_n(k) + \dfrac{\Delta t}{\Delta x}\left(\varphi_n(k) - \varphi_{out}(k)\right), \end{cases} \tag{2.18}$$

where $\varphi_i(k)$ is the Godunov numerical flux between cells defined as

$$\varphi_i(k) = \min\left\{D(\rho_{i-1}(k)), S(\rho_i(k))\right\}, \tag{2.19}$$

with $D(\rho_{i-1}(k))$ and $S(\rho_i(k))$ being the discretized demand and supply functions that can be taken as in (2.17). Thus, the amount of flow transmitted from the left cell $i-1$ to the right cell i corresponds to the minimum between the demand of $i-1$ and supply of i, see Figure 2.4 for the illustration of the concept.

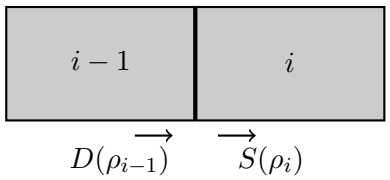

Figure 2.4: Schematic illustration of the demand-supply concept.

Notice that the discrete version of LWR model given by (2.18) together with demand and supply functions corresponding to triangular FD (2.17) is known as the cell transmission model (CTM). The CTM is by far the most widely used traffic model due to its simplicity and straightforward extension to networks.

The boundary flows $\varphi_{in}(k)$ and $\varphi_{out}(k)$ from (2.18) are respectively set by specifying the density at cells with indices $i = 0$ and $i = n+1$. These are called *ghost cells*, since they do not belong to the domain but are used to denote state at the boundaries:

$$\begin{aligned} \varphi_{in}(k) &= \min\left\{D(\rho_0(k)), S(\rho_1(k))\right\}, \\ \varphi_{out}(k) &= \min\left\{D(\rho_n(k)), S(\rho_{n+1}(k))\right\}. \end{aligned} \tag{2.20}$$

In the uncontrolled case, we set $\rho_0(k) = \rho_1(k)$ and $\rho_{n+1}(k) = \rho_n(k)$, which gives $\varphi_{in}(k) = \varphi_1(k)$ and $\varphi_{out}(k) = \varphi_n(k)$, thus the system evolves freely. In the controlled case, we set $\rho_0(k) = u_{in}(k)$ for the free-flow regime and $\rho_{n+1}(k) = u_{out}(k)$ for the congested regime, where u_{in} and u_{out} represent boundary control laws.

2.1.7 Hamilton-Jacobi formulation

As we have seen previously in Section 2.1.3, the kinematic wave theory for traffic incorporated by the LWR model can have complications that arise when characteristic lines with different ρ intersect at some (x,t). This led to the necessity to introduce shocks in order to guarantee the conservation of the number of vehicles across the pass, and handling shocks can sometimes become a tedious task. To simplify the issue of handling nonlinearities within the LWR formulation, an alternative formulation of highway traffic flow on a macroscopic level was proposed by Newell [106, 107, 108]. He proposed to describe the traffic state in terms of **Moskowitz function** $M(x,t)$ (or shortly, MF). The name of this function comes after Karl Moskowitz, an engineer who first used it to investigate traffic in [104], although it was first mentioned only some decades later in [106].

Physically, MF corresponds to the *cumulative number of vehicles*. Its value is obtained by numbering vehicles at highway's entry and following the isolines of the functions representing vehicle numbers at all times and locations. It is assumed that vehicles can not pass each other, thus the ordering of the vehicles is preserved everywhere. Recall that traffic flow $\phi(x,t)$ is the rate at which vehicles pass some point $x \in \mathbb{R}^+$, and the traffic density $\rho(x,t)$ is defined as the number of vehicles per unit length of road. Then, the cumulative number of vehicles can be easily obtained by integrating flow in space or by integrating density in time. This relation is formalized as follows:

$$\rho(x,t) = -\frac{\partial M(x,t)}{\partial x}, \quad \phi(x,t) = \frac{\partial M(x,t)}{\partial t}. \tag{2.21}$$

Recall that the key assumption of the kinematic wave theory for traffic is the existence of a concave relation between flow and density. Let us now rewrite this fundamental law $\Phi\left(\rho(x,t)\right) = \phi(x,t)$ using (2.21) as

$$\frac{\partial M(x,t)}{\partial t} - \Phi\left(-\frac{\partial M(x,t)}{\partial x}\right) = 0, \tag{2.22}$$

which is a **Hamilton-Jacobi PDE** with a Lipschitz continuous function $M(x,t) : [0,L] \times \mathbb{R}^+ \to \mathbb{R}$ being its state. The corresponding boundary conditions for (2.22) will be added in Section 2.1.8, where we will again consider traffic evolution along a road of length L. In terms of viability theory, $M(x,t)$ can also be called the *congestion function* (see [11]), since (2.22) can be considered as an optimal control problem minimizing a congestion functional $M(x,t)$. In particular, vehicles tend to minimize the traffic congestion by adapting their individual (microscopic) velocities to the kinematic wave velocity (a macroscopic quantity). Thus, function Φ plays the role of a Hamiltonian that governs the congestion function through the H-J PDE (2.22). More details on how to treat the H-J PDE as an optimal control problem are given in Section 2.1.8.

Note that the LWR PDE can be obtained if (2.22) is differentiated w.r.t. space and expressed in terms of density. Intuitively, one can see a relation between H-J and LWR by performing a formal computation, that is by taking the derivative of density w.r.t. time and

the derivative of flow w.r.t. space (assuming both of them being continuous) and by using (2.21), and thus obtaining the LWR PDE:

$$\frac{\partial \rho(x,t)}{\partial t} + \frac{\partial \Phi\left(\rho(x,t)\right)}{\partial x} = 0 \;\Leftrightarrow\; \frac{\partial^2 M(x,t)}{\partial x \partial t} - \frac{\partial^2 M(x,t)}{\partial t \partial x} = 0.$$

The rigorous relation was shown in [76].

Note that (2.22) depends only on the derivatives of $M(x,t)$. Therefore, for any solution $M(x,t)$ adding any constant M_0 gives also a solution $M(x,t) + M_0$. This is obvious, since we can start numeration of cars from any particular number. The existence of $M(x,t)$ itself guarantees the conservation of number of vehicles. Being an integral form of the LWR PDE, the solution of Hamilton–Jacobi PDE is a continuous function that has no shocks. A shock in the vehicle density function corresponds to a discontinuity in the first derivative of $M(x,t)$. Then, the conservation equations are still valid if $M(x,t)$ is continuous across the shock path, which also must be "stable". This requirement corresponds to the entropy condition in the LWR framework, where the characteristics must run into the shock (Lax admissibility condition). Thus, if a kinematic wave problem such as (2.10) is a well-posed problem, then it has a unique solution with stable shocks.

Let us now express the Moskowitz function $M(x,t)$ through inflows $\phi_{in}(t)$ and outflows $\phi_{out}(t)$ of the system. This can be simply done by using the definitions from (2.21). Namely, we can define a conservative field $(-\rho(x,t),\, \phi(x,t))$, which is a gradient of $M(x,t)$ $\forall (x,t) \in [0,L] \times \mathbb{R}^+$ (consider again a road of length L). By the gradient theorem, it follows that the value of the line integral of this field does not depend on a particular chosen path, and equals to only the difference between the values of the Moskowitz function between ending and starting points of the path in space-time. Since $M(x,t)$ is an integral function that is defined up to a constant, we are free to assign a reference value to this function at some particular point in space-time. Let us choose a starting point $(L,0)$ corresponding to the end of the road at inital time. Then, we also set $M(L,0) = 0$, since congestion functions are decreasing functions of position and increasing functions of time, see Chapter 14 of [11]. Thus, taking the ending point of the path as (x,t), one possible integration path is:

$$M(x,t) = \int_0^t \phi_{out}(\tau)\, d\tau + \int_x^L \rho(s,t)\, ds, \tag{2.23}$$

or if the starting point is $(0,0)$, then the integration path is

$$M(x,t) = \int_0^L \rho_0(s)\, ds + \int_0^t \phi_{in}(\tau) d\tau - \int_0^x \rho(s,t)\, ds. \tag{2.24}$$

2.1.8 Variational theory

Equation (2.22) is a scalar Hamilton-Jacobi PDE that can be solved semi-analytically using initial condition function $M_{\mathrm{Ini}}(x)$, upstream $M_{\mathrm{Up}}(t)$ and downstream $M_{\mathrm{Down}}(t)$ boundary

condition functions. Note that the boundary conditions should be consistent with the weak boundary conditions formulation (2.15)-(2.16). Thus, let us define the following IBVP for the H-J PDE with weak boundary conditions $\forall (x,t) \in [0,L] \times \mathbb{R}^+$:

$$\begin{cases} \dfrac{\partial M(x,t)}{\partial t} - \Phi\left(-\dfrac{\partial M(x,t)}{\partial x}\right) = 0, \\ M(x,0) = M_{\text{Ini}}(x), \\ M(0,t) = M_{\text{Up}}(t), \\ M(L,t) = M_{\text{Down}}(t). \end{cases} \tag{2.25}$$

For convenience, let us introduce the value condition function $c(x,t) : \text{Dom}(c) \to \mathbb{R}^+$, where $\text{Dom}(c) = (\{0,L\} \times \mathbb{R}^+) \cup ((0,L) \times \{0\})$. It aggregates the initial and boundary conditions of (2.25) (as in [28]):

$$c(x,t) = \begin{cases} M_{\text{Ini}}(x), & t = 0, \\ M_{\text{Up}}(t), & x = 0, \\ M_{\text{Down}}(t), & x = L. \end{cases} \tag{2.26}$$

Let us determine this value condition function (2.26), which implies the calculation of $M_{\text{Up}}(t)$, $M_{\text{Down}}(t)$ and $M_{\text{Ini}}(x)$. The upstream boundary condition should be expressed through inflow ϕ_{in}. Thus, we obtain $M_{\text{Up}}(t)$ by considering (2.24) for $x = 0$, which results into

$$M_{\text{Up}}(t) = c(0,t) = \int_0^t \phi_{in}(\tau)\, d\tau + \int_0^L \rho_0(s)\, ds, \qquad \forall t \in \mathbb{R}^+. \tag{2.27}$$

Then, the downstream boundary condition $M_{\text{Down}}(t)$ can be expressed by considering (2.23) for $x = L$:

$$M_{\text{Down}}(t) = c(L,t) = \int_0^t \phi_{out}(\tau)\, d\tau, \qquad \forall t \in \mathbb{R}^+. \tag{2.28}$$

Finally, we can obtain the initial condition by considering either (2.24) or (2.23) for $t = 0$, which gives us

$$M_{\text{Ini}}(x) = c(x,0) = \int_x^L \rho_0(s)\, ds, \qquad \forall x \in [0,L]. \tag{2.29}$$

The solution of a well-posed IBVP (2.25) is a set of least-cost paths in space-time, as it was shown in [36]. In order to obtain its analytical solution, one should treat (2.25) as a capacity-constrained optimization problem, which should be interpreted as follows. Traffic flow at any point is upper bounded by the road capacity ϕ_{max} at this point, which, in general, depends on the number of lanes and speed limits. A similar capacity constraint holds, if the road is viewed from a rigid reference frame (observer) moving along this road at a speed $v' \in [-\omega, v]$ next to a traffic stream that is characterized by density ρ and flow ϕ. Then, the maximum

rate at which the observer attached to the frame can be passed by the traffic stream is $\phi - \rho v'$ (the "relative capacity").

The fundamental diagram from the observer's viewpoint becomes $\Phi(\rho(x,t)) - \rho v'$, and its relative capacity is

$$\forall v' \in [-\omega, v], \qquad L(v') = \sup_{\rho \in [0, \rho_{max}]} \left(\Phi(\rho) - \rho v' \right), \tag{2.30}$$

where v and $-\omega$ are related to kinematic wave speeds for zero density and for the traffic jam density, respectively, i.e.,

$$v = \Phi'(0), \qquad -\omega = \Phi'(\rho_{max}).$$

Note that $L(v')$ corresponds to the *Legendre-Fenchel transform* of the flux function $\Phi(\rho)$. Thus, $L(v') \geq 0$ is a convex and strictly decreasing function $\forall v' \in [-\omega, v]$, see Figure 2.5. It achieves minimum if the observer tends to adapt his/her velocity to the maximal kinematic wave speed v, whereas its maximal value is achieved for $v' = -\omega$. Thus, $L(v')$ corresponds to the "cost" per unit time [37], and the observer moves such that this cost is minimized.

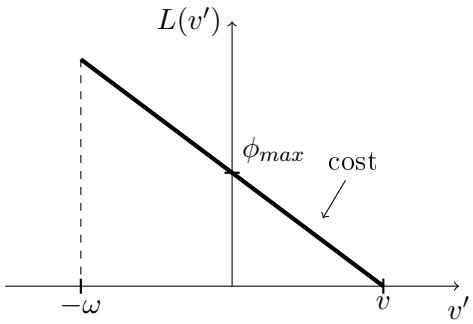

Figure 2.5: Legendre-Fenchel transform of triangular FD.

The observer traveling at time t along a valid space-time path with starting time $t_s \in \mathbb{R}^+$ can not perceive a change in its associated cumulative vehicle number greater than

$$\Delta M(x,t) = \int_{t_s}^{t} L(v')dt = (t - t_s)\, L(v').$$

In general, its associated cumulative vehicle number $M(x,t)$ can not be larger than the value at its origin boundary $c(x-(t-t_s)v', t_s)$ ("starting cost") plus the maximal possible change in its vehicle number $\Delta M = (t - t_s)\, L(v')$ caused by other vehicles that have passed the observer:

$$\begin{aligned} M(x,t) \leq \inf & \left(c(x - (t-t_s)v', t_s) + (t-t_s)L(v') \right) \\ & \text{s.t.} \quad (v', t - t_s) \in [-\omega, v] \times \mathbb{R}^+ \\ & \text{and} \quad (x - (t-t_s)v', t_s) \in \mathrm{Dom}(c). \end{aligned} \tag{2.31}$$

According to the variational theory presented in [17], this capacity constraint (2.31) is binding, i.e., the actual value of $M(x,t)$ is the largest possible allowed by this constraint. We introduce a time interval $T = t - t_s$ to make the notations shorter. Thus, the unique solution to (2.25) is found as

$$\begin{aligned} M(x,t) = &\inf \left(c(x - Tv', t - T) + TL(v') \right) \\ &\text{s.t.} \quad (v', T) \in [-\omega, v] \times \mathbb{R}^+ \\ &\text{and} \quad (x - Tv', t_s) \in \mathrm{Dom}(c). \end{aligned} \tag{2.32}$$

This expression is known as the *Lax-Hopf formula*, which provides a semi-analytical unique solution to the Hamilton-Jacobi system (2.25). Thus, the unique solution $M(x,t)$ is the infimum of the infinite number of functions of the value condition (see also [10]).

With a slight abuse of notation, we introduce two-argument functions $M_{\mathrm{Up}}(x,t)$, $M_{\mathrm{Down}}(x,t)$ and $M_{\mathrm{Ini}}(x,t)$ as solutions to the Lax-Hopf formula (2.32) for corresponding domains of the value condition function c, which are $M_{\mathrm{Up}}(t)$ (2.27), $M_{\mathrm{Down}}(t)$ (2.28) and $M_{\mathrm{Ini}}(x)$ (2.29). Thus, $M_{\mathrm{Up}}(x,t)$ comes from the upstream boundary with a given "initial cost" $M_{\mathrm{Up}}(t)$, then $M_{\mathrm{Down}}(x,t)$ comes from the downstream boundary with a known $M_{\mathrm{Down}}(t)$, and $M_{\mathrm{Ini}}(x,t)$ comes from the initial condition $M_{\mathrm{Ini}}(x)$. For example, $M_{\mathrm{Up}}(x,t)$ is obtained by

$$\begin{aligned} M_{\mathrm{Up}}(x,t) = &\inf \left(c(x - Tv', t - T) + TL(v') \right) \\ &\text{s.t.} \quad (v', T) \in [-\omega, v] \times \mathbb{R}^+ \\ &\text{and} \quad (x - Tv', t - T) \in \{0\} \times \mathbb{R}^+, \end{aligned} \tag{2.33}$$

and the same formula yields $M_{\mathrm{Down}}(x,t)$ for $(x - Tv', t - T) \in \{L\} \times \mathbb{R}^+$ and $M_{\mathrm{Ini}}(x,t)$ for $(x - Tv', t - T) \in [0, L] \times \{0\}$.

This enables us to restate the solution to the Hamilton-Jacobi problem (2.25) as a minimum of three possible "solution candidates" $M_{\mathrm{Up}}(x,t)$, $M_{\mathrm{Down}}(x,t)$ and $M_{\mathrm{Ini}}(x,t)$ $\forall (x,t) \in [0, L] \times \mathbb{R}^+$. By properties of infimum, the original Lax-Hopf formula (2.32) can be rewritten as

$$M(x,t) = \min \left\{ M_{\mathrm{Ini}}(x,t), M_{\mathrm{Up}}(x,t), M_{\mathrm{Down}}(x,t) \right\}. \tag{2.34}$$

In some special cases, e.g., for a triangular FD defined in (2.2), we can calculate the solution to the H-J PDE in explicit form as it is shown in Appendix B.2.

2.2 Robust tracking boundary control design

In this section, we address two seldom studied issues: tracking time- and space-varying desired profiles (rather than stabilizing to an equilibrium), and dealing with uncertainties due to a possible model mismatch. In particular, we consider an optimal boundary control problem to track a desired vehicle density on a single road with a state being subject to unknown space-dependent disturbances. For instance, imagine traffic evolving along a road, for which we want to achieve some desired density profile by controlling the vehicle flow at the boundary of this road. However, even if we know the flow-density relation for this road, the tracking control problem might be challenging due to unknown number of vehicles originating from minor roads. Thus, we solve the problem of controlling the vehicle density whose value we can not predict exactly. For this, we include the disturbance term to model the unknown change in the number of vehicles coming from minor roads.

2.2.1 Introductions

Most works devoted to traffic control have addressed the homogeneous (ideal) case, where the discrepancies between model and system are ignored (like in classical LWR). Some of the studies related to the disturbance rejection problem were devoted to disturbance attenuation on a boundary by action from another boundary [1, 130, 6]. For example, in [130] the sliding mode control is used to stabilize a hyperbolic system with boundary input disturbance. [1] proposed a controller able to reject disturbance at the boundary where this disturbance acts. Later on, [6] proposed a controller for disturbance rejection at an arbitrary point within the domain. A model reference adaptive control problem has been solved for hyperbolic PDEs in [7]. Therein, the authors considered harmonic disturbances with known frequencies and designed a filter-based control law. In a related work on robust control design for systems of conservation laws [117], the problem of stabilization to a steady-state profile was considered. Boundary control design was addressed previously in [20] for the problem of stabilizing the vehicle density to a constant equilibrium.

The main contribution of this section is the *optimal* boundary controller, which leads to attenuation of a *general in-domain* space-dependent disturbance. This is the first result devoted to a robust controller tracking a *space- and time-dependent* desired traffic density. Space- and time-dependency of traffic density is an important aspect to handle, since in realistic traffic situations it is more likely to obtain non-stationary profiles due to rapidly changing traffic conditions.

The control design is based on two components. These are the feedforward control component used to track the trajectory, whereas the feedback control component is used to minimize spatial L_2 and L_∞ error norms for asymptotic time. We show that the optimal feedback term takes different forms according to the norm to be minimized. The feedback law is given in its implicit but computationally feasible form, thus we can apply it without any explicit knowledge about the disturbance. In addition, we also compute the L_2 and L_∞ gains resulting from the application of the respective control laws. The special thing about these gains is that they

depend only on system physical parameters such as length of the road stretch and parameters of the fundamental diagram.

2.2.2 Preliminaries

The goal of this section is to design a *robust* boundary control law for a vehicle density governed by equation (2.1) with disturbance such that the state tracks a desired time- and space-dependent profile. Let us now describe the problem in more concrete terms by performing the following steps: present the state equation with disturbance, perform motion planning, analyze error dynamics and solve it explicitly by using the method of characteristics. We will also present the general structure of the boundary controller to be designed.

2.2.2.1 System with disturbance

We assume that the vehicle density is quite high, i.e., we consider a road being in the *congested traffic regime*, which is a common problem arising during rush hours. Here we consider traffic on a bounded domain (road of length L), which implies that boundary conditions must also be included as in IBVP (2.10). In case of traffic that is restricted to the congested regime, the system (2.10) becomes linear (like a transport equation), since it is considered only for $\rho(x,t) \in (\rho_c, \rho_{max}]\ \forall (x,t) \in [0,L] \times \mathbb{R}^+$ that lets us write $\partial_x \Phi(\rho(x,t)) = -\omega \partial_x \rho(x,t)$ (we assume a triangular FD). For this case, let us also introduce an *unknown* disturbance term $\delta(x) : [0,L] \to \mathbb{R}$ that is assumed to be *bounded*. Then, the inhomogeneous initial-boundary value problem reads:

$$\Sigma = \begin{cases} \dfrac{\partial \rho(x,t)}{\partial t} - \omega \dfrac{\partial \rho(x,t)}{\partial x} = \delta(x), \\ \rho(x,0) = \rho_0(x), \\ \rho(L,t) = u(t), \end{cases} \tag{2.35}$$

where $u(t)$ is a controller to be designed. The control action is applied at the downstream boundary, since in the congested regime the kinematic wave is moving backwards. In the free-flow regime the kinematic wave propagates forwards, and then we would control the state by actuating the upstream boundary $x = 0$. Note that the linear system Σ given by (2.35) allows us to use the fact that characteristics always propagate only in one direction. Thus, the downstream boundary conditions can always be enforced, which enables us to consider them in a strong sense.

Physically, the disturbance term $\delta(x)$ in (2.35) corresponds to the additional unknown vehicle density per time unit, an example is illustrated in Figure 2.6. Also notice that the actual control of traffic at road boundaries can be done only in terms of vehicle flow, which can be changed by, e.g., appropriately timing the traffic light signals. However, in this section, the boundary conditions are prescribed in terms vehicle density, which is the state of system Σ, since it makes the analysis of the effect of boundary values on the system solution pretty straightforward. Then, if we want to transfer the control result that is going to be designed

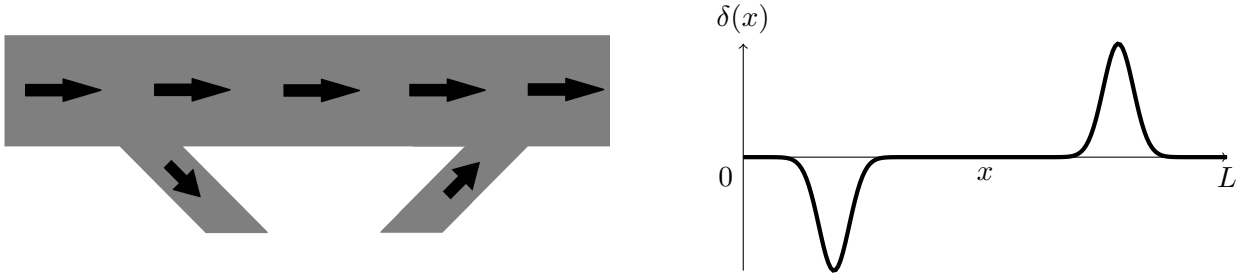

Figure 2.6: Example of a highway road with exit/entry minor roads (left) and the corresponding disturbance function (right).

for system Σ into real life, we should use the flow-density function that allows us to obtain the corresponding flow value to be achieved at the boundary, which is then translated into, e.g., time intervals during which the traffic lights are green/red.

2.2.2.2 Motion planning

Let us now define the desired trajectory for the vehicle density $\rho_d(x,t)$ that we want to achieve via the boundary control. An admissible desired trajectory $\rho_d(x,t)$ must be a solution of the following system Σ_d:

$$\Sigma_d = \begin{cases} \dfrac{\partial \rho_d(x,t)}{\partial t} - \omega \dfrac{\partial \rho_d(x,t)}{\partial x} = 0, \\ \rho_d(x,0) = \rho_{d_0}(x), \\ \rho_d(L,t) = \rho_{d_{out}}(t), \end{cases} \tag{2.36}$$

where $\rho_{d_{out}}$ is the desired state at the downstream boundary and $\rho_{d_0}(x)$ is the initial state in the desired system. Notice that system Σ_d is an IBVP that looks exactly like (2.35) but with $\delta(x) = 0$, i.e., Σ_d is a homogeneous system.

To guarantee that the system Σ_d is well-posed, its state $\rho_d(x,t)$ must always remain in the congested traffic regime along the road, i.e., $\rho_d(x,t) : [0,L] \times \mathbb{R}^+ \to (\rho_c, \rho_{max}]$.

2.2.2.3 Error dynamics

Let us now determine the dynamic system for the error density $\tilde{\rho}(x,t)$ defined as in (1.4). Systems Σ and Σ_d given by (2.35) and (2.36) are linear. Thus, we can simply subtract Σ_d from Σ and obtain the following IBVP for the error $\tilde{\rho}(x,t)$:

$$\Sigma_{err} = \begin{cases} \dfrac{\partial \tilde{\rho}(x,t)}{\partial t} - \omega \dfrac{\partial \tilde{\rho}(x,t)}{\partial x} = \delta(x), \\ \tilde{\rho}(x,0) = \tilde{\rho}_0(x), \\ \tilde{\rho}(L,t) = u(t) - \rho_{d_{out}}(t). \end{cases} \tag{2.37}$$

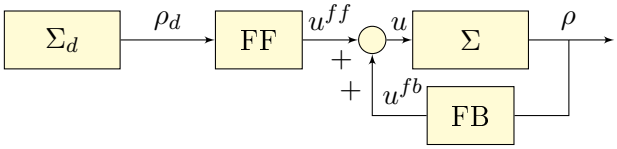

Figure 2.7: Control scheme.

2.2.2.4 Control design

We aim to design a boundary control law that can be schematically represented as in Figure 2.7. Thus, the input is a sum of feedforward $u^{ff}(t)$ and feedback $u^{fb}(\rho, t)$ terms:

$$u(\rho, t) = u^{ff}(t) + u^{fb}(\rho, t). \tag{2.38}$$

For simplicity of notations, the arguments of the controls are omitted, and in the following they will be included only if not clear from the context.

Remark 2.1
Note that the feedforward term is needed to track the desired trajectory $\rho_d(x, t)$, while the feedback term is needed for disturbance attenuation.

2.2.2.5 Solution of Σ_{err}

Let us now consider (2.37). To analyze its solution, we apply the method of characteristics presented in [46]. The details are given in Appendix B.1, where we find that the error term $\tilde{\rho}(x, t)$ evolves along the characteristic lines as

$$\tilde{\rho}(x,t) = \begin{cases} \tilde{\rho}\left(x + \omega t, 0\right) + \Delta(x) - \Delta(x + \omega t), & \forall t \in \left[0, \dfrac{L-x}{\omega}\right), \\ \tilde{\rho}\left(L, t - \frac{L-x}{\omega}\right) + \Delta(x), & \forall t \in \left[\dfrac{L-x}{\omega}, +\infty\right), \end{cases} \tag{2.39}$$

where $\Delta(x)$ is the integral of the disturbance (disturbance accumulated along the road stretch) defined as

$$\Delta(x) = \frac{1}{\omega} \int_x^L \delta(s)\, ds. \tag{2.40}$$

Remark 2.2
Note that $t_{ctr} = \frac{L}{\omega}$ is the minimum time for control action to propagate to the end of the road from $x = L$ to $x = 0$, that is why in the following we consider solutions only for $t \geq \frac{L}{\omega}$, i.e., the second expression in (2.39).

Let us rewrite (2.39) using the expression for the downstream boundary in the error system (2.37), which reads $\tilde{\rho}\left(L, t - \frac{L-x}{\omega}\right) = u\left(t - \frac{L-x}{\omega}\right) - \rho_{d_{out}}\left(t - \frac{L-x}{\omega}\right)$. Thus, we get the following

solution for the error system:

$$\tilde{\rho}(x,t) = u\left(t - \frac{L-x}{\omega}\right) - \rho_{d_{out}}\left(t - \frac{L-x}{\omega}\right) + \Delta(x). \tag{2.41}$$

Note that the time dependency in the error solution (2.41) is caused by the time dependency of the desired trajectory $\rho_{d_{out}}(t)$. If there would be no disturbance ($\Delta(x) = 0$), the desired trajectory could be achieved by using only the feedforward term. Therefore, from now on we set $u^{ff}(t) = \rho_{d_{out}}(t)$, and write the solution of (2.41) only as a function of a feedback term (since $u - u^{ff} = u^{fb}$):

$$\tilde{\rho}(x,t) = u^{fb}\left(t - \frac{L-x}{\omega}\right) + \Delta(x). \tag{2.42}$$

2.2.3 Problem statement

We also introduce notations for the density error and feedback term in asymptotic time:

$$\tilde{\rho}_\infty(x) = \lim_{t\to\infty} \tilde{\rho}(x,t), \qquad u_\infty^{fb} = \lim_{t\to\infty} \tilde{\rho}_{out}(t),$$

where the latter definition comes from comparing (2.42) with (2.39). Then, the density error solution (2.42) is given by the following relation for $t \to \infty$:

$$\tilde{\rho}_\infty(x) = u_\infty^{fb} + \Delta(x). \tag{2.43}$$

The role of u_∞^{fb} is thus to ensure that $\tilde{\rho}(x,t) \to \tilde{\rho}_\infty(x)$, and u_∞^{fb} is such that the effect of the cumulated disturbance $\Delta(x)$ is minimized in the sense of L_2-space norm (Problem 2.1) and L_∞-space norm (Problem 2.2). This is formalized as follows:

Problem 2.1
Find the optimal control law u^* composed of (2.38) such that:

(*i*) $\tilde{\rho}(x,t) \to \tilde{\rho}_\infty(x)$,

(*ii*) $u^* = \underset{u}{\operatorname{argmin}} \|\tilde{\rho}_\infty(x)\|_2^2$.

Problem 2.2
Find the optimal control law u^* composed of (2.38) such that:

(*i*) $\tilde{\rho}(x,t) \to \tilde{\rho}_\infty(x)$,

(*ii*) $u^* = \underset{u}{\operatorname{argmin}} \|\tilde{\rho}_\infty(x)\|_\infty$,

For the definition of L_2 and L_∞ norms see (1.2) and (1.3). Note that in both Problems 2.1 and 2.2, the argmin is taken over a set of all possible control functions u such that the density from (2.35) remains in the congested regime.

Note that due to the presence of in-domain disturbance $\delta(x)$, we can not drive the error $\tilde{\rho}(x,t)$ to zero as $t \to \infty$ by acting only from the boundary.

2.2.4 Convergence to an equilibrium

Let us now consider the error system Σ_{err} given by (2.37). We will first prove that a feedback controller u_∞^{fb} that is *constant* for asymptotic time acting such that the error term converges to a steady-state (as in statements (i) in Problems 2.1 and 2.2). Then, we will also derive the optimal control law u^* that satisfies statements (ii) of Problems 2.1 and 2.2.

Lemma 2.1. *Let $u(t) = u^{ff}(t) + u_\infty^{fb}$ with $u^{ff}(t) = \rho_{d_{out}}(t)$ and u_∞^{fb} being some constant. Then, the following statement holds:*

$$\lim_{t\to\infty} \|\tilde{\rho}(x,t) - \tilde{\rho}_\infty(x)\|_2 = 0.$$

Proof. Similar to [147], we define the following Lyapunov function candidate

$$V(t) = \frac{1}{2}\int_0^L e^{\omega x}\left(\tilde{\rho}(x,t) - \tilde{\rho}_\infty(x)\right)^2 dx, \tag{2.44}$$

where $e^{\omega x}$ plays the role of a weighting function. The time derivative of (2.44) is

$$\dot{V}(t) = \int_0^L e^{\omega x}\left(\tilde{\rho}(x,t) - \tilde{\rho}_\infty(x)\right)\frac{\partial\tilde{\rho}(x,t)}{\partial t}\,dx = \int_0^L e^{\omega x}\left(\tilde{\rho}(x,t) - \tilde{\rho}_\infty(x)\right)\left(\delta(x) + \omega\frac{\partial\tilde{\rho}(x,t)}{\partial x}\right)dx,$$

where the last expression comes from the error dynamics given by (2.37).

From (2.40), (2.43), and the fact that u_∞^{fb} does not depend on x, the derivative of $\tilde{\rho}_\infty(x)$ with respect to x is

$$\frac{\partial\tilde{\rho}_\infty(x)}{\partial x} = -\frac{1}{\omega}\delta(x),$$

and thus we get

$$\dot{V}(t) = \omega\int_0^L e^{\omega x}\left(\tilde{\rho}(x,t) - \tilde{\rho}_\infty(x)\right)\frac{\partial\left(\tilde{\rho}(x,t) - \tilde{\rho}_\infty(x)\right)}{\partial x}dx.$$

Integration by parts yields

$$\begin{aligned}\dot{V}(t) &= \frac{\omega}{2}e^{\omega x}\left(\tilde{\rho}(L,t) - \tilde{\rho}_\infty(L)\right)^2 - \frac{\omega}{2}\left(\tilde{\rho}(0,t) - \tilde{\rho}_\infty(0)\right)^2 - \omega^2 V(t)\\ &\leqslant \frac{\omega}{2}e^{\omega L}\left(u_\infty^{fb} - \tilde{\rho}_\infty(L)\right)^2 - \omega^2 V(t),\end{aligned} \tag{2.45}$$

where the last inequality comes from the fact that $\tilde{\rho}(L,t) = u(t) - \rho_{d_{out}} = u^{ff}(t) + u_\infty^{fb} - \rho_{d_{out}}$, and using that $u^{ff}(t) = \rho_{d_{out}}(t)$ we obtain $\tilde{\rho}(L,t) = u_\infty^{fb}$, i.e., the error at the boundary becomes constant as well. It follows then from (2.43) and (2.40) for $x = L$ that $\Delta(L) = 0$, which results for (2.45) into

$$\dot{V}(t) \leq \frac{\omega}{2}e^{\omega L}\Delta(L)^2 - \omega^2 V(t) = -\omega^2 V(t).$$

Lemma statement follows directly from $\|\tilde{\rho}(x,t) - \tilde{\rho}_\infty(x)\|_2^2 \leqslant 2V(t)\,e^{-\omega L}$, thus $V(t) \to 0$ implies $\|\tilde{\rho}(x,t) - \tilde{\rho}_\infty(x)\|_2 \to 0$. □

2.2.5 Disturbance attenuation in sense of L_2 norm

The following theorem completes the previous result and gives the optimal form of u^{fb*} that acts to minimize the L_2 norm of the error term as $t \to \infty$ as specified in Problem 2.1(*ii*). Although the feedback term depends on unmeasured disturbance, we will be still able to present it in a computationally feasible form.

Theorem 2.1
For the density error $\tilde{\rho}(x,t)$ given by IBVP (2.37), the optimal boundary controller minimizing the limit of its L_2 norm as $t \to \infty$ is given by

$$u^* = u^{ff} + u^{fb*}, \quad \textit{where} \quad u^{ff} = \rho_{d_{out}}(t) \quad \textit{and} \tag{2.46}$$

$$u^{fb*}(t) = \begin{cases} 0, & \textit{if} \quad 0 \le t < L/\omega, \\ -\frac{1}{L}\int\limits_0^L \left(\rho\left(x,t\right) - u^*\left(t - \frac{L-x}{\omega}\right)\right) dx, & \textit{if} \quad t \ge L/\omega. \end{cases}$$

Proof. First, assume that $u^{fb*}(t)$ is a constant for $t \ge L/\omega$. Thus note that minimization over $u(t) = u^{ff}(t) + u^{fb}$ in Problem 2.1(*ii*) is equivalent to the minimization over $u^{fb} = u^{fb}_\infty = \text{const}$:

$$u^{fb*} = \underset{u^{fb}}{\operatorname{argmin}} \|\tilde{\rho}_\infty(x)\|_2^2 = \underset{u^{fb}}{\operatorname{argmin}} \left\|u^{fb} + \Delta(x)\right\|_2^2 = \underset{u^{fb}}{\operatorname{argmin}} \int\limits_0^L \left(u^{fb} + \Delta(x)\right)^2 dx,$$

where we have used the relation (2.43) and the definition of L_2 norm from equation (1.2). Expanding the quadratic form in the integral, we obtain

$$\int\limits_0^L \left(u^{fb} + \Delta(x)\right)^2 dx = (u^{fb})^2 L + 2u^{fb} \int\limits_0^L \Delta(x)dx + \int\limits_0^L \Delta^2(x)dx. \tag{2.47}$$

In order to compute u^{fb*} minimizing the quadratic form (2.47), we need to take the derivative of (2.47) with respect to u^{fb} and set this expression to zero. This allows us to obtain the optimal feedback term:

$$u^{fb*} = -\frac{1}{L}\int\limits_0^L \Delta(x)dx. \tag{2.48}$$

This expression corresponds to the subtraction of the mean value of cumulative disturbance $\Delta(x)$. However, we should recall that $\Delta(x)$ is an unmeasured function. Using the solution of the error term $\tilde{\rho}(x,t)$ (2.39) obtained by the method of characteristics, we can express the integral disturbance as

$$\Delta(x) = \rho(x,t) - \rho_d(x,t) - u^*\left(t - \frac{L-x}{\omega}\right) + \rho_{d_{out}}\left(t - \frac{L-x}{\omega}\right),$$

where the last two terms come from the definition of the boundary conditions in the error system (2.37). Recall that the desired density $\rho_d(x,t)$ satisfies system Σ_d given by (2.36), which

is a homogeneous transport equation. Then, we can again apply the method of characteristics and get $\rho_d(x,t) = \rho_{d_{out}}(t - \frac{L-x}{\omega})$, which results into the following expression for the integral disturbance:

$$\Delta(x) = \rho(x,t) - u^*\left(t - \frac{L-x}{\omega}\right). \tag{2.49}$$

Thus, the disturbance term in (2.49) can be computed if we know the current density $\rho(x,t)$ and the control action on previous time steps $u^*(t - \frac{L-x}{\omega})$. Finally, note that the quantity on the left-hand side of (2.49) is constant in time provided that the right-hand side is well-defined, i.e. for all $t \geq L/\omega$, irrespectively of the control action $u^*(t)$. Thus, our initial assumption that u^{fb*} becomes constant is valid. The combination of (2.48) and (2.49) yields the final expression (2.46) stated in Theorem 2.1. □

Thus, the optimal controller given by (2.46) should be seen as a compensator for the average effect of disturbance in number of vehicles within the whole road.

Corollary 2.1. *The optimal controller (2.46) provides the following bound for the L_2 norm of the density error as $t \to \infty$:*

$$\|\tilde{\rho}_\infty(x)\|_2^2 \leq k\,\|\delta(x)\|_2^2, \qquad \textit{with}\ \ k = \frac{L^2}{2\omega^2}.$$

Proof. Let us first explicitly calculate the L_2 norm of the density error $\tilde{\rho}_\infty(x)$ for $t \to \infty$ under the optimal feedback control, for which we make use of (2.48) and get

$$\|\tilde{\rho}_\infty(x)\|_2^2 = \left\|u^{fb*} + \Delta(x)\right\|_2^2 = \int_0^L \Delta^2(x)\,dx - \frac{1}{L}\left(\int_0^L \Delta(x)\,dx\right)^2.$$

Using the definition of the integral disturbance (2.40), we obtain

$$\left\|u^{fb*} + \Delta(x)\right\|_2^2 \leq \int_0^L \Delta^2(x)\,dx = \frac{1}{\omega^2}\int_0^L \left(\int_x^L \delta(s)\,ds\right)^2 dx.$$

Using the Cauchy-Schwartz inequality we can provide an upper bound for the latter expression:

$$\left\|u^{fb*} + \Delta(x)\right\|_2^2 \leq \frac{1}{\omega^2}\int_0^L \left((L-x)\int_x^L \delta^2(s)\,ds\right) dx \leq \frac{1}{\omega^2}\,\|\delta(x)\|_2^2 \int_0^L (L-x)\,dx,$$

and finally we get

$$\left\|u^{fb*} + \Delta(x)\right\|_2^2 \leq \frac{L^2}{2\omega^2}\,\|\delta(x)\|_2^2,$$

which shows that there is an upper bound of the error norm as $t \to \infty$ and concludes the proof. □

2.2.6 Disturbance attenuation in sense of L_∞ norm

Theorem 2.2
For the density error $\tilde{\rho}(x,t)$ given by IBVP (2.37), the optimal boundary controller minimizing the limit of its L_∞ norm as $t \to \infty$ is given by

$$u^* = u^{ff} + u^{fb*}, \quad \textit{where} \quad u^{ff} = \rho_{d_{out}}(t) \quad \textit{and} \tag{2.50}$$

$$u^{fb*}(t) = \begin{cases} 0, & \textit{if} \quad 0 \le t < \dfrac{L}{\omega}, \\ -\dfrac{\sup\limits_{x\in[0,L]} \left(\rho(x,t) - u^*\left(t - \dfrac{L-x}{\omega}\right)\right) + \inf\limits_{x\in[0,L]} \left(\rho(x,t) - u^*\left(t - \dfrac{L-x}{\omega}\right)\right)}{2}, & \textit{if} \quad t \ge \dfrac{L}{\omega}. \end{cases}$$

Proof. Following the proof of Theorem 2.1, the minimization over u^* in Problem 2.2(ii) is again equivalent to the minimization over $u^{fb} = u^{fb}_\infty = \text{const}$:

$$u^{fb*} = \underset{u^{fb}}{\operatorname{argmin}} \left\|\tilde{\rho}_\infty(x)\right\|_\infty = \underset{u^{fb}}{\operatorname{argmin}} \left\|u^{fb} + \Delta(x)\right\|_\infty = \underset{u^{fb}}{\operatorname{argmin}} \sup_{x\in[0,L]} |u^{fb} + \Delta(x)|.$$

Expanding the supremum term, we get

$$\begin{aligned} \sup_{x\in[0,L]} |u^{fb} + \Delta(x)| &= \max\left\{ \sup_{x\in[0,L]} \left(u^{fb} + \Delta(x)\right), \; -\inf_{x\in[0,L]} \left(u^{fb} + \Delta(x)\right) \right\} \\ &= \max\left\{ u^{fb} + \sup_{x\in[0,L]} \Delta(x), \; -u^{fb} - \inf_{x\in[0,L]} \Delta(x) \right\}. \end{aligned} \tag{2.51}$$

The first argument in (2.51) is a monotonically increasing function with respect to u^{fb}, while the second argument is a monotonically decreasing one. Thus, the minimum can be achieved only at the intersection point of both functions, i.e.,

$$u^{fb*} = -\frac{1}{2}\left(\sup_{x\in[0,L]} \Delta(x) + \inf_{x\in[0,L]} \Delta(x) \right). \tag{2.52}$$

Substituting (2.49) in (2.52) in order to eliminate the explicit dependency on unknown disturbance, we obtain the optimal feedback term (2.50) as stated in Theorem 2.2. □

As in case of L_2 norm, let us estimate the upper bound of L_∞ norm of the error state that this controller is able to achieve as $t \to \infty$.

Corollary 2.2. *The control law given by (2.50) provides the following bound*

$$\left\|\tilde{\rho}_\infty(x)\right\|_\infty \le \mu \left\|\delta(x)\right\|_\infty, \quad \textit{with} \quad \mu = \frac{L}{\omega}.$$

Proof. In order to estimate bounds on $\|\tilde{\rho}_\infty(x)\|_\infty$, we need to find bounds on $\sup_{x\in[0,L]} \Delta(x)$ and $-\inf_{x\in[0,L]} \Delta(x)$. Let us start with the supremum:

$$\sup_{x\in[0,L]} \Delta(x) = \sup_{x\in[0,L]} \left(\frac{1}{\omega} \int_x^L \delta(s)\, ds \right) \leq \sup_{x\in[0,L]} \left(\frac{L-x}{\omega} \sup_{s\in[0,x]} \delta(s) \right) \leq$$
$$\sup_{x\in[0,L]} \left(\frac{L-x}{\omega} \sup_{s\in[0,L]} \delta(s) \right) \leq \begin{cases} 0, & \text{if } \sup_{x\in[0,L]} \delta(x) \leq 0, \\ \dfrac{L}{\omega} \sup_{x\in[0,L]} \delta(x), & \text{if } \sup_{x\in[0,L]} \delta(x) > 0. \end{cases} \tag{2.53}$$

For the infimum we proceed in the same way and obtain:

$$\inf_{x\in[0,L]} \Delta(x) = \inf_{x\in[0,L]} \left(\frac{1}{\omega} \int_x^L \delta(s)\, ds \right) \geq \inf_{x\in[0,L]} \left(\frac{L-x}{\omega} \inf_{s\in[0,x]} \delta(s) \right) \geq$$
$$\inf_{x\in[0,L]} \left(\frac{L-x}{\omega} \inf_{s\in[0,L]} \delta(s) \right) \geq \begin{cases} 0, & \text{if } \inf_{x\in[0,L]} \delta(x) \geq 0, \\ \dfrac{L}{\omega} \inf_{x\in[0,L]} \delta(x), & \text{if } \inf_{x\in[0,L]} \delta(x) < 0. \end{cases} \tag{2.54}$$

From the bounds on supremum (2.53) and infimum (2.54), we distinguish three possible cases:

1. Both $\sup_{x\in[0,L]} \delta(x)$ and $\inf_{x\in[0,L]} \delta(x)$ are positive. Then, $\|\delta(x)\|_\infty = \sup_{x\in[0,L]} \delta(x)$ and
$$\|\tilde{\rho}_\infty(x)\|_\infty = \frac{1}{2} \left(\sup_{x\in[0,L]} \Delta(x) - \inf_{x\in[0,L]} \Delta(x) \right) \leq \frac{L}{2\omega} \sup_{x\in[0,L]} \delta(x) = \frac{L}{2\omega} \|\delta(x)\|_\infty .$$

2. Both $\sup_{x\in[0,L]} \delta(x)$ and $\inf_{x\in[0,L]} \delta(x)$ are negative. Then $\|\delta(x)\|_\infty = -\inf_{x\in[0,L]} \delta(x)$ and
$$\|\tilde{\rho}_\infty(x)\|_\infty = \frac{1}{2} \left(\sup_{x\in[0,L]} \Delta(x) - \inf_{x\in[0,L]} \Delta(x) \right) \leq -\frac{L}{2\omega} \inf_{x\in[0,L]} \delta(x) = \frac{L}{2\omega} \|\delta(x)\|_\infty .$$

3. The signs of $\sup_{x\in[0,L]} \delta(x)$ and $\inf_{x\in[0,L]} \delta(x)$ are different. Then
$$\sup_{x\in[0,L]} \delta(x) - \inf_{x\in[0,L]} \delta(x) \leqslant 2 \sup_{x\in[0,L]} |\delta(x)| = 2 \|\delta(x)\|_\infty ,$$
which leads to
$$\|\tilde{\rho}_\infty(x)\|_\infty = \frac{1}{2} \left(\sup_{x\in[0,L]} \Delta(x) - \inf_{x\in[0,L]} \Delta(x) \right)$$
$$\leq \frac{L}{2\omega} \left(\sup_{x\in[0,L]} \delta(x) - \inf_{x\in[0,L]} \delta(x) \right) \leq \frac{L}{\omega} \|\delta(x)\|_\infty .$$

Thus, we can provide the following bound for the L_∞ norm as $t \to \infty$:

$$\|\tilde{\rho}_\infty(x)\|_\infty \leqslant \frac{L}{\omega} \|\delta(x)\|_\infty .$$

□

2.2.7 Numerical simulation

To verify our theoretical results, we provide a numerical example, which intends to illustrate the performance of the feedback term u^{fb*} used to minimize the L_2 and L_∞ norms of $\tilde{\rho}(x,t)$ as $t \to \infty$. For the simulation, we use the Godunov scheme (2.18) described in Section 2.1.6, and the numerical grid is divided into $n = 500$ cells.

2.2.7.1 Simulation setup

Notice that we simulate the system only in the congested regime, thus in (2.19) the minimum is always resolved to the benefit of the supply function, i.e., $\forall (i,k) \in \{1,\dots,n\} \times \mathbb{Z}^+$:

$$\varphi_i(k) = S(\rho_i(k)), \quad \varphi_{in}(k) = S(\rho_1(k)).$$

We also set $\rho_{n+1}(k) = \rho_n(k)$ if no boundary conditions are specified (freely evolving system), and $\rho_{n+1}(k) = u(k)$ in case of boundary control so that $\varphi_{out}(k) = S(u(k))$.

For the simulation we set the following parameters, which are taken from real traffic data [143]:

$$\begin{aligned} &v = 16.667\,\text{m/s},\ \omega = 7.114\,\text{m/s},\ L = 1000\,\text{m}, \\ &\rho_{max} = 0.181\,\text{veh/m},\ \rho_c = 0.0541\,\text{veh/m}. \end{aligned} \tag{2.55}$$

Notice that the free-flow speed $v = 16.667$ m/s corresponds to 60 km/h. We also fix the initial condition $\forall i \in \{1,\dots,n\}$

$$\rho_i(0) = 0.1 - 0.03\cos(\pi i \Delta x/50),$$

the desired trajectory

$$\rho_{d_i}(k) = 0.11 + 0.03\sin\left(\pi(k\Delta t - \frac{L - i\Delta x}{\omega}) * 0.01\right),$$

and the disturbance term

$$\delta_i = \begin{cases} -0.0002, & \text{if } \ i \in \{1,\dots,\frac{n}{2}\} \\ 0.0006, & \text{otherwise.} \end{cases}$$

There are three possible control strategies, which can be applied at the downstream boundary of the system:

1. No control action is performed.

2. Only feedforward control $u(k) = u^{ff}(k)$ is applied.

3. Full control $u^*(k) = u^{ff}(k) + u^{fb*}(k)$ is applied. For the computation of the integral from the feedback term in case of (2.46), we use the Riemann summation over all cells inside the domain.

2.2.7.2 Simulation results

In Figure 2.8 we illustrate the effect of the feedback term on disturbance attenuation in sense of both L_2 and L_∞ norms by acting from the downstream boundary. The desired density profile $\rho_d(x,t)$ and the freely evolving uncontrolled state $\rho(x,t)$ with disturbance are shown in Figures 2.8a) and 2.8b), respectively. The density values can be read from the colormap: the smallest values are denoted by blue color, while the most congested zones are marked in red. The disturbance term acts so that the freely evolving system becomes entirely congested in the right part of the road, as we can see from Figure 2.8b).

In Figure 2.8c) we show what happens to the state $\rho(x,t)$, when only the feedforward control is applied ($u = u^{ff}$) by setting $\rho_d(L,t)$ at the downstream boundary. This technique provides results that are already considerably better than just letting the state evolve freely. Finally, the state under the optimal control laws u^{fb*} from (2.46) and (2.50) minimizing $\|\tilde{\rho}_\infty(x)\|_2$ and $\|\tilde{\rho}_\infty(x)\|_\infty$, respectively, are shown in Figures 2.8d) and 2.8e). The feedback term started acting after the minimal controllability time $t_{ctr} = \frac{L}{\omega} \approx 140$ s, while only feedforward control was activated prior to this time threshold. In this particular case, minimization of L_2 norm has led us to better results, since the corresponding controlled state in Figure 2.8d) is less congested than in case of L_∞ minimization, as we can observe from Figure 2.8e).

Comparing Figure 2.8c) with Figures and 2.8d) and 2.8e), we see that the optimally controlled density reaches a profile that looks more similar to the desired one from 2.8a), however they are not identical (but the best that could be obtained for in-domain disturbance and boundary control). In general, it is easy to see that disturbance attenuation results into a state characterized by a much lower congestion level, which is a desirable effect when it comes to control applications.

In Figure 2.9 we can see that the optimal control law applied to minimize $\|\tilde{\rho}_\infty(x)\|_2$ in Figure 2.9a) and $\|\tilde{\rho}_\infty(x)\|_\infty$ in Figure 2.9b) performs better in both cases with respect to the case with no feedback. The feedback controller is a constant that is switched on after the minimal controllability time $t_{ctr} \approx 140$ s has passed. Then, in both cases the norms achieve their minimal values already after $2t_{ctr}$, since another time period equal to the minimal controllability time must pass for the control action to propagate to the end of the road.

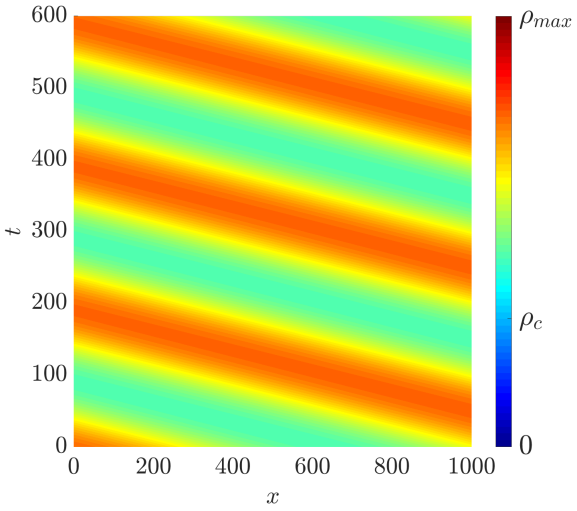

a) desired density profile

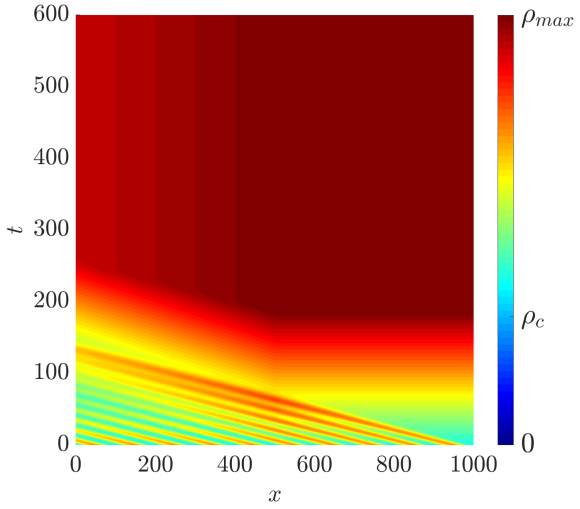

b) uncontrolled state

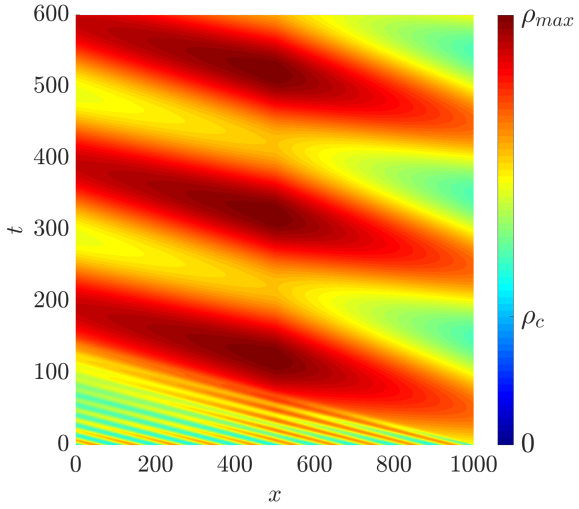

c) state obtained by applying only $u = u^{ff}$

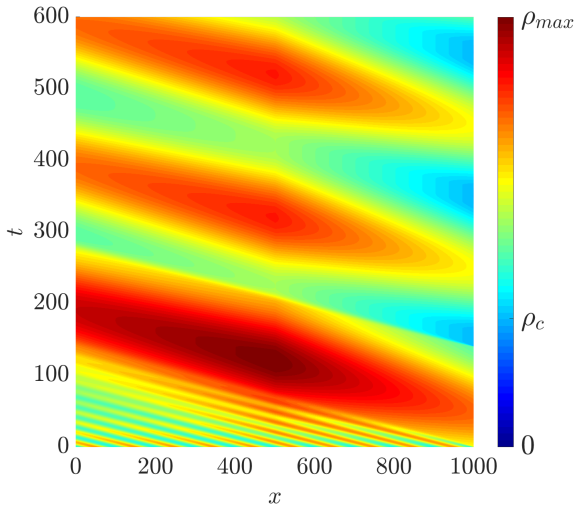

d) state under u^{fb*} minimizing L_2 norm

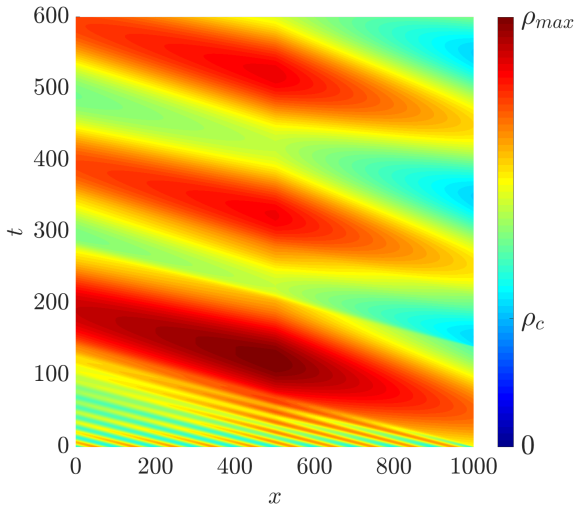

e) state under u^{fb*} minimizing L_∞ norm

Figure 2.8: a) Desired density profile, b) freely evolving state, and in c),d),e) the density evolution under the disturbance term for different control choices.

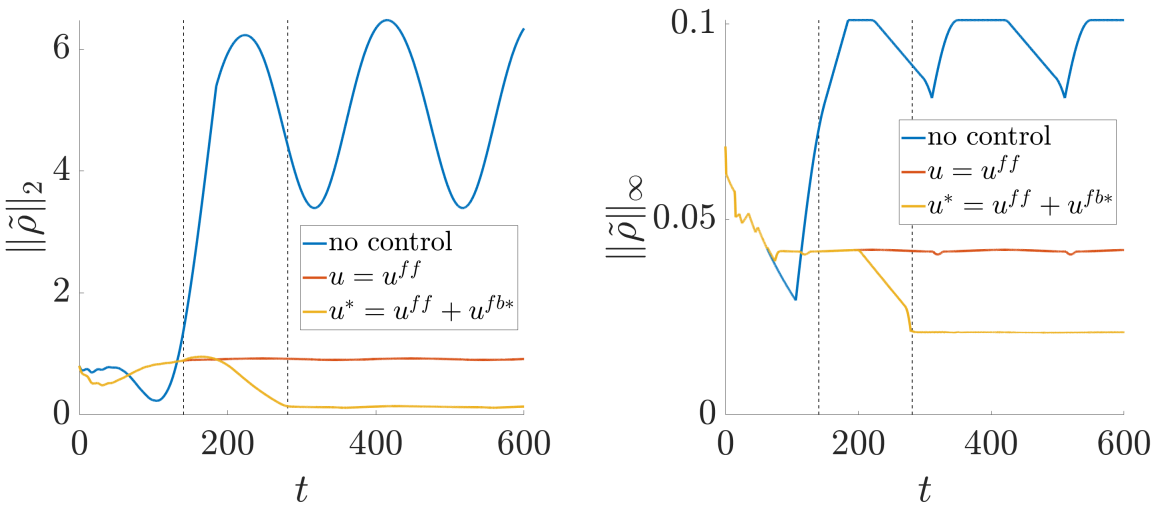

a) L_2 norm b) L_∞ norm

Figure 2.9: Temporal evolution of density error norms obtained for the uncontrolled case (blue line), with feedforward control only (red line), and then also with the feedback part u^{fb*} (yellow line) for a) L_2 norm, and b) L_∞ norm. The black dashed lines indicate t_{ctr} and $2t_{ctr}$.

2.2.8 Discussions

In this section, we have designed a feedback control law that minimizes the deviation of the state from the desired time- and space-dependent trajectory as time goes to infinity in sense of L_2 and L_∞ spatial norms. The vehicle density, for which we were designing the boundary control, is restricted to the congested traffic regime, which allowed us to deal with a linear problem. The control is actuated at road's downstream boundary, and physically it corresponds to controlling the amount of traffic flow to leave the road. The congested traffic state can become unpredictably worth (such as becoming a full traffic jam with $\rho(x,t) = \rho_{max}$ $\forall x \in [0, L]$) due to the presence of in-domain disturbance that has been included into the LWR equation. This included disturbance is used to capture the contribution of vehicles originating from minor roads having a non-zero inflow into the road to control. The desired trajectory solves an ideal (homogeneous) linear LWR in the same regime. The problem was posed and solved as the disturbance attenuation problem. The results have been verified by a numerical example, which clearly illustrates that the feedback plays an important role in the designed controller, which performs significantly better for the error norm minimization than the one including only the feedforward part.

The obtained controllers for minimization of both L_2 and L_∞ norms are optimal. The corresponding norm to be minimized should be chosen in accordance with the available knowledge about the source of disturbance. For example, the controller to minimize the L_2 norm should be chosen if the disturbance comes from a large number of minor roads, then it makes sense to minimize the mean-square deviation from the desired state. The controller for L_∞ norm minimization should be chosen, if the maximal deviation from the desired state should be

attenuated. This can be a good practical choice, if the disturbance source corresponds to vehicles coming from, e.g., another important road in case of merge intersections.

In the the following section, we extend our analysis to a more complex problem, i.e., the traffic state is not restricted to any particular regime, which yields a fully nonlinear problem with all the technical challenges related to this nonlinearity, i.e., crossing characteristics and shocks in the solution.

2.3 Boundary control design for traffic with nonlinear dynamics

In this section, we again consider a tracking problem to be solved by properly actuating road boundaries. This time, both the traffic state and the desired trajectory are vehicle densities that can take any value from its range. We consider a mixed traffic problem, e.g., traffic is in the free-flow regime at one part of the road, and congested at the other part. Hence, we are going to analyze a fully nonlinear LWR model as in (2.10). The main technical challenge thereby occurs when characteristics intersect (as in the case of kinematic waves moving with different speeds), which causes the emergence of shocks, see Section 2.1.3. In order to handle shocks, we make use of the Hamilton-Jacobi formulation, which is an integral formulation of LWR that does not contain shocks, see Section 2.1.7 for more details.

2.3.1 Introduction

There exist many works that used the structure of the Hamilton-Jacobi PDE to solve control tasks for traffic. For instance, optimal control methods for a traffic network based on viability framework are proposed in [93, 94]. The framework has also been used to develop a convex optimization approach to reduce the fuel consumption in [153]. Also [16] considered a H-J PDE with viscous term that allowed to perform a feedback linearization, which enabled tracking a desired time-dependent state on some fixed space point. One of the most recent works [141] used the analytical solution to the LWR PDE to formulate an optimization control problem for traffic on networks with variable speed limit and ramp metering control.

The main contributions of this section are the following:

- Tracking space- and time-dependent trajectory: we extend the results presented in [20, 14] and present a controller able to drive a state with shocks to any *time- and space-dependent* vehicle density that also may contain shocks. This is the first boundary controller in the traffic community able to solve such general tasks. Moreover, if we compare it to [16], our analysis is done for the original LWR system without linearization and viscosity term.
- The explicit solution of H-J PDE is used to provide conditions on when and which control can be applied: we consider a general case with weak boundary conditions, when it is not guaranteed that control can be imposed pointwise (see Section 2.1.4). To handle this limitation of control, we have formulated weak boundary conditions in terms of *control restriction functions*, and then we use them to show that even in case of "non acceptance" of boundary control laws the goal can still be achieved.

2.3.2 Preliminaries

We seek to design a feedback boundary control law that is able to track any desired space- and time-dependent vehicle density. Unlike in the previous Section 2.2 where only congested

traffic has been considered, here we deal with a full nonlinear traffic system as in (2.10). Thus, prior to stating the boundary control problem, we will first do the following: present the nonlinear state equation, perform motion planning to define admissible trajectories to track, then we also mention assumptions that need to hold in this section, and then we give an explicit Hamilton-Jacobi solution describing the temporal evolution of the traffic system.

2.3.2.1 Nonlinear traffic system

Let us formulate a nonlinear IBVP for traffic evolving along a single road with $x \in [0, L]$ as in (2.10), but for convenience we now specify the boundary values in terms of flows ϕ_{in}, ϕ_{out}. Thus, we introduce the following IBVP $\forall (x,t) \in [0,L] \times \mathbb{R}^+$:

$$\begin{cases} \partial_t \rho(x,t) + \partial_x \Phi\left(\rho(x,t)\right) = 0, \\ \Phi\left(\rho(0,t)\right) = \phi_{in}(t), \ \Phi\left(\rho(L,t)\right) = \phi_{out}(t), \\ \rho(x,0) = \rho_0(x). \end{cases} \tag{2.56}$$

Thereby, the flux function $\Phi(\rho)$ is again assumed to have a triangular shape as in (2.2) with $\rho_c = \rho_{max}/3$, and inflows $\phi_{in}(t)$ and outflows $\phi_{out}(t)$ are defined $\forall t \in \mathbb{R}^+$ as

$$\begin{cases} \phi_{in}(t) = \min\left\{u_{in}(t), S(\rho(0,t))\right\}, \\ \phi_{out}(t) = \min\left\{D(\rho(L,t)), u_{out}(t)\right\}, \end{cases} \tag{2.57}$$

where u_{in} and u_{out} denote the proposed flow values for the upstream and for the downstream boundary, correspondingly. Here, we treat u_{in} and u_{out} as control variables. By comparing (2.57) to the boundary Riemann problems for $x = 0$ and $x = L$ given by (2.15) and (2.16), we establish that $\forall t \in \mathbb{R}^+$

$$u_{in}(t) = D(\rho_{in}(t)), \quad \text{and} \quad u_{out}(t) = S(\rho_{out}(t)),$$

which means that u_{in} physically corresponds to control of the demand to enter the road, i.e, we decide how much vehicles to let enter the domain, while u_{out} should be viewed as control of the supply of the exit of the road, i.e., we decide how much vehicles to let leave the domain. Notice that both u_{in} and u_{out} can not always be applied, i.e., these boundary conditions (2.57) are equivalent to the weak boundary conditions formulation in terms of densities given in [129], see also Section 2.1.4. Thus, the problem given by (2.56) and (2.57) is well-posed.

2.3.2.2 Motion planning

Now we define a desired space- and time-varying density $\rho_d(x,t)$ $\forall (x,t) \in [0,L] \times \mathbb{R}^+$ that should be tracked with the help of boundary control. In order to be *admissible*, $\rho_d(x,t) \in \mathbb{R}^+$ must be a weak entropy solution of the following system:

$$\begin{cases} \dfrac{\partial \rho_d(x,t)}{\partial t} + \dfrac{\partial \Phi\left(\rho_d(x,t)\right)}{\partial x} = 0, \\ \Phi\left(\rho_d(0,t)\right) = \phi_{in_d}(t), \ \Phi\left(\rho_d(L,t)\right) = \phi_{out_d}(t), \\ \rho_d(x,0) = \rho_{0_d}(x), \end{cases} \tag{2.58}$$

where inflows and outflows in the desired system must also satisfy $\phi_{in_d}(t) \leq S(\rho_d(0,t))$ and $\phi_{out_d}(t) \leq D(\rho_d(L,t))$ (weak boundary conditions). Notice that unlike Σ_d given by (2.36) in Section 2.2, the system (2.58) is a nonlinear hyperbolic PDE system, in which discontinuities may evolve even for smooth initial data.

Thus, this section is devoted to finding $\forall t \in \mathbb{R}^+$ boundary control laws $u_{in}(t)$ and $u_{out}(t)$ such that the density achieves a desired trajectory $\rho_d(x,t)$ as $t \to \infty$. Thereby, they can take any values from their range, i.e., $\rho \in [0, \rho_{max}]$ and $\rho_d \in [0, \rho_{max}]$.

2.3.2.3 Assumptions

Finally, throughout this section we make the following assumptions:

Assumption 2.1
The initial conditions have left the system, thus, the solution of system (2.56) is determined by the values at the boundaries only.

Assumption 2.2
There exists $\varepsilon > 0$ such that ϕ_{in} and ϕ_{out} from system (2.56) satisfy the following inequalities in time average:

$$\int_t^{t+T} \phi_{in}(\tau)d\tau \leq T\phi_{max} - \varepsilon \quad \text{and} \quad \int_t^{t+T} \phi_{out}(\tau)d\tau \leq T\phi_{max} - \varepsilon,$$

$$\text{where} \quad t > 0 \quad \text{and} \quad T = \min\left\{\frac{L}{v}, \frac{L}{\omega}\right\}.$$

Thus, flows can not hold their maximal values during the time interval given by T.

Note that Assumption 2.2 is needed to prove the exponential convergence to a desired vehicle density profile, see details in the proof of Theorem 2.3.

Remark 2.3
Note that if Assumption 2.2 is satisfied, then Assumption 2.1 holds trivially $\forall t \in [t_{min}, +\infty)$, where t_{min} is defined as

$$t_{min} = \min\left\{\frac{L}{v}, \frac{L}{\omega}\right\}\left(1 + \left\lceil \frac{L}{\varepsilon}(\rho_{max} + \rho_c)\right\rceil\right), \tag{2.59}$$

as it is shown in Appendix B.3.

2.3.2.4 Hamilton-Jacobi system

Note that control enters the system through the minimum function (2.57), and in several situations it can not be applied pointwise. Hence, control variables should be understood only

as proposed functions. If traffic is restricted only to the congested regime, then $\phi_{out}(t) = u_{out}(t)$ is always satisfied, as it was the case for the linear system (2.35) considered in the previous section. However, to solve control problems for a traffic state in the mixed regime, we must handle (2.57), since the actual flow passing through the boundary is determined by the traffic state. For instance, if for some time t there are only a few cars at the end of the road, we would obtain from (2.57)

$$\phi_{out}(t) = D\left(\rho(L,t)\right) \quad \Rightarrow \quad u_{out}(t) \text{ is not imposed.}$$

In order to enable analytical treatment of weak boundary conditions, we use the Hamilton-Jacobi formulation, which is an integral form of the LWR PDE that was explained in Section 2.1.7. In particular, we will be able to analyze, when and for how long the proposed control values are accepted by the system. This is possible due to a cumulative description of traffic within the H-J approach, since the state corresponds to the cumulative number of vehicles also known as Moskowitz function $M(x,t)$ (MF).

Let us recall the IBVP in the H-J formulation as in (2.25), i.e., $\forall (x,t) \in [0,L] \times \mathbb{R}^+$:

$$\begin{cases} \dfrac{\partial M(x,t)}{\partial t} - \Phi\left(-\dfrac{\partial M(x,t)}{\partial x}\right) = 0, \\ M(x,0) = M_{\text{Ini}}(x), \\ M(0,t) = M_{\text{Up}}(t), \\ M(L,t) = M_{\text{Down}}(t). \end{cases}$$

As already discussed in Section 2.1.8, the solution of this system can be obtained explicitly using the Lax-Hopf formula (2.32) for the case of a triangular FD (2.2), which is also the case here. The derivation of the solution is presented in Appendix B.2. Here we consider the solution of the system for large enough time, which equivalently means that the effect of initial conditions should have left the system (Assumption 2.1):

$$\begin{aligned} &\forall (x,t) \in [0,L] \times [t_{min}, +\infty) : \\ &M(x,t) = \min\left\{ \int_0^{t-\frac{x}{v}} \phi_{in}(\tau)\, d\tau + \int_0^{L} \rho_0(s)\, ds, \quad \int_0^{t-\frac{L-x}{\omega}} \phi_{out}(\tau)\, d\tau + \rho_{max}(L-x) \right\}, \end{aligned} \tag{2.60}$$

where t_{min} was estimated in Appendix B.3, which requires that Assumption 2.2 holds as well.

2.3.3 Problem statement in H-J formulation

The desired MF is obtained similar to (2.60):

$$\begin{aligned} &\forall (x,t) \in [0,L] \times [t_{min}, +\infty) : \\ &M_d(x,t) = \min\left\{ \int_0^{t-\frac{x}{v}} \phi_{in_d}(\tau)\, d\tau + \int_0^{L} \rho_{d_0}(s)\, ds, \quad \int_0^{t-\frac{L-x}{\omega}} \phi_{out_d}(\tau)\, d\tau + \rho_{max}(L-x) \right\}. \end{aligned} \tag{2.61}$$

Note that both $M(x,t)$ and $M_d(x,t)$ are defined up to a constant since the starting point for the numeration of cars can be arbitrary. Therefore, we state our problem in Hamilton-Jacobi formulation as a pointwise convergence of Moskowitz functions $M(x,t)$ to $M_d(x,t)$ as $t \to \infty$. This is formalized as follows.

Problem 2.3
Given a desired trajectory $\rho_d(x,t)$ governed by system (2.58), find $\forall t \in \mathbb{R}^+$ boundary control laws $u_{in}(t)$ and $u_{out}(t)$ for system (2.56) such that

$$\exists M_0 \in \mathbb{R} \,:\, \forall x \in [0,L] \quad \lim_{t\to\infty} \left(M(x,t) - M_d(x,t)\right) = M_0.$$

The constant M_0 should be understood as some historical difference in the cumulative number of vehicles in both systems, and it does not have any effect on the traffic evolution.

After we have stated Problem 2.3 in H-J formulation, let us establish the link to the LWR formulation.

Lemma 2.2. *Problem (2.3) is equivalent to the integral convergence of densities over arbitrarily small intervals, i.e., $\forall a, b$: $0 \le a < b \le L$ we obtain*

$$\lim_{t\to\infty} \int_a^b \left(\rho(s,t) - \rho_d(s,t)\right) ds = 0, \tag{2.62}$$

where a and b can be arbitrarily close points in space.

Proof. By the definition of the Moskowitz function (2.23), we can write

$$M(a,t) - M(b,t) = \int_a^L \rho\,(s,t)\, ds - \int_b^L \rho\,(s,t)\; ds = \int_a^b \rho(s,t) ds, \tag{2.63}$$

and

$$M_d(a,t) - M_d(b,t) = \int_a^b \rho_d\,(s,t)\, ds. \tag{2.64}$$

For $x = a$ and $x = b$ in Problem (2.3) we get $M(a,t) \to M_d(a,t) + M_0$ and $M(b,t) \to M_d(b,t) + M_0$. This is equivalent to $M(a,t) - M(b,t) \to M_d(a,t) - M_d(b,t)$, which by (2.63) and (2.64) can be rewritten as

$$\int_a^b \rho\,(s,t)\, ds \to \int_a^b \rho_d\,(s,t)\, ds.$$

□

Remark 2.4
Notice that pointwise convergence of two functions does not imply the convergence for their derivatives in any of L^p norms. However, we pose Problem 2.3 to reach the equality of the densities over arbitrarily small intervals, which means that the state approximates the desired trajectory as time goes to infinity.

Thus, the density approximates the desired trajectory as in (2.62) if we find a control law for system (2.56) that solves Problem 2.3 stated in the Hamilton-Jacobi formulation.

2.3.4 Control law design

Theorem 2.3
Given system (2.56) for which Assumptions 2.1 and 2.2 hold with the MF solution given by (2.60), and the desired vehicle trajectory solving system (2.58) for which Assumption 2.1 holds with the MF solution (2.61). Then a control law that achieves the goal stated in Problem 2.3 is given by

$$\begin{aligned} &(1)\ u_{in}(t) = \phi_{in_d}(t) - ke(t), \\ &(2)\ u_{out}(t) = \phi_{out_d}(t) + ke(t), \end{aligned} \quad t \in \mathbb{R}^+$$
$$\text{where } e(t) = \int_0^L (\rho(s,t) - \rho_d(s,t))\, ds \quad \text{and} \quad k > 0. \tag{2.65}$$

Remark 2.5
Physically, the control law given by (2.65) makes us control inflows and outflows such that all the "excess" cars, given by the integral difference in densities, leave the domain, and then inflows and outflows match the desired ones. When the goal is achieved, the following conditions hold for $\forall t \geq t_{min}$:

$$(i)\ \ \phi_{in}(t) = \phi_{in_d}(t), \qquad (ii)\ \phi_{out}(t) = \phi_{out_d}(t),$$

$$(iii)\ \int_0^{t-\frac{x}{v}} (\phi_{in}(\tau) - \phi_{in_d}(\tau))\, d\tau + \int_0^L (\rho_0(s) - \rho_{d_0}(s))\, ds = \int_0^{t-\frac{L-x}{\omega}} (\phi_{out}(\tau) - \phi_{out_d}(\tau))\, d\tau. \tag{2.66}$$

The derivation of these conditions is given in Appendix B.4.

Proof of Theorem 2.3. This proof consists of five parts: it is shown that $e(t)$ goes to zero as $t \to \infty$ in Sections 2.3.4.1 - 2.3.4.3, and then we show that this is enough for the convergence of Moskowitz functions in Sections 2.3.4.4 and 2.3.4.5.

Error $e(t)$ is defined as the difference in the overall number of cars in the real and the desired systems (1.5). Using (2.23) for $x = 0$ we can rewrite the definition of error as

$$e(t) = M(0,t) - M_d(0,t) + \int_0^t (\phi_{out_d}(\tau) - \phi_{out}(\tau))\, d\tau,$$

which by using (2.24) to evaluate $M(0,t) - M_d(0,t)$ can be further modified as

$$e(t) = \int_0^t (\phi_{in}(\tau) - \phi_{out}(\tau) + \phi_{out_d}(\tau) - \phi_{in_d}(\tau))\, d\tau + \int_0^L (\rho_0(s) - \rho_{0_d}(s))\, ds. \tag{2.67}$$

Error dynamics are found as the time derivative of (2.67)

$$\dot{e}(t) = \phi_{in}(t) - \phi_{out}(t) - \phi_{in_d}(t) + \phi_{out_d}(t). \tag{2.68}$$

Recall that the main challenge in controlling system (2.56) is related to the fact that the boundary flows ϕ_{in} and ϕ_{out} are not always equal to u_{in} and u_{out}, respectively. Thus, for some periods of time, we lose the ability to impose any control u_{in} or u_{out} on the boundaries. Let us investigate this problem in more details.

2.3.4.1 Analysis of flow restrictions

By definition of the Moskowitz function (2.21), inflows and outflows are time derivatives of $M(0,t)$ and $M(L,t)$, respectively. Let us first focus on the inflow defined as $\phi_{in}(t) = \partial M(0,t)/\partial t$, which allows us to express $M(0,t)$ by taking the time integral of $\phi_{in}(t)$ and get

$$M(0,t) = \int_0^t \phi_{in}(\tau)\, d\tau + M(0,0), \tag{2.69}$$

where $M(0,0) = \int_0^L \rho_0(s)\, ds$ is obtained from the definition (2.23) for the space-time point $(x,t) = (0,0)$.

From now on, let us consider only $t \geq t_{min}$ with t_{min} being defined in (2.59). Then, we can also consider the MF solution (2.60) for $x = 0$ and obtain

$$M(0,t) = \min\left\{ \int_0^t \phi_{in}(\tau)\, d\tau + \int_0^L \rho_0(s)\, ds,\ \int_0^{t-\frac{L}{\omega}} \phi_{out}(\tau)\, d\tau + L\rho_{max} \right\}. \tag{2.70}$$

Combining (2.69) with (2.70), we obtain the following minimum problem:

$$\int_0^t \phi_{in}(\tau)d\tau + \int_0^L \rho_0(s)ds = \min\left\{ \int_0^t \phi_{in}(\tau)d\tau + \int_0^L \rho_0(s)ds,\ \int_0^{t-\frac{L}{\omega}} \phi_{out}(\tau)d\tau + L\phi_{max} \right\}. \tag{2.71}$$

From (2.71) one can see that the following inequality holds

$$\int_0^t \phi_{in}(\tau)\,d\tau + \int_0^L \rho_0(s)\,ds \leq \int_0^{t-\frac{L}{\omega}} \phi_{out}(\tau)\,d\tau + L\phi_{max}. \tag{2.72}$$

In case of equality in (2.72), we must provide that the right-hand term grows more quickly than the left-hand term. Thus, by taking the time derivative of (2.71) we obtain $\phi_{in}(t) \leq \phi_{out}(t-\frac{L}{\omega})$. Notice that if the left-hand term is strictly smaller than the right-hand term in (2.72), then the inflow is less constrained and we should be able to set $\phi_{in}(t) = u_{in}(t)$.

All this can be combined in the following property. We define a *control restriction function* for the upstream boundary

$$g_{in}(t) = \int_0^{t-\frac{L}{\omega}} \phi_{out}(\tau)\,d\tau + L\rho_{max} - \int_0^t \phi_{in}(\tau)\,d\tau - \int_0^L \rho_0(s)\,ds,$$

which represents the difference between two arguments of the minimum from (2.71). By (2.72) we obtain that $g_{in}(t) \geq 0$ always. Moreover, using the definition of $\phi_{in}(t)$ given by (2.57), the condition on inflow restriction can be formulated as:

$$\begin{aligned} g_{in}(t) > 0: &\quad \phi_{in}(t) = u_{in}(t), \\ g_{in}(t) = 0: &\quad \phi_{in}(t) = \min\left\{u_{in}(t), \phi_{out}\left(t - \frac{L}{\omega}\right)\right\}. \end{aligned} \tag{2.73}$$

Note that the notation of control restriction should be understood as saturation control with $\phi_{out}\left(t - \frac{L}{\omega}\right)$ being the saturation time-varying threshold.

Similarly, we proceed by considering the MF solution (2.34) for $x = L$ to analyze $\phi_{out}(t)$ for the downstream boundary, and get its control restriction function that reads

$$g_{out}(t) = \int_0^{t-\frac{L}{v}} \phi_{in}(\tau)\,d\tau + \int_0^L \rho_0(s)\,ds - \int_0^t \phi_{out}(\tau)\,d\tau,$$

and the following condition on the *outflow restriction*

$$\begin{aligned} g_{out}(t) > 0: &\quad \phi_{out}(t) = u_{out}(t), \\ g_{out}(t) = 0: &\quad \phi_{out}(t) = \min\left\{u_{out}(t), \phi_{in}\left(t - \frac{L}{v}\right)\right\}. \end{aligned} \tag{2.74}$$

Thus, any boundary control can be imposed if $g_{in} > 0$ and $g_{out} > 0$.

Defining $R(t) = \int_0^L \rho(s,t)ds$ and $R_0 = R(0)$, and using the equality of (2.23) and (2.24) (independence of chosen integration path), we obtain for $\forall t' \in \mathbb{R}^+$ and $x = 0$

$$R(t') = R_0 + \int_0^{t'} \phi_{in}(\tau)\,d\tau - \int_0^{t'} \phi_{out}(\tau)\,d\tau. \tag{2.75}$$

Thus, the control restriction functions can be rewritten as

$$\begin{aligned} g_{in}(t) &= L\rho_{max} - R(t') - \int\limits_{t-\frac{L}{\omega}}^{t'} \phi_{out}(\tau)\,d\tau - \int\limits_{t'}^{t} \phi_{in}(\tau)\,d\tau, \\ g_{out}(t) &= R(t') - \int\limits_{t-\frac{L}{v}}^{t'} \phi_{in}(\tau)\,d\tau - \int\limits_{t'}^{t} \phi_{out}(\tau)\,d\tau. \end{aligned} \tag{2.76}$$

Note also that inflows and outflows are upper bounded by the road capacity, i.e., $\phi_{in} \le \phi_{max}$ and $\phi_{out} \le \phi_{max}$, where $\phi_{max} = v\rho_c$ (see Figure 2.1). To find a time interval, during which no control law can be imposed, we set $g_{in}(t) = 0$ and then express $R(t')$ from (2.76):

$$\begin{aligned} R(t') &= L\rho_{max} - \int\limits_{t-\frac{L}{\omega}}^{t'} \phi_{out}(\tau)\,d\tau - \int\limits_{t'}^{t} \phi_{in}(\tau)\,d\tau \\ &\ge L\rho_{max} - \int\limits_{t-\frac{L}{\omega}}^{t'} \phi_{max}\,d\tau - \int\limits_{t'}^{t} \phi_{max}\,d\tau = L\rho_{max} - \frac{L}{\omega}\phi_{max} = L\rho_c. \end{aligned}$$

The same steps are performed for $g_{out}(t) = 0$, and we get

$$\begin{aligned} g_{in}(t) = 0 \quad &\Rightarrow \quad R(t') \ge L\rho_c \quad \forall t' \in \left[t - \frac{L}{\omega}, t\right], \\ g_{out}(t) = 0 \quad &\Rightarrow \quad R(t') \le L\rho_c \quad \forall t' \in \left[t - \frac{L}{v}, t\right]. \end{aligned} \tag{2.77}$$

This means that not any control law can be applied at the upstream boundary at time t, if during the preceding time interval $\left[t - \frac{L}{\omega}, t\right]$ the mean density was bigger than the critical density (and inversely for the downstream boundary).

Using Assumption 2.2 and the fact that the critical density $\rho_c = \rho_{max}/3$, we set $g_{in}(t) = 0$ in (2.76), which implies $R(t) \ge L\rho_c + \varepsilon$ and $R(t - L/\omega) \ge L\rho_c + \varepsilon$, as well as $g_{out}(t) = 0$ implies $R(t) \le L\rho_c - \varepsilon$ and $R(t - L/v) \le L\rho_c - \varepsilon$.

Let us consider (2.77) to investigate whether it is possible that control can not be imposed at both boundaries simultaneously. We pick some time point t such that $g_{in}(t) = 0$ and some time point $t' \in [t, t + L/v]$ with $g_{out}(t') = 0$. As written above, $g_{in}(t) = 0$ implies $R(t) \ge L\rho_c + \varepsilon$. However, $t \in [t' - L/v, t']$, thus $R(t) \le L\rho_c$ for $g_{out}(t') = 0$ by (2.77). This is a contradiction, since satisfying both $R(t) \ge L\rho_c + \varepsilon$ and $R(t) \le L\rho_c$ at the same t is impossible. Thus, the time point t' when $g_{out}(t') = 0$ can occur at least after the interval L/v has passed since the last $g_{in}(t) = 0$.

Moreover, if $t' \ge t + L/v$ and $g_{out}(t') = 0$, then $R(t' - L/v) \le L\rho_c - \varepsilon$. The maximal inflow is always bounded from above by ϕ_{max}, therefore the difference in the integral densities

$R(t' - L/v) - R(t)$ can be passed at least in time $t' - L/v - t \geq 2\varepsilon/\phi_{max}$. Performing the same analysis for the inverse case, we conclude that

$$\begin{aligned} g_{in}(t) = 0 \quad &\Rightarrow \quad g_{out}(t') > 0 \qquad \forall t' \in \left[t, t + \frac{L}{v} + \frac{2\varepsilon}{\phi_{max}}\right], \\ g_{out}(t) = 0 \quad &\Rightarrow \quad g_{in}(t') > 0 \qquad \forall t' \in \left[t, t + \frac{L}{\omega} + \frac{2\varepsilon}{\phi_{max}}\right]. \end{aligned} \tag{2.78}$$

Thus, it is impossible for two boundaries to be unable to accept the control simultaneously, and the periods of "uncontrollability" are separated in time by at least $\frac{L}{v} + \frac{2\varepsilon}{\phi_{max}}$ or $\frac{L}{\omega} + \frac{2\varepsilon}{\phi_{max}}$.

2.3.4.2 Dynamics of $e(t)$

Thus, in Section 2.3.4.1 we have established that at each moment either one of control restriction functions or none of them is zero (2.78). Hence, we separate the dynamics of the integral error term $e(t)$ (1.5) into three possible cases.

1. Assume both $g_{in}(t) > 0$ and $g_{out}(t) > 0$. Then all the boundary control terms u_{in} and u_{out} can be applied, which by (2.65) implies that $\phi_{in}(t) = \phi_{in_d}(t) - ke(t)$ and $\phi_{out}(t) = \phi_{out_d}(t) + ke(t)$. According to (2.68), the error dynamics are given by

$$\dot{e}(t) = -2ke(t), \tag{2.79}$$

and, thus, $e(t)$ converges exponentially to zero.

2. Assume $g_{in}(t) = 0$. Then, the control can not be applied at the upstream boundary, i.e., $\phi_{in}(t) \leq \phi_{in_d}(t) - ke(t)$ and $\phi_{out}(t) = \phi_{out_d}(t) + ke(t)$, which means

$$\dot{e}(t) \leq -2ke(t). \tag{2.80}$$

Thus, a positive error $e(t) > 0$ implies even faster convergence to zero. If $e(t) < 0$, such dynamics can diverge from zero. However, it is possible to show that after a period of not being able to impose any control at the upstream boundary, the error will not be further away from zero than at the beginning of the period. Consider the control restriction function $g_{in_d}(t)$ for the upstream boundary of the desired system:

$$g_{in_d}(t) = L\rho_{max} - R_d(t') - \int\limits_{t-\frac{L}{\omega}}^{t'} \phi_{out_d}(\tau)\, d\tau - \int\limits_{t'}^{t} \phi_{in_d}(\tau)\, d\tau \geq 0, \quad \text{for } t' \in \left[t - \frac{L}{\omega}, t\right].$$

Using $e(t') = R(t') - R_d(t')$, we obtain

$$g_{in_d}(t) - g_{in}(t) = \int\limits_{t-\frac{L}{\omega}}^{t'} (\phi_{out}(\tau) - \phi_{out_d}(\tau))\, d\tau + \int\limits_{t'}^{t} (\phi_{in}(\tau) - \phi_{in_d}(\tau))\, d\tau + e(t') \geq 0. \tag{2.81}$$

Using the properties $\phi_{in}(t) \leq \phi_{in_d}(t) - ke(t)$ and $\phi_{out}(t) = \phi_{out_d}(t) + ke(t)$, we obtain

$$e(t') + k \int_{t-\frac{L}{\omega}}^{t'} e(\tau)\, d\tau - k \int_{t'}^{t} e(\tau)\, d\tau \geq 0.$$

We substitute $t' = t$ to get the first inequality, and then $t' = t - \frac{L}{\omega}$ to get the second one:

$$1)\ e(t) + k \int_{t-\frac{L}{\omega}}^{t} e(\tau)\, d\tau \geq 0, \qquad 2)\ e\left(t - \frac{L}{\omega}\right) - k \int_{t-\frac{L}{\omega}}^{t} e(\tau) d\tau \geq 0,$$

and the sum of these inequalities yields

$$e(t) + e\left(t - \frac{L}{\omega}\right) \geq 0. \tag{2.82}$$

3. Assume $g_{out}(t) = 0$. Then, the control can not be applied at the downstream boundary, i.e., $\phi_{out}(t) \leq \phi_{out_d}(t) + ke(t)$ and $\phi_{in}(t) = \phi_{in_d}(t) - ke(t)$, which yields the following error dynamics

$$\dot{e}(t) \geq -2ke(t). \tag{2.83}$$

Using the same analysis as above for $e(t) > 0$, we obtain

$$e(t) + e\left(t - \frac{L}{v}\right) \leq 0. \tag{2.84}$$

2.3.4.3 Proof that $e(t)$ converges to zero

In Table 2.1 we have summarized three regimes of error dynamics. The regimes can alternate

Table 2.1: Summary of error regimes

Regime 1	$g_{in}(t) > 0, \quad g_{out}(t) > 0$	$\dot{e}(t) = -2ke(t)$
Regime 2	$g_{in}(t) = 0, \quad g_{out}(t') > 0,$ $\forall t' \in \left[t, t + \frac{L}{v} + \frac{2\varepsilon}{\phi_{max}}\right]$	$\dot{e}(t) \leq -2ke(t)$
Regime 3	$g_{out}(t) = 0, \quad g_{in}(t') > 0,$ $\forall t' \in \left[t, t + \frac{L}{\omega} + \frac{2\varepsilon}{\phi_{max}}\right]$	$\dot{e}(t) \geq -2ke(t)$

as depicted in Figure 2.10. In this part of the proof, we will show that the error can enter the second dynamic regime (Regime 2) only being positive, while it enter Regime 3 only being negative. Thus, if the error is positive in Regime 1 (green circle), it either remains there forever and the exponential convergence to zero is guaranteed by (2.79), or it enters Regime 2 (violet circle). Then, being positive, by (2.80) the error converges to zero even faster than in Regime 1. However, it can also become negative, and in this case the error might diverge from

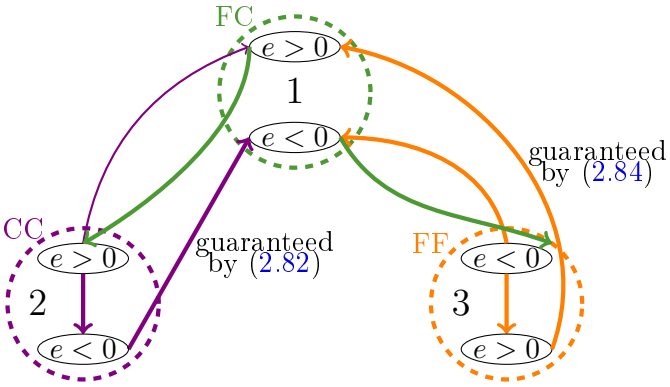

Figure 2.10: Diagram of regimes illustrating how they can alternate. Arrows denote possible regime switches. FC, CC and FF are used to denote regimes at both boundaries, where F stays for free-flow and C for congested regime.

zero. Nevertheless, the divergence from zero can last only for a bounded time interval, and by (2.82) the absolute value of the error term can not exceed the value it had some time ago. As this happens, the error enters again Regime 1 as a negative term. It either stays there forever, or switches to Regime 3, where it goes to zero even more quickly by (2.83). The rest can be described in a symmetric manner. Recall also that Regimes 2 and 3 are always separated in time by at least $\frac{L}{v} + \frac{2\varepsilon}{\phi_{max}}$ or $\frac{L}{\omega} + \frac{2\varepsilon}{\phi_{max}}$. Further, we provide a strict proof of the exponential convergence of the error term to zero.

Imagine a time axis split into three types of intervals corresponding to three different error dynamic regimes as shown in Figure 2.11. Recalling that Regimes 2 and 3 cannot occur in a row, we can observe, e.g., a sequence like this: 12121313121.... Thus, it is possible that after Regime 2 and then Regime 1, the second regime comes again, since nothing prohibits $g_{in}(t)$ to become zero again almost immediately. We denote this sequence of regimes as "$g_{in}(t) = 0$ *sometimes*", which is defined as the largest row of Regimes 1 and 2 that starts and ends with Regime 2 and does not contain any time interval with Regime 3. The same can be done with the regime sequence containing Regimes 1 and 3 called "$g_{out}(t) = 0$ *sometimes*". These sequences "$g_{in}(t) = 0$ *sometimes*" and "$g_{out}(t) = 0$ *sometimes*" alternate strictly, always having Regime 1 between them. Finally, for a time interval corresponding to the regime (or regime sequence) with index i we can define entrance time $\underline{t}_i$ and exit time $\bar{t}_i$. By (2.78) we see that $\underline{t}_i - \bar{t}_{i-1} \geq \frac{L}{\omega} + \frac{2\varepsilon}{\phi_{max}}$ if Regime i is "$g_{in}(t) = 0$ *sometimes*", and $\underline{t}_i - \bar{t}_{i-1} \geq \frac{L}{v} + \frac{2\varepsilon}{\phi_{max}}$ if Regime i is "$g_{out}(t) = 0$ *sometimes*".

Let us fix i corresponding to "$g_{in}(t) = 0$ *sometimes*" (the other case is symmetric). First of all, by (2.82) we obtain

$$g_{in}(\underline{t}_i) = 0 \quad \text{and} \quad g_{in}(\bar{t}_i) = 0.$$

Therefore

$$e(\underline{t}_i) + e\left(\underline{t}_i - \frac{L}{\omega}\right) \geq 0 \tag{2.85}$$

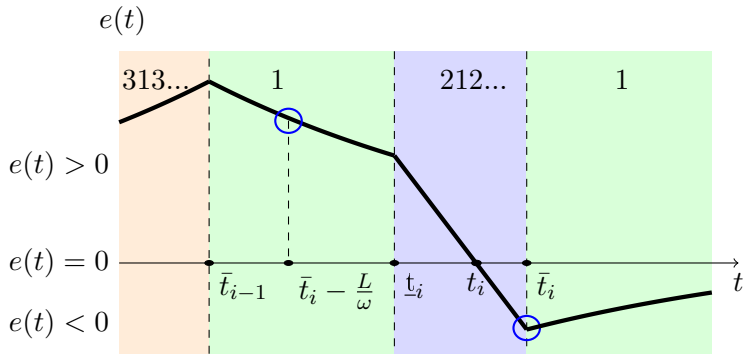

Figure 2.11: A possible error behaviour $e(t)$ (thick black line). From left to right: divergence for "$g_{out}(t) = 0$ *sometimes*" (in orange); exponential convergence in Regime 1 (in green); fast convergence for "$g_{in}(t) = 0$ *sometimes*" (in blue); then divergence for $e(t') < 0\ \forall t' \in [t_i, \bar{t}_i]$; exponential convergence in Regime 1. Blue empty circles are related to (2.86).

and

$$e(\bar{t}_i) + e\left(\bar{t}_i - \frac{L}{\omega}\right) \geq 0. \tag{2.86}$$

It is clear that $\underline{t}_i - \frac{L}{\omega} \geq \bar{t}_{i-1}$, which means that the dynamics of e in the interval $[\underline{t}_i - \frac{L}{\omega}, \underline{t}_i]$ are exponential. Thus, both $e(\underline{t}_i)$ and $e\left(\underline{t}_i - \frac{L}{\omega}\right)$ have the same sign, and by (2.85) they are both positive. A similar analysis can be done for the regime sequence "$g_{out}(t) = 0$ *sometimes*", which means that from $g_{out}(t) = 0$ to $g_{in}(t) = 0$ the error term is positive and from $g_{in}(t) = 0$ to $g_{out}(t) = 0$ the error term is negative (and thus $e(\bar{t}_i) < 0$). Consequently, inside each regime sequence i there should be a time point t_i, when $e(t_i) = 0$.

Now, by (2.86) and using that $e(\bar{t}_i)$ is negative, we see that $e\left(\bar{t}_i - \frac{L}{\omega}\right) \geq 0$, which means that $\bar{t}_i - \frac{L}{\omega} \leq t_i$ (see Figure 2.11).

During the time interval $[\bar{t}_{i-1}, \underline{t}_i]$ it is clear that the convergence is exponential (Regime 1). During the time interval $[\underline{t}_i, t_i]$ the dynamics are $\dot{e} \leq -2ke$, and $e(t) \geq 0$. The time point $\bar{t}_i - \frac{L}{\omega} \in [\bar{t}_{i-1}, t_i]$, therefore

$$e\left(\bar{t}_i - \frac{L}{\omega}\right) \leq e(\bar{t}_{i-1}) \exp^{-2k(\bar{t}_i - \frac{L}{\omega} - \bar{t}_{i-1})},$$

which is also valid for its absolute values

$$\left|e\left(\bar{t}_i - \frac{L}{\omega}\right)\right| \leq |e(\bar{t}_{i-1})| \exp^{-2k(\bar{t}_i - \frac{L}{\omega} - \bar{t}_{i-1})}.$$

Now from (2.86) and the fact that $e(\bar{t}_i) < 0$ we see that $|e(\bar{t}_i)| \leq \left|e\left(\bar{t}_i - \frac{L}{\omega}\right)\right|$, thus

$$|e(\bar{t}_i)| \leq |e(\bar{t}_{i-1})| \exp^{-2k(\bar{t}_i - \frac{L}{\omega} - \bar{t}_{i-1})}.$$

We can write $\bar{t}_i - \bar{t}_{i-1} \geq \underline{t}_i - \bar{t}_{i-1} \geq \frac{L}{\omega} + \frac{2\varepsilon}{\phi_{max}}$, which yields

$$\frac{\bar{t}_i - \frac{L}{\omega} - \bar{t}_{i-1}}{\bar{t}_i - \bar{t}_{i-1}} = 1 - \frac{\frac{L}{\omega}}{\bar{t}_i - \bar{t}_{i-1}} \geq 1 - \frac{\frac{L}{\omega}}{\frac{L}{\omega} + \frac{2\varepsilon}{\phi_{max}}} = \frac{\frac{2\varepsilon}{\phi_{max}}}{\frac{L}{\omega} + \frac{2\varepsilon}{\phi_{max}}} = \frac{2\varepsilon\omega}{L\phi_{max} + 2\varepsilon\omega},$$

which allows us to bound time interval in the exponential function from below by

$$\bar{t}_i - \frac{L}{\omega} - \bar{t}_{i-1} \geq \left(\frac{2\varepsilon\omega}{L\phi_{max} + 2\varepsilon\omega}\right)(\bar{t}_i - \bar{t}_{i-1})\,.$$

This finally leads to

$$|e(\bar{t}_i)| \leq |e(\bar{t}_{i-1})| \exp^{-2k\left(\frac{2\varepsilon\omega}{L\phi_{max}+2\varepsilon\omega}\right)(\bar{t}_i - \bar{t}_{i-1})}, \tag{2.87}$$

which proves the exponential convergence to zero of $e(t)$.

2.3.4.4 Proof that integral inflows converge

In order to further proceed with the proof of Theorem 2.3, we need to show that the integral of inflow difference in the real (2.56) and in the desired system (2.58) has a limit, as it is required for the convergence of Moskowitz functions as stated in Problem 2.3 (see Section 2.3.4.5, where the existence of this limit is used for the introduction of constant M_0):

$$\exists \lim_{t\to\infty} \int_0^t (\phi_{in}(\tau) - \phi_{in_d}(\tau))\, d\tau. \tag{2.88}$$

By the Cauchy criterion for the convergence of functions, it suffices to show that

$$\lim_{t_1,t_2\to\infty} \int_{t_1}^{t_2} (\phi_{in}(\tau) - \phi_{in_d}(\tau))\, d\tau = 0, \qquad \forall t_1, t_2 \,:\, t_2 > t_1. \tag{2.89}$$

First, we find an upper bound for this limit (2.89). By combining (2.73) with (2.65) we obtain $\phi_{in}(t) \leq \phi_{in_d}(t) - ke(t)\ \forall t \in \mathbb{R}^+$, thus, we can write $\forall t_1, t_2 \to \infty$

$$\int_{t_1}^{t_2} (\phi_{in}(\tau) - \phi_{in_d}(\tau))\, d\tau \leq -k \int_{t_1}^{t_2} e(\tau)\, d\tau \to 0,$$

where we have used the exponential convergence result for the error term (2.87). This in turn implies that the upper bound is 0:

$$\lim_{t_1,t_2\to\infty} \int_{t_1}^{t_2} (\phi_{in}(\tau) - \phi_{in_d}(\tau))\, d\tau \leq 0. \tag{2.90}$$

Now let us estimate the lower bound for the limit (2.89). Thereby, we distinguish two possible cases:

1. Assume $g_{in}(t) > 0$. In this case, we can write

$$\int_{t-\frac{L}{\omega}}^{t} (\phi_{in}(\tau) - \phi_{in_d}(\tau))\, d\tau \geq -k \int_{t-\frac{L}{\omega}}^{t} |e(\tau)|\, d\tau.$$

2. Assume $g_{in}(t) = 0$. Using (2.81) for $t' = t - \frac{L}{\omega}$, we get

$$\int_{t-\frac{L}{\omega}}^{t} (\phi_{in}(\tau) - \phi_{in_d}(\tau))\, d\tau \geq -e(t - \frac{L}{\omega}) \geq -\left|e(t - \frac{L}{\omega})\right|.$$

The combination of these two cases yields

$$\int_{t-\frac{L}{\omega}}^{t} (\phi_{in}(\tau) - \phi_{in_d}(\tau))\, d\tau \geq -k \int_{t-\frac{L}{\omega}}^{t} |e(\tau)|\, d\tau - \left|e(t - \frac{L}{\omega})\right|. \tag{2.91}$$

Now let us divide the time interval $[t_1, t_2]$ into equal subintervals of length L/ω. Thus, (2.91) can be rewritten for a larger time interval as

$$\int_{t_1}^{t_2} (\phi_{in}(\tau) - \phi_{in_d}(\tau))\, d\tau \geq -k \int_{t_1}^{t_2} |e(\tau)|\, d\tau - \sum_{n=0}^{\left\lfloor \frac{t_2 - t_1}{L/\omega} \right\rfloor} \left|e\left(t_1 + n\frac{L}{\omega}\right)\right|.$$

where the sum goes over intervals of size L/ω, i.e., t_1, $t_1 + L/\omega$, ..., t_2. If we take the time limit of the latter expression for $t_1, t_2 \to \infty$, both right-hand terms converge to zero, as for the sum term we can apply the integral test for convergence. Finally, we obtain the lower bound:

$$\lim_{t_1, t_2 \to \infty} \int_{t_1}^{t_2} (\phi_{in}(\tau) - \phi_{in_d}(\tau))\, d\tau \geq 0. \tag{2.92}$$

The combination of (2.92) and (2.90) provides that the limit is zero, which proves the existence of the limit of the integral difference between inflows in both systems as in (2.88).

2.3.4.5 Proof that Moskowitz functions converge

Finally we arrived at the last part of the proof of Theorem (2.3). Let us define two auxiliary Moskowitz functions as

$$M_1(x,t) = R_0 - R_{0_d} + \int_{0}^{t-\frac{x}{v}} (\phi_{in}(\tau) - \phi_{in_d}(\tau))\, d\tau, \tag{2.93}$$

$$M_2(x,t) = \int_{0}^{t-\frac{L-x}{\omega}} (\phi_{out}(\tau) - \phi_{out_d}(\tau))\, d\tau. \tag{2.94}$$

Notice that $M_1(x,t)$ and $M_2(x,t)$ correspond to the left- and to the right-hand side of (2.66)(iii), which must hold for large t. First of all, using $e_0 = R_0 - R_{0_d}$ and the dynamics of

$e(t)$ given by (2.68), we obtain that $\forall x \in [0, L]$

$$\lim_{t\to\infty}(M_1(x,t) - M_2(x,t)) = \int_0^\infty (\phi_{in}(\tau) - \phi_{in_d}(\tau) - \phi_{out}(\tau) + \phi_{out_d}(\tau))\, d\tau + e_0 = \lim_{t\to\infty} e(t) = 0. \tag{2.95}$$

Moreover, as it was proven in the previous Section (2.3.4.4), $M_1(x,t)$ has a limit due to (2.88) and e_0 being constant in time. Therefore, we can define

$$M_0 := \lim_{t\to\infty} M_1(x,t),$$

and by (2.95) we get

$$\lim_{t\to\infty} M_2(x,t) = M_0.$$

We can also define the MF error terms as

$$\tilde{M}_1(x,t) = M_1(x,t) - M_0 \quad \text{and} \quad \tilde{M}_2(x,t) = M_2(x,t) - M_0.$$

Finally, recall that the desired MF given by (2.61) can be expressed as

$$M_d(x,t) = \min\left\{M_{\mathrm{Up}_d}(x,t), M_{\mathrm{Down}_d}(x,t)\right\},$$

since this is the general definition of a solution which is not affected by the initial conditions (see Assumption 2.1). Thus, by using the MF solution (2.60) together with $M_1(x,t)$ (2.93) and $M_2(x,t)$ (2.94), we obtain

$$M(x,t) = \min\left\{M_{\mathrm{Up}_d}(x,t) + M_1(x,t), M_{\mathrm{Down}_d}(x,t) + M_2(x,t)\right\},$$

or

$$M(x,t) = \min\left\{M_{\mathrm{Up}_d}(x,t) + \tilde{M}_1(x,t), M_{\mathrm{Down}_d}(x,t) + \tilde{M}_2(x,t)\right\} + M_0.$$

Minimum is a continuous function on both arguments, thus we obtain for $t \to \infty$ that

$$M(x,t) \to M_d(x,t) + M_0, \qquad \forall x \in [0, L], \tag{2.96}$$

as stated in Problem 2.3, which finally concludes the proof. □

Remark 2.6

Note that Assumption 2.2 is non-limiting. Indeed, it requires that the flow integral over time T is less than its maximum value by at least ε, which is always possible, except when vehicles enter and leave the system at maximum rate during T. Obviously, in this case, it is also possible to reach the goal.

The need to use Assumption 2.2 comes from the fact that at maximum flow by (2.77) both $g_{in}(t) = 0$ and $g_{out}(t) = 0$ for the same t, which means that with the slightest fluctuation a boundary becomes "uncontrollable". Thus, the state with maximum flows at both boundaries during time interval T is "unstable", and therefore for this case it is impossible to prove the exponential convergence of the error term $e(t)$.

2.3.5 Numerical example

We illustrate the efficiency of the feedback boundary control law (2.65) by driving a state being initially almost completely in a traffic jam to a desired vehicle density trajectory being in a mixed regime. This is done by providing results from a numerical simulation, for which we again use the standard Godunov scheme that is described in Section 2.1.6.

2.3.6 Simulation setup

As in Section 2.2.7, here we also consider a space interval $[0, L]$ that is divided into $n = 500$ cells. The feedback term given by the integral error (1.5) is computed using the Riemann summation over cells $i \in \{2, \dots, n-1\}$. Thus, here we seek to demonstrate the efficiency of using a state feedback for a road whose first quarter is initially empty, and the traffic jam is formed at the rest of the road:

$$\rho_0(0 \leq x < 1/4L) = 0 \quad \text{and} \quad \rho_0(1/4L \leq x \leq L) = \rho_{max}.$$

Thus, we consider here a system being almost completely in the traffic jam as initial condition. For the simulation, we use the same parameter set as in (2.55).

As a target state, we consider a vehicle density trajectory in a mixed traffic regime (a space- and time-dependent function), whose evolution is given by "ghost" cells (which are set by copying the value from the neighbor cell) with

$$\rho_{d_{in}}(t) = 0.04 + 0.04 \sin(t/8) \quad \text{and} \quad \rho_{d_{out}}(t) = 0.1 + 0.06 \sin(t/4).$$

Here, for convenience, the boundary values are prescribed in terms of densities, since it allows a straightforward implementation of the Godunov scheme (2.18). Then, these density values are transformed into inflows and outflows by using the supply-demand formulation for the case of a triangular FD (2.17).

We will demonstrate how the feedback term given by $-ke(t)$ for the upstream and $+ke(t)$ for the downstream boundary improves the result and provides the asymptotic convergence targeting the desired profile. Two control strategies are compared:

1. No feedback is performed, i.e., only $u_{in}(t) = \phi_{in_d}(t)$ and $u_{out}(t) = \phi_{out_d}(t)$.
2. Feedback terms are applied, i.e., $u_{in}(t) = \phi_{in_d}(t) - ke(t)$, $u_{out}(t) = \phi_{out_d}(t) + ke(t)$.

2.3.6.1 Simulation results

The simulation results are presented in Figure 2.12. Thereby, Figure 2.12a) illustrates the evolution of a desired density trajectory being in a mixed traffic regime. The results of achieving this state with and without feedback are shown below, i.e., see Figures 2.12c) - f).

Thereby, the left column shows the evolution of traffic under the control action, whereas on the right column one can see the corresponding evolution of the absolute difference between the real and the desired states, i.e., L_1 spatial norm defined in (1.1). Figures 2.12c) and 2.12d) illustrate the result if no feedback is applied at the boundaries, while plots e) and f) depict the situation if feedback with gain $k = 0.1$ is applied. The corresponding error behaviour for different gains is shown in Figure 2.12b).

Comparing these plots, we can see that control including the feedback term performs considerably better. Without feedback the congested regime almost completely occupies the domain as time runs, while the feedback term makes the system approach the desired state after the time inferior to the minimal controllability time, which is $t_{ctr} = \frac{L}{v} + \frac{L}{\omega} = 200.5$ s. The convergence results in sense of L_1 norm are compared for different control gains ($k = 0$, $k = 0.005$ and $k = 0.1$) in Figure 2.12b). Thereby, we observe a faster convergence rate for the largest controller gain.

Note that an open-loop control (such as applying absorbing boundary conditions until the road becomes empty, and then applying desired inflows and outflows) will not achieve the goal at all due to the difference in initial densities (2.67).

2.3.7 Discussion

In this section, we have designed boundary control laws that enable tracking a target space- and time-dependent vehicle density on a single road. Both real and desired states are governed by LWR PDEs with triangular fundamental diagram, and they are allowed to be in a mixed traffic regime. This means that the controller is activated at both road boundaries. It allows us to drive any state, being in a partly congested and partly free-flow regime or even being completely congested, to some desired state that is also governed by a fully nonlinear LWR PDE.

The main challenge in control design was related to the fact that we can not apply the boundary conditions pointwise in a general nonlinear LWR system, since one always has to deal with demand-supply concept. We could handle this issue by using the explicit solution formula to H-J PDE that was obtained using the properties of triangular FDs due to the convenient shape of its Legendre transform. The cumulative representation of traffic in terms of number of vehicles within the H-J approach allowed us to formulate and to analyze the control restriction functions. These functions describe time periods, when a domain boundary can accept a proposed controller. These control restriction functions could be defined by exploiting the system evolution at previous times due to the integral structure of the H-J solution. The designed controller has a feedback term, which physically corresponds to the difference between the given number of vehicles on a road and in the desired system multiplied by some controller gain. The numerical example verified the results and illustrated that feedback is absolutely necessary to achieve the goal.

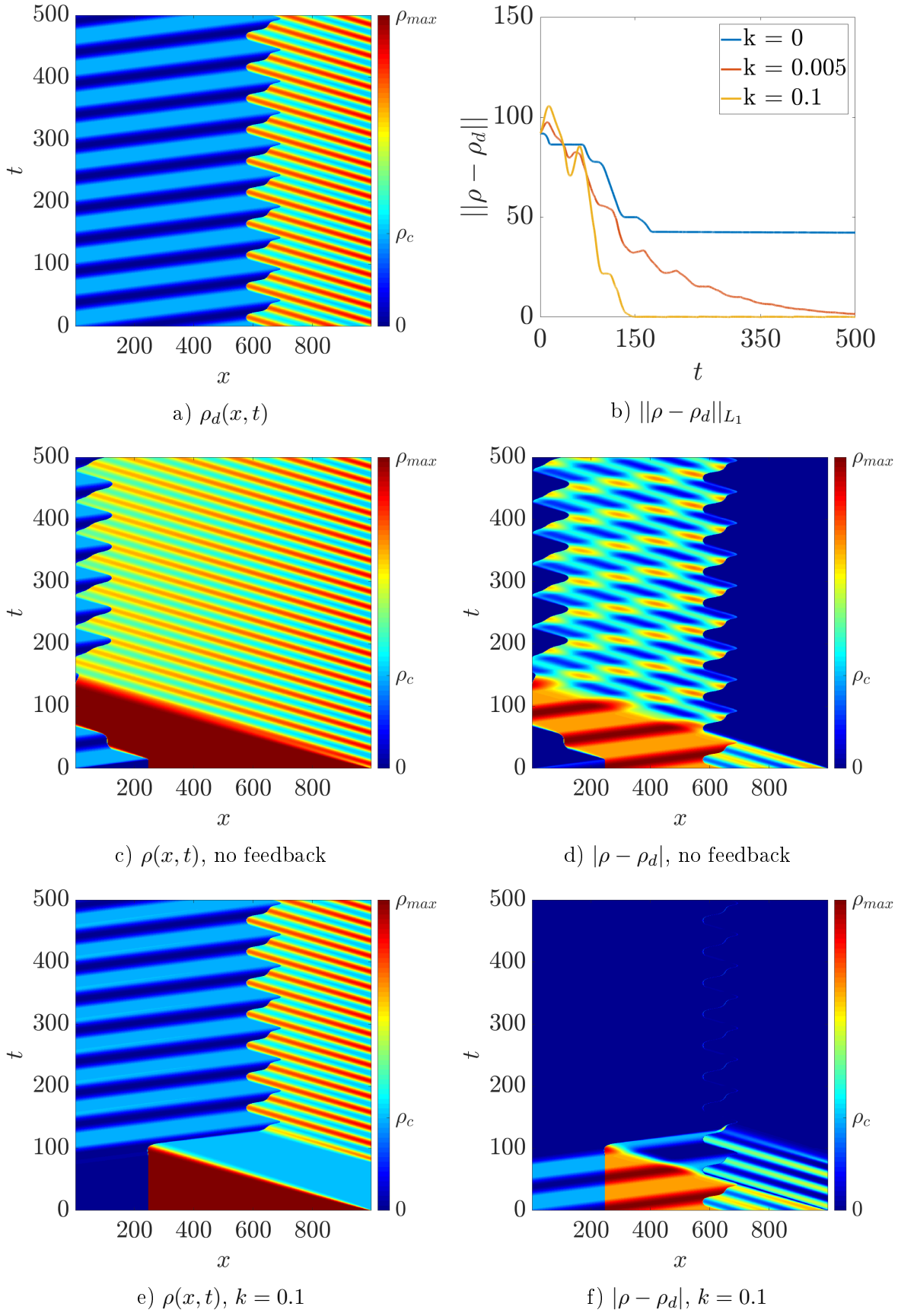

a) $\rho_d(x,t)$

b) $||\rho - \rho_d||_{L_1}$

c) $\rho(x,t)$, no feedback

d) $|\rho - \rho_d|$, no feedback

e) $\rho(x,t)$, $k = 0.1$

f) $|\rho - \rho_d|$, $k = 0.1$

Figure 2.12: a) Desired profile in space-time, b) L_1 error as a function of time for different control gains. Spatio-temporal evolution of the density (left) and of the absolute difference between the real and the target state (right) for: c),d) $k = 0$; e),f) $k = 0.1$.

2.4 Chapter conclusions

In this chapter, we have investigated traffic dynamics evolution on a single road of finite length. This was done within the LWR modeling approach that was described in Section 2.1. Further, we have formulated tracking problems for a desired density being a space- and time-dependent trajectory. These dependencies were included for a better approximation of some realistic traffic situations when traffic conditions change rapidly, e.g., it is common to have non constant inflows and outflows at different day times. Moreover, an equilibrium desired state is just a special case of a general space- and time-varying profile, which can also be covered by the theoretical results derived in this chapter. Such a general target profile results into a non-trivial error dynamics that have been analyzed in both Sections 2.2 and 2.3.

Then, we have also designed feedback boundary control laws on a single road for two different systems. The first traffic system that we have considered in Section 2.2 corresponds to a linear LWR model describing traffic in a congested regime that incorporates a possible mismatch between the model and the reality in terms of unknown in-domain disturbance function. We formulated disturbance attenuation problems while reaching the desired profile in terms of L_2 and L_∞ spatial norms (Problems 2.1 and 2.2). We were able to handle unknown disturbance using characteristics method that allowed us to express the disturbance function through known (measured) variables such as vehicle density and control actions applied at previous time steps. The achieved results stated in Theorems 2.1 and 2.2 were validated with the help of a numerical simulation example, which illustrated considerable improvements of a traffic state under the boundary controller compared to a freely evolving traffic system with no boundary control. In particular, we were able to observe how easily a system can get into a complete traffic jam along the whole road, if we do not apply at least the feedforward control, which is used to track the desired density. The feedforward control is able to considerably reduce the congestion level, although the desired state must remain in the congested regime for the well-posedness of the problem. Then, it was also shown that if in addition to the feedforward controller we also include the feedback part used, then we track the desired state even better. This became obvious from the temporal behaviour of L_2 and L_∞ norms of the deviation from the desired trajectory illustrated in Figure 2.9.

Further, in Section 2.3, we have considered a more complex problem for the case, when both the state and the desired trajectory are governed by full nonlinear LWR models as in its original formulation (also without the disturbance). The main challenge thereby was related to shocks (discontinuities), which arise in such systems for smooth initial data in finite time. This makes an explicit analysis a tedious ask, since then we have to consider the solution only in a weak sense (no classical solutions any more) and track shocks dynamics. Another challenge to deal with was related to the weak boundary conditions, which implies the non-ability to impose any boundary control. To handle both of these issues, we translated the LWR traffic system into its integral form corresponding to the Hamilton-Jacobi PDE that is free of discontinuities, and in the worst case it can only become non-differentiable. Its state corresponds to a cumulative number of vehicles that can be obtained by integrating the vehicle density. The H-J system can be seen as an optimal control problem, and its solution is

obtained semi-explicitly as the minimum of all valid paths. In case of triangular FD that we assumed in this chapter, the solution is obtained as the minimum over only three valid paths each associated with one of the boundary conditions or with the initial condition. For the analysis of the system in asymptotic time, we were able to estimate the minimal time (2.59) upon which it is guaranteed that the initial conditions do not affect the H-J solution any more. The solution can then just be formulated as a minimum of two valid paths associated with the boundary conditions. Thus, the integral formulation of Hamilton-Jacobi traffic system, as well as the ability to express its solution exactly, allowed us to explicitly analyze the periods of time, when boundaries are restricted to accept control action as a function of the actual traffic state. These so-called control restriction functions enabled to divide the error dynamics into three different regimes depending on which boundaries can currently accept control actions. The main result of Section 2.3 is given by Theorem 2.3. Thereby, we have shown that even when boundaries are sometimes unable to accept proposed controls, the system converges to the desired trajectory exponentially. The designed boundary controller also consists of a feedforward and a feedback part, where the latter is an essential component to achieve the goal. The results have been validated numerically for different control gains.

In the next chapter, we are going to extend this result to a large scale, i.e., we will pose and solve various control tasks for the vehicle density defined in some urban area using a scalable modeling approach by considering a conservation law for traffic in 2D.

Chapter 3

Uni-Directional Traffic on Networks

This chapter is devoted to traffic control problems in large-scale urban networks with a preferred direction of traffic flow. The analysis and control design will be done within the same modeling approach as in the previous Chapter 2 but in two dimensions (2D).

3.1 Preliminaries

In case of traffic modeling on large-scale urban networks, one needs to look for macroscopic approaches due to increasing computational complexity. However, prior to [142] who used data from microsimulations, there has been no evidence of any existence of macroscopic relation between density and flow on a city level as it was established on single roads by Greenshields [58]. Later, in 2008, Geroliminis and Daganzo observed a similar relation during data collection in a real-life experiment conducted during a rush-hour in the city of Yokohama, Japan [53, 40]. The discovery of the so-called *macroscopic fundamental diagram* (or shortly, MFD) gave rise to reservoir models, which track the number of cars in a urban area. MFD-based models are intuitive, simple, and do not require a high computational effort to be applied. For an MFD to be well-defined, there must exist only one flow value for a given number of vehicles. This feature is preserved only in regions that consist of links that have similar congested levels, while this causes problems in case of regions with heterogeneous links. To overcome this problem, [63, 87] presented partitioning algorithms that intend to split an urban area into multiple homogeneous zones each having its own well-defined MFD.

3.1.1 LWR model in 2D

Let us present here a macroscopic model presented in [103] that corresponds to a conservation law on a two-dimensional plane, where the conserved quantity is the total number of vehicles in this plane. This model will be used to investigate the macroscopic traffic behaviour in a urban network that is represented by a 2D continuum plane $(x, y) \in \Omega \in \mathbb{R}^2$ that is a bounded rectangular domain, i.e., $\Omega : [x_{min}, x_{max}] \times [y_{min}, y_{max}]$. The size of the rectangular domain is determined by the size of the urban network, i.e., x_{min} is associated to the intersection with the minimal x space coordinate among all intersections (the rest is defined similarly).

This 2D model can be seen as an extension of the classical 1D LWR model (2.1) to two dimensions that describes the traffic density evolution over a continuum plane $\forall(x, y, t) \in$

$\Omega \times \mathbb{R}^+$ as:

$$\begin{cases} \dfrac{\partial \rho(x,y,t)}{\partial t} + \nabla \cdot \vec{\Phi}(x,y,\rho(x,y,t)) = 0, \\ \rho(x,y,0) = \rho_0(x,y), \end{cases} \tag{3.1}$$

where $\rho(x,y,t) : \Omega \times \mathbb{R}^+ \to \mathbb{R}^+$ is now a two-dimensional density that aggregates the number of vehicles per square meter, $\rho_0(x,y)$ is its value at initial time. The flux function in (3.1) is now an explicitly space-dependent vector function with the magnitude $\Phi(x,y,\rho) : E \to [0, \phi_{max}]$ with the set of departure being $E = \{(x,y,\rho) : (x,y) \in \Omega,\ \rho \in [0, \rho_{max}(x,y)]\}$. The flux magnitude $\Phi(x,y,\rho)$ is again a concave Lipschitz continuous function that reflects the empirically established law relating the average 2D flow with the average 2D density (fundamental diagram), i.e., $\phi(x,y,t) = \Phi(x,y,\rho)$. The flux vector function is then defined as a product of the magnitude $\Phi(x,y,\rho)$ and the direction vector $\vec{d_\theta}$ (unit vector):

$$\vec{\Phi}(x,y,\rho) = \Phi(x,y,\rho)\vec{d_\theta}(x,y), \tag{3.2}$$

where

$$\vec{d_\theta} = \begin{pmatrix} \cos(\theta(x,y)) \\ \sin(\theta(x,y)) \end{pmatrix} \tag{3.3}$$

is a vector that depends on the network geometry given by angle $\theta(x,y) : \Omega \to [0, 2\pi)$ that must be smooth enough (more details on its smoothness are given in Section 3.2). Angle $\theta(x,y)$ is related to the orientation of roads in a urban network, thus, it determines the direction of traffic flow. Hence, from now on, we will call $\vec{d_\theta}$ the *direction field* to stress its physical meaning. The details on how to obtain this vector $\vec{d_\theta}(x,y)\,\forall(x,y) \in \Omega$ are given in Section 3.1.3.1. Finally, the nabla operator in (3.1) is defined as

$$\nabla = \left(\frac{\partial}{\partial x}, \frac{\partial}{\partial y} \right).$$

Thus, the divergence term $\nabla \cdot \vec{\Phi}(x,y,\rho(x,y,t))$ in (3.1) is a scalar. The existence and uniqueness of solutions for a system like (3.1) were shown in [81] (see p.223 for the conditions of uniqueness, and existence is discussed on p.230). The boundary conditions of (3.1) will be discussed later in Section 3.1.4.

As the 2D model (3.1) represents an extension of the standard 1D LWR model (2.1), their units and structure are compared in Table 3.1. In general, 2D models like (3.1) are not expected to describe very precisely the density evolution in space coordinates. They are rather used to capture the main traffic features on a global scale such as the location and propagation of congested areas in a transportation network.

Table 3.1: Comparison of 2D and 1D LWR models

	1D LWR	2D LWR
density	$[\rho]$ = veh/m (scalar)	$[\rho]$ = veh/m^2 (scalar)
velocity	$[v]$ = m/s (scalar)	$[\vec{v}]$ = m/s (vector)
flux	$[\Phi]$ = veh/s (scalar)	$[\vec{\Phi}]$ = veh/(s·m) (vector)
equation	$\partial_t \rho + \partial_x \Phi(\rho) = 0$	$\partial_t \rho + \nabla \cdot \vec{\Phi}(x,y,\rho) = 0$

3.1.2 Space-dependent fundamental diagram

In general, the flux magnitude in 2D (3.1) is very similar to the flux function in 1D (e.g., it can be the triangular FD (2.2)) both being Lipschitz continuous concave functions. However, unlike in the 1D case, the 2D flux magnitude $\Phi(x, y, \rho)$ incorporates network infrastructure parameters by having an explicit space-dependency. Imagine a urban network containing roads that may have different speed limits and number of lanes, i.e., roads usually have different transportation capacities. For instance, compare some major three-lane roads with 50 km/h as a speed limit with minor single-lane roads with 30 km/h that can clearly accommodate less cars than the major roads. This kind of infrastructure differences are captured by space-varying parameters $\rho_{max}(x, y)$, $\rho_c(x, y)$ and $v(x, y)$. Thus, we can see that in a 2D representation of traffic, the assumption that the FD parameters are identical everywhere, does not hold any more, since the network geometry should also be taken into account.

All these parameters still have the same physical meaning as in the 1D case introduced in Sections 2.1.1 and 2.1.2, but their units are consistent with those in Table 3.1. For example, $\rho_{max}(x, y)$ and $\rho_c(x, y)$ are referred to the maximal and the critical number of cars per square meter (veh/m^2), correspondingly. Thus, space-dependent fundamental diagrams are functions with space-dependent parameters, e.g., the triangular FD is defined $\forall(x, y, \rho) \in E$ as:

$$\Phi(x, y, \rho) = \begin{cases} v(x, y)\rho, & \rho \in [0, \rho_c(x, y)], \\ -\omega(x, y)(\rho - \rho_{\max}(x, y)), & \rho \in (\rho_c(x, y), \rho_{max}(x, y)], \end{cases} \tag{3.4}$$

and, similarly, the Greenshields space-dependent FD is defined $\forall(x, y, \rho) \in E$ as:

$$\Phi(x, y, \rho) = v_{max}(x, y) \left(1 - \frac{\rho}{\rho_{max}(x, y)}\right) \rho. \tag{3.5}$$

Note that all FDs can still be depicted as in Figures 2.1a) and 2.1b) having in mind that they can have different peaks and slopes for different space points $(x, y) \in \Omega$.

3.1.3 Continuous approximation of parameters

In general, two-dimensional continuum models with a structure similar to (3.1) are commonly used in pedestrian (crowd) modeling [64, 71]. It is however worth noting that crowds evolve in open spaces, and, unlike vehicles, pedestrians are not constrained to move on traffic roads. Here, we are going to use the 2D model (3.1) to predict the propagation of traffic in a urban network, which represents a set of roads (links) and intersections (nodes). Thus, the equation (3.1) is a valid model for traffic modeling, if we assume that the urban network is dense enough to be approximated as a continuum. As already mentioned above, we will use the network geometry to parametrize the model, e.g., we will estimate the values of velocity and direction field as a function of the distance to physical roads. Let us explain parametrization on an example of a flux with the magnitude corresponding to the Greenshields FD:

$$\vec{\Phi}(x, y, \rho) = v_{max}(x, y)\vec{d}_\theta(x, y) \left(1 - \frac{\rho}{\rho_{max}(x, y)}\right) \rho. \tag{3.6}$$

3.1.3.1 Inverse distance weighting

From (3.1) and (3.6) we can see that the traffic flow direction is determined by the *velocity field*, which is a product of direction field $\vec{d}_\theta$ (3.3) and the maximal kinematic wave speed v_{max}. Thus, we expect more traffic to be concentrated in areas with densely located roads and along roads with high speed limits, e.g., highways. We achieve that by applying the *inverse distance weighting* method (IDW), which assignes larger weights to space points that are close to roads, see [103] for a detailed explanation, while in the next paragraph we will give a brief idea.

Let us denote roads of the network by $q \in \{1, \dots, Q\}$. For the sake of computation, each road is parametrized by $s \in \{1, \dots, s_{max}\}$ such that variable s allows to progress along the road curvature from one intersection to the next one. Then, the velocity field $\vec{d}_\theta(x,y)\, v_{max}(x,y)$ can be computed $\forall (x,y) \in \Omega$ as:

$$\vec{d}_\theta(x,y)\, v_{max}(x,y) = \frac{\sum_{q=1}^{Q} \sum_{s=1}^{s_{max}} w\left(\|(x,y) - p(q,s)\|\right)\, \vec{d}_{\theta_q}\, v_{max_q}}{\sum_{q=1}^{Q} \sum_{s=1}^{s_{max}} w\left(\|(x,y) - p(q,s)\|\right)}, \tag{3.7}$$

where $p(q,s)$ is the spatial coordinate of cell s of road q, and the weighting function $w(l) : \mathbb{R}^+ \to \mathbb{R}^+$ is a decreasing function of the (Euclidean) distance, e.g., here we use the exponential function:

$$w(l) = e^{-\mu l} \quad \text{and} \quad l = \sqrt{(x - p(q,s)_x)^2 + (y - p(q,s)_y)^2},$$

where μ is a weighting parameter that needs to be tuned according to the desired "accuracy" of reproducing the network structure in a 2D representation: for a small μ the velocity field follows only the global trend of the network geometry, while for a large μ the velocity field follows the roads in a detailed way. These two extreme cases are illustrated in Figure 3.1, where a small Manhattan grid area is taken as a network example.

In this work, we would like to capture the evolution of a 2D vehicle density quite accurately but without over-resolving the network geometry, for example, see Figure 3.2a) that illustrates the direction field estimated for $\mu = 50$ for a network representing the city center of Grenoble of the total area 1×1.4 km^2. Thereby, we can also notice that the integral lines of the direction field drawn in Figure 3.2b) do not cross. This results from the model structure, since the integral lines can be seen as unique solutions to the differential equation governed by $\vec{d}_\theta$. Moreover, we assume that there are no loops in the urban network, i.e., there exists a preferred direction of motion. Indeed, if there would be a loop, then there would be a point inside of every loop where θ is undefined, since the direction lines cannot cross each other. Moreover, any loop would have no boundary, thus the cars following this path would never be created nor destroyed. The condition on not having loops plays an essential role in the coordinate transformation that will be explained in Section (3.2). In terms of integral lines, we require that any integral line of the directional field $\vec{d}_\theta$ begins and ends at the boundary of the domain. In terms of network structure, we consider only networks (or urban areas) with uni-directional roads that are located such that no loops arise. This is the main restriction of

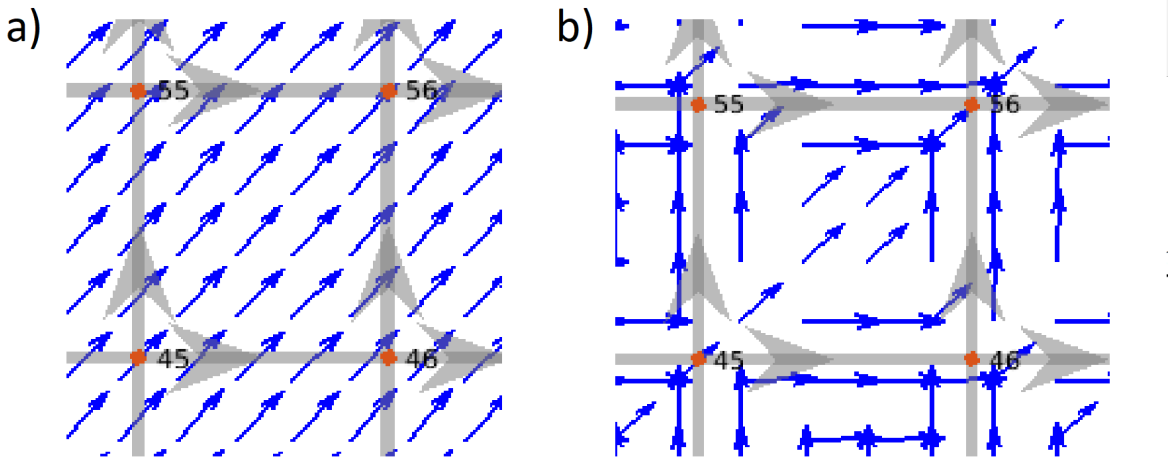

Figure 3.1: Direction field estimation (blue arrows) for: a) small $\mu = 10$, b) large $\mu = 100$. The figure is taken from Chapter 2 of [101]. Grey arrows indicate the direction of real roads in a Manhattan-grid network.

the model (3.1), which limits its usability for general traffic applications although being still useful in several situations. For example, imagine a rush hour (e.g., at 9 am), when many people are driving to the business center of the city located in some particular point, then the assumption of the preferred direction of motion is realistic.

Thus, equation (3.7) constructs a velocity field $\vec{d}_\theta(x,y)\, v_{max}(x,y)$ at any point in the domain as a normalized weighted average of the road directions $\vec{d}_{\theta_q}\, v_{max_q}$ such that the traffic flow direction at some point is mostly impacted by the nearest roads to this point.

3.1.3.2 Kernel density estimation

To complete the definition of FD parameters, we also need to determine density-related parameters of the fundamental diagram, i.e., the critical density $\rho_c(x,y)$ and the maximal density $\rho_{max}(x,y)\ \forall(x,y) \in \Omega$. Let us first concentrate on the maximal density $\rho_{max}(x,y)$, and then it will be straightforward to determine $\rho_c(x,y)$, if we know the particular FD shape, e.g., from real traffic measurements.

In a 2D representation of traffic, the maximal density depends not only on the number of lanes of particular roads but can also increase in areas with high concentration of roads. In order to estimate $\rho_{max}(x,y)\ \forall(x,y) \in \Omega$, we fill each road of the network by placing a vehicle at a minimum headway distance of 6 m, since this is an approximate distance between two consecutive vehicles in a traffic jam. Thus, we place vehicles as close as possible to determine the maximal density by using the *kernel density estimation* (KDE).

The idea of this method is that each individual vehicle contributes to the total vehicle density as a Gaussian function with a kernel located around the vehicle position. The total estimated density then corresponds to the superposition of all their contributions.

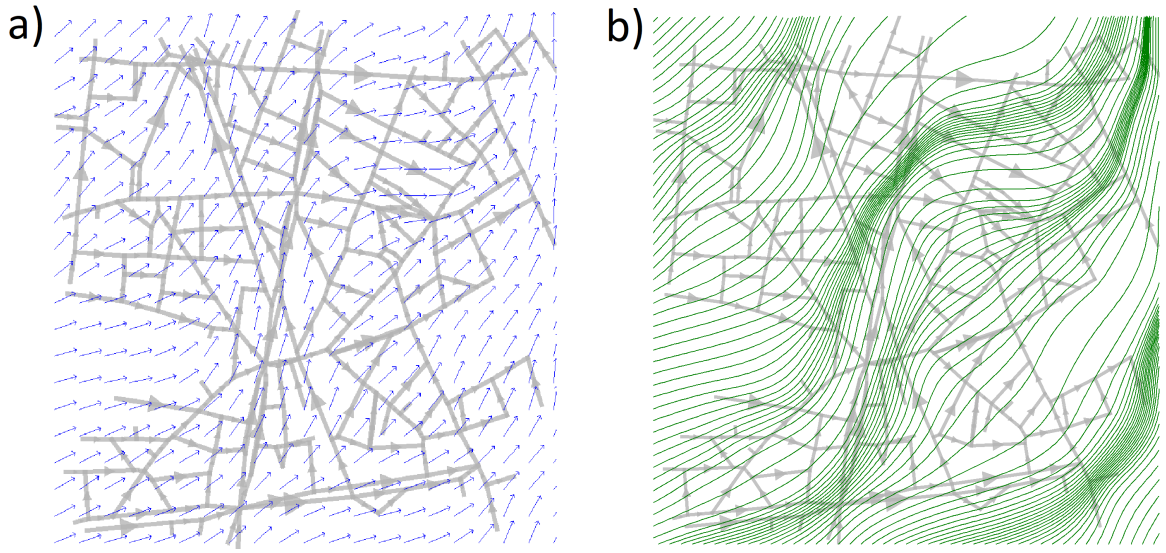

Figure 3.2: Result for an intermediate value of the weighting parameter $\mu = 50$: a) estimated direction field (blue arrows), b) integral lines of traffic flow direction (tangent of $\vec{d_\theta}$). Grey lines represent real roads in Grenoble city center, arrows indicate the direction of traffic.

Let the position of a vehicle $v \in \{1, \dots, V(t)\}$ be denoted by $(x_v(t), y_v(t))$ at some time t. Then, the vehicle density can be estimated as follows:

$$\tilde{\rho}(x, y, t) = \frac{1}{2\pi d_0^2} \sum_{v=1}^{V(t)} e^{-\frac{1}{2d_0^2}\left((x-x_v)^2+(y-y_v)^2\right)}, \tag{3.8}$$

where d_0 is a standard deviation of a Gaussian function. Note that Gaussians are used to preserve the conservation of vehicles, since density integrals are normalized to 1.

Parameter d_0 in (3.8) determines the range of impact of the Gaussian kernel that has to be chosen. For example, in Figure 3.3b) we can see how equidistant vehicles on a road contribute to the global density by its Gaussian functions. In the upper plot, each car has an impact on the density in the range of $d_0 = 25$ m around its position, which results into a constant density along the road. The lower plot illustrates the situation when the range of impact is set to $d_0 = 100$ m, which is too high, since then the reconstructed density has a bell shape due to boundary effects. There are several works regarding the optimal choice of this parameter, see [47, 48]. The authors rely on the idea that the parameter d_0 should be chosen such that equidistant cars should provide constant density.

The same qualitative effects can be observed also in 2D, see [103] for more details. Note that the maximal density ρ_{max} can be estimated by KDE (3.8), with the only difference being that all the vehicles are placed as densely as possible. An application example of KDE is illustrated in Figure 3.3a), where the density (colormap value) is obtained by using KDE from vehicles' positions denoted by blue dots. The positions of vehicles were generated using commercial software Aimsun that takes any network geometry as input and produces microsimulations of traffic on this network with the possibility to specify boundary inflows. Note that unlike

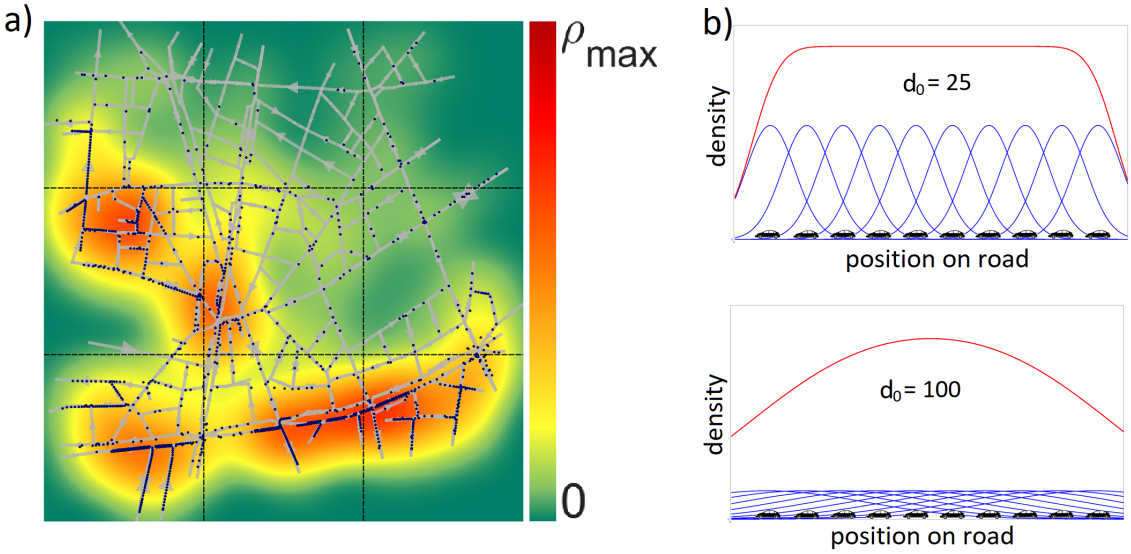

Figure 3.3: Density reconstruction from car positions by KDE: a) 2D density is reconstructed from vehicle positions (blue dots) that move along a network with the geometry of Grenoble city center (grey arrows), b) 1D density estimation from equidistant vehicles with Gaussians having different standard deviations: $d_0 = 25$ m (upper plot) and $d_0 = 100$ m (lower plot).

in previous density representation in 1D, the colormap in Figure 3.3a) is used to denote the ratio of the density value to the maximal density over the whole network (absolute maximal density), i.e., $\rho_{max} = \max\limits_{(x,y)\in\Omega} \rho_{max}(x,y)$. Moreover, due to the space-dependency of FD, the critical density $\rho_c(x,y)$ is different $\forall (x,y) \in \Omega$.

3.1.4 Boundary conditions

To complete the 2D LWR model (3.1) that describes traffic dynamics on a bounded domain, we need to introduce the boundary conditions, as we did in Section 2.1.4 for the 1D case.

Define a set $\Gamma \subset \Omega$ as the boundary of a rectangular domain Ω. The boundary consists of two subsets $\Gamma = \Gamma_{in} \cup \Gamma_{out}$. Thereby, Γ_{in} is a set of boundary points (x,y) for which $\vec{n}(x,y)\cdot\vec{d}_\theta(x,y) > 0$, where $\vec{n}(x,y)$ is a unit normal vector to the boundary oriented inside the domain. In a similar way, we also define Γ_{out} such that $\forall (x,y) \in \Gamma_{out} : \vec{n}(x,y)\cdot\vec{d}_\theta(x,y) < 0$.

Now let us fix boundary flows $\phi_{in}(x,y,t)$ and $\phi_{out}(x,y,t)$ for the 2D system given by (3.1) and formulate the following IBVP:

$$\begin{cases} \dfrac{\partial \rho(x,y,t)}{\partial t} + \nabla \cdot \vec{\Phi}(x,y,\rho(x,y,t)) = 0, \\ \vec{\Phi}(x,y,t) = \begin{cases} \phi_{in}(x,y,t)\vec{d}_\theta(x,y), & \forall (x,y) \in \Gamma_{in} \\ \phi_{out}(x,y,t)\vec{d}_\theta(x,y), & \forall (x,y) \in \Gamma_{out} \end{cases} \\ \rho(x,y,0) = \rho_0(x,y), \end{cases} \tag{3.9}$$

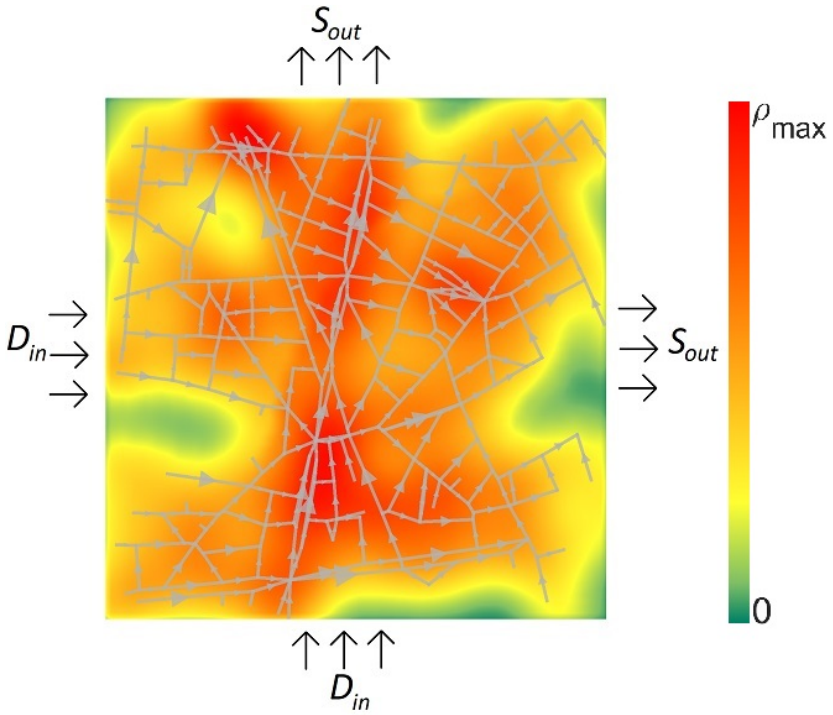

Figure 3.4: The vehicle density in a 2D domain with indicated upstream and downstream boundaries. The underlying network geometry corresponds to Grenoble city center (grey arrows).

where inflows $\phi_{in}(x, y, t)$ and outflows $\phi_{out}(x, y, t)$ are defined as

$$\begin{cases} \phi_{in}(x, y, t) = \min\left\{D(\rho_{in}(x, y, t)), S\left(\rho(x, y, t)\right)\right\}, & (x, y) \in \Gamma_{in} \\ \phi_{out}(x, y, t) = \min\left\{D\left(\rho(x, y, t)\right), S\left(\rho_{out}(x, y, t)\right)\right\}, & (x, y) \in \Gamma_{out} \end{cases} \tag{3.10}$$

where $D(\rho)$ and $S(\rho)$ are demand and supply functions defined as in Section 2.1.5 but depending on space and in two dimensions. The well-posedness of IBVP given by (3.9) and (3.10) will be discussed in Section 3.2.

The upstream Γ_{in} and downstream Γ_{out} boundaries are the ones that should be actuated when it comes to control applications. As an illustrative example, these boundaries are indicated by black arrows in Figure 3.4.

3.1.5 Comparison between 2D LWR and MFD-based models

This section is devoted to the comparison between the newly introduced continuum model in 2D (3.9) to reservoir models based on a macroscopic fundamental diagram, which are very popular in traffic applications due to their simplicity. We seek to show that 2D conservation law models such as (3.9) have their own advantages. By running the same traffic scenario on a Manhattan grid network with these two different approaches and comparing the steady state results to those predicted by microsimulator Aimsun, we will motivate the use of the

2D LWR model that can be a reasonable choice for many traffic control applications in large urban networks.

3.1.5.1 Macroscopic fundamental diagram

As described in [3], MFD-based models (also known as reservoir models) describe the evolution of accumulation of vehicles in some urban zone. Let us consider a heterogeneous network partitioned into N reservoirs, e.g., $N = 4$ as illustrated in Figure 3.5. Let $n_i(t)$ be the accumulation of vehicles in reservoir i at time t. The main assumption of reservoir models is the existence of MFD $\phi_i(n_i(t))$, which relates the number of cars in a reservoir i with the outflow from this reservoir $\phi_{i,out}$. Let us also define $\mathcal{N}_{in,i}$ as a set of neighboring reservoirs, from which cars can directly reach reservoir i, and $\mathcal{N}_{out,i}$ as a set of neighboring reservoirs that can be directly reached by cars from reservoir i, as illustrated in Figure 3.5. Then, the rate of change in the number of cars $n_i(t)$ in reservoir i is given by the difference in its inflow and outflow, that is:

$$\begin{aligned} &\frac{dn_i(t)}{dt} = \phi_{in,i}(t) - \phi_{out,i}(t), \quad \text{with} \\ &\phi_{in,i}(t) = \sum_{j \in \mathcal{N}_{in,i}} r_{ji} \min\{D_j, S_i\} \quad \text{and} \quad \phi_{out,i}(t) = \sum_{j \in \mathcal{N}_{out,i}} r_{ij} \min\{D_i, S_j\}, \end{aligned} \tag{3.11}$$

where r_{ji} and r_{ij} are numbers of roads leading from reservoir j to reservoir i and from reservoir i to reservoir j, respectively. Demand D_i and supply S_i functions are defined as

$$D_i(n_i(t)) = \begin{cases} \phi_i(n_i(t)), & \text{if} \quad n_i < n_{c,i} \\ \phi_{max,i}, & \text{if} \quad n_i \geq n_{c,i} \end{cases} \quad S_i(n_i(t)) = \begin{cases} \phi_{max,i}, & \text{if} \quad n_i \leq n_{c,i} \\ \phi_i(n_i(t)), & \text{if} \quad n_i > n_{c,i}, \end{cases} \tag{3.12}$$

thereby, n_c denotes the critical car number that has the same implication as the critical density ρ_c in (3.4), i.e., we observe the free-flow regime if $n_i \leq n_c$, otherwise it indicates that the congestion has occurred. We compute MFD for each reservoir by using the GPS data (velocities) from the microsimulator Aimsun at each t:

$$\phi_i(n_i(t)) = \left(\frac{1}{n_i} \sum_{m=1}^{n_i(t)} v_{im} \right) \left(\frac{n_i}{\sum_{q=1}^{Q_i} L_{iq}} \right) = \frac{1}{\sum_{q=1}^{Q_i} L_{iq}} \sum_{m=1}^{n_i(t)} v_{im},$$

where L_{iq} corresponds to the length of road $q \in \{1, \ldots, Q_i\}$ in reservoir i, and v_{im} is the velocity of vehicle m in reservoir i. Note this expression is the product of average velocity and density in reservoir i. Having data as (n_i, ϕ_i), we fit a cubic polynomial as it was done in [3], and extract the maximal flow $\phi_{max,i}$. The final step to complete the definition of MFD is to get the maximal car number obtained by counting cars placed in a reservoir at the minimal headway distance (6 meters).

[3] presented a method to perform a network partition depending on the traffic state such that each part has its own well-defined MFD (low scattering of the MFD curve). However, to

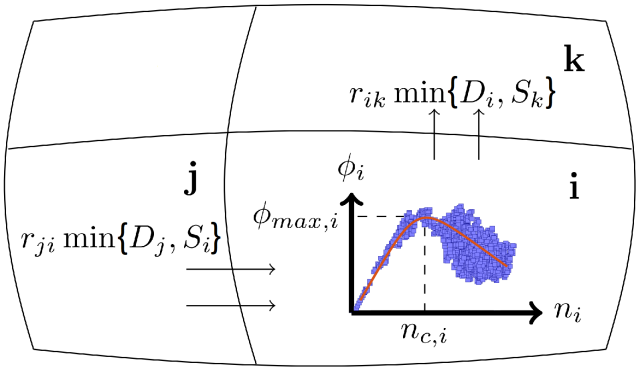

Figure 3.5: Schematic illustration of a network divided into $N = 4$ zones. The variables are defined with respect to reservoir i, which has its own MFD $\phi_i(n_i)$ (fitted data, in red) with the maximum flow $\phi_{max,i}$ attained with the critical number of cars $n_{c,i}$. The change in vehicle's accumulation $n_i(t)$ is determined by flows from $\mathcal{N}_{in,i} = \{j\}$ and by flows into $\mathcal{N}_{out,i} = \{k\}$.

make a fair comparison between MFD-based models (3.11) and 2D LWR (3.9), we divide a Manhattan grid network into $N = 16$ equal parts each having its own MFD, and then compare the steady states achieved by using two different models with the steady state obtained by using the microsimulator Aimsun for the same inflow and outflow data.

A steady state in a reservoir model is reached when the accumulation of vehicles stops changing its value over time, i.e., $dn_i(t)/dt = 0\ \forall i \in \{1, \dots, N\}$. Further, by (3.11) we obtain for each reservoir i that the number of cars is preserved whenever inflow equals to outflow:

$$\phi^*_{in,i}(t) = \phi^*_{out,i}(t), \tag{3.13}$$

where the asterisk is used to denote a steady state.

We will compare steady states predicted by both models (3.1) and (3.11) with the one obtained with microsimulator Aimsun, which simulates the dynamics of vehicle positions in a given urban area. The vehicle positions are then used to reconstruct the density using the kernel density estimation method that was presented in Section 3.1.3.2.

To enable a quantitative comparison of steady states, we will compute the L_2 norm of the deviation of the density predicted by one of the models $\rho^*_{\text{pred}}(x, y)$ from the "ground true" distribution $\rho^*_{\text{sim}}(x, y)$ obtained by Aimsun in the steady state, i.e.,

$$\|\tilde{\rho}^*(x, y)\|_2\,, \quad \text{where} \quad \tilde{\rho}^*(x, y) = \rho^*_{\text{pred}}(x, y) - \rho^*_{\text{sim}}(x, y).$$

The L_2 norm in 2D is computed as in (1.7). Note that in case of MFD-based model, $\rho^*_{\text{pred}}(x, y)$ is a piecewise constant function obtained from the accumulation of vehicles in a zone multiplied by its area.

3.1.6 Scenario description

We consider a 10×10 Manhattan grid network with a total surface of 1 km^2, which is drawn by grey lines on all three plots of Figure 3.6. Positions of nodes (intersections) are slightly disordered with white noise of standard deviation that equals 10 m. We assume that all roads are single-lane and are globally oriented towards the North-East direction (grey arrows in Figure 3.6 are used to point the direction of traffic on each road). The network contains a topological bottleneck in the middle, e.g., a river with some bridges. The speed limits on most of the roads are set to 30 km/h, and there are also two roads with 50 km/h.

In order to obtain a non-trivial congestion pattern in the steady state, we create a congestion formation scenario in the Western part of the network, while the rest of the network should remain in the free-flow regime. We achieve that by setting appropriate inflows (demand functions). The domain contains 15 incoming roads in total: 8 roads are coming from the North and 7 are coming from the West. We can identify the incoming roads from Figure 3.6a), where the green and red arrows are assigned to points, through which vehicles enter the domain. Thereby, we provide a large demand in the South-Western area by setting $D_{in} = 1200$ veh/h on 8 incoming roads (red arrows), while a lower demand $D_{in} = 300$ veh/h is created for the remaining boundary roads (green arrows). Notice that veh/h is the basic Aimsun unit for traffic flow, while this should be veh/s in the 2D LWR model, which we can easily get by dividing by 3600. Although we have marked these arrows only for the results related to the MFD-based simulation, the same inflow values are set at the same points in Aimsun (Figure 3.6c)).

We set the inflow demand at the upstream boundary for the numerical simulation of the 2D model (3.9) by deploying the 1D kernel density estimation method. Namely, KDE is used to reconstruct the density created by vehicles entering the domain through the continuous boundary line. The numerical scheme for 2D LWR system given by (3.9) was discussed in [103]. The brief idea is to perform dimensional splitting, and then for each dimension the numerical flux is computed using the Godunov scheme. However, the simulation result in Figure 3.6 was obtained with our own numerical method for this model that will be presented later in the next section. To produce the result depicted in Figure 3.6b), we perform a numerical simulation of vehicle density governed by a 2D model, until the steady-state is reached. It is also worth noting that the supply of the downstream boundary is set to ϕ_{max} so that cars can freely leave the domain. Notice that the result in Figure 3.6b) was obtained with a low weighting parameter $\mu = 20$ for the continuous approximation of velocity field (see Section 3.1.3.1).

Thus, we run a dynamic scenario on Aimsun for 2 hours of simulation time setting the time-constant inflow values indicated above. Thereby, we see that the shape of a congested zone does not change much after a certain simulation time indicating that the steady-state was reached. In order to set up a simulation, Aimsun requires also to define turning ratios at each intersection. A turning ratio is assigned to a pair of roads i and j connected by a junction, and it denotes a percentage of vehicles that turn from road i to road j. On a global scale, turning ratios determine the overall traffic flow direction. Since the applicability of the 2D

LWR model (3.9) is limited to networks that have a preferred direction of motion, we set the turning ratios accordingly. Thus, at each 2×2 intersection, 75% of vehicles will turn and the rest 25% continue moving straightforward, while at each 1×2 intersection the turning ratios are set to 50%. During the Aimsun simulation, we save the position of all cars at each time step, i.e., generate car trajectories. Finally, from the vehicle positions (blue dots in Figure 3.6c)) we reconstruct a two dimensional density using KDE (see Section 3.1.3.2). The density in Figure 3.6c) was estimated with a Gaussian standard deviation $d_0 = 50$ m, i.e., we assume that every car contributes to the total density in 50 m range around its position. Finally, the state governed by the MFD-based model (3.11) was updated using the forward Euler method with the time step $\Delta t = 0.01$ until the convergence to the steady state (3.13) was reached.

3.1.7 Comparison of steady states

In Figure 3.6 we present the steady state results predicted by the MFD-based model (panel a)), the numerical simulation of 2D LWR (panel b)) and those obtained by running a simulation on Aimsun (panel c)). For the case with MFD, we performed a partition into 16 zones (black dashed lines). Then, we used Aimsun velocity data to define MFD for each zone as described in Section 3.1.5.1, and using (3.11) we find the number of cars for each zone n_i^*, as depicted in Figure 3.6a). Then, the vehicle density in each reservoir $i \in \{1, \dots, N\}$ is obtained by:

$$\rho^*_{\text{mfd}}(x, y) = \frac{n_i^*}{s_i}, \quad \text{where} \quad i : (x, y) \in R_i, \tag{3.14}$$

where s_i is the area (in m^2) of reservoir with index i, and R_i is the domain taken by this reservoir.

By comparing Figures 3.6a) and 3.6c), we can see that the MFD-based model captures quite well the phenomenon of traffic congestion in zones where it arises, although it provides only 16 values in our case. To enable a quantitative comparison, we use (3.14) to compute the L_2 norm of the deviation from Aimsun and obtain $\|\tilde{\rho}^*(x, y)\|_2 = 0.58$, where $\tilde{\rho}^*(x, y)$ is the difference in the steady state densities predicted by MFD-based model and Aimsun.

By comparing Figures 3.6b) and 3.6c), we can observe that both steady states look very similar, the congestion shape reproduced by the 2D LWR model (3.9) looks even better than in the case of MFD-based model (3.11). For a quantitative comparison, we again compute the L_2 norm and obtain $\|\tilde{\rho}^*(x, y)\|_2 = 0.38$, which is a way smaller value than in the case with MFD. Thus, the steady state obtained by numerical simulation of 2D LWR captures the spatial distribution of congestion significantly better than the result predicted by numerical integration of MFD-based model.

There exist also other arguments to prefer the 2D continuum model to MFD-based models in several situations. Thus, MFD-based models are discrete in space and, by their nature, they do not really enable us to develop model-based control approaches. This is related to the fact that the result of the network partitioning algorithm as in [3] depends on the current traffic state for MFD-based models, since the main point thereby is to define zones consisting of roads with similar congestion levels. Thus, if traffic conditions change, e.g., a higher inflow

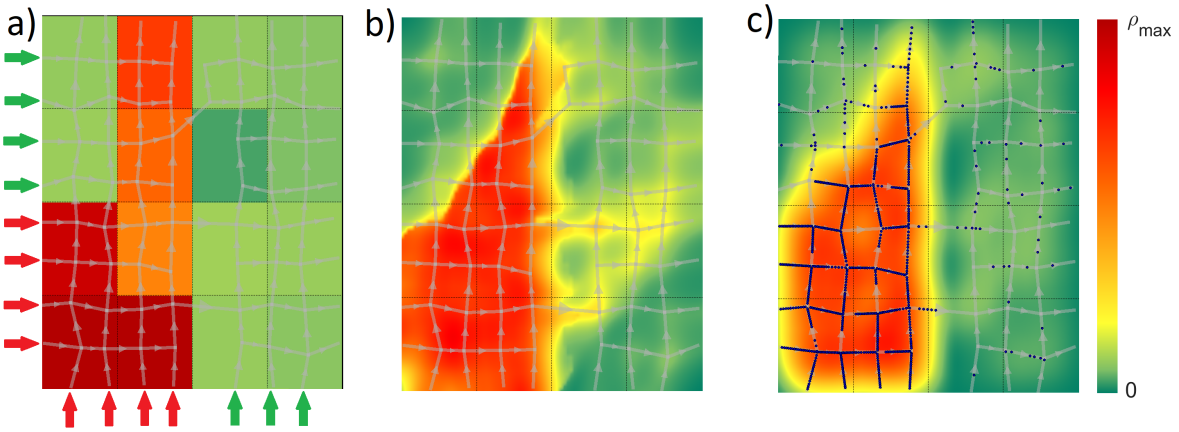

Figure 3.6: Steady-states obtained by: a) MFD-based model, b) numerical simulation of 2D LWR, c) microsimulator.

comes through roads that did not provide a high inflow before, this might lead to invalid MFDs, which causes the necessity to perform the network partitioning again. Moreover, even for stationary inflows, the performance of the model degrades as reservoirs' areas enlarge.

Thus, we have shown that the 2D LWR model is a beneficial representation of traffic, especially in a urban network with multiple congestion zones that may relocate in time. The 2D LWR model is a scalable model and it does not cost a high computational effort to be applied. Moreover, unlike MFD-based models, it is able to track the shape of congestion evolution quite well without the necessity to perform network partitioning. In the next Section 3.2 we will present a method to translate the 2D LWR model in a form that can be easily analyzed for a large variety of model-based control design tasks that will be considered in the current chapter.

3.2 Curvilinear coordinate transformation

The structure of the 2D LWR model (3.9) implies that the direction field of traffic flow $\vec{d}_\theta$ given by (3.3) depends only on the network geometry and not on the state. This enables us to describe the traffic flow trajectories that do not change with time. These trajectories are obtained by building tangents to the direction field $\vec{d}_\theta$. This gives us the integral lines illustrated in Figure 3.2b).

In the following, we will perform a **curvilinear coordinate transformation** that translates these integral curves into a set of straight parallel lines as illustrated in Figure 3.7. Afterwards, a traffic state evolving along a straight line can be treated as a 1D system, which would significantly simplify any analysis of the 2D system (3.9).

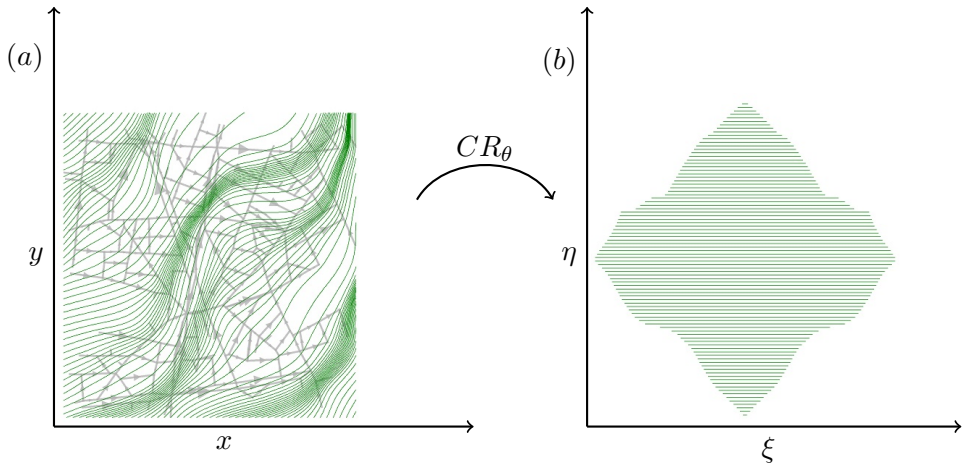

Figure 3.7: Coordinate transformation mapping: (a) curved trajectories in Grenoble downtown in (x, y)-plane into (b) straight lines in (ξ, η)-plane.

3.2.1 General idea

Let us assume that angle $\theta \in C^1(\Omega)$. We introduce new coordinates (ξ, η) in a differential form:

$$\begin{pmatrix} d\xi \\ d\eta \end{pmatrix} = C(x,y)R_\theta(x,y) \begin{pmatrix} dx \\ dy \end{pmatrix}, \tag{3.15}$$

where $R_\theta(x, y)$ is a *rotation* matrix given by

$$R_\theta(x,y) = \begin{pmatrix} \cos(\theta(x,y)) & \sin(\theta(x,y)) \\ -\sin(\theta(x,y)) & \cos(\theta(x,y)) \end{pmatrix}, \tag{3.16}$$

and $C(x, y)$ is a diagonal *scaling* matrix given by

$$C(x,y) = \begin{pmatrix} \alpha(x,y) & 0 \\ 0 & \beta(x,y) \end{pmatrix}, \tag{3.17}$$

where $\alpha(x, y)$ and $\beta(x, y)$ are positive and bounded scaling parameters needed for the existence of the coordinate transformation (will be defined later in this section).

Thus, matrix $R_\theta(x, y)$ provides the rotation of the integral lines in (x, y)-plane, and the scaling matrix $C(x, y)$ acts such that these lines have the same metric, see Figure 3.7. In Figure 3.7a) we have used the topological structure of Grenoble downtown (the same as in Figure 3.2) where the direction at each road is set such that loops and flow crossings are impossible, i.e., all roads need to be uni-directional and there exists a preferred direction of motion. Thus, on a global scale, the motion on this network is oriented towards North-East of the city.

3.2.2 Intuition: straight lines

In the case of straight lines depicted in Figure 3.7b) we have $\theta = 0\ \forall(x, y) \in \Omega$, which implies that the rotation (3.16) and scaling matrices (3.17) become identity matrices, i.e., $C = R_\theta = \mathbb{I}$. Then, by (3.15) the new coordinates (ξ, η) would completely coincide with (x, y) up to a constant shift. In this case, the direction field defined in (3.3) becomes $\vec{d}_\theta(\xi, \eta) = (1, 0)$, and by (3.2) we obtain:

$$\vec{\Phi} = \Phi(\xi, \eta, \rho) \begin{pmatrix} 1 \\ 0 \end{pmatrix}, \tag{3.18}$$

which can be inserted into the divergence term in (3.9) resulting into:

$$\begin{pmatrix} \frac{\partial}{\partial \xi}, & \frac{\partial}{\partial \eta} \end{pmatrix} \begin{pmatrix} 1 \\ 0 \end{pmatrix} \Phi(\xi, \eta, \rho) = \frac{\partial \Phi(\xi, \eta, \rho)}{\partial \xi}. \tag{3.19}$$

Notice that in case of straight lines, the divergence (3.19) contains only one term instead of two as it was in the original system with curved trajectories (3.9). Thus, the traffic flow evolves only along ξ coordinates, which are tangent to the flow motion. At the same time there is no motion in the orthogonal direction of η, which can be treated as a parameter (a label numbering the flow path). Afterwards, we can treat each such line of constant η as a 1D equation, for which we will be able to solve different control tasks.

3.2.3 Curvilinear coordinate transformation

After providing an intuitive explanation on how this coordinate transformation should work, let us first define scaling parameters α and β from (3.17). Then, we will be able to perform the coordinate transformation of the original 2D system (3.9) in order to turn it into a continuous 1D LWR model like (2.10) parametrized by an additional parameter $\eta \in \mathbb{R}$ used to label the flow paths.

Lemma 3.1. *Assume $\theta \in C^1(\Omega)$ and $\alpha, \beta \in C^1(\Omega)$. Then there exists a bijective transformation (ξ, η) in $C^2(\Omega)$ satisfying (3.15) if and only if the following PDEs hold $\forall(x, y) \in \Omega$:*

$$-\sin\theta \frac{\partial(\ln\alpha)}{\partial x} + \cos\theta \frac{\partial(\ln\alpha)}{\partial y} = \cos\theta \frac{\partial\theta}{\partial x} + \sin\theta \frac{\partial\theta}{\partial y} \tag{3.20}$$

and

$$\cos\theta \frac{\partial(\ln\beta)}{\partial x} + \sin\theta \frac{\partial(\ln\beta)}{\partial y} = \sin\theta \frac{\partial\theta}{\partial x} - \cos\theta \frac{\partial\theta}{\partial y}. \tag{3.21}$$

Proof. For any function in C^2, mixed partial derivatives must be equal by the Schwarz theorem. In our case, this is equivalent to the invariance in the order of taking partial derivatives of ξ and η w.r.t. x and y, i.e.,

$$\frac{\partial}{\partial y}\left(\frac{\partial \xi(x, y)}{\partial x}\right) = \frac{\partial}{\partial x}\left(\frac{\partial \xi(x, y)}{\partial y}\right), \tag{3.22}$$

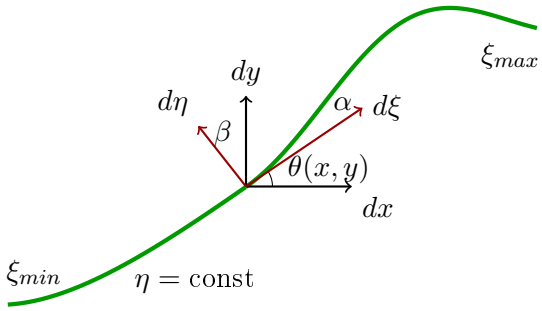

Figure 3.8: Coordinate transformation for one single line of constant η that is parametrized by $\xi(\eta) \in [\xi_{min}(\eta), \xi_{max}(\eta)]$.

and

$$\frac{\partial}{\partial y}\left(\frac{\partial \eta(x,y)}{\partial x}\right) = \frac{\partial}{\partial x}\left(\frac{\partial \eta(x,y)}{\partial y}\right). \tag{3.23}$$

By applying (3.22) and (3.23) to the definition of the coordinate transformation (3.15) given matrices (3.16) and (3.17), we obtain (3.20)-(3.21). Finally, ξ and η can be obtained by integrating (3.15). Bijectivity follows since the determinant of the Jacobian (3.15) is given by $\alpha(x,y)\beta(x,y)$, and by (3.20)-(3.21) both $\alpha(x,y)$ and $\beta(x,y)$ are strictly positive. □

Thus, $\alpha(x,y)$ and $\beta(x,y)$ being functions of angle $\theta(x,y)$ only, can be computed from the network geometry. In Figure 3.8 we illustrate the role of these parameters in the coordinate transformation by considering a single line of constant η. As we can see, α and β are used to scale the distances between the lines of constant ξ and between the lines of constant η, respectively. In (ξ,η)-space the flow evolves only along lines of constant η as in (3.19).

3.2.4 Model in (ξ,η)-space

According to Chapter 2 of [9], we can apply the divergence formula to calculate $\nabla \cdot \vec{\Phi}$ in (ξ,η)-space:

$$\nabla \cdot \vec{\Phi}(\xi,\eta,\rho) = \frac{1}{h_\xi h_\eta}\left[\frac{\partial\left(\vec{\Phi}_\xi h_\eta\right)}{\partial \xi} + \frac{\partial\left(\vec{\Phi}_\eta h_\xi\right)}{\partial \eta}\right], \tag{3.24}$$

where h_ξ and h_η are known as Lamé coefficients, which correspond to the lengths of the basis vectors in (ξ,η)-space:

$$\vec{h_\xi} = \left(\tfrac{\partial x}{\partial \xi}, \quad \tfrac{\partial y}{\partial \xi}\right)^T \quad \text{and} \quad \vec{h_\eta} = \left(\tfrac{\partial x}{\partial \eta}, \quad \tfrac{\partial y}{\partial \eta}\right)^T. \tag{3.25}$$

For the computation of (3.25), we invert the Jacobian (3.15) and get:

$$\begin{pmatrix} dx \\ dy \end{pmatrix} = \begin{pmatrix} \frac{1}{\alpha}\cos\theta & -\frac{1}{\beta}\sin\theta \\ \frac{1}{\alpha}\sin\theta & \frac{1}{\beta}\cos\theta \end{pmatrix}\begin{pmatrix} d\xi \\ d\eta \end{pmatrix}. \tag{3.26}$$

The combination of (3.26) and (3.25) yields the basis vectors in (ξ, η)-space:

$$\vec{h_\xi} = \frac{1}{\alpha}\begin{pmatrix}\cos\theta\\ \sin\theta\end{pmatrix}, \quad \vec{h_\eta} = \frac{1}{\beta}\begin{pmatrix}-\sin\theta\\ \cos\theta\end{pmatrix}. \tag{3.27}$$

We then find the lengths of these vectors (3.27), which gives us Lamé coefficients:

$$h_\xi = |\vec{h_\xi}| = \frac{1}{\alpha}, \quad h_\eta = |\vec{h_\eta}| = \frac{1}{\beta}. \tag{3.28}$$

Using (3.28), we are able to normalize the basis vectors by dividing (3.27) by their length (3.28):

$$\begin{cases}\vec{e}_\xi = \vec{e}_x\cos\theta + \vec{e}_y\sin\theta,\\ \vec{e}_\eta = -\vec{e}_x\sin\theta + \vec{e}_y\cos\theta,\end{cases} \tag{3.29}$$

where $\vec{e}_x$ and $\vec{e}_y$ are the normalized basis vectors of (x, y)-space, and $\vec{e}_\xi$ and $\vec{e}_\eta$ are the normalized basis vectors of (ξ, η)-space.

Let us now rewrite vector $\vec{\Phi}$ given by (3.2) in (ξ, η)-space. Notice that in (x, y)-space this vector reads:

$$\vec{\Phi}(x, y, \rho) = \Phi(x, y, \rho)\cos(\theta(x, y))\vec{e}_x + \Phi(x, y, \rho)\sin(\theta(x, y))\vec{e}_y. \tag{3.30}$$

Then, by using (3.29) we obtain:

$$\vec{\Phi}(\xi, \eta, \rho) = \Phi(\xi, \eta, \rho)\vec{e}_\xi. \tag{3.31}$$

Having Lamé coefficients (3.28) and the flux vector in (ξ, η)-space (3.31), we finalize the calculation of the divergence term (3.24) in (ξ, η)-space as:

$$\nabla\cdot\vec{\Phi}(\xi, \eta, \rho) = \alpha(\xi, \eta)\beta(\xi, \eta)\left[\frac{\partial(\Phi(\xi, \eta, \rho)/\beta)}{\partial\xi}\right]. \tag{3.32}$$

Thus, we have shown that our curvilinear coordinate transformation (3.15) does really reformulate the 2D divergence term into 1D. This means that the temporal change of vehicle density in a 2D plane is caused by the change of traffic flow along only one coordinate in (ξ, η)-space, as we were showing by (3.19) for the case of straight lines.

For simplicity, we also introduce some new functions by scaling density, flows, demand and supply functions as:

$$\begin{aligned}&\bar{\rho} = \frac{\rho}{\alpha\beta}, \quad \bar{\Phi} = \frac{\Phi}{\beta}, \quad \bar{\phi}_{in} = \frac{\phi_{in}}{\beta},\\ &\bar{\phi}_{out} = \frac{\phi_{out}}{\beta}, \quad \bar{S} = \frac{S}{\beta}, \quad \bar{D} = \frac{D}{\beta}.\end{aligned} \tag{3.33}$$

Finally, the last thing that needs to be clarified prior to rewriting the 2D LWR system (3.9) in (ξ, η)-space, is the definition of a spatial domain, on which the system in new coordinates will evolve. Thus, the new spatial domain $\bar{\Omega}$ is a compact domain defined as:

$$\bar{\Omega} = \{(\xi, \eta) \,:\, \exists\,(x, y) \in \Omega,\, \xi = \xi(x, y),\, \eta = \eta(x, y)\}.$$

Then, the domain boundary in (x, y)-space can be uniquely projected into the boundary in (ξ, η)-space, i.e., $\Gamma_\Omega \to \Gamma_{\bar{\Omega}}$. In particular, $\Gamma_{\bar{\Omega}}$ consists of points $(\xi_{min}(\eta), \xi_{max}(\eta))$ such that

$$\xi_{min}(\eta) = \min_{\substack{(x,y)\in\Omega,\\ \eta(x,y)=\eta}} \xi(x,y), \quad \xi_{max}(\eta) = \max_{\substack{(x,y)\in\Omega,\\ \eta(x,y)=\eta}} \xi(x,y),$$

and we can also define the maximal and minimal values of η as

$$\eta_{min} = \min\{\eta \mid \exists \xi : (\xi, \eta) \in \bar{\Omega}\}, \quad \eta_{max} = \max\{\eta \mid \exists \xi : (\xi, \eta) \in \bar{\Omega}\}.$$

Now, using the divergence term in (ξ, η)-space (3.32), we can rewrite the 2D LWR system (3.9) that now reads $\forall (\xi, \eta, t) \in \bar{\Omega} \times \mathbb{R}^+$:

$$\begin{cases} \dfrac{\partial \bar{\rho}(\xi,\eta,t)}{\partial t} + \dfrac{\partial \bar{\Phi}(\xi,\eta,\bar{\rho})}{\partial \xi} = 0, \\ \bar{\phi}_{in}(\eta,t) = \min\left\{\bar{D}\left(\bar{\rho}_{in}(\eta,t)\right), \bar{S}\left(\bar{\rho}\left(\xi_{min}(\eta),\eta,t\right)\right)\right\}, \\ \bar{\phi}_{out}(\eta,t) = \min\left\{\bar{D}\left(\bar{\rho}\left(\xi_{max}(\eta),\eta,t\right)\right), \bar{S}\left(\bar{\rho}_{out}(\eta,t)\right)\right\}, \\ \bar{\rho}(\xi,\eta,0) = \bar{\rho}_0(\xi,\eta), \end{cases} \tag{3.34}$$

where $\bar{\Phi}(\xi, \eta, \bar{\rho})$ is now a scalar function that preserves all the FD properties such as being Lipschitz continuous and concave, e.g., consider the Greenshields FD in (ξ, η)-space:

$$\bar{\Phi}(\xi,\eta,\bar{\rho}) = \bar{v}_{max}(\xi,\eta)\left(1 - \frac{\bar{\rho}}{\bar{\rho}_{max}(\xi,\eta)}\right)\bar{\rho}, \quad \text{where} \quad \bar{v}_{max} = \alpha v_{max}, \quad \bar{\rho}_{max} = \frac{\rho_{max}}{\alpha\beta}. \tag{3.35}$$

The general rule in scaling functions is the following: all functions that have flow units (ϕ_{in}, ϕ_{out}, $S(\rho)$, $D(\rho)$, $\Phi(\rho)$, ϕ_{max}) have to be divided by β, all density-related functions (ρ, ρ_{max} and ρ_c) must be divided by $\alpha\beta$, and velocity-related functions (v_{max} in case of Greenshields FD and v, ω in case of triangular FD) must be multiplied by α. Note that also here the demand $\bar{D}(\bar{\rho})$ and supply $\bar{S}(\bar{\rho})$ functions are defined as in Section 2.1.5 but depending on (ξ, η)-space and in two dimensions.

We can see that the traffic flow evolves now only along lines of constant η in (ξ, η)-space. Thus, the system in new coordinates (3.34) should be seen as a continuous set of 1D LWR equations each following a path parametrized by η. This means that we can also analyze its solution in the same way as we do it in case of 1D LWR. Namely, in system (3.34) shocks arise when characteristics cross at some point of space, and thus we need to consider its solution in a weak sense, and then the unique (entropy) solution is the one that satisfies the Lax condition (see Section 2.1.3). Moreover, to guarantee that the weak solution $\bar{\rho}(\xi, \eta, t)$ is the entropy one $\forall (\xi, \eta, t) \in \bar{\Omega} \times \mathbb{R}^+$, one needs to consider the boundary conditions in the weak sense, see Section 2.1.4. Notice, that the boundary conditions $\bar{\phi}_{in}(\eta, t)$ and $\bar{\phi}_{out}(\eta, t)$ in (3.34) are formulated using the demand-supply concept (see Section 2.1.5 for the explanation). Thus, the initial boundary value problem (3.34) is well-posed, see more details in [22, 146] for entropy conditions for inhomogeneous LWR model.

Let us now summarize all the steps that need to be performed in order to be able to describe the evolution of traffic in (ξ, η)-space by system (3.34) in some urban area.

1. As an input, we get some urban network as a collection of roads and junctions with known coordinates in (x, y)-space, speed limits and the number of lanes.

2. We define a rectangular plane Ω such that the corresponding urban network is contained in it. Then, we apply approximations to find all variables and FD parameters $\forall (x, y) \in \Omega$: the inverse distance weighting to find the vector field $\vec{d}_\theta(x, y)v_{max}(x, y)$ (see Section 3.1.3.1), then the kernel density estimation to obtain $\rho_{max}(x, y)$ (see Section 3.1.3.2).

3. Apply 1D kernel density estimation to the boundary conditions given as inflows and outflows of particular roads of the city.

4. Given road orientation angle $\theta(x, y)$ $\forall (x, y) \in \Omega$ obtained as arctangent of the velocity field, calculate functions $\alpha(x, y)$ and $\beta(x, y)$ by solving PDEs (3.20) and (3.21).

5. Using $\alpha(x, y)$ and $\beta(x, y)$, calculate new coordinates $(\xi, \eta) \in \bar{\Omega}$ by numerical integration of (3.15).

6. Rescale all the FD parameters, density- and flow-related variables as in (3.33). For example, demand and supply functions at the boundaries should be rescaled as:

$$\bar{D}_{in}(\eta) = \frac{D_{in}(\eta)}{\beta(\xi_{min}(\eta), \eta)}, \qquad \bar{S}_{out}(\eta) = \frac{S_{out}(\eta)}{\beta(\xi_{max}(\eta), \eta)}.$$

For the rest of this chapter we will be always referring to the system written in (ξ, η)-space (3.34). Thus, with a slight abuse of notations, we will omit bars for all the variables from (3.34), however leaving the notations for domains $\bar{\Omega}$ and its boundary $\bar{\Gamma} \in \bar{\Omega}$.

3.2.5 Numerical scheme

Since the system (3.34) is essentially just a set of 1D LWR equations, its numerical solution is found using the same Godunov scheme as described in Section 2.1.6. The differences emerge from the dependency on the additional dimension η and also from the space-dependency of FD parameters $\rho_{max}(\xi, \eta)$ and $v_{max}(\xi, \eta)$. For convergence results for the Godunov scheme applied to kinematic wave systems with space-dependent fundamental diagrams see [22].

We start by defining a numerical grid in $\bar{\Omega} \times \mathbb{R}^+$ by setting

- m to be number of cells to discretize η dimension,
- $\Delta\eta = (\eta_{max} - \eta_{min})/m$ to be the space cell size in η dimension,
- $\eta_j = \eta_{min} + j\Delta\eta$ to be the grid point in η dimension for $j \in \{1, ..., m\}$,
- $\Delta\xi$ to be the space cell size in ξ dimension,
- $n_j = \lceil (\xi_{max}(\eta_j) - \xi_{min}(\eta_j))/\Delta\xi \rceil$ to be the number of cells in ξ dimension for particular $\eta = \eta_j$ for $j \in \{1, ..., m\}$,

- $\xi_{ij} = \xi_{min}(\eta_j) + i\Delta\xi$ to be the grid point in ξ dimension for $i \in \{1, ..., n_j\}$ and $j \in \{1, ..., m\}$,
- Δt to be the time cell size,
- $t_k = k\Delta t$ for $k \in \mathbb{Z}^+$ to be the grid point in time.

Similarily to Section 2.1.6, the mesh sizes $\Delta\xi$ and Δt are chosen sucht that they satisfy the Courant-Friedrichs-Lewy condition [33]:

$$\Delta t \max_{(\xi,\eta,\rho)} |\Phi'(\xi, \eta, \rho)| \leq \frac{\Delta\xi}{2}.$$

The discrete density is then $\rho_{i,j}(k)$, and according to the Godunov scheme, we update it $\forall j \in \{1, \dots, m\}, \forall i \in \{1, \dots, n_j\}$ and $\forall k \in \mathbb{Z}^+$ as follows:

$$\begin{cases} \rho_{1,j}(k+1) = \rho_{1,j}(k) + \dfrac{\Delta t}{\Delta\xi}\left(\varphi_{in,j}(k) - \varphi_{2,j}(k)\right), \\ \rho_{i,j}(k+1) = \rho_{i,j}(k) + \dfrac{\Delta t}{\Delta\xi}\left(\varphi_{i,j}(k) - \varphi_{i+1,j}(k)\right), \\ \rho_{n_j,j}(k+1) = \rho_{n_j,j}(k) + \dfrac{\Delta t}{\Delta\xi}\left(\varphi_{n_j,j}(k) - \varphi_{out,j}(k)\right), \end{cases} \tag{3.36}$$

where $\varphi_{i,j}(k)$ is the Godunov numerical flux defined as

$$\varphi_{i,j}(k) = \min\left\{D(\rho_{i-1,j}(k)), S(\rho_{i,j}(k))\right\}, \tag{3.37}$$

with $D(\rho_{i-1,j}(k))$ and $S(\rho_{i,j}(k))$ being the discretized demand and supply functions same as in Section 2.1.6 except that the numerical flux in (3.36) has space-dependent parameters $\rho_{max}(\xi, \eta)$ and $v_{max}(\xi, \eta)$, which should be used for the computation of $D(\rho_{i-1,j}(k))$ and $S(\rho_{i,j}(k))$ in (3.37).

The boundary flows $\varphi_{in,j}(k)$ and $\varphi_{out,j}(k)$ from (3.36) are determined by specifying the density at the ghost cells with indices $i = 0$ and $i = n_j + 1$ for $j \in \{1, \dots, m\}$:

$$\begin{aligned} \varphi_{in,j}(k) &= \min\left\{D(\rho_{0,j}(k)), S(\rho_{1,j}(k))\right\}, \\ \varphi_{out,j}(k) &= \min\left\{D(\rho_{n_j,j}(k)), S(\rho_{n_j+1,j}(k))\right\}. \end{aligned} \tag{3.38}$$

3.2.6 Hamilton-Jacobi formulation

Let us now consider the parametrized set of 1D LWR equations with space-dependent FD (3.34) (2D LWR in curvilinear coordinates) in Hamilton-Jacobi formulation. The Hamilton-Jacobi formalism here is quite similar to the one presented in Section 2.1.7. The only difference here is that we must carefully handle the space-dependency of FD and the additional space parameter $\eta \in [\eta_{min}, \eta_{max}]$ that is just used as a label of the flow path rather than the

second space dimension. Thus, let us again consider the cumulative vehicle number function $M(\xi,\eta,t)$ that is an integral function of flow in time or density in a 2D space (see (2.21) for 1D). This integral function can be expressed through domain outflows as in (2.23), if the starting point of the integration is set to the downstream boundary of flow path η at initial time, i.e., $M(\xi_{max}(\eta),\eta,0)=0$. Then, the Moskowitz function in the 2D plane is defined $\forall(\xi,\eta,t)\in\bar{\Omega}\times\mathbb{R}^+$ as

$$M(\xi,\eta,t)=\int_0^t \phi_{out}(\eta,\tau)d\tau+\int_{\xi}^{\xi_{max}(\eta)}\rho(\hat{\xi},\eta,t)d\hat{\xi}. \tag{3.39}$$

Also we can express the Moskowitz function through domain inflows and initial density distribution as in (2.24), if the starting point is set to the upstream boundary of η-line at initial time, i.e., $M(\xi_{min}(\eta),\eta,0)=0$. In this case we obtain:

$$M(\xi,\eta,t)=\int_{\xi_{min}(\eta)}^{\xi_{max}(\eta)}\rho_0(\hat{\xi},\eta)d\hat{\xi}+\int_0^t \phi_{in}(\eta,\tau)d\tau-\int_{\xi_{min}(\eta)}^{\xi}\rho(\hat{\xi},\eta,t)d\hat{\xi}. \tag{3.40}$$

The relation of H-J formulation to the LWR formulation is the same as discussed in Section 2.1.7. Thus, the H-J PDE with space-dependent Lipschitz continuous Hamiltonian can be obtained from the space-dependent flow-density relation $\Phi(\xi,\eta,\rho)=\phi(\xi,\eta,t)$, where the flow and density functions are then replaced by formulas similar to (2.21).

Let us introduce the following initial boundary value problem $\forall(\xi,\eta,t)\in\Omega\times\mathbb{R}^+$ in Hamilton-Jacobi formulation:

$$\begin{cases}\dfrac{\partial M(\xi,\eta,t)}{\partial t}-\Phi\left(\xi,\eta,-\dfrac{\partial M(\xi,\eta,t)}{\partial\xi}\right)=0,\\ M(\xi,\eta,0)=M_{\text{Ini}}(\xi,\eta),\\ M(\xi_{min}(\eta),\eta,t)=M_{\text{Up}}(\eta,t),\\ M(\xi_{max}(\eta),\eta,t)=M_{\text{Down}}(\eta,t).\end{cases} \tag{3.41}$$

The main advantage of the H-J PDE is that we can indeed formulate its solution in terms of a minimization problem. For several shapes of Hamiltonian (for example, triangular FD), the solution to the minimization problem can be found explicitly.

Solution of the H-J IBVP (3.41) can be obtained analytically in accordance with the variational principle using only its boundary and initial conditions, which can be encoded in the general value condition function c. For 1D it was already done in (2.26), however, in 2D it has a different set of departure, i.e., $c(\xi,\eta,t):\text{Dom}(c)\to\mathbb{R}^+$, where

$$\begin{aligned}\text{Dom}(c)=&\left\{(\xi,\eta,t)\ :\ \eta\in[\eta_{min},\eta_{max}],\ \xi\in\{\xi_{min}(\eta),\xi_{max}(\eta)\},\ t\in\mathbb{R}^+\right\}\\ &\cup\left\{(\xi,\eta,0)\ :\ \eta\in[\eta_{min},\eta_{max}],\ \xi\in[\xi_{min}(\eta),\xi_{max}(\eta)]\right\}.\end{aligned}$$

This function generalizes the initial $M_{\text{Ini}}(\xi,\eta)$ and boundary conditions $M_{\text{Up}}(\eta,t)$ and

$M_{\text{Down}}(\eta, t)$ of (3.41) that are then used for the computation of the infimum problem:

$$c(\xi, \eta, t) = \begin{cases} M_{\text{Ini}}(\xi, \eta), & t = 0, \\ M_{\text{Up}}(\eta, t), & \xi = \xi_{min}(\eta), \\ M_{\text{Down}}(\eta, t), & \xi = \xi_{max}(\eta). \end{cases} \tag{3.42}$$

Now we specify the value condition function (3.42) by calculating $M_{\text{Up}}(\eta, t)$, $M_{\text{Down}}(\eta, t)$ and $M_{\text{Ini}}(\xi, \eta)$. We proceed in a similar way as in Section 2.1.8. Thus, the upstream boundary condition $M_{\text{Up}}(\eta, t)$ can be obtained by considering (3.40) for $\xi = \xi_{min}(\eta)$, which results into

$$M_{\text{Up}}(\eta, t) = c(\xi_{min}(\eta), t) = \int_0^t \phi_{in}(\eta, \tau) d\tau + \int_{\xi_{min}(\eta)}^{\xi_{max}(\eta)} \rho_0(\hat{\xi}, \eta) d\hat{\xi}, \quad \forall (\eta, t) \in [\eta_{min}, \eta_{max}] \times \mathbb{R}^+. \tag{3.43}$$

Then, the downstream boundary condition $M_{\text{Down}}(\eta, t)$ can be expressed from (3.39) for $\xi = \xi_{max}(\eta)$:

$$M_{\text{Down}}(\eta, t) = c(\xi_{max}(\eta), t) = \int_0^t \phi_{out}(\eta, \tau) d\tau, \quad \forall (\eta, t) \in [\eta_{min}, \eta_{max}] \times \mathbb{R}^+. \tag{3.44}$$

Finally, the initial condition $M_{\text{Ini}}(\xi, \eta)$ can be expressed from either (3.40) or (3.39) for $t = 0$, which yields

$$M_{\text{Ini}}(\xi, \eta) = c(\xi, \eta, 0) = \int_{\xi}^{\xi_{max}(\eta)} \rho_0(\hat{\xi}, \eta) d\hat{\xi}. \tag{3.45}$$

Further, we introduce a Legendre-Fenchel transform of the space-dependent flux function $\Phi(\xi, \eta, \rho)$ as:

$$\begin{gathered} \forall v' \in [-\omega(\xi, \eta), v(\xi, \eta)] : \\ L(\xi, \eta, v') = \sup_{\rho \in [0, \rho_{max}(\xi, \eta)]} (\Phi(\xi, \eta, \rho) - v'\rho), \end{gathered} \tag{3.46}$$

where $v(\xi, \eta)$ and $-\omega(\xi, \eta)$ are related to the maximal and minimal kinematic wave speeds in free-flow and congested traffic regime (not necessarily as in triangular FD). This function achieves minimum, if an observer moving in a traffic stream adapts his/her individual speed to the maximal kinematic wave speed (see the discussion in Section 2.1.8).

Finally, the closed-form solution to (3.41) corresponding to the infimum among all viable evolutions that start at initial time $t - T$ and arrive at (ξ, η) at terminal time t reads as:

$$M(\xi, \eta, t) = \inf_{(T, v') \in S} \left(c\left(\hat{\xi}(0), \eta, t - T\right) + \int_0^T L\left(\hat{\xi}(\tau), \eta, v'(\tau)\right) d\tau \right), \tag{3.47}$$

where the infimum is taken over domain S defined as:

$$\begin{aligned} S = \Big\{ (T, v') \;\Big|\; & T \in \mathbb{R}^+,\ v'(\cdot) \in L^1(0,T),\ \ \dot{\hat{\xi}}(\tau) = v'(\tau), \\ & \hat{\xi}(T) = \xi,\ \ v'(\tau) \in \left[-\omega \left(\hat{\xi}(\tau), \eta \right), v \left(\hat{\xi}(\tau), \eta \right) \right], \\ & \left(\hat{\xi}(0), \eta, t - T \right) \in \mathrm{Dom}(c) \Big\}. \end{aligned} \tag{3.48}$$

Here $\hat{\xi}(\tau)$ denotes the trajectory of an observer moving along a traffic stream with possibly non-constant speed $v'(\tau)$ unlike in Lax-Hopf formula (2.32), since now we consider space-dependent FDs that include inhomogeneity of the network infrastructure. Trajectory $\hat{\xi}(\tau)$ originates at $\tau = 0$ on a boundary of the domain of c and arrives at the point ξ at terminal time $\tau = T$.

As already mentioned, in case of a triangular FD (3.4) the solution to H-J PDE (3.41) can be found explicitly. We show the derivation of the explicit solution in Appendix B.5, where the solution was considered for large enough time such that the effect of initial conditions is negligible. This result will be then used in Section 3.5, where we consider a boundary control problem for traffic in a mixed regime evolving on a large urban network and prove its exponential convergence to the desired trajectory.

3.3 Equilibrium manifolds

Analysis of steady states emerging in large urban networks is of a key importance in understanding traffic dynamics. In particular, steady states need to be studied to enable comparison of different models or to solve optimal control tasks of driving a state to some desired equilibrium. This section is devoted to the model-based estimation of steady states for traffic density evolving on arbitrary large-scale urban networks. The traffic state is governed by a two-dimensional conservation law (3.9).

In the previous Section 3.2, we presented the curvilinear coordinate transformation for the 2D conservation law model that could be translated into a parametrized inhomogeneous 1D LWR system (3.34), i.e., each such 1D system incorporates space-dependency in the flux function that is related to bottlenecks and varying speed limits along the traffic flow path.

This section demonstrates the first analytic result that can be easily obtained for this kind of systems. In particular, we present the first model-based steady state estimation result for large traffic networks, which became possible due to this curvilinear coordinate transformation. Thereby, we will use only the information about the network geometry and infrastructure parameters, as well as demand and supply at network boundaries. For a 1D inhomogeneous case (one road with bottlenecks) this was done in [146], who used the wave entropy conditions derived in [149] to ensure the physically relevant solution. We will rely on this previous result [146] to extract the "correct" density from the steady state flow, which provides the entropy solution of system (3.34).

3.3.1 Problem statement

Let us consider the parametrized inhomogeneous PDE system (3.34). Assume that demand at the upstream boundary and the supply at the downstream boundary are constant in time, i.e., $D(\rho_{in}(\eta))$ and $S(\rho_{out}(\eta))$ are given $\forall \eta \in \bar{\Omega}$. We seek to develop a technique that yields the steady state of (3.34) analytically. This is formalized as follows:

Problem 3.1
Given system (3.34) with constant demand and supply functions $D(\rho_{in}(\eta))$ and $S(\rho_{out}(\eta))\, \forall \eta \in \bar{\Omega}$, find a time-invariant density distribution $\rho^*(\xi, \eta)$ such that

$$\frac{\partial \Phi^*(\xi, \eta, \rho^*)}{\partial \xi} = 0, \qquad \forall (\xi, \eta) \in \bar{\Omega}. \tag{3.49}$$

3.3.2 Steady state density

Stationary solutions to system (3.34) might be space-varying functions $\rho^*(\xi, \eta)$ due to the space-dependency of the fundamental diagram. By the mass conservation law, the steady state traffic flow in (3.34) should be constant along its evolution path (lines of constant η), that is:

$$\phi^*(\eta) := \Phi^*(\xi, \eta, \rho^*).$$

Recall that, in general, traffic operates at maximum efficiency when $\Phi(\xi, \eta, \rho) = \phi_{max}(\xi, \eta)$, i.e., when the traffic conditions allow to exploit roads at their capacity. However, $\phi_{max}(\xi, \eta)$ can not be the steady state flow, since it should not depend on ξ. The equilibrium traffic flow can not exceed the capacity of the "worst" bottleneck along its path (line of constant η). If traffic conditions do not allow that (e.g., congested traffic along the whole η line), we need to mind the boundary conditions as well. Assume that demand at the upstream boundary $D(\rho_{in}(\eta))$ and supply at the downstream boundary $S(\rho_{out}(\eta))$ are given $\forall \eta \in [\eta_{min}, \eta_{max}]$. In accordance with the analysis performed in [146], we obtain that the steady state flow along its path is the minimum of three functions

$$\phi^*(\eta) = \min\{D(\rho_{in}(\eta)), \phi^{min}_{max}(\eta), S(\rho_{out}(\eta))\}, \tag{3.50}$$

where $\phi^{min}_{max}(\eta)$ is the transportation capacity at the strongest bottleneck along the η-line defined as:

$$\phi^{min}_{max}(\eta) = \min_{\xi \in [\xi_{min}(\eta), \xi_{max}(\eta)]} \phi_{max}(\xi, \eta), \tag{3.51}$$

and the point where the minimum is achieved is the location of the strongest bottleneck denoted by $\xi^*(\eta)$:

$$\xi^*(\eta) = \operatorname*{argmin}_{\xi \in [\xi_{min}(\eta), \xi_{max}(\eta)]} \phi_{max}(\xi, \eta). \tag{3.52}$$

If there are several points ξ^* or it is an interval, then we take the left-most value (the first point on the flow path), i.e., $\xi^* = \xi^*_1$ in Figure 3.11.

Thus, the steady state traffic flow along a line of constant η is the minimum between the demand at its entry, the supply at its exit and the minimum bandwidth (3.51), which is determined by the strongest bottleneck of the η-line. On a physical road, such a bottleneck can be caused by a reduced number of lanes or by a lower speed limit. Recall that lines of constant η are used to describe the traffic flow path, and they are different from the physical roads as these lines are defined on a continuum 2D plane using approximations of all parameters (see Sections 3.1.3.1 and 3.1.3.2). Thus, the strongest bottleneck is determined by the level of compression of roads, i.e., the smallest capacity is achieved in areas with highly compressed roads. This dependency is incorporated in the scaling factor $\beta(\xi, \eta)$, since recall that every term in (3.50) was divided by it (as in (3.33), and then the bars were omitted to simplify the notations).

As a next step, we need to find the corresponding steady state density. Due to the concavity of the fundamental diagram (see Figure 2.1), for each flow value (except the maximal flow ϕ_{max}), there exist two densities corresponding to this flow: the lower value denotes the free-flow traffic regime, and the higher value denotes the congested regime.

Based on the result obtained by solving the minimum (3.50), we can distinguish three possible cases:

1. $\phi(\eta)^* = \phi^{min}_{max}(\eta)$. Then, the steady state ρ^* should be chosen to guarantee the congested regime $\forall \xi \in [\xi_{min}(\eta), \xi^*(\eta))$, while it must provide the free-flow regime $\forall \xi \in (\xi^*(\eta), \xi_{max}(\eta)]$. This is the only solution satisfying the wave entropy condition for inhomogeneous roads (space-dependent FDs) as presented in [146, 149]. This means that the strongest bottleneck creates congestion, and after passing it, vehicles can move freely. As mentioned above, such bottlenecks can be caused by highly compressed roads (characterized by a high scaling parameter $\beta(\xi, \eta)$), low maximal density $\rho_{max}(\xi, \eta)$ (e.g., on a river's bridge), or low speed limits $v_{max}(\xi, \eta)$.

2. $\phi(\eta)^* = D(\rho_{in}(\eta))$. This implies that the demand to enter this "road" is too small, and all cars can pass through the system freely. Therefore, the whole domain is in the free-flow traffic regime and $\xi^*(\eta) = \xi_{min}(\eta)$.

3. $\phi(\eta)^* = S(\rho_{out}(\eta))$. This implies that the supply at the exit of this "road" is too low, and the cars get blocked there. The strongest bottleneck is at the exit of η-line, i.e., $\xi^*(\eta) = \xi_{max}(\eta)$. Therefore, the whole domain is in the congested traffic regime.

Notice that the steady state ρ^* is obtained by taking the inverse of the fundamental diagram, and the correct traffic regime providing the entropy solution of (3.34) should be set depending on the steady state flow (3.50), as discussed above for three possible cases. As a final step, we need to rescale the density back as:

$$\rho(\xi, \eta) = \bar{\rho}(\xi, \eta)\alpha(\xi, \eta)\beta(\xi, \eta),$$

which allows us to compare steady states obtained by a numerical simulation of (3.9) and by performing a model-based analysis of (3.34) (see next Section 3.3.3).

3.3.3 Steady state example

Let us now demonstrate a steady state example that can be obtained by following the steps described in Section 3.3.2. For this, let us take a synthetic 10×10 Manhattan network as described earlier in Section 3.1.6. The demand at the upstream boundary $D(\rho_{in}(\eta))$ is also set as in Section 3.1.6, and the supply at the downstream boundary $S(\rho_{out}(\eta)) = \phi_{max}(\xi_{max}(\eta), \eta)$, i.e., all vehicles can leave the domain freely. Further, we discretize η dimension into $m = 180$ cells. Following the steps described in Section 3.3.2, we obtain a steady state for a parametrized inhomogeneous 1D LWR system (3.34) shown in Figure 3.9b). The continuous approximation was again performed for a low weighting parameter $\mu = 20$. We thus seek to capture only the global trend of the velocity field in this example.

We compare now this steady state to the one obtained by running a numerical simulation of traffic density governed by a 2D LWR model (3.9), which is illustrated in Figure 3.9a). Thereby, we use the Godunov scheme in 2D presented in Section 3.2.5 for an unscaled system (3.34), which is the same system as (3.9) with the only difference that it is written in different coordinates. Additionally, we also compare the obtained steady state distribution to the one that results from running the microsimulator Aimsun, see Figure 3.9c). Recall that Aimsun produces vehicle trajectories, and then we use the kernel density estimation (see Section 3.1.3.2) to reconstruct the 2D density from vehicle positions. For the density reconstruction, we again use the standard deviation of the Gaussian $d_0 = 50$ m as in Section 3.1.6. Notice also that Figures 3.9a) and 3.9c) are exactly the same as Figures 3.6b) and 3.6c), since we use here the same congestion formation scenario as in Section 3.1.6.

Thus, we can observe that the analytical steady state solution presented in Figure 3.9b) captures quite well the spatial distribution of congested and free-flow areas compared to the "ground true" steady state density obtained from Aimsun (Figure 3.9c)). In particular, in plots b) and c) the lines separating congested and free-flow areas in the South-Western part are very similar, while in case of steady state density obtained by the numerical simulation (Figure 3.9a)) this line lies notably lower. The L_2 norm of the deviation from the Aimsun density yields $\|\tilde{\rho}^*(x, y)\|_2 = 0.4$ for b) , which is almost the same as for a). Thus, the model-based steady state calculation yields quite accurate results, which are obtained analytically without any need to run long simulations as required in the case of 2D LWR model in Figure 3.9a) (2 hours of simulation time).

3.3.4 Discussions

In this section, we demonstrated the first result that can be obtained by analysing the 2D LWR model in (ξ, η)-coordinates. The rewritten model (3.34) represents a parametrized 1D LWR model with a space-dependent FD, where the second dimension is used to label the traffic flow path. We described how to obtain its steady state that corresponds to a space-varying density distribution by following two steps: first, solving the minimum (3.50) between the demand flow at the upstream boundary, the supply flow at the downstream boundary and the capacity at the strongest bottleneck, and second, by extracting the density satisfying the wave entropy

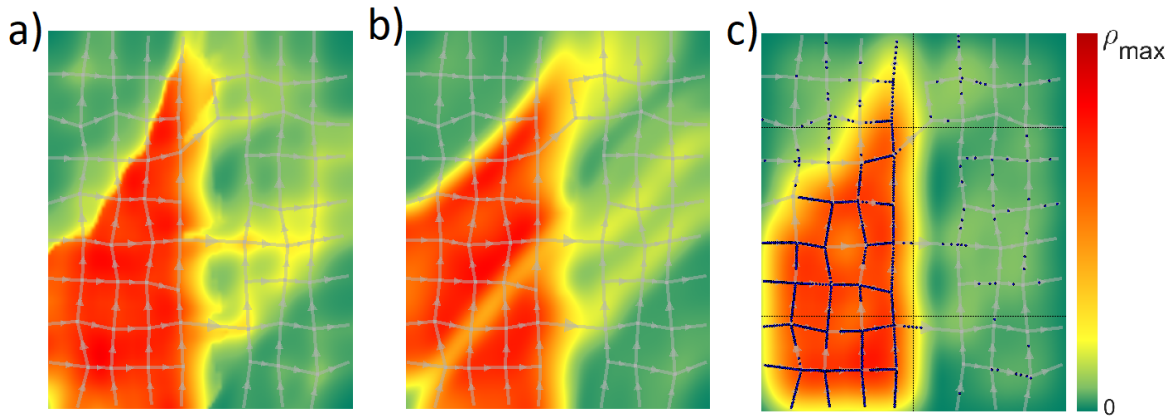

Figure 3.9: Steady state obtained by: a) numerical simulation of density governed by the 2D LWR system (3.9), b) model-based analysis of (3.34), c) density reconstruction from vehicle positions predicted by Aimsun.

condition.

We then provided an example for a steady state that can be obtained by this model-based analysis, which was then compared to the previous results obtained by running a congestion formation scenario for 2 hours of simulation time. For this, we referred to Section 3.1.7, where the steady-state distribution obtained by simulating a traffic density governed by the 2D LWR (3.34) in (x, y)-coordinates was compared to the reference steady state distribution predicted by microsimulator Aimsun. Thus, the analytically obtained steady state from the model in (ξ, η)-coordinates (3.34) appeared to provide quite accurate results by capturing the shape of traffic congestion even better in comparison to the result obtained numerically. There are two main advantages of model-based steady state prediction: first, it saves a lot of computational time, since there is no more need to run simulations until the steady state is achieved, and second, being an explicit result it can be used to solve control related tasks for traffic in large urban networks. This will be shown in the following section, where the explicitly estimated steady state will be used as a desired equilibrium to reach via a boundary control.

3.4 Boundary control for congested areas

In this section, we seek do design a boundary control for a congested area within a large urban network using the same modeling approach as in Section 3.3. Thus, we again describe the traffic state by its density whose temporal evolution is given by the 2D LWR model rewritten in curvilinear coordinates (3.34). We will consider a urban network that includes congested areas that will be controlled from their downstream boundary as shown in Figure 3.10. The control should drive the traffic system to the equilibrium that provides the maximal throughput of the system. This stabilized system is then characterised by a reduced average latency and a higher average velocity.

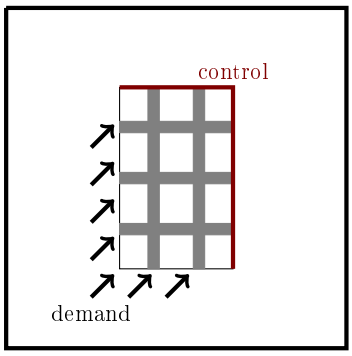

Figure 3.10: A sketch of a urban network that contains a congested area (grey Manhattan greed) to be controlled from its downstream boundary (in red).

Our main contribution here is to suggest a model-based control design technique that requires only the knowledge about the network geometry and its infrastructure, i.e., speed limits and transportation capacities. This is the first work of this kind for two-dimensional traffic systems providing an explicit solution to the problem.

First, we will discuss the desired equilibrium to be achieved in a congested urban area. Then, the boundary control result will be presented. Finally, the theoretical results will be verified with the help of a numerical example, where we demonstrate the performance of the designed controller.

3.4.1 Optimal equilibrium

In this section, our main goal is to design a boundary controller that can drive a 2D traffic system governed by (3.34) to a steady state providing the maximal throughput of the system. Thereby, we rely on the steady state analysis from the previous Section 3.3.

3.4.1.1 General steady states

Recall that a steady state $\rho^*(\xi,\eta)$ implies space-independent $\phi^*(\eta)$, which can be achieved only for time constant $D(\rho_{in}(\eta))$ and $S(\rho_{out}(\eta))$. We obtained that the steady state flow along the line of constant η (3.50) is the minimum of demand at the entry, supply at the exit and the capacity of the strongest bottleneck located at $\xi^*(\eta)$ (3.51). By bottlenecks we mean permanent capacity constraints in the network itself, e.g., a road segment with low speed limit or with a few lanes (see Figure 3.11).

Thus, from the steady state flow given by (3.50), we need to extract the steady state density ρ^* that provides the physically relevant solution (entropy solution), which was already discussed in Section 3.3.2. Here we need to consider the minimum (3.50) of only two functions, as the demand at the upstream boundary $D(\rho_{in}(\eta))$ is always larger than capacity at the

bottleneck. This happens, since $\rho_{in}(\eta)$ is assumed to be very high for all η-lines, which implies by (2.13) that

$$D(\rho_{in}(\eta)) = \phi_{max}(\xi_{min}(\eta), \eta), \quad \forall \eta \in [\eta_{min}, \eta_{max}]. \tag{3.53}$$

If supply at the downstream boundary is also larger $S(\rho_{out}(\eta)) > \phi^{min}_{max}$, then ρ^* should be chosen to provide the congested regime $\forall \xi \in [\xi_{min}, \xi^*)$, and the free-flow regime occurs $\forall \xi \in (\xi^*, \xi_{max}]$. If there are several such ξ^* (or it is an interval), then we take the left-most value, i.e., $\xi^* = \xi^*_1$ in Figure 3.11. If $S(\rho_{out}(\eta))$ is smaller than the capacity at the bottleneck, then the whole domain is in the congested traffic regime.

3.4.1.2 Optimal steady state

Here we consider congested urban areas, and thus the inflow demand is assumed to be very high as in (3.53). This also means that the minimum function in the demand-supply problem (2.16) is resolved to the supply at the domain exit, which is treated as a control variable. Thus, we control the area outflow from its downstream boundary, i.e., $u(\eta) = S\left(\rho_{out}(\eta)\right)$ $\forall \eta \in [\eta_{min}, \eta_{max}]$ (as it was done in Section 2.2 but now it is on a 2D domain).

From (3.50) it is clear that the maximal throughput of the system in the equilibrium is achieved for $\phi^*(\eta) = \phi^{min}_{max}(\eta)$ for all η-lines. In order to provide a steady state that ensures the maximal throughput, we can actuate the downstream boundary accordingly, i.e., $u(\eta) = \phi^{min}_{max}(\eta)$. However, this control would lead to the violation of the congested regime, since the wave entropy condition prescribes the free-flow traffic regime $\forall \xi \in (\xi^*(\eta), \xi_{max}(\eta)]$, where $\xi^*(\eta)$ is given by (3.52) (see (3.50) and the discussion above). This is a situation that we would like to avoid, since this section deals exclusively with congested areas for mathematical simplicity.

Thus, we would like to define a desired steady state flow to be as close as possible to the maximal possible steady state flow (determined by the capacity at the strongest bottleneck) that still respects the constraint on the congested traffic regime in the whole area. For this purpose, we introduce a small constant $\epsilon > 0$ (small flow), and then the desired steady state flow can be defined as

$$\phi_d\left(\eta\right) = \phi^{min}_{max}\left(\eta\right) - \epsilon, \quad \forall \eta \in [\eta_{min}, \eta_{max}]. \tag{3.54}$$

By setting the control variable $u(\eta) = \phi_d(\eta)$, we translate the bottleneck to the end of the η-line, i.e., $\xi^*(\eta) = \xi_{max}(\eta)$. In this case, we guarantee that the congested traffic regime is preserved within the whole interval $[\xi_{min}(\eta), \xi_{max}(\eta)]$, see Figure 3.11. This allows us to control the system from the exit, and this control is applied in the strong sense, since the whole system is assumed to operate in one traffic regime (as in Section 2.2).

From the practical viewpoint, subtraction of ϵ does not change much the desired state, since ϵ can be set to an arbitrarily small value. Thus, in the following we will call the desired state an *ϵ-optimal equilibrium w.r.t. throughput maximization*. Note that controlling the domain exit can be physically realized by installing, e.g., traffic lights.

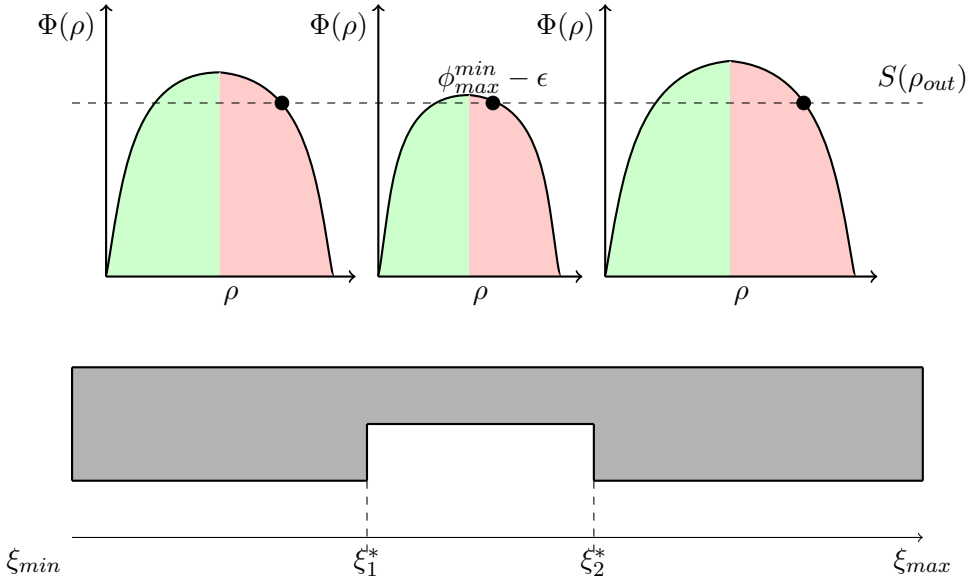

Figure 3.11: A single η-line with inhomogeneous capacities. Its worst bottleneck occupies a road segment $\xi^* = [\xi_1^*, \xi_2^*]$. The flow-density relation $\Phi(\rho)$ is Greenshields FD: green and red areas indicate free-flow and congested traffic regimes, respectively.

Definition 3.1
The desired ϵ-optimal equilibrium $\rho_d(\xi,\eta)$ w.r.t. the throughput maximization is defined $\forall(\xi,\eta) \in \bar{\Omega}$ as

$$\rho_d(\xi,\eta) = \frac{\rho_{max}(\xi,\eta)}{2} + \sqrt{\frac{\rho_{max}^2(\xi,\eta)}{4} - \frac{\rho_{max}(\xi,\eta)}{v_{max}(\xi,\eta)}\phi_d(\eta)}, \tag{3.55}$$

where $\phi_d(\eta)$ is defined in (3.54) and $\epsilon > 0$, see Figure 3.11.

Note that (3.55) was obtained by taking the inverse of (3.35) for $\Phi(\xi,\eta,\rho_d) = \phi_d(\eta)$, which leads us to the quadratic formula with two possible roots. To provide the congested traffic regime, we need to pick the plus sign.

3.4.2 Boundary control design

Problem 3.2
Given a urban network and its infrastructure parameters $v_{max}(\xi,\eta)$, $\rho_{max}(\xi,\eta)$ and $\phi_{max}(\xi,\eta)$ $\forall(\xi,\eta) \in \bar{\Omega}$ with initially congested traffic $\rho_0(\xi,\eta) \in (\rho_c(\xi,\eta), \rho_{max}(\xi,\eta)]$ whose dynamics are governed by (3.34) with Greenshields FD (3.35), and given large constant inflow demand at domain entry $D(\rho_{in}(\eta)) = \phi_{max}(\eta)$ $\forall\eta \in [\eta_{min}, \eta_{max}]$, design a boundary control law $u(\eta) = S_{out}(\eta)$ such that $\forall(\xi,\eta) \in \bar{\Omega}$:

$$\lim_{t\to\infty} \|\tilde{\rho}(\xi,\eta,t)\|_2 = 0, \tag{3.56}$$

where $\tilde{\rho}(\xi,\eta,t)$ is the L_2 norm of the deviation from the desired equilibrium (3.55). The L_2 norm and the error term are defined as in (1.7) and (1.9), respectively, but in (ξ,η)-space.

Theorem 3.1
The boundary control problem of driving a congested urban area to the desired ϵ-optimal equilibrium (3.55), as formulated in Problem 3.2, is solved with

$$u(\eta)=\phi_d(\eta), \quad \textit{where} \quad \phi_d(\eta)=\phi_{max}^{min}(\eta)-\epsilon, \qquad \forall\eta\in[\eta_{min},\eta_{max}]. \tag{3.57}$$

Proof. Let us define the following Lyapunov function candidate $\forall\eta\in[\eta_{min},\eta_{max}]$

$$V(\eta,t)=\frac{1}{2}\int\limits_{\xi_{min}(\eta)}^{\xi_{max}(\eta)} e^{\xi}\tilde{\rho}^2(\xi,\eta,t)d\xi, \tag{3.58}$$

where e^{ξ} is a weighting function used to provide the exponential convergence of the Lyapunov function (similar as in (2.44)). For simplicity of notations, we neglect variable η as an argument. The time derivative of (3.58) is

$$\dot{V}(t)=\int\limits_{\xi_{min}}^{\xi_{max}} e^{\xi}\tilde{\rho}(\xi,t)\frac{\partial\tilde{\rho}(\xi,t)}{\partial t}d\xi. \tag{3.59}$$

To simplify (3.59), we use the time-independence of ρ_d as:

$$\frac{\partial\tilde{\rho}(\xi,t)}{\partial t}=\frac{\partial\rho(\xi,t)}{\partial t}\equiv-\frac{\partial\Phi\left(\xi,\rho\right)}{\partial\xi}=-\frac{\partial\Phi\left(\xi,\rho_d+\tilde{\rho}\right)}{\partial\xi}. \tag{3.60}$$

We consider the most right-hand-side term and linearize the flux function around the desired state as follows:

$$\Phi\left(\xi,\rho_d+\tilde{\rho}\right)\approx\Phi\left(\xi,\rho_d\right)+\frac{\partial\Phi\left(\xi,\rho_d\right)}{\partial\rho}\tilde{\rho}, \tag{3.61}$$

which being inserted in (3.60) yields

$$\frac{\partial\tilde{\rho}(\xi,t)}{\partial t}=-\frac{\partial\Phi(\xi,\rho_d)}{\partial\xi}-\frac{\partial\left(\Phi'\left(\xi,\rho_d\right)\tilde{\rho}\right)}{\partial\xi}, \tag{3.62}$$

where the prime denotes $\Phi'=\partial\Phi/\partial\rho$.

Recall that, in general, the conservation law prescribes that

$$\frac{\partial\rho(\xi,t)}{\partial t}=-\frac{\partial\Phi(\xi,\rho)}{\partial\xi}.$$

Hence, if we consider a time-constant density $\rho_d(\xi)$, then by the conservation law we obtain $\partial\Phi(\xi,\rho_d)/\partial t=0$. This allows us to simplify (3.62) to

$$\frac{\partial\tilde{\rho}(\xi,t)}{\partial t}=-\frac{\partial\left(\Phi'\left(\xi,\rho_d\right)\tilde{\rho}(\xi,t)\right)}{\partial\xi}. \tag{3.63}$$

To simplify the notations, we omit the arguments of $\tilde{\rho}(\xi,t)$ and insert (3.63) into (3.59), which yields

$$\begin{aligned}\dot{V}(t) &= -\int_{\xi_{min}}^{\xi_{max}} e^{\xi}\tilde{\rho}\frac{\partial\left(\Phi'\left(\xi,\rho_d\right)\tilde{\rho}\right)}{\partial\xi}d\xi = -\int_{\xi_{min}}^{\xi_{max}} e^{\xi}\frac{2\Phi'\left(\xi,\rho_d\right)}{2\Phi'\left(\xi,\rho_d\right)}\tilde{\rho}\frac{\partial\left(\Phi'\left(\xi,\rho_d\right)\tilde{\rho}\right)}{\partial\xi}d\xi \\ &= -\int_{\xi_{min}}^{\xi_{max}} \frac{e^{\xi}}{2\Phi'\left(\xi,\rho_d\right)}\frac{\partial\left(\Phi'\left(\xi,\rho_d\right)\tilde{\rho}\right)^2}{\partial\xi}d\xi.\end{aligned} \tag{3.64}$$

We now consider $\Phi'\left(\xi,\rho_d\right)$, which is obtained by taking a derivative of (3.35) w.r.t. density:

$$\Phi'\left(\xi,\rho_d\right) = v_{max}\left(\xi\right)\left(1-\frac{2\rho_d\left(\xi\right)}{\rho_{max}\left(\xi\right)}\right). \tag{3.65}$$

In order to estimate an upper bound of (3.64), we will evaluate the derivative Φ' at ξ^*, which is the location of the bottleneck. Note that being the derivative of a concave function, Φ' achieves its maximum at the bottleneck in the congested regime (in the free-flow regime it is vice versa).

First, let us obtain the desired density at ξ^* using (3.35). Recall that by (2.5), in general, the capacity is given by $\phi_{max} = v_{max}\rho_{max}/4$, which lets us write:

$$\Phi\left(\xi^*,\rho_d(\xi^*)\right) = \phi_{max}(\xi^*) - \epsilon \Rightarrow \Phi\left(\xi^*,\rho_d(\xi^*)\right) = \frac{v_{max}(\xi^*)\rho_{max}(\xi^*)}{4} - \epsilon.$$

By using (3.35), this can be further rewritten as:

$$\begin{aligned}&v_{max}\left(\xi^*\right)\rho_d\left(\xi^*\right) - \frac{v_{max}\left(\xi^*\right)\rho_d^2\left(\xi^*\right)}{\rho_{max}\left(\xi^*\right)} = \frac{v_{max}\left(\xi^*\right)\rho_{max}\left(\xi^*\right)}{4} - \epsilon \\ &\Rightarrow \rho_d^2\left(\xi^*\right) - \rho_d\left(\xi^*\right)\rho_{max}\left(\xi^*\right) + \frac{\rho_{max}^2\left(\xi^*\right)}{4} - \frac{\epsilon\rho_{max}(\xi^*)}{v_{max}\left(\xi^*\right)} = 0 \\ &\Rightarrow \rho_d\left(\xi^*\right) = \frac{\rho_{max}\left(\xi^*\right)}{2} + \sqrt{\frac{\epsilon\rho_{max}(\xi^*)}{v_{max}\left(\xi^*\right)}}.\end{aligned} \tag{3.66}$$

Recall that in the solution of the quadratic equation, we need to choose the plus sign to respect the congested traffic regime. Thus, we insert (3.66) into (3.65) and introduce a variable ν used to denote Φ' at the bottleneck:

$$\Phi'\left(\xi^*\right) = -\sqrt{\frac{v_{max}\left(\xi^*\right)\epsilon}{\rho_{max}(\xi^*)}} = -\nu. \tag{3.67}$$

Notice that Φ' in (3.67) has the same physical meaning as velocity, which can be seen from its physical units by having in mind that ϵ is measured in [veh/s], see (3.54).

Let us now again use the arguments of $\tilde{\rho}$ and η. We can bound (3.64) from above using (3.67):

$$\dot{V}(\eta,t) \leq \frac{1}{2\nu}\int_{\xi_{min}(\eta)}^{\xi_{max}(\eta)} e^{\xi}\frac{\partial\left(\Phi'\left(\xi,\eta,\rho_d\right)\tilde{\rho}(\xi,\eta,t)\right)^2}{\partial\xi}d\xi. \tag{3.68}$$

Integration by parts of (3.68) yields

$$\begin{aligned}\dot{V}(\eta,t) =& \frac{e^{\xi_{max}(\eta)}}{2\nu(\eta)}\Phi'^2\left(\xi_{max}(\eta),\eta,\rho_d\right)\tilde{\rho}^2\left(\xi_{max}(\eta),\eta,t\right)\\ &- \frac{e^{\xi_{min}(\eta)}}{2\nu(\eta)}\Phi'^2\left(\xi_{min}(\eta),\eta,\rho_d\right)\tilde{\rho}^2\left(\xi_{min}(\eta),\eta,t\right)\\ &- \frac{1}{2\nu(\eta)}\int\limits_{\xi_{min}(\eta)}^{\xi_{max}(\eta)} e^{\xi}\left(\Phi'\left(\xi,\eta,\rho_d\right)\tilde{\rho}\left(\xi,\eta,t\right)\right)^2 d\xi.\end{aligned} \tag{3.69}$$

The last term in (3.69) can be again bounded by $\nu(\eta)$ as follows:

$$\begin{aligned}&-\frac{1}{2\nu(\eta)}\int\limits_{\xi_{min}(\eta)}^{\xi_{max}(\eta)} e^{\xi}\left(\Phi'\left(\xi,\eta,\rho_d\right)\tilde{\rho}\left(\xi,\eta,t\right)\right)^2 dx\\ &\qquad\leq -\frac{\nu(\eta)}{2}\int\limits_{\xi_{min}(\eta)}^{\xi_{max}(\eta)} e^{\xi}\tilde{\rho}^2\left(\xi,\eta,t\right)d\xi = -\nu(\eta)V(\eta,t).\end{aligned} \tag{3.70}$$

Inserting (3.70) into (3.69), we see that the only positive term is the first one, which can be eliminated by providing $\tilde{\rho}\left(\xi_{max}(\eta),\eta,t\right)=0$, i.e., $\rho\left(\xi_{max}(\eta),\eta,t\right)=\rho_d\left(\xi_{max}(\eta),\eta\right)$. This can be achieved by accordingly adjusting the boundary control

$$u(\eta)=\phi_d(\eta), \quad \text{where} \quad \phi_d(\eta)=\phi_{max}^{min}(\eta)-\epsilon, \qquad \forall\eta\in[\eta_{min},\eta_{max}], \tag{3.71}$$

as stated in Theorem 3.1. Note that the control term is different for each η. Thus, with (3.71) and (3.70), we can rewrite (3.69) as

$$\dot{V}(\eta,t) = -\frac{e^{\xi_{min}(\eta)}}{2\nu(\eta)}\Phi'^2\left(\xi_{min}(\eta),\eta,\rho_d\right)\tilde{\rho}^2\left(\xi_{min}(\eta),\eta,t\right) - \nu(\eta)V(\eta,t).$$

Thus, we have proved the L_2 convergence of $\rho\left(\xi,\eta,t\right)$ to the desired ϵ-optimal equilibrium $\rho_d\left(\xi,\eta\right)$ as $t\to\infty$ $\forall\eta\in[\eta_{min},\eta_{max}]$. It also follows that the pointwise convergence in η is achieved, which implies the L_∞ convergence in η. In bounded spaces (which is the case for η-space) this also implies the L_2 convergence in η. This proves the asymptotic L_2 convergence in the whole (ξ,η)-space.

□

3.4.3 Numerical example

Now let us demonstrate how this boundary control law (3.57) provides the convergence to the desired equilibrium with the help of a numerical example. For this purpose, we will again take a synthetic Manhattan grid network as in Section 3.1.6. The only difference is a larger noise

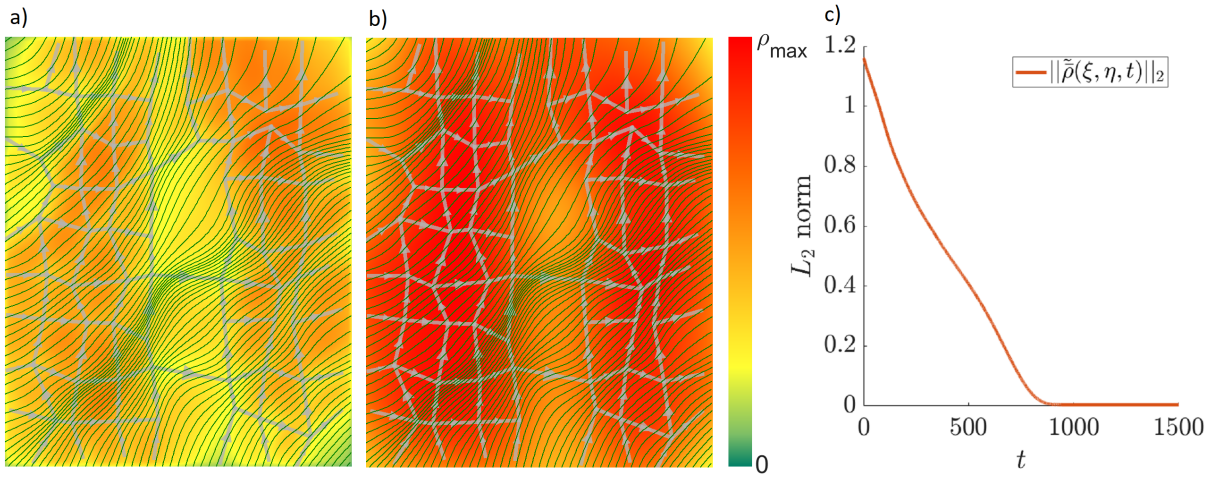

Figure 3.12: Control of urban traffic from the downstream boundary: a) desired steady state distribution, b) initial state of traffic jam, c) L_2 norm of the density error as a function of time.

in the positions of intersections with the standard deviation of 20 m (network is drawn in grey in Figures 3.12a) and 3.12b)). For a continuous approximation of the velocity field $v_{max}\vec{d}_\theta$, we use the weighting parameter $\mu = 20$ (the same as in Sections 3.3.3 and 3.1.6).

Thus, we will apply the boundary control to a fully congested urban area with the initial density distribution given by

$$\rho_0(\xi,\eta) = \rho_{max}(\xi,\eta), \qquad \forall(\xi,\eta) \in \bar{\Omega}.$$

There are a lot of vehicles at the upstream boundary of this area, i.e., $\rho_{in}(\eta,t) = \rho_{max}(\xi_{min}(\eta),\eta)\ \forall(\eta,t) \in [\eta_{min},\eta_{max}] \times \mathbb{R}^+$. These vehicles permanently provide a maximal possible inflow into the system, that is $D(\rho_{in}(\eta)) = \phi_{max}\left(\xi_{min}(\eta),\eta\right)$. This traffic jam distribution is illustrated in Figure 3.12b). Thereby, the differences in the heatmap are caused by the variation of $\rho_{max}(\xi,\eta)$ along the domain. Thus, more yellow zones are the those characterized by a low maximal density, which is usually achieved in areas with low concentration of roads.

The desired ϵ-optimal steady state given by (3.55) is illustrated in Figure 3.12a) for $\epsilon = 10^{-5}$ veh/s. Notice that the desired density distribution is space-dependent, which is caused by the variety of the infrastructure in the considered domain, e.g., inhomogeneous distribution of roads, different speed limits, etc. Recall that this desired distribution provides the maximal possible throughput of the system at equilibrium up to a small constant ϵ that is introduced to guarantee that the vehicle density is always larger than the critical value (congested traffic regime).

For the numerical simulation, we first discretize the domain by η into $m = 180$ cells, and then the Godunov scheme (3.36) is implemented for every constant η. The boundary conditions are assigned to the ghost cells, which are the cells that do not belong to the domain

(see Section 3.2.5 for more details). Thus, for the congested system the boundary flows (3.38) in the numerical scheme are set to

$$\phi_{in,j} = S(\rho_{1,j}), \qquad \phi_{out,j} = u(j), \quad \forall j \in \{1, \dots, m\},$$

where u_j is the boundary controller (3.57) that was shown to provide the convergence to the desired steady state. The performance of this controller is shown in Figure 3.12c), from which we observe that the spatial L_2 norm of the error from the desired equilibrium converges to zero in finite time. The finite time convergence can be explained by the fact that in a linear traffic system (obtained if we consider only one regime, as we did here and in Section 2.2), the boundary condition is propagated in the whole domain with the characteristic line that has a finite propagation speed.

3.4.4 Discussions

In this section, we considered large-scale urban networks from the control point of view. In particular, we again used the 2D LWR model rewritten in curvilinear coordinates (3.34), and demonstrated how it can be used for control design. The control goal was to drive a fully congested area to the equilibrium state characterized by the maximal throughput of the system, which also implies shorter traveling times. The maximal throughput at each line of constant η (flow path in a continuum plane) is constrained from above by the capacity of its strongest bottleneck. For instance, imagine a road (or η-line in our terms) that consists of segments characterized by different speed limits, e.g., 30 km/h and 50 km/h. Then, the steady state flow is constant along the road, and its value is determined by the capacity of the road segment with the lowest speed limit.

To simplify the problem mathematically, we restricted this part to traffic being only in the congested regime. This allows us to consider a linear problem (as it was done in Section 2.2), which is a set of transport PDEs parametrized by η with space-dependent FD. This simplification allows us to consider boundary conditions in a strong sense, and moreover, we do not have to handle discontinuities in the solution. We provide the congested regime by adding a small constant ϵ, and subtract it from the desired equilibrium flow, which corresponds to the maximal throughput minus ϵ. Hence, we call the desired state the ϵ-optimal state w.r.t. throughput maximization. Notice that this constant was introduced for mathematical simplicity, and its value can be arbitrarily small. Thus, the desired state can still be seen as the equilibrium of (almost) maximal throughput.

The control design should be realized by actuating only the downstream boundary of the congested domain. It again relies on the model (as in the previous section) and requires only the information about the network geometry and its infrastructure parameters. The controller (3.57) includes only the feedforward component, since the curvilinear coordinate transformation and the restriction to only one traffic regime allowed us to considerably simplify the 2D network control problem. Lyapunov methods were used to prove the exponential convergence to the desired equilibrium. Finally, we demonstrated the performance of the

boundary controller on an example of a heavily congested network with a large inflow demand at its entry. The L_2 norm of the error term showed a finite time convergence.

In the next section, we are going to extend the boundary control problem to the mixed regime traffic, which implies considering a nonlinear PDE for a urban network (3.34).

3.5 Boundary control for mixed regime traffic

In this section, we consider control problem for large-scale urban networks with mixed regime traffic. Thereby, we again rely on the 2D LWR model resulting from the curvilinear coordinate transformation (3.34), i.e., an assumption on uni-directional traffic must still hold. Unlike in the previous Section 3.4, here the traffic state satisfies a fully nonlinear PDE system without being restricted to any particular regime. Thus, we now consider a much more general problem that poses a lot of technical issues to handle due to discontinuities in the solutions and weak boundary conditions.

We design a boundary control law for some uni-directional urban transportation area explicitly by relying only on intrinsic model properties and network geometry. The main contribution of this section is to present the first explicitely derived boundary controller for a 2D conservation law model that is able to track a space- and time-dependent trajectory that admits discontinuities in its solutions. To make this possible, we use the Hamilton-Jacobi framework as it was done in Section 2.3, but extending it to 2D and handling space-dependency of the fundamental diagram, see Section 3.2.6 for a general theory on Hamilton-Jacobi PDE with space-dependent Hamiltonians. This means that instead of the classical Lax-Hopf formula (2.32), we have to apply the viability theory to the solution of a Hamilton-Jacobi-Moskowitz problem with a space-dependent Hamiltonian explained in [44, 11].

3.5.1 Problem statement

Problem 3.3
Our objective is to design boundary control laws $u_{in}(\eta,t)$ and $u_{out}(\eta,t)$ $\forall(\eta,t)\in[\eta_{min},\eta_{max}]\times\mathbb{R}^+$ such that the vehicle density $\rho(\xi,\eta,t)$ given by the system (3.34) tracks a desired trajectory as $t\to\infty$.

In Section 2.3 a similar problem was posed for a single homogeneous road (see Problem 2.3 and Lemma 2.2) but there was no space-dependency in the FD. Here we extend this result for a large urban area whose infrastructure is captured by the space-dependency in the FD, which makes its solution more technically involved. Throughout this section we make the following assumptions:

Assumption 3.1
Inflows $\phi_{in}(\eta,t)$ and outflows $\phi_{out}(\eta,t)$ of the 2D traffic system (3.34) must satisfy the follow-

ing inequalities $\forall(\eta,t)\in[\eta_{min},\eta_{max}]\times\mathbb{R}^+$

$$\phi_{in}(\eta,t)\le\phi^{min}_{max}(\eta),\quad \phi_{out}(\eta,t)\le\phi^{min}_{max}(\eta), \tag{3.72}$$

where $\phi^{min}_{max}(\eta)$ *is the transportation capacity at the strongest bottleneck along the* η*-line defined in* (3.51).

Moreover, there exists $\varepsilon>0$ *such that* $\phi_{in}(\eta,t)$ *and* $\phi_{out}(\eta,t)$ *additionally satisfy:*

$$\begin{aligned}&\int_{t}^{t+t_{ctr}(\eta)}\phi_{in}(\eta,\tau)d\tau\le t_{ctr}(\eta)\phi^{min}_{max}(\eta)-\varepsilon\quad \textit{and}\\ &\int_{t}^{t+t_{ctr}(\eta)}\phi_{out}(\eta,\tau)d\tau\le t_{ctr}(\eta)\phi^{min}_{max}(\eta)-\varepsilon,\end{aligned} \tag{3.73}$$

where $t_{ctr}(\eta)$ *is the minimal controllability time for* η*-line, i.e., the time needed for a solution evolving from one end of* η*-line to reach the opposite end:*

$$t_{ctr}(\eta)=\min\left\{\int_{\xi_{min}(\eta)}^{\xi_{max}(\eta)}\frac{1}{v(\hat\xi,\eta)}d\hat\xi,\int_{\xi_{min}(\eta)}^{\xi_{max}(\eta)}\frac{1}{\omega(\hat\xi,\eta)}d\hat\xi\right\}. \tag{3.74}$$

It means that inflows and outflows for each η-line are not allowed to exceed the capacity of the strongest bottleneck of the corresponding line instantly (3.72), and (3.73) means that they must be strictly lower during the time interval given by $t_{ctr}(\eta)$ (3.74). This assumption is necessary for the proof of Theorem 3.2.

Assumption 3.2
The solution of IBVP (3.34) *is determined by the boundary conditions only, i.e., the initial conditions have left the system.*

Remark 3.1
Note that if Assumption 3.1 is satisfied, then Assumption 3.2 holds trivially by taking $t\ge t_{min}$*, where* t_{min} *is the largest time, after which it is guaranteed that the initial conditions will have left the domain* $\bar\Omega$*. The value of* t_{min} *is given by*

$$\begin{aligned}t_{min}&=\max_{\eta\in[\eta_{min},\eta_{max}]}t_{min}(\eta),\quad \textit{where}\\ t_{min}(\eta)&=t_{ctr}(\eta)\left(1+\left\lceil\frac{1}{\epsilon}\int_{\xi_{min}(\eta)}^{\xi_{max}(\eta)}\Big(\rho_{max}(\hat\xi,\eta)+\rho_c(\hat\xi,\eta)\Big)\,d\hat\xi\right\rceil\right),\end{aligned}$$

which corresponds to equations (B.40) *and* (B.41) *that were derived in Appendix B.5.4.*

Here we consider a vehicle density given by system (3.34). To analyze this system for a boundary control task (as it was done in the proof of Theorem 2.3), one can obtain its solution

in explicit form for the equivalent H-J system (3.41). Let us assume that the space-dependent flow-density relation in (3.34) has a triangular shape (3.4), and then apply the variational principle (3.47) to calculate the solution to (3.41). The derivation of its solution is quite technical and, therefore, we shift it to Appendix B.5. Thus, if Assumptions 3.1 and 3.2 hold, the solution $M(\xi,\eta,t)$ reads $\forall(\xi,\eta,t)\in\bar{\Omega}\times[t_{min},+\infty)$:

$$\begin{aligned} M(\xi,\eta,t) = \min\Bigg\{ &\int_0^{t-T_v(\xi,\eta)} \phi_{in}(\eta,\tau)\,d\tau + \int_{\xi_{min}(\eta)}^{\xi_{max}(\eta)} \rho_0(\hat{\xi},\eta)\,d\hat{\xi}, \\ &\int_0^{t-T_\omega(\xi,\eta)} \phi_{out}(\eta,\tau)\,d\tau + \int_{\xi}^{\xi_{max}(\eta)} \rho_{max}(\hat{\xi},\eta)\,d\hat{\xi}\Bigg\}, \end{aligned} \tag{3.75}$$

where

$$T_v(\xi,\eta) = \int_{\xi_{min}(\eta)}^{\xi} \frac{1}{v(\hat{\xi},\eta)}d\hat{\xi}, \qquad T_\omega(\xi,\eta) = \int_{\xi}^{\xi_{max}(\eta)} \frac{1}{\omega(\hat{\xi},\eta)}d\hat{\xi}. \tag{3.76}$$

Recall that $t\in[t_{min},+\infty)$ implies that the effect of initial conditions has left the system (see Remark 3.1).

Remark 3.2
We widely use the solution (3.75) obtained in H-J formalism to analyze the properties of system (3.34) in order to design the boundary control. The major reason lies in weak boundary conditions given by (3.37), which imply that not any control can be imposed at the boundaries at any time. Thus, (3.75) is used to estimate time periods during which controls might not be accepted by the system in terms of control restriction functions, as it was done in Section 2.3.

3.5.2 Boundary control design

Theorem 3.2
Consider a vehicle density function $\rho(\xi,\eta,t)$ governed by system (3.34) $\forall(\xi,\eta,t)\in\bar{\Omega}\times\mathbb{R}^+$, for which Assumptions 3.1 and 3.2 hold, and the corresponding Hamilton-Jacobi solution given by (3.75). Assume also the desired density profile $\rho_d(\xi,\eta,t)$ and boundary flows $\phi_{in_d}(\eta,t)$ and $\phi_{out_d}(\eta,t)$ that are also given by (3.34). Then, if $\forall(\eta,t)\in[\eta_{min},\eta_{max}]\times\mathbb{R}^+$ the boundary controllers in (3.34) are set to

$$\begin{aligned} &(1)\ u_{in}(\eta,t) = \phi_{in_d}(\eta,t) - ke(\eta,t), \\ &(2)\ u_{out}(\eta,t) = \phi_{out_d}(\eta,t) + ke(\eta,t), \\ &\text{where } e(\eta,t) = \int_{\xi_{min}(\eta)}^{\xi_{max}(\eta)} \Big(\rho(\hat{\xi},\eta,t) - \rho_d(\hat{\xi},\eta,t)\Big)\,d\hat{\xi} \quad \text{and} \quad k>0, \end{aligned} \tag{3.77}$$

then $\forall a, b$: $\xi_{min}(\eta) \leq a < b \leq \xi_{max}(\eta)$ *we obtain* $\forall \eta \in [\eta_{min}, \eta_{max}]$

$$\lim_{t\to\infty} \int_a^b \left(\rho(\hat{\xi}, \eta, t) - \rho_d(\hat{\xi}, \eta, t)\right) d\hat{\xi} = 0.$$

Notice that the boundary controllers $u_{in}(\eta, t)$ and $u_{out}(\eta, t)$ are applied by changing the demand at domain entry and the supply at domain exit, respectively. The control functions enter the system (3.34) through the minimum function (and therefore are not necessarily fulfilled pointwise):

$$u_{in}(\eta, t) = D\left(\rho_{in}(\eta, t)\right), \quad u_{out}(\eta, t) = S\left(\rho_{out}(\eta, t)\right).$$

Proof of Theorem 3.2. The proof shows that the MF solutions converge pointwise up to a constant shift as $t \to \infty$, see Lemma 2.2 and Remark 2.4 for implications of this convergence. Thus, the procedure here is the same as in the proof of Theorem 2.3 for a problem in 1D apart from a few differences listed in Appendix B.6. □

Remark 3.3
Note that the integral convergence of densities stated in Theorem 3.2 implies that the state approximates the desired trajectory as time goes to infinity, since a and b can be arbitrarily close in space, i.e., $\rho \approx \rho_d$ *as* $t \to \infty$.

3.5.3 Numerical example

Here we demonstrate the efficiency of our boundary controller (3.77) applied to traffic evolving on a urban network with geometry as in Grenoble downtown. The total surface of the chosen Grenoble area is approximately 1.4×1 km^2. We track a desired density profile that is space-dependent and periodic in time. The geometry of the studied area in Grenoble is shown in grey in Figure 3.13. The directions of traffic motion on roads were however modified for this example (numerically) such that all roads are uni-directional. Thus, there exists some global direction of traffic flow towards North-East of the city and no loops are allowed, which is exactly how it is illustrated in Figure 3.7. The speed limits on roads are taken from real Grenoble network data: some roads can be driven with 30 km/h, and others can be driven with 50 km/h.

We define a numerical grid in $\bar{\Omega} \times \mathbb{R}^+$ and deploy the Godunov scheme in 2D, as described in Section 3.2.5. First, discretize the η dimension into $m = 180$ cells. Then, we use the 2D Godunov scheme (3.36) for every $j \in \{1, \dots, m\}$ with a discretization step $\Delta\xi = 5$ m (space cell size in ξ dimension). We also set the time cell size $\Delta t = 0.1$ s, which provides that the CFL condition is satisfied. In order to compute the integral related to the feedback term in (3.77) we perform the Riemann summation for every $j \in \{1, \dots, m\}$ over all ξ cells, i.e., $i \in \{1, \dots, n_j\}$, where n_j is the number of ξ cells contained in each cell j.

Recall that triangular FD is characterized by $\rho_c = \rho_{max}/3$. The initial vehicle density distribution is given $\forall(\xi,\eta) \in \bar{\Omega}$ by

$$\rho_0(\xi,\eta) = \rho_{max}(\xi,\eta).$$

We set the inflow demand $D\left(\rho_{in_d}(\eta,t)\right)$ and the outflow supply $S\left(\rho_{out_d}(\eta,t)\right)$ in the desired system to be time-periodic functions:

$$D\left(\rho_{in_d}(\eta,t)\right) = \phi^{min}_{max}(\eta)\Big[0.6 + 0.4\sin\Big(2\pi\big(\frac{t}{1200} + 2\frac{\eta-\eta_{min}}{\eta_{max}-\eta_{min}}\big)\Big)\Big],$$

$$S\left(\rho_{out_d}(\eta,t)\right) = \phi^{min}_{max}(\eta)\Big[0.6 + 0.4\sin\Big(2\pi\big(\frac{t}{2400} + 2\frac{\eta-\eta_{min}}{\eta_{max}-\eta_{min}}\big)\Big)\Big].$$

Hence, these boundary flow functions are guaranteed to be smaller than the minimal capacity on each line of constant η. Note that these functions were chosen such to generate a mixed regime desired trajectory $\rho_d(\xi,\eta,t)$ with a period of $\tau = 2400$ seconds. Such a desired trajectory is generated on purpose, since the biggest advantage of boundary controllers (3.77) is the ability to handle mixed traffic regimes, which is mathematically a tricky case.

We demonstrate here, how the boundary control law enhances the traffic state if there is a feedback, i.e., $k > 0$ in (3.77). The controller is applied at both upstream and downstream boundaries of the domain, and it physically corresponds to demand at the entry and supply of the exit, as illustrated in Figure 3.4. Thus, we will compare two possible strategies:

1. Both feedforward and feedback terms are used, i.e., $\forall(\eta,t) \in [\eta_{min},\eta_{max}] \times \mathbb{R}^+$:
$$u_{in}(\eta,t) = \phi_{in_d}(\eta,t) - ke(\eta,t) \quad \text{and} \quad u_{out}(\eta,t) = \phi_{out_d}(\eta,t) + ke(\eta,t).$$
2. Only feedforward term is used (no feedback), i.e., $\forall(\eta,t) \in [\eta_{min},\eta_{max}] \times \mathbb{R}^+$:
$$u_{in}(\eta,t) = \phi_{in_d}(\eta,t) \quad \text{and} \quad u_{out}(\eta,t) = \phi_{out_d}(\eta,t).$$

In Figure 3.13 the evolution of traffic density within the time interval of $2\tau = 4800$ seconds is shown, i.e., 2 time periods of $\rho_d(\xi,\eta,t)$. The middle column illustrates the evolution of density controlled with the gain $k = 5\cdot 10^{-5}$, i.e., strategy 1). The left column corresponds to the density evolution using only the boundary conditions of the desired system, i.e., strategy 2). The right column is related to the time-periodic desired density trajectory with the boundary conditions as described above. We can observe the convergence to the desired profiles for the case with feedback that becomes visible already at $t = 2\tau$, while this does not happen for the case without feedback. Notice that all the density distributions are drawn in (x,y)-coordinates in Figure 3.13, i.e., we had to rescale the functions and to perform the back transformation from (ξ,η)-space to (x,y)-space.

In Figure 3.14, the L_1 norm of the error in the number of cars is depicted as a function of time for different control gains. The density error $\tilde{\rho}(x,y,t)$ is defined as in (1.10), and its L_1 norm can be computed as in (1.6). We can clearly see that a higher control gain $k = 10^{-3}$ provides a higher convergence speed in comparison to a controller with a smaller gain $k = 5\cdot 10^{-5}$. On the contrary, $k = 0$ will not achieve the goal even if we would start from an empty city without any cars. This could work only if there is absolutely no difference in the initial conditions with the desired profile, which is hardly ever possible.

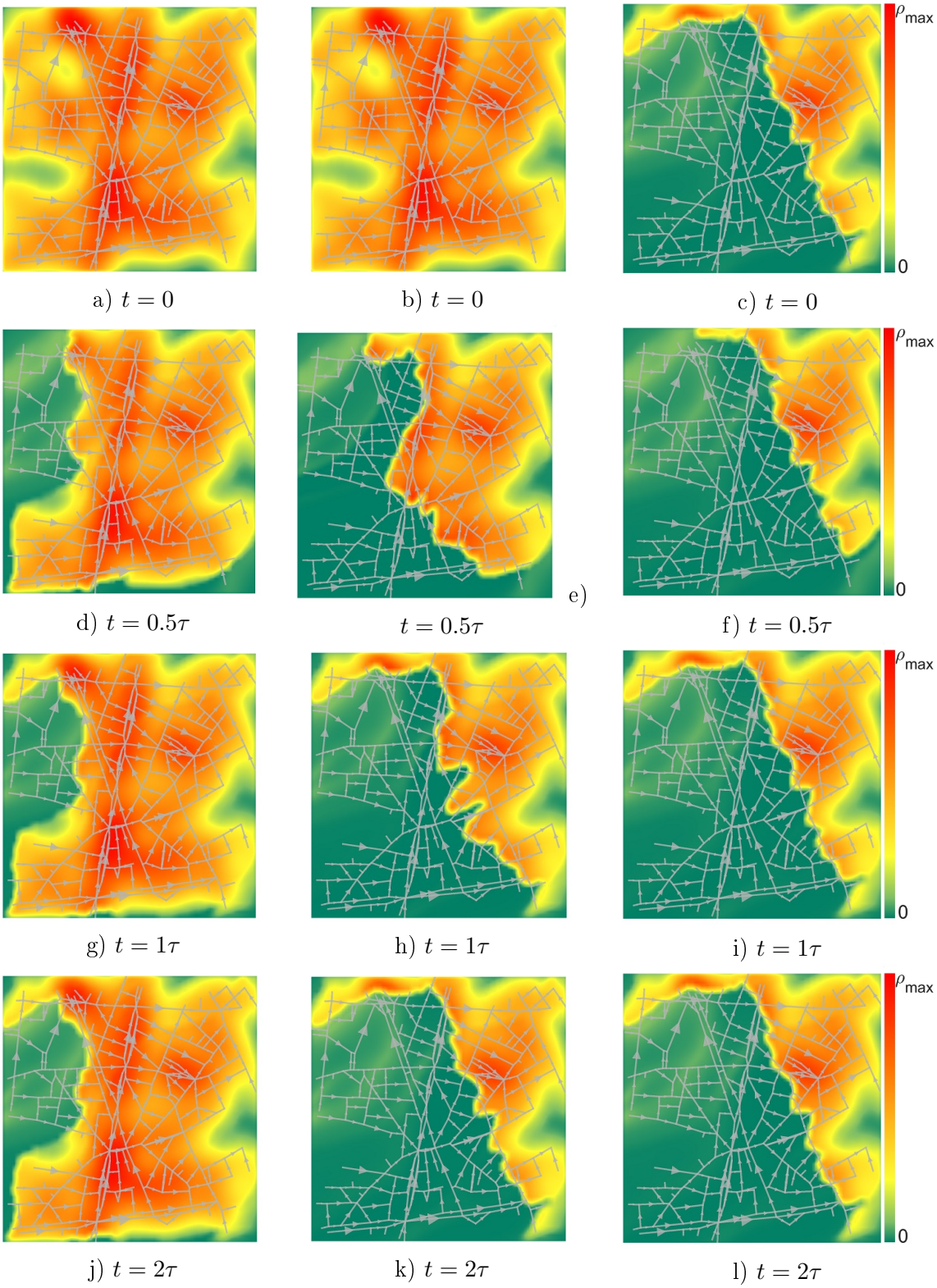

Figure 3.13: Traffic control in Grenoble downtown. **Right column**: desired density $\rho_d(x, y, t)$; **middle column**: evolution of $\rho(x, y, t)$ with $k = 5 \cdot 10^{-5}$; **left column**: evolution of $\rho(x, y, t)$ with $k = 0$. All the plots represent snapshots made at: a), b), c) $t = 0$; d), e), f) $t = 0.5\tau$; g), h), i) $t = 1\tau$; j), k), l) $t = 2\tau$.

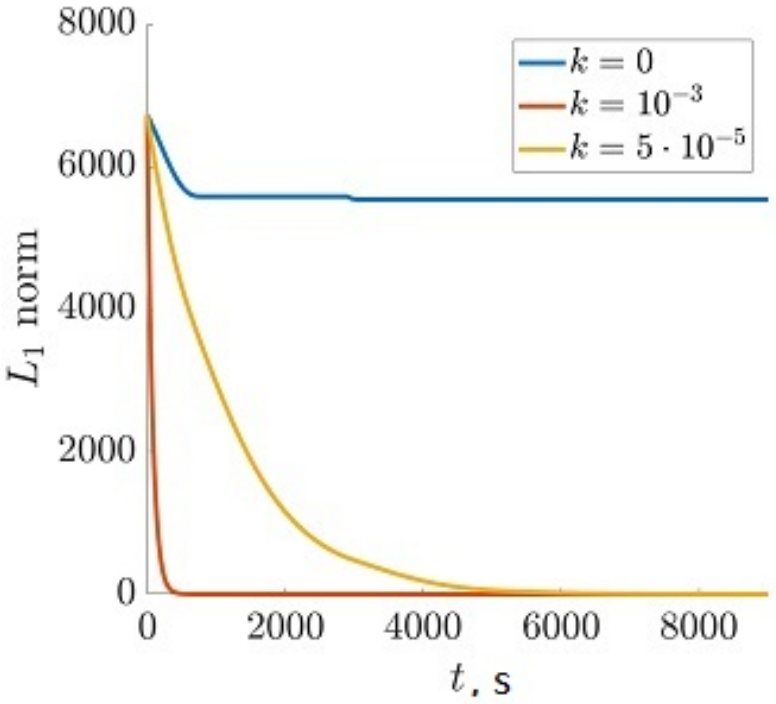

Figure 3.14: The L_1 norm of the density error as a function of time for different control gains.

3.5.4 Discussions

In this section, a boundary control technique was presented for a mixed regime traffic density evolving on a large urban network with a preferred direction of motion. The control goal was formulated in a similar way as in Section 2.3 but in two dimensions, which caused additional technical difficulties. The viability solution of the Hamilton-Jacobi PDE with space-dependent Hamiltonian (3.75) was used to prove Theorem 3.2 stating that the desired trajectory is approximated even if controls can not be directly imposed at the boundaries, i.e., we are able to handle weak boundary conditions in 2D using control restriction functions as in Section 2.3. Approximating desired density trajectory implies that the number of vehicles tracks pointwise the desired number of vehicles. Thus, from the practical view point, this control goal has even more sense than pointwise tracking of the desired density.

The controller (3.77) is applied at all boundaries of the urban area, and it acts as to track a space- and time-dependent trajectory that can be in any traffic regime. Its performance has been verified with the help of a numerical example using the geometry of an area in Grenoble downtown. Thereby, the initial density distribution corresponded to a traffic jam. We compared two control strategies: without the feedback part and with it. As expected from the theoretical results, feedback plays an essential role in tracking the desired density profile in the mixed traffic regime. Moreover, the control gain affects the convergence speed.

3.6 Traffic control using variable speed limit

Let us now demonstrate how to solve control tasks using a variable speed limit (VSL) in a 2D-plane by stating a new problem in (ξ, η)-space.

We consider the following IBVP on the same bounded domain $(\xi, \eta, t) \in \bar{\Omega} \times \mathbb{R}^+$:

$$\begin{cases} \dfrac{\partial \rho(\xi,\eta,t)}{\partial t} + \dfrac{\partial \Phi(\xi,\eta,\rho(\xi,\eta,t),u)}{\partial \xi} = 0, \\ \phi_{in}(\eta,t,u) = \min\left\{D\left(\xi_{min},\eta,\rho_{in}(\eta,t),u\right), S\left(\xi_{min},\eta,\rho\left(\xi_{min},\eta,t\right),u\right)\right\}, \\ \phi_{out}(\eta,t,u) = \min\left\{D\left(\xi_{max},\eta,\rho\left(\xi_{max},\eta,t\right),u\right), S\left(\xi_{max},\eta,\rho_{out}(\eta,t),u\right)\right\}, \\ \rho(\xi,\eta,0) = \rho_0(\xi,\eta), \end{cases} \tag{3.78}$$

where the flux function Φ now depends also on a control parameter $u \in [0,1]$ that represents the variable speed limit ratio: no VSL is applied if $u = 1$, and no movement is allowed if $u = 0$. Applying variable speed limits should be understood as a flexible (temporary) restriction on speed at which vehicles can drive on a given stretch of road. The speed limit varies according to the current environmental and road conditions and is displayed on electronic traffic signs. Setting $u = 1$ implies that vehicles can drive at speeds bounded by the legal maximum (e.g., 130 km/h on French highways, or by the comfort zone of drivers on German highways).

Note that flux Φ is still a concave function with respect to ρ, and Φ is continuous in u. Moreover, $\Phi(\xi,\eta,\rho,0) = \Phi(\xi,\eta,0,u) = 0$. One should see u as the **in-domain controller** that affects the traffic flow. It is applied in the whole domain including its boundaries. Therefore, the demand and supply functions in (3.78) have u as an additional argument.

3.6.1 Contributions

The material presented in this section was inspired by a previous work [78]. However, there are four major points that were not considered in [78], and thus will be addressed here:

1. *2D systems*: this is the first time that VSL control is applied on a large transportation network directly using the intrinsic properties of the model only. Hence, the VSL controller is designed by analysing the structure of a 2D conservation law (3.78) without any discretization that needs to be done to obtain a numerical solution.

2. *Space-dependent diagrams*: we extend the result of [78] by considering space-dependent diagrams, which imply space-dependent desired equilibrium profiles.

3. *Realistic FDs*: in [78] it was assumed that $\partial\Phi(\xi,\eta,\rho,u)/\partial u > 0$ holds, see Figure 3.15a). This assumption was made for simplicity to avoid multi-valued functions, i.e., there is only one value of u for each flow ϕ. In this section, we omit this condition by allowing more general forms of FD. In general, applying speed limits ($u < 1$) can cause a shift of the critical density towards larger values in realistic fundamental diagrams. This is

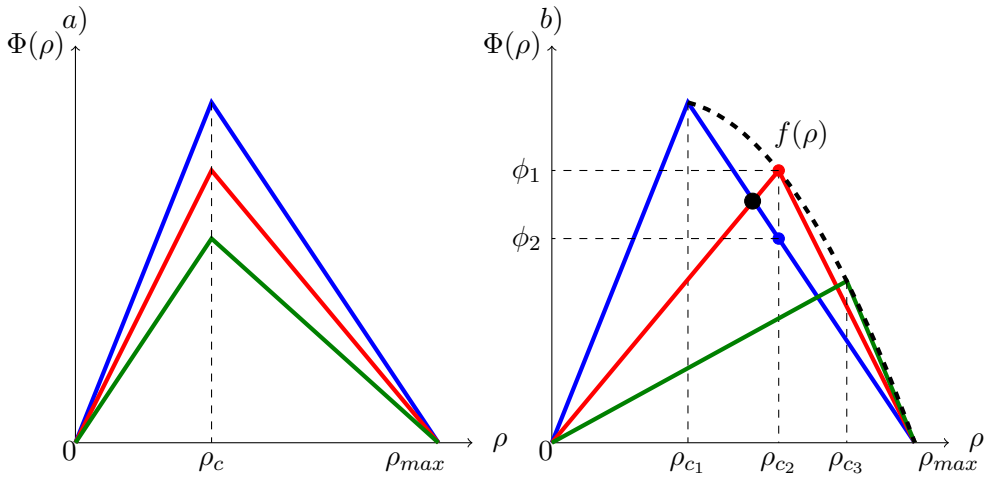

Figure 3.15: Fundamental diagrams and their dependence on speed limits: a) monotonic dependence $\partial\Phi(\xi,\eta,\rho,u)/\partial u > 0$ used in [78]; b) dependence we assume here, i.e., possible increase of ρ_c when stronger speed limits are applied (from real data, see [24]). Blue line: $u = 1$. Red line: $u = 0.7$. Green line: $u = 0.5$. Bold dashed line: maximal flow function defined in (3.80).

schematically depicted in Figure 3.15b), see red FD for $u = 0.7$ and green FD for $u = 0.5$ and compare ρ_{c3} and ρ_{c2} with ρ_{c1} achieved with $u = 1$. This means that applying speed limits can increase the range of vehicle density, for which the free-flow regime is preserved. There it is also shown how VSL can enhance traffic flow for some given densities in the congested regime, e.g., compare flows ϕ_2 with ϕ_1 that can be achieved with different speed limits for the same vehicle density ρ_{c2}. These VSL effects on the shape of FD were revealed from data obtained due to a real-life experiment conducted on a European VSL-equipped motorway, see [24]. In general, we have no restrictions on how FD must depend on VSL apart from $\Phi(\xi,\eta,\rho,0) = 0$, i.e., the flux function is zero if there is no movement allowed.

4. *Investigate the smoothness of VSL controller*: considering such a general class of fundamental diagrams may lead to irregular control policies. We investigate whether any conditions must be imposed on the functional dependence of FD on VSL in order to provide smoothness.

3.6.2 Problem statement

Let us first introduce the following notations:

$$\min_{\eta} \triangleq \min_{\eta\in[\eta_{min},\eta_{max}]}, \qquad \min_{\xi} \triangleq \min_{\xi\in[\xi_{min}(\eta),\xi_{max}(\eta)]},$$

and now we can formulate the stabilization problem as follows.

Problem 3.4
Given $\forall(\xi,\eta) \in \bar{\Omega}$ the fundamental diagram $\Phi(\xi,\eta,\rho,u)$ and the initial density $\rho_0(\xi,\eta)$ with dynamics governed by (3.78), find a VSL controller $u(\xi,\eta,t)$ such that

$$\lim_{t\to\infty} \tilde{\rho}(\xi,\eta,t) = 0, \quad \forall(\xi,\eta) \in \bar{\Omega} \tag{3.79}$$

where $\tilde{\rho}(\xi,\eta,t)$ is the deviation from a desired equilibrium $\rho_d(\xi,\eta) \in (0, \rho_{max}(\xi,\eta))$.

3.6.3 VSL control design

Let us define a *maximal flow function* $f(\xi,\eta,\rho)$, which is the maximum possible flow that can be achieved at a given space point for a given vehicle density over all the VSL values (see the thick dashed line in Figure 3.15):

$$f(\xi,\eta,\rho) = \max_{u\in[0,1]} \Phi(\xi,\eta,\rho,u). \tag{3.80}$$

We also introduce a multi-valued function $G(\xi,\eta,\rho,\phi)$, which is the inverse image of the fundamental diagram with respect to the speed limit:

$$G(\xi,\eta,\rho,\phi) = \{u \in [0,1] : \Phi(\xi,\eta,\rho,u) = \phi\}. \tag{3.81}$$

In general, it is possible that several values of speed limits u provide the same flow value, see the black dot in Figure 3.15. Therefore, $G(\xi,\eta,\rho,\phi)$ for a fixed set of parameters represents a set, not a single value.

Theorem 3.3
Let the controller $u = u(\xi,\eta,\rho)$ be given $\forall(\xi,\eta) \in \bar{\Omega}$ and for $\rho = \rho(\xi,\eta,t)$ by the following inclusion

$$\begin{aligned} &u(\xi,\eta,\rho) \in G(\xi,\eta,\rho,\phi_d(\xi,\eta,\rho)), \qquad \textit{with} \\ &\phi_d(\xi,\eta,\rho) = B(\xi,\eta,\rho) \min_{\xi'} \frac{f(\xi',\eta,\rho(\xi',\eta,t))}{B(\xi',\eta,\rho)} \\ &\textit{and} \quad B(\xi,\eta,\rho) = 1 + \gamma \int_{\xi_{min}(\eta)}^{\xi} \tilde{\rho}(\hat{\xi},\eta,t)d\hat{\xi}, \end{aligned} \tag{3.82}$$

where the control gain γ is a positive constant defined as

$$0 < \gamma < \min_{\eta} \left(\int_{\xi_{min}(\eta)}^{\xi_{max}(\eta)} \rho_{max}(\hat{\xi},\eta)d\hat{\xi} \right)^{-1}.$$

Then there exists $c = c(\gamma,\rho_0) > 0$ such that for every $\rho_0 \in C^1(\bar{\Omega})$ the system (3.78) with initial condition $\rho(\xi,\eta,0) = \rho_0(\xi,\eta)$ has a unique solution $\rho \in C^1(\bar{\Omega}\times\mathbb{R}^+)$, which satisfies

$$\max_{(\xi,\eta)\in\bar{\Omega}} |\tilde{\rho}(\xi,\eta,t)| \le e^{-ct} \max_{(\xi,\eta)\in\bar{\Omega}} |\tilde{\rho}(\xi,\eta,0)|, \qquad \forall t \in \mathbb{R}^+, \tag{3.83}$$

and moreover, $\forall(\xi,\eta) \in \bar{\Omega}$

$$\lim_{t\to\infty} \Phi(\xi,\eta,\rho(\xi,\eta,t),u(\xi,\eta,\rho)) = \min_{\xi'} f(\xi',\eta,\rho_d(\xi',\eta)). \tag{3.84}$$

Remark 3.4
Note that the VSL in-domain controller $u(\xi,\eta,\rho)$ depends on the state, i.e., it is a feedback control law. Let us give several comments on the controller structure:

1. *Such a controller choice (3.82) assures that the system flow is immediately set to the desired flow ϕ_d, i.e.:*
$$\Phi\left(\xi,\eta,\rho,u\right)=\phi_d(\xi,\eta,\rho),\qquad \forall(\xi,\eta,t)\in\bar{\Omega}\times\mathbb{R}^+.$$
2. *The desired flow $\phi_d(\xi,\eta,\rho)$ is designed such that it does not exceed the maximal flow function $f(\xi,\eta,\rho)$ in any point, i.e., $\forall(\xi,\eta,t)\in\bar{\Omega}\times\mathbb{R}^+$. The space-dependency of the desired flow is incorporated into function $B(\xi,\eta,\rho)$.*
3. *The function $B(\xi,\eta,\rho)$ is constructed in such a way that it acts as a feedback linearization for system (3.78). Thus, the system loses the conservation law structure, and we do not have to handle discontinuities in the solution. This will be shown later in the proof of Theorem 3.3.*
4. *The lower and upper bound on control gain γ are set such to guarantee that function $B(\xi,\eta,\rho)$ is positive, i.e., $B:\bar{\Omega}\times\mathbb{R}^+\to\mathbb{R}^+$. The upper bound on γ is required for situations when the density error $\tilde{\rho}$ has a negative value, which can appear since we design a general controller that drives any state to any desired equilibrium.*

Proof of Theorem 3.3. First of all, we need to prove that the controller given by (3.82) is well-defined. Namely, we will show that the set $G(\xi,\eta,\rho,\phi_d(\xi,\eta,\rho))$ is not empty, i.e., the desired flow takes values in a bounded range that can be achieved by the VSL control. Indeed, for all $(\xi,\eta)\in\bar{\Omega}$ we get from (3.82) that
$$\frac{\phi_d(\xi,\eta,\rho)}{B(\xi,\eta,\rho)}=\min_{\xi'}\frac{f(\xi',\eta,\rho)}{B(\xi',\eta,\rho)}\le\frac{f(\xi,\eta,\rho)}{B(\xi,\eta,\rho)},\tag{3.85}$$
and, thus, by the positivity of function $B(\xi,\eta,\rho)$ (see item 4 in Remark 3.4), we get $\phi_d(\xi,\eta,\rho)\in[0,f(\xi,\eta,\rho)]\ \ \forall(\xi,\eta,t)\in\bar{\Omega}\times\mathbb{R}^+$. This interval exactly corresponds to the range of the flux function $\Phi(\xi,\eta,\rho,u(\xi,\eta,\rho))$ w.r.t. u, therefore the set function $G(\xi,\eta,\rho,\phi_d(\xi,\eta,\rho))$ is not empty.

Now we substitute the constructed flux function
$$\Phi(\xi,\eta,\rho,u(\xi,\eta,\rho))=B(\xi,\eta,\rho)\min_{\xi'}\frac{f(\xi',\eta,\rho)}{B(\xi',\eta,\rho)}\tag{3.86}$$
into IBVP (3.78) and obtain:
$$\frac{\partial\tilde{\rho}(\xi,\eta,t)}{\partial t}+\min_{\xi'}\frac{f(\xi',\eta,\rho)}{B(\xi',\eta,\rho)}\frac{\partial B(\xi,\eta,\rho)}{\partial\xi}=0.$$
Then, if we insert the definition of function $B(\xi,\eta,\rho)$ from (3.82), this equation can be further simplified as
$$\frac{\partial\tilde{\rho}(\xi,\eta,t)}{\partial t}=-\gamma\tilde{\rho}(\xi,\eta,t)\min_{\xi'}\frac{f(\xi',\eta,\rho(\xi',\eta,t))}{B(\xi',\eta,\rho)}.\tag{3.87}$$

This equation does not contain any partial space derivatives, and thus the controller really acts such that the conservation law structure is lost. Moreover, this dynamic equation has a stable equilibrium at zero. By [78], we obtain an exponential convergence to the desired equilibrium with rate $c > 0$, which depends on controller gain γ and the maximal flow function f defined in (3.80).

Finally, we see that the convergence of densities $\forall(\xi,\eta) \in \bar{\Omega}\ \rho(\xi,\eta,t) \to \rho_d(\xi,\eta)$ as $t \to +\infty$ implies that function $B(\xi,\eta,\rho) \to 1$, and thus (3.86) results into

$$\Phi(\xi,\eta,\rho(\xi,\eta,t),u(\xi,\eta,\rho)) \to \min_{\xi'} f(\xi',\eta,\rho_d(\xi',\eta)),$$

which coincides with (3.84), and thus concludes the proof. □

Remark 3.5
Property (3.84) means that the highest possible equilibrium constant flow is achieved for a given $\rho_d(\xi,\eta)$. Namely, by definition of (3.80), the following double inequality holds $\forall\eta \in [\eta_{min},\eta_{max}]$

$$\min_{\xi} \Phi(\xi,\eta,\rho_d,1) \le \min_{\xi} f(\xi,\eta,\rho_d) \le \phi^{min}_{max}(\eta), \tag{3.88}$$

where $\phi^{min}_{max}(\eta)$ is the capacity at the strongest bottleneck along the η-line (3.51). The left inequality in (3.88) implies that the same or higher traffic flow can be achieved with lower speed limits than for $u = 1$. Thus, any VSL controller in the system can provide at most the flow $\min_{\xi} f(\xi,\eta,\rho_d)$, which is indeed achieved by controller (3.82) due to the property (3.84).

3.6.4 Smoothness of VSL controller

The VSL controller (3.82) is defined via inclusion, and in general it can result in a discontinuous function in space. For example, imagine that two different speed limits are able to provide the desired traffic flow. In this case, our fear would be that the speed limits jump from one value to another along the road infinitely many times. However, if we assume additional properties on how the flux function should depend on the speed limit, we will obtain that $u(\xi,\eta,\rho)$ is differentiable almost everywhere.

Theorem 3.4
Assume that $\forall(\xi,\eta) \in \bar{\Omega}$, $\forall\rho \in [0,\rho_{max}(\xi,\eta)]$ and $\forall u \in [0,1]$ the flux function $\Phi(\xi,\eta,\rho,u)$ is differentiable. Moreover, assume that it is either twice differentiable and strictly concave in u (congested regime) or monotonic in u and reaches its maximum at $u = 1$ (free-flow regime). Then using controller provided in Theorem 3.3 and assuming $\rho \in C^1(\bar{\Omega})$ $\forall t > 0$, we can choose the speed limit function $u(\xi,\eta,\rho)$ such that it is differentiable almost everywhere w.r.t. ξ.

Remark 3.6
This additional assumption on the functional dependence of $\Phi(\xi,\eta,\rho,u)$ on u can be interpreted as follows. When traffic is in the congested regime and speed limit decreases, the traffic flow can first increase for a fixed value density as illustrated in Figure 3.16b), and then it drops to zero as the speed limit approaches zero. On the contrary, when traffic is in the free-flow

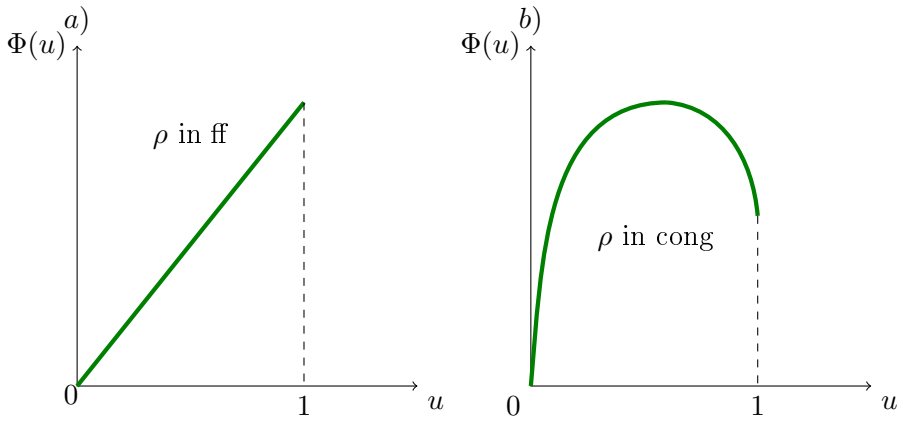

Figure 3.16: FD as a function of u: a) monotonic dependence for a fixed ρ in the free-flow regime, b) concave dependence for a fixed ρ in the congested regime.

regime, the flow of vehicles is maximal if there are no speed limits ($u = 1$), and when speed limits are applied the flow decreases monotonically as u decreases, see Figure 3.16a).

Remark 3.7
Notice that by Theorem 3.3, vehicle density is a differentiable function $\rho \in C^1(\bar{\Omega})\ \forall t \in \mathbb{R}^+$ if the initial condition function of system (3.78) is differentiable, i.e., $\rho_0 \in C^1(\bar{\Omega})$.

Proof of Theorem 3.4. For the proof, we fix time t and line η. Let us consider an interval of all possible ξ values and split it in two subsets H_1 and H_2 as:

$$[\xi_{min}(\eta), \xi_{max}(\eta)] = H_1 \cup H_2, \quad \text{where}$$
$$H_1 = \left\{ \xi \in [\xi_{min}(\eta), \xi_{max}(\eta)] \,\middle|\, \frac{\partial \Phi(\xi, \rho(\xi), u(\xi, \rho))}{\partial u} \neq 0 \right\},$$
$$H_2 = \left\{ \xi \in [\xi_{min}(\eta), \xi_{max}(\eta)] \,\middle|\, \frac{\partial \Phi(\xi, \rho(\xi), u(\xi, \rho))}{\partial u} = 0 \right\}.$$

We introduce also further subsets of H_1 and H_2 that correspond to their interiors:

$$E_1 = \text{int}(H_1), \qquad E_2 = \text{int}(H_2).$$

Moreover, we introduce a complementary subset E_0 as

$$E_0 = (H_1 \setminus E_1) \cup (H_2 \setminus E_2),$$

such that $E_0 \cup E_1 \cup E_2 = H_1 \cup H_2 = [\xi_{min}(\eta), \xi_{max}(\eta)]$.

It is clear that sets E_1 and E_2 have the same Lebesgue measure as sets H_1 and H_2, respectively. Thus, the set E_0 is of measure zero. This means that showing that the controller

function $u(\xi) = u(\xi, \rho(\xi))$ is differentiable on sets E_1 and E_2 would imply that it is differentiable almost everywhere. Let us first consider set E_1 with the following function defined from (3.86):

$$F_1(\xi, u) = \Phi(\xi, \rho(\xi), u) - B(\xi, \rho(\xi))k, \quad \text{where } k = \min_{\xi'} \frac{f(\xi', \rho(\xi'))}{B(\xi', \rho(\xi'))}.$$

This function is differentiable by the assumptions made in Theorem 3.4 and is equal to zero by (3.86). Moreover, the derivative of $\Phi(\xi, \rho(\xi), u)$ with respect to u is non-zero on set E_1 by its definition. This immediately implies that the derivative of $F_1(\xi, u)$ with respect to u is also non-zero. Therefore, we can use the Implicit Function Theorem, which assures that there exists a differentiable function $u(\xi)$ on this set satisfying (3.86).

In the second set E_2 we define another function as

$$F_2(\xi, u) = \frac{\partial \Phi(\xi, \rho(\xi), u)}{\partial u}.$$

Notice that $F_2(\xi, u)$ is zero by the definition of set E_2, and it has a negative derivative with respect to u, since we assumed concavity of the flux function for the congested traffic regime (in a pure free-flow regime set E_2 would be empty). This means that we can use the Implicit Function Theorem again, thus a differentiable function $u(\xi)$ exists on set E_2 as well.

Finally, combining these results, we obtain that the controller function $u(\xi)$ is differentiable on $E_1 \cup E_2$, i.e., almost everywhere. □

Proposition 3.1. *In case of concave dependence of FD on speed limits, $u(\xi, \eta, \rho)$ can sometimes be chosen from two values $G(\xi, \eta, \rho, \phi_d)$ for ρ being in congested regime, see Figure 3.16 b). Then, the most appropriate choice from the practical point of view is the minimal value, since it provides the free-flow traffic regime:*

$$u(\xi, \eta, \rho) := \min\{G(\xi, \eta, \rho, \phi_d)\}.$$

As an example, consider the intersection point (black dot) in Figure 3.15b) corresponding to the flow-density pair that can be achieved using either $u = 1$ or $u = 0.7$. In this case, we should choose $u = 0.7$, since this provides the free-flow regime and, thus, a more smooth traffic motion.

To conclude, we have shown that the VSL controller is differentiable almost everywhere if the fundamental diagram depends on u is a special way, i.e., monotonically increasing function of u in free-flow regime and a concave function of u in congested regime. In order to be able to apply the designed VSL controller (3.82) in practice (or in our case, it will be a numerical example), we should first discuss flux functions depending on u by suggesting an explicit relation satisfying assumptions made in Theorem 3.4.

3.6.5 Parametrization of fundamental diagram

Let us assume that the basic shape of FD is triangular as in (3.4), which should be modified due to the dependence on speed limits. We denote $v_1(\xi, \eta)$ and $\omega_1(\xi, \eta)$ as kinematic wave

speeds for $u = 1$ in the free-flow and in the congested regime, respectively. We can assume a linear dependence of kinematic wave speeds on speed limits, e.g.,

$$\begin{cases} v(\xi, \eta, u) = u\, v_1(\xi, \eta), \\ \omega(\xi, \eta, u) = \omega_1(\xi, \eta) + (1 - u)\omega_{add}(\xi, \eta), \end{cases} \tag{3.89}$$

where $\omega_{add}(\xi, \eta)$ is an additional value expressing the effect of speed limit on the kinematic wave speed in the congested regime. This value is bounded and will be defined later. Thus, if speed limits are high ($u \ll 1$), drivers are moving slowly, and therefore start braking late (larger safety distance for lower speeds). Let us estimate the range of reasonable values for $\omega_{add}(\xi, \eta)$ such that $\forall(\xi, \eta) \in \bar{\Omega}$

$$\frac{\partial \phi_{max}(\xi, \eta, u)}{\partial u} \geq 0. \tag{3.90}$$

Condition (3.90) means that it is not possible to enhance the transportation capacity by applying speed limits, see (3.88). This comes from the fact that ϕ_{max} is determined by the number of lanes and free-flow kinematic wave speed, which depends on the legal maximum speed that takes specific values depending on a country and road type. Thus, the transportation capacity is a property of urban network geometry and it should not be changed with a variable speed limit. In the following, we skip the dependence on (ξ, η) for simplicity of notations. We insert $\omega(u)$ and $v(u)$ from (3.89) into the definition of ϕ_{max} for triangular FD (2.3) and get

$$\phi_{max}(u) = v_1 \rho_{max} \frac{u\,(\omega_1 + (1 - u)\omega_{add})}{\omega_1 + v_1 u + (1 - u)\omega_{add}}. \tag{3.91}$$

We take the partial derivative of (3.91) w.r.t. u and obtain

$$\frac{\partial \phi_{max}(u)}{\partial u} = v_1 \rho_{max} \frac{(\omega_1 + (1 - u)\,\omega_{add})^2 - u^2 v_1 \omega_{add}}{(\omega_1 + v_1 u + (1 - u)\omega_{add})^2}. \tag{3.92}$$

In accordance with condition (3.90), we need to find such range of ω_{add} that (3.92) is positive. We distinguish two different cases, for which the nominator of (3.92) takes non-negative values $\forall u \in [0, 1]$:

1. Case $\omega_{add} \leq 0$. Then, obviously $\partial \phi_{max}(u)/\partial u > 0$ holds always.
2. Case $\omega_{add} > 0$. Then, we must provide that

$$\omega_1 + (1 - u)\,\omega_{add} \geq u\sqrt{\omega_{add} v_1} \Rightarrow \omega_1 + \omega_{add} \geq u\,(\omega_{add} + \sqrt{\omega_{add} v_1})\,.$$

In the worst case, this inequality must be satisfied for $u = 1$, which results into

$$\omega_{add} \leq \frac{\omega_1^2}{v_1}.$$

This expression yields the upper bound for ω_{add}. By the definition (3.89) and the fact that $\omega(u)$ should be non-negative, the lowest bound is $-\omega_1$. Thus, the reasonable range reads

$$\omega_{add} \in \Big[-\omega_1, \frac{\omega_1^2}{v_1} \Big].$$

For the numerical example, we will pick the largest possible value $\omega_{add} = \omega_1^2/v_1$, since by (3.92) this value provides $\partial\phi_{max}(u)/\partial u = 0$ at $u = 1$. From the physical viewpoint, this choice implies the largest possible influence of VSL on FD in the congested regime (the largest possible surface enclosed by the blue line in the congested regime and the thick dashed line in Figure 3.17).

3.6.6 Optimal equilibrium

The controller given by (3.82) can be applied to achieve any type of desired equilibrium $\rho_d(\xi,\eta) \in (0, \rho_{max}(\xi,\eta))\ \forall(\xi,\eta) \in \bar{\Omega}$. However, for the following numerical example, we seek to achieve an optimal equilibrium ρ_d^{opt} that corresponds to the throughput maximization and, at the same time, to the density maximization, i.e., the highest possible number of cars should be able to pass the system at maximal flow. Thereby, the number of cars in a urban area is directly related to the vehicle density in it that can be increased due to the change in the shape of fundamental diagram caused by $u(\xi,\eta,\rho)$, as it is shown in Figure 3.17.

The method to compute exactly equilibrium profiles providing the maximal flow in the system was presented in Section 3.4.1. However, there it was done for $u = 1$, i.e., no speed limits were applied. With the help of speed limits, we are now able to extend the result of Section 3.4.1 by maximizing also the number of vehicles that can pass the system at maximal flow. In particular, we seek to find $\forall(\xi,\eta) \in \bar{\Omega}$ speed limits $u^{opt}(\xi,\eta)$ such that

$$\phi_{max}(\xi,\eta,u^{opt}) = \phi_{max}^{min}(\eta,1),$$

where $\phi_{max}^{min}(\eta,1)$ is the maximal possible steady state flow determined by the capacity at the strongest bottleneck along the η-line (3.51). Thus, the VSL controller must provide that this steady state flow is achieved, and at the same time

$$\rho_d^{opt}(\xi,\eta) = \rho_c(\xi,\eta,u^{opt}).$$

Thus, the desired equilibrium density corresponds to the critical density achieved for u^{opt}. In terms of Figure 3.17, this means that if $\phi_{max}^{min}(u=1) = \phi_{max}(u^{opt})$ for some $(\xi,\eta) \in \bar{\Omega}$, then u^{opt} is such that $\rho_d^{opt} = \rho_c(u^{opt})$. Speaking in terms of Theorem 3.3, the desired flow $\phi_d = \phi_{max}(u^{opt})$. Hence, the controller should act such to provide the same maximal possible flow, while the density is increased, since $\rho_d^{opt} > \rho_1$. Notice that due to the change of FD shape, at the desired equilibrium traffic operates only at critical density, i.e., there are no congestions in the whole area.

Let us again skip (ξ,η) in the notations for simplicity. In order to find $u^{opt}\ \forall(\xi,\eta) \in \bar{\Omega}$, we use (3.91) and (2.3), and obtain

$$\phi_{max}(u^{opt}) = v_1\frac{v_1+\omega_1}{\omega_1}\rho_c\frac{u^{opt}\left(\omega_1+(1-u^{opt})\omega_{add}\right)}{\omega_1+v_1u^{opt}+(1-u^{opt})\omega_{add}}, \tag{3.93}$$

where ρ_c corresponds to the critical density as in (2.3) for $v = v_1$ and $\omega = \omega_1$.

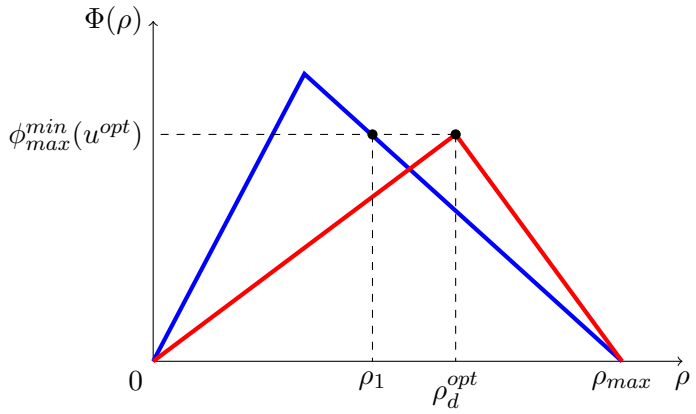

Figure 3.17: Blue line: FD for $u = 1$. Red line: FD for $u = u^{opt}$.

Further, we use $\rho_c v_1 = \phi_{max_1}$ with ϕ_{max_1} being the highest possible flow for some $(\xi, \eta) \in \bar{\Omega}$ reached with $u = 1$, and $\omega_{add} = \omega_1^2/v_1$ to rewrite (3.93) as

$$\phi_{max}(u^{opt}) = \phi_{max_1} \frac{u^{opt}\left(v_1 + (1 - u^{opt})\omega_1\right)}{\omega_1 + (v_1 - \omega_1)\, u^{opt}}. \tag{3.94}$$

Let us now introduce a coefficient $\kappa \in (0, 1]$ to denote the ratio of the flow at the strongest bottleneck along the η-line to the maximal possible flow at space point (ξ, η) for $u = 1$:

$$\kappa(\xi, \eta) = \frac{\phi_{max}^{min}(\eta, 1)}{\phi_{max}(\xi, \eta, 1)}.$$

From (3.94) we get the following equation $\forall(\xi, \eta) \in \bar{\Omega}$ to be solved for u^{opt}:

$$\kappa = \frac{u^{opt}\left(v_1 + (1 - u^{opt})\omega_1\right)}{\omega_1 + (v_1 - \omega_1)\, u^{opt}},$$

which can be further expanded as

$$\left(u^{opt}\right)^2 + u^{opt}\left(\kappa\left(\frac{v_1}{\omega_1} - 1\right) - \frac{v_1}{\omega_1} - 1\right) + \kappa = 0.$$

This is a quadratic equation with respect to u^{opt}, which yields two possible solutions. We pick the one with the minus sign, since this guarantees that u^{opt} remains below 1:

$$u^{opt} = \frac{\mu + 1 - \kappa(\nu - 1) - \sqrt{\left(\nu + 1 - \kappa(\nu - 1)\right)^2 - 4\kappa}}{2}, \tag{3.95}$$

with $\nu = v_1/\omega_1$. Finally, the optimal equilibrium is the critical density defined in (2.3) obtained for u^{opt} from (3.95):

$$\rho_d^{opt} = \frac{\omega(u^{opt})}{v(u^{opt}) + \omega(u^{opt})}\rho_{max}, \tag{3.96}$$

where $v(u^{opt})$ and $\omega(u^{opt})$ can be taken from (3.89) for $u = u_{opt}$ and $\omega_{add} = \omega_1^2/v_1$.

3.6.7 Numerical example

As a network we again take the downtown of Grenoble. All the infrastructure parameters and the two-dimensional discretization scheme are exactly the same as described in the numerical example for 2D boundary control presented in Section 3.5.3.

It is again assumed that the critical density in triangular FD is $\rho_c = \rho_{max}/3$. The initial datum is given $\forall(\xi,\eta) \in \bar{\Omega}$ by

$$\rho_0(\xi,\eta) = 3\rho_{max}(\xi,\eta)/4,$$

thus, it is in the congested traffic regime. The inflow demand and the outflow supply are set to the maximal possible steady-state flows for $u = 1$, that is

$$D\left(\xi_{min},\eta,\rho_{in}(\eta),u\right) = \phi^{min}_{max}(\eta,1), \quad S\left(\xi_{max},\eta,\rho_{out}(\eta),u\right) = \phi^{min}_{max}(\eta,1),$$

which are the only possible values, if we want to maximize the throughput of the system.

The desired optimal steady state (3.96) is constructed following the steps described above, and it is depicted in Figure 3.18b). This state is characterized by the maximal possible flow through the system achieved for the maximal possible number of vehicles. The numerical scheme needed to discretize the PDE system (3.78) is again the Godunov scheme in 2D that was described in Section 3.2.5. The only difference is that the for every grid point in space and time $\forall(i,j,k) \in \{1,\dots,m\}\times\{1,\dots,n_j\}\times\mathbb{Z}^+$, the flux function must include dependence on VSL controller as in (3.89) for $u = u^{opt}$ from (3.95).

Note that in (3.82) there exists an upper bound for the controller gain γ that guarantees that $B(\xi,\eta,\rho) > 0$ $\forall(\xi,\eta,t) \in \bar{\Omega}\times\mathbb{R}^+$. However, one can accelerate the convergence rate by choosing the maximal possible $\gamma(\eta,t)$ for each line of constant η and for each time. Thus, we will compare the control results obtained with two different control gains:

1. A constant control gain $\gamma = 0.14$ that is the largest possible value for a given urban network (Grenoble downtown) that matches the bounds stated in Theorem 3.3.

2. A time- and space-varying control gain $\gamma(\eta,t)$:

$$\gamma(\eta,t) = \frac{1-\epsilon}{\max\left\{-\min\limits_{\xi}\int\limits_{\xi_{min}(\eta)}^{\xi}\tilde{\rho}(\hat{\xi},\eta,t)d\hat{\xi},\delta\right\}}, \tag{3.97}$$

   where $\delta > 0$ is chosen to get $\gamma > 0$ even if the minimum is positive (since the arbitrarily large γ can be used), and $\epsilon > 0$ provides the lower bound for $B(\xi,\eta,\rho)$.

Notice that Theorem 3.3 was proved for the case of constant γ (as in item 1). However, the convergence can be accelerated also with γ that depends on η and t as in (3.97). The only issue is that function B must be always positive, and also that γ can not depend on dimension ξ, since in this case the feedback linearization would not work such that the dynamic equation turns into(3.87) due to an additional derivative term w.r.t. ξ.

Figure 3.18c) - f) illustrates the temporal evolution of traffic density under the VSL control (3.95) with a time-varying gain given by (3.97) with $\epsilon = 0.01$ and $\delta = 0.1$. Thereby, at every time step, the demand and supply functions at domain boundaries are set to the maximal possible throughput corresponding to the desired flow in the system. We observe that the state converges to the desired equilibrium, which becomes visible already after $t = 2$ hours of simulation time.

Remark 3.8
Notice that at the desired equilibrium the critical density at each point of space will be higher than at initial time, since the VSL control changes the FD shape and affects the desired density is as in (3.96). Therefore, the results presented in Figure 3.18 may look like driving the traffic state towards more congested regime, although it is still the free-flow (recall that in the desired equilibrium the traffic operates at critical density, which becomes higher with VSL control). The traffic flow corresponds to the maximal possible steady state flow that is only determined by the network geometry (capacities at strongest bottlenecks).

Further, we compute the L_1 norm of the error in the number of cars as in (1.6) with $\rho_d^{opt}(\xi, \eta)$ from (3.96) being the desired state. Its temporal evolutions for two different control gains are shown in Figure 3.18a). As in the previous example, we again observe that a larger control gain (3.97) provides a higher convergence speed in comparison to the constant $\gamma = 0.14$. Recall that as soon as we start applying control, the traffic system is completely set to the free-flow regime, since we always choose the minimal VSL value (see Proposition 3.1).

3.6.8 Discussions

In this section, we designed an in-domain controller for the traffic state evolving on urban networks with dynamics governed by (3.78). This controller is a parameter incorporated into the flux function, and it should be interpreted as the ratio of a variable speed limit to the regular maximal allowed speed, i.e., $u < 1$ means that the speed limit is applied. Real data confirmed however that the traffic flow can be enhanced for a given density in the congested regime, i.e., applying VSL might be an efficient solution to manage congestions. It also revealed that the VSL changes the shape of the fundamental diagram such that the critical density is increased, i.e., applying speed limits may result into setting the traffic state to the free-flow regime. This, in general, results into a more smooth traffic motion without sudden breaking, which has also a positive ecological impact.

The VSL controller is presented in Theorem 3.3. It is applied continuously in space and time, and the controller affects the state such that the desired flow is immediately achieved, and the vehicle density converges to the desired equilibrium as in (3.87). Thus, the controller changes the structure of the PDE system (3.78) such that it is not a conservation law, i.e., the controller performs a feedback linearization. This considerably simplifies the analysis, since for continuous initial datum the solution to the state equation is a continuous function (and no weak formulation is required). Thus, it was shown that the exponential convergence to the

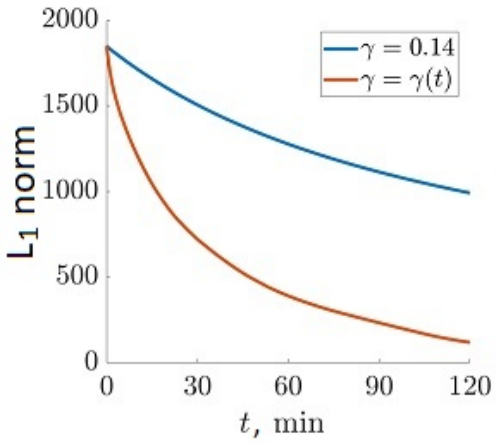

a) L_1 error

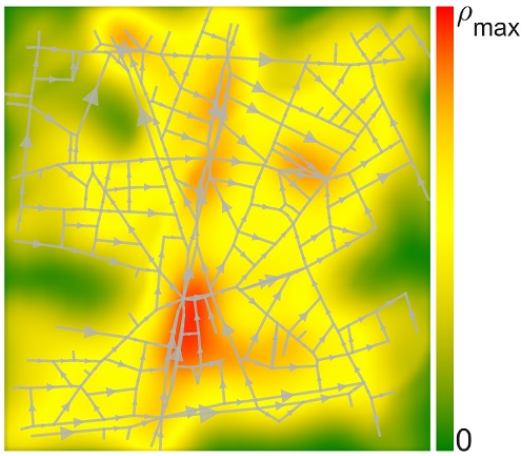

b) ρ_d^{opt}

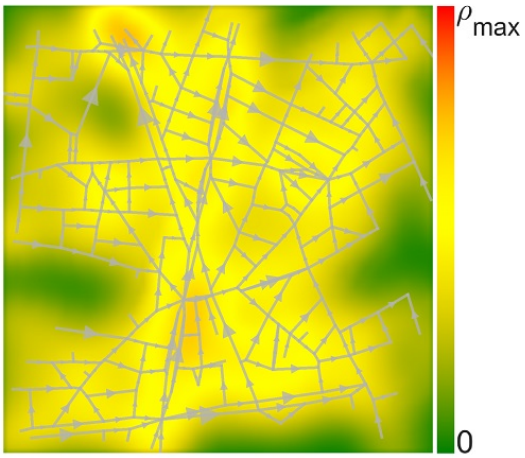

c) $t = 0$

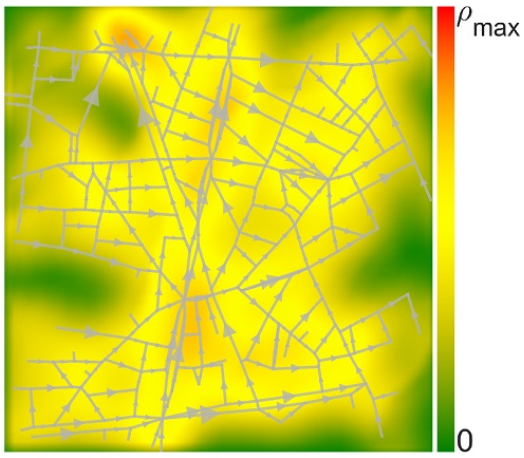

d) $t = 10$ min

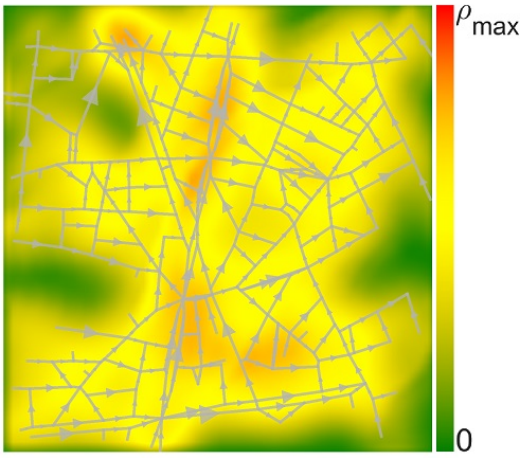

e) $t = 30$ min

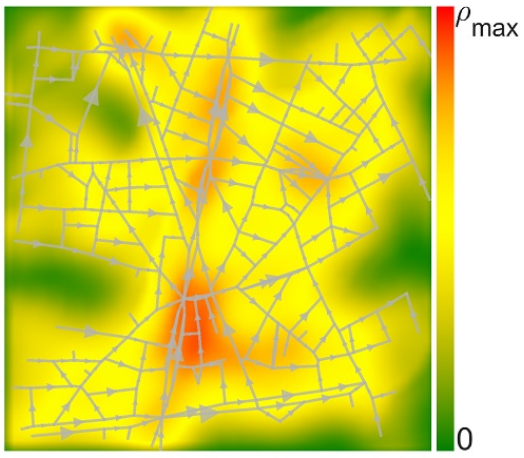

f) $t = 2$ hours

Figure 3.18: a) L_1 norm of density error as a function of time for different control gains, b) the desired optimal equilibrium as in (3.96). Traffic flow control by VSL in Grenoble downtown. Density $\rho(x, y, t)$ at: c) $t = 0$, d) $t = 10$ min, e) $t = 30$ min, f) $t = 2$ hours.

desired state is guaranteed under the proposed VSL controller (3.82).

Further, we analyzed the structure of the proposed controller in Theorem 3.4. Thereby, it was assumed that FD depends on speed limits such that it monotonically increases with u for the free-flow traffic regime and it reveals a concave dependence for the congested traffic regime. Under these assumptions, the controller was shown to be differentiable almost everywhere with respect to ξ-dimension, which determines the flow motion.

Then, we suggested a specific way to parametrize the triangular FD with u such that all these assumptions hold. This analysis allowed us to obtain the explicit form of FD, which was then analyzed to obtain the controller (3.95) providing the optimal steady state (3.96). This desired equilibrium corresponds to the throughput maximization for the maximal possible number of vehicles, i.e., as many vehicles as possible pass a urban area at maximal flow (for the same total traveling time). This is guaranteed by the modifications in the shape of FD introduced by the VSL controller that shifts the critical density such that the desired state corresponds to the critical density. Thus, the traffic is in the free-flow regime everywhere in the domain, while the maximum throughput is experienced by the maximal possible number of vehicles. The performance of the designed VSL controller was demonstrated on a numerical example, where a congested traffic is driven to the optimal equilibrium. The convergence to the desired state was observed after 2 hours. Notice that the convergence speed is determined by the controller gain that can be chosen larger, although its upper bound must not be violated. The value of the upper bound depends on the network infrastructure. The convergence happens also faster if the state is close to the desired equilibrium.

3.7 Chapter conclusions

This chapter was devoted to control of traffic on urban networks of any size whose dynamics are described by a conservation law in two dimensions such as 2D LWR (3.1). Traffic is viewed from the macroscopic point of view within this modeling approach. As in the 1D case, traffic is treated as a fluid that now propagates on a continuum 2D plane.

In Section 3.1 the 2D LWR model was presented. The model is inspired from crowd modeling with the only difference being the restriction for vehicles to move on real physical roads. Thus, the model requires to assume that the urban network is dense enough to be viewed as a continuum plane. This plane is bounded by the size of the considered urban area. To model traffic, one needs to have information about geometry and infrastructure of the urban network under study, i.e., the location of roads and intersections, number of lanes at each road and its speed limits. This information is used to define the maximal density and capacities on the network. Then, all these parameters are approximated on a continuum plane by applying the inverse distance weighting method that assigns values to variables everywhere as a function of the distance to real roads. All these parameters being specific for different urban networks are incorporated into the fundamental diagram that becomes an explicitly space-dependent function.

The 2D LWR model was compared to an MFD-based model in Section 3.1.5 using a steady-state vehicle density predicted by commercial microsimulator Aimsun as a reference distribution. It appeared that the 2D LWR model is able to predict steady-states even more accurately than the MFD-based model. Moreover, it tracks more precisely shapes of congested areas, which may play an important role for localized congestion mitigation control tasks. Thus, the 2D LWR model was justified as a reasonable choice for model-based control design. However, a direct analysis of such a model is a complicated task due to the second space derivative. It is also unclear which boundary point should be actuated to affect a specific in-domain point or area.

We had to find an approach to analyze this model such that one gets information about the trajectories followed by vehicles in the urban area. Such analysis became possible, since the structure of the 2D LWR model limits its applicability only for networks that consist of uni-directional roads. The direction field depends only on network geometry and not on state. If there are no loops in a network we can define a curvilinear coordinate transformation that was presented in Section 3.2. This coordinate transformation translates the 2D traffic system into a parametrized set of 1D systems with space-dependent fundamental diagram (3.34), which is a way easier to analyze. Mathematically, it means that instead of two partial derivatives with respect to space the modified system has only one. Although this coordinate transformation could be defined due to specific restrictions of 2D LWR model, this model can still be used to predict traffic evolution in several frequently occurring situations, e.g., when during the morning rush hour all vehicles stream to the city center where most companies are located.

Further, we have presented several results obtained by analysing the 2D LWR system in curvilinear coordinates. Namely, in Section 3.3 we have elaborated a technique to obtain steady-state vehicle distribution only by knowing inflow and outflow data of a urban area. This ability to analyze equation in 2D to obtain admissible equilibria is an essential result that enables formulating control tasks for stabilization of traffic evolving on large-scale urban networks. Further, this result was directly used in Section 3.4, where the model was analyzed for a boundary control design to mitigate congestions in some urban area. Thereby, traffic was restricted to the congested regime for mathematical simplicity, since otherwise one would have to deal with solution discontinuities.

The Hamilton-Jacobi formalism enabled to handle discontinuities for the boundary control design in Section 3.5, where the 2D LWR model in curvilinear coordinates was considered. There, the problem of approximating the desired vehicle trajectory has been posed for a mixed traffic regime in asymptotic time. The problem was solved in a similar way as it was done for the 1D case in Section 2.3. The additional difficulty was introduced due to the explicit space-dependency in the fundamental diagram such that the classical Lax-Hopf formula could not be applied. Instead, we had to apply the viability theory elaborated for the case of space-dependent Hamiltonians. For a numerical example, we took the structure of Grenoble downtown as a urban network. Simulation results revealed that the feedback part in the boundary controller is an essential component that makes the convergence to the desired vehicle trajectory possible.

Finally, we used the 2D LWR model in curvilinear coordinates to design a variable speed limit controller in Section 3.6. The VSL controller is used to directly affect the traffic flow by imposing temporary restrictions on allowed speed, which is often used for specific situations such as accidents, bad weather conditions, etc. This is an in-domain controller that is applied continuously in space in the whole domain. It acts as a feedback linearization such that the state equation loses its conservation law structure, which exempts us from considering the solution in the weak formulation due to shocks if the initial datum is continuous. The VSL controller can be used to stabilize the 2D system to any desired space-varying equilibrium. If FD has a concave dependence on controller in the congested traffic regime and a linear one in the free-flow regime (which is a physically intuitive assumption), then the controller is differentiable almost everywhere in space. The smoothness of the VSL controller has been studied, since the desired vehicle flow can sometimes be achieved for several speed limit ratio values. We have also investigated how to design an optimal steady state that corresponds to the throughput maximization achieved for the maximal possible number of cars. In a numerical example, we again used the structure of Grenoble downtown, and then demonstrated how the VSL controller makes the vehicle density converge to the desired equilibrium.

In the next Chapter 4, we will extend all these results to capture urban traffic that admits multiple directions and flow crossings, since assuming a network without loops was the main limitation of this chapter.

Chapter 4

Multi-Directional Traffic on Networks

This chapter is devoted to modeling and control of **multi-directional** traffic evolving on large-scale networks. Here we directly address the main limitation of the previous Chapter 3, which was the assumption on the existence of some preferred direction of motion on a network level. We propose a novel model that is able to describe traffic evolving in multiple directions on a urban network on a macroscopic level in Section 4.1. Thereby, we provide the derivation of this model step-by-step from the CTM at one intersection. Then, in Section 4.2, the model is validated using synthetic data from microsimulator, as well as using **real data** that we get from real sensors installed in the center of Grenoble. Finally, in Section 4.3, we design a boundary controller for traffic governed by our new model that acts to mitigate congestion.

4.1 Multi-directional continuous traffic model

In this section, we propose a new multi-directional two-dimensional continuous traffic model. It is called the NEWS model, since it consists of four PDEs that describe the evolution of vehicle density in four cardinal directions: North, East, West and South. This model can be applied to predict traffic evolution on a general urban network of arbitrary size by knowing only the information about its boundary flows, as well as network topology, turning ratios at each intersection and infrastructure parameters. The literature review on existing works in this direction is given in Chapter 1.

The contribution of this section is the formal derivation of a macroscopic model describing traffic propagation in a large traffic urban network of arbitrary size by using the classical CTM at each intersection. The resulting NEWS model is a hyperbolic system with bounded densities in each layer. It will also be shown that the model also corresponds to a conservation law with the conserved quantity being the vehicle density in the domain. The main novelty of our model is that it includes mixing between different density layers, i.e., it allows cars to change their original direction of movement. For example, imagine a car going to the North that changed its direction and turned to the East. Thus, there is a non-zero flow from one layer to another, which is captured by our model. We present a method allowing to transform traffic evolving on arbitrarily sparse networks into a continuum model, i.e., PDE. This is a beneficial form when it comes to modeling on a large scale, since it allows to describe traffic in terms of aggregated variables rather than tracking the motion of each individual vehicle.

First of all, we review the CTM for one intersection in Section 4.1.1, thereby introducing

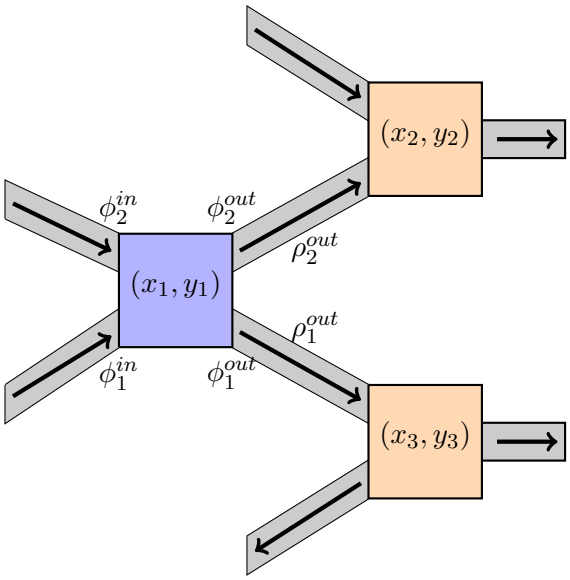

Figure 4.1: Example of a small traffic network consisting of 3 intersections. We consider the intersection filled in blue.

several important assumptions that must hold in this chapter. Then, we present the NEWS modeling framework with all the concepts and notations in Section 4.1.2. Further, we derive the NEWS model from the CTM in Section 4.1.3. Thereby, the model is expanded from one intersection to cover the whole network by applying the continuation method which was recently introduced in [110]. The continuation method turns an ordinary differential equation (CTM) into a partial differential equation. Therefore, **NEWS model** is a macroscopic (PDE-based) model that can be seen as a direct **extension** of the classical **LWR** to **general urban networks**.

4.1.1 Traffic model for one intersection

In this section, we seek to derive a multi-directional macroscopic traffic model that is able to predict the temporal evolution of traffic density. To achieve this, we need first of all to derive a traffic flow model for **one intersection**. During this derivation we will be able to define several important variables that will be later used to derive a continuous model for the whole network. In particular, we use the cell transmission model (CTM) [38] at one intersection to introduce the concept of *partial flows* from one road to another. Partial flows will then be used to express the traffic flow directions as a function of the network topology (more details are given below).

Let us consider an intersection located at (x_1, y_1) with two incoming and two outgoing roads (as illustrated in Figure 4.1), and show a step-by-step derivation of the traffic model at this intersection. Then, the traffic model will be generalized for an intersection with an arbitrary number of roads.

4.1.1.1 Flows at intersections: example

We use the demand-supply concept described in Section 2.1.5 to derive a traffic model for the intersection at (x_1, y_1) as illustrated in Figure 4.1. In particular, we need to determine inflows $\phi^{in}(t)$ and outflows $\phi^{out}(t)$ for this intersection that stay in balance

$$\phi_1^{in} + \phi_2^{in} = \phi_1^{out} + \phi_2^{out}.$$

Notice that unlike in previous chapters of this thesis, we now indicate the inflow and outflow w.r.t. some particular intersection (and not a domain boundary as it was meant, e.g., in (2.57)). Thus, we use a subscript to number roads, and a superscript is used to indicate whether this particular road is incoming or outgoing, e.g., $\phi_{max,1}^{in}$ is the capacity of incoming road number 1.

Assume that the flow-density relation at any road is given by a triangular FD as in (2.2). Then, the demand and supply functions are given by (2.17).

Remark 4.1
Notice that, in general, the derivation of the model relies only on the demand-supply concept, which is applicable also for a more general FD shape (not only triangular) as long as it is a concave function of density. We assumed the triangular shape only to gain more clarity during the upcoming step-by-step model derivation.

Each incoming road has its own flow demand to enter the intersection (illustrated in Figure 4.1) that reads with (2.17):

$$D_1 = \min\{v_1^{in}\rho_1^{in}, \phi_{max,1}^{in}\}, \qquad D_2 = \min\{v_2^{in}\rho_2^{in}, \phi_{max,2}^{in}\}. \tag{4.1}$$

A part of the flow entering the intersection goes to the first outgoing road and the other part goes to the second outgoing road. These flows are split according to the *turning ratios* (TR) $\alpha_{ij} \in [0, 1]$, where i is the index of the incoming road and j is the index of the outgoing road. For instance, if $\alpha_{11} = 0.6$ and $\alpha_{12} = 0.4$, then 60% of the cars from the first incoming road turn to the first outgoing road, and 40% turn to the second outgoing road. Note also that the sum of turning ratios for each incoming road must be 1, i.e.,

$$\alpha_{11} + \alpha_{12} = 1, \qquad \alpha_{21} + \alpha_{22} = 1.$$

The concept of TR was discussed, for example, in [39] for the case of diverging intersections.

Let us now introduce the concept of **partial demands**. A partial demand refers to the demand flow of an incoming road to enter a *particular* outgoing road. These are equal to the overall demands (4.1) (demand to enter an intersection) multiplied by the corresponding TR:

$$\begin{aligned} D_{11} &= \min\{\alpha_{11}v_1^{in}\rho_1^{in}, \alpha_{11}\phi_{max,1}^{in}\}, & D_{12} &= \min\{\alpha_{12}v_1^{in}\rho_1^{in}, \alpha_{12}\phi_{max,1}^{in}\}, \\ D_{21} &= \min\{\alpha_{21}v_2^{in}\rho_2^{in}, \alpha_{21}\phi_{max,2}^{in}\}, & D_{22} &= \min\{\alpha_{22}v_2^{in}\rho_2^{in}, \alpha_{22}\phi_{max,2}^{in}\}, \end{aligned}$$

where the first number in the subscript of D is related to the incoming road, and the second number is related to the outgoing road.

In accordance with [39], each outgoing road provides supply for the flow coming from an intersection, which in case of triangular FD (2.17) reads:

$$\begin{aligned} S_1 &= \min\{\omega_1^{out}(\rho_{max,1}^{out} - \rho_1^{out}), \phi_{max,1}^{out}\}, \\ S_2 &= \min\{\omega_2^{out}(\rho_{max,2}^{out} - \rho_2^{out}), \phi_{max,2}^{out}\}. \end{aligned} \tag{4.2}$$

Let us also *assume* that each outgoing road has a *particular* supply for each incoming road, e.g., S_1 is split into S_{11} and S_{21} (recall that the first number is referred to an incoming road). In order to define these *partial supplies*, we introduce **supply ratios** (SR) $\beta_{ij} \in [0, 1]$ used to denote the proportion of supply of outgoing road j that it provides for the maximal flow coming from a particular incoming road i relative to the supply it provides for all the incoming roads. The supply ratio β_{ij} is thus defined as

$$\beta_{ij} = \frac{\alpha_{ij}\phi_{max,i}^{in}}{\sum_{k=1}^{n_{in}} \alpha_{kj}\phi_{max,k}^{in}}, \tag{4.3}$$

where n_{in} is the overall number of incoming roads for some intersection, here $n_{in} = 2$. Notice that for each outgoing road the sum of its SR must be 1, i.e.,

$$\beta_{11} + \beta_{21} = 1, \qquad \beta_{12} + \beta_{22} = 1.$$

With the definition of supply ratios (4.3), we are now ready to formulate **partial supplies** as the overall (intersection-related) supply given by (4.2) multiplied by the corresponding SR:

$$S_{ij} = \beta_{ij}S_j = \min\{\beta_{ij}\omega_j^{out}(\rho_{max,j}^{out} - \rho_j^{out}), \beta_{ij}\phi_{max,j}^{out}\}.$$

Under the assumption of SR, we can also define **partial flows** as the minimum between partial demand and partial supply, e.g., $\phi_{11} = \min\{D_{11}, S_{11}\}$ yields:

$$\phi_{11} = \min\{\alpha_{11}v_1^{in}\rho_1^{in}, \beta_{11}\omega_1^{out}(\rho_{max,1}^{out} - \rho_1^{out}), \alpha_{11}\phi_{max,1}^{in}, \beta_{11}\phi_{max,1}^{out}\}.$$

Finally, the intersection-related flows from incoming and to outgoing roads are expressed as sums of the corresponding partial flows, i.e.,

$$\begin{aligned} \phi_1^{in} &= \phi_{11} + \phi_{12}, \qquad \phi_2^{in} = \phi_{21} + \phi_{22}, \\ \phi_1^{out} &= \phi_{11} + \phi_{21}, \qquad \phi_2^{out} = \phi_{12} + \phi_{22}. \end{aligned}$$

Notice that the sum of flows before and after the intersection is always conserved, i.e., $\phi_1^{in} + \phi_2^{in} = \phi_1^{out} + \phi_2^{out}$. Thus, we have established a traffic flow model at one particular intersection from Figure 4.1 by explicitly deriving expressions for its inflows and outflows.

4.1.1.2 Flows at intersections: generalization

We can now generalize the calculations from above to any intersection with n_{in} incoming roads with densities ρ_i^{in} and flows ϕ_i^{in} for $i \in \{1, \dots, n_{in}\}$, and n_{out} outgoing roads with densities ρ_j^{out} and flows ϕ_j^{out} for $j \in \{1, \dots, n_{out}\}$.

Every incoming road i has its own flow demand D_i to enter its source intersection:

$$D_i = \min\{v_i^{in}\rho_i^{in}, \phi_{max,i}^{in}\}.$$

Then, we define partial demands from road i to road j as

$$D_{ij} = \alpha_{ij} D_i = \min\{\alpha_{ij} v_i^{in}\rho_i^{in}, \alpha_{ij}\phi_{max,i}^{in}\}.$$

Supply S_j of the outgoing road j is simply given by

$$S_j = \min\{\omega_j^{out}(\rho_{max,j}^{out} - \rho_j^{out}), \phi_{max,j}^{out}\}.$$

Partial flow ϕ_{ij} from incoming road i towards outgoing road j is given by

$$\begin{aligned} \phi_{ij} &= \min\{D_{ij}, S_{ij}\} = \\ &= \min\{\alpha_{ij} v_i^{in}\rho_i^{in},\ \beta_{ij}\omega_j^{out}(\rho_{max,j}^{out} - \rho_j^{out}),\ \alpha_{ij}\phi_{max,i}^{in},\ \beta_{ij}\phi_{max,j}^{out}\}. \end{aligned} \tag{4.4}$$

Finally, the flow from incoming road ϕ_i^{in} is the sum over all the flows exiting this road, and the flow into outgoing road ϕ_j^{out} is the sum over all the flows coming into this road:

$$\phi_i^{in} = \sum_{j=1}^{n_{out}} \phi_{ij}, \qquad \phi_j^{out} = \sum_{i=1}^{n_{in}} \phi_{ij}. \tag{4.5}$$

For a better overview, we have summarized all the notations introduced in this section in Appendix A.3.1.

4.1.2 NEWS framework

We seek to develop a model capable of predicting the evolution of multi-directional traffic in a large-scale network that may consist of thousands of intersections. The main challenge thereby is that roads at every intersection may be oriented arbitrarily. Hence, we would like to obtain a model in terms of flows that are parallel to the cardinal directions: North (**N**), East (**E**), West (**W**) and South (**S**). This will enable us to formulate the model in macroscopic terms, if every intersection will be described in a unified way. Let us call it the **NEWS**-model. Its state variables should be denoted by bars, and they represent 4-dimensional vectors, e.g., $\bar{\phi}^{in} = (\bar{\phi}_N^{in}, \bar{\phi}_E^{in}, \bar{\phi}_W^{in}, \bar{\phi}_S^{in})^T$.

Notice that the resulting model is intended to describe the evolution of densities in four direction layers, although an urban area can in general be represented as a 2D plane (x and y). The reason to consider traffic evolution in opposite directions (e.g., North and South) independently is related to the idea to preserve flow values positive, since we want to keep information about the number of vehicles moving in each direction.

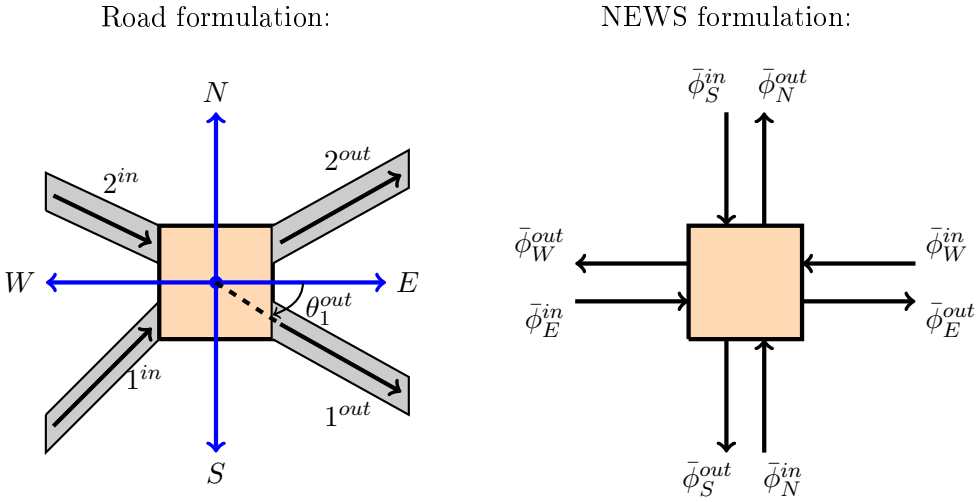

Figure 4.2: Idea of NEWS framework: map road original directions into North, East, West and South directions, and then traffic flow can be described in terms of 4 direction layers.

4.1.2.1 Projection from roads to NEWS

In order to formulate the traffic model in terms of NEWS, *we will use only the geometric properties of the network*, such as angles of the road orientations with respect to the East direction counter-clockwise denoted by θ that ranges from 0 to 2π, see Figure 4.2. Thereby, roads 1^{in} and 2^{out} are oriented towards North-East, and roads 2^{in} and 1^{out} are oriented towards South-East.

Let us consider the projection of flows into the North. We calculate the flow to the North as a weighted sum of all flows on the roads that have angles less than $\pi/2$ with the North direction, i.e., these are roads 1^{in} and 2^{out} in Figure 4.2. This also means that, in general, an angle of road's direction with non-zero projection to the North is bounded to the range $\theta \in (0, \pi)$, while for non-zero projections to the East, West and South the angle must be $\theta \in (0, \frac{\pi}{2}) \cup (\frac{3\pi}{2}, 2\pi)$, $\theta \in (\pi/2, 3\pi/2)$ and $\theta \in (\pi, 2\pi)$, respectively. Then, outflows in NEWS formulation can be found from the road formulation by applying the following projection:

$$\bar{\phi}_N^{out} = p^N_{\theta_1^{out}} \phi_1^{out} + p^N_{\theta_2^{out}} \phi_2^{out}, \qquad \bar{\phi}_E^{out} = p^E_{\theta_1^{out}} \phi_1^{out} + p^E_{\theta_2^{out}} \phi_2^{out},$$
$$\bar{\phi}_W^{out} = p^W_{\theta_1^{out}} \phi_1^{out} + p^W_{\theta_2^{out}} \phi_2^{out}, \qquad \bar{\phi}_S^{out} = p^S_{\theta_1^{out}} \phi_1^{out} + p^S_{\theta_2^{out}} \phi_2^{out},$$

where $p_\theta \in [0, 1]$ are *projection coefficients* that should satisfy the following properties:

1. If a road goes exactly to the North, then $p_\theta^N = 1$.
2. If a road has an angle equal to or greater than $\pi/2$ with the North direction, then $p_\theta^N = 0$.
3. The sum $p_\theta^N + p_\theta^E + p_\theta^W + p_\theta^S = 1$ to ensure the conservation of flows.

Notice that these properties are defined for the North direction, while the same holds also for other directions. The simplest choice for the projection coefficients p_θ, satisfying all these properties, is

$$
\begin{aligned}
p_\theta^N &= \begin{cases} \dfrac{\sin(\theta)}{|\cos(\theta)| + |\sin(\theta)|}, & \theta \in (0, \pi), \\ 0, & \text{elsewhere}, \end{cases} \\
p_\theta^E &= \begin{cases} \dfrac{\cos(\theta)}{|\cos(\theta)| + |\sin(\theta)|}, & \theta \in (0, \frac{\pi}{2}) \cup (\frac{3\pi}{2}, 2\pi), \\ 0, & \text{elsewhere}. \end{cases} \\
p_\theta^W &= \begin{cases} \dfrac{-\cos(\theta)}{|\cos(\theta)| + |\sin(\theta)|}, & \theta \in (\frac{\pi}{2}, \frac{3\pi}{2}), \\ 0, & \text{elsewhere}, \end{cases} \\
p_\theta^S &= \begin{cases} \dfrac{-\sin(\theta)}{|\cos(\theta)| + |\sin(\theta)|}, & \theta \in (\pi, 2\pi), \\ 0, & \text{elsewhere}, \end{cases}
\end{aligned}
\tag{4.6}
$$

where θ is a positive angle between the direction of the road and the East direction.

Notice that, in general, *each road can have non-zero weights with at most two directions.* For example, in Figure 4.2 the flow along the first outgoing road 1^{out} has non-zero weights with South and East direction, i.e., $p^S_{\theta_1^{out}} > 0$ and $p^E_{\theta_1^{out}} > 0$.

4.1.2.2 Flows in NEWS formulation

Flows *at each intersection* in NEWS formulation should be given by vectors $\bar{\phi}^{in} = (\bar{\phi}^{in}_N, \bar{\phi}^{in}_E, \bar{\phi}^{in}_W, \bar{\phi}^{in}_S)^T$ and $\bar{\phi}^{out} = (\bar{\phi}^{out}_N, \bar{\phi}^{out}_E, \bar{\phi}^{out}_W, \bar{\phi}^{out}_S)^T$. This allows us to establish the following relation with flows from the original road formulation given by (4.5):

$$
\bar{\phi}^{in} = \begin{pmatrix} \bar{\phi}^{in}_N \\ \bar{\phi}^{in}_E \\ \bar{\phi}^{in}_W \\ \bar{\phi}^{in}_S \end{pmatrix} = \begin{bmatrix} p^N_{\theta_1^{in}} & p^N_{\theta_2^{in}} \\ p^E_{\theta_1^{in}} & p^E_{\theta_2^{in}} \\ p^W_{\theta_1^{in}} & p^W_{\theta_2^{in}} \\ p^S_{\theta_1^{in}} & p^S_{\theta_2^{in}} \end{bmatrix} \begin{pmatrix} \phi^{in}_1 \\ \phi^{in}_2 \end{pmatrix}
$$

and

$$
\bar{\phi}^{out} = \begin{pmatrix} \bar{\phi}^{out}_N \\ \bar{\phi}^{out}_E \\ \bar{\phi}^{out}_W \\ \bar{\phi}^{out}_S \end{pmatrix} = \begin{bmatrix} p^N_{\theta_1^{out}} & p^N_{\theta_2^{out}} \\ p^E_{\theta_1^{out}} & p^E_{\theta_2^{out}} \\ p^W_{\theta_1^{out}} & p^W_{\theta_2^{out}} \\ p^S_{\theta_1^{out}} & p^S_{\theta_2^{out}} \end{bmatrix} \begin{pmatrix} \phi^{out}_1 \\ \phi^{out}_2 \end{pmatrix}.
$$

For a general case of n_{in} incoming and n_{out} outgoing roads, we introduce **projection matrices** $P_{in} \in \mathbb{R}^{4 \times n_{in}}$ and $P_{out} \in \mathbb{R}^{4 \times n_{out}}$ consisting of coefficients $p_{\theta_i^{in}}$ and $p_{\theta_j^{out}}$, respectively.

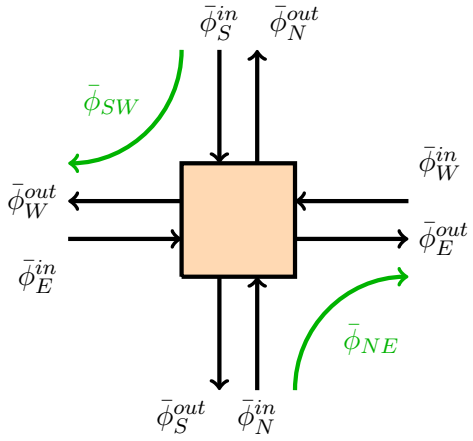

Figure 4.3: Schematic explanation of flow directions in NEWS formulation.

Thus, in general, flows are transformed into the NEWS formulation as follows:

$$\bar{\phi}^{in} = P_{in}\phi^{in}, \quad \bar{\phi}^{out} = P_{out}\phi^{out}. \tag{4.7}$$

In general, $\bar{\phi}_N^{in}$ is the flow on incoming roads going to the North direction before the intersection, and $\bar{\phi}_N^{out}$ is the flow on outgoing roads going to the North after the intersection, see Figure 4.3 for the illustration of this concept. They can also be represented by the sums over *partial flows in the NEWS formulation*:

$$\bar{\phi}_N^{in} = \bar{\phi}_{NN} + \bar{\phi}_{NE} + \bar{\phi}_{NW} + \bar{\phi}_{NS}, \tag{4.8}$$

and

$$\bar{\phi}_N^{out} = \bar{\phi}_{NN} + \bar{\phi}_{EN} + \bar{\phi}_{WN} + \bar{\phi}_{SN}, \tag{4.9}$$

where, for example, $\bar{\phi}_{NE}$ is the flow consisting of cars going to the North before the intersection and to the East after they have passed this intersection, as it is illustrated in Figure 4.3. Thus, $\bar{\phi}_N^{in}$ (4.8) is composed of all such flows that were going to the North before the intersection and then continued their way either to the North or changed to the East, West or South after passing the intersection.

In the NEWS formulation, partial flows are defined from the road formulation as follows:

$$\bar{\phi}_{EN} = \sum_{i=1}^{n_{in}} \sum_{j=1}^{n_{out}} p^E_{\theta_i^{in}} p^N_{\theta_j^{out}} \phi_{ij}, \tag{4.10}$$

where p_θ are the projection coefficients from (4.6). Notice that the correctness of this definition of partial flows can be verified by inserting (4.10) into (4.9):

$$\bar{\phi}_N^{out} = \sum_{j=1}^{n_{out}} p^N_{\theta_j^{out}} \left[\sum_{i=1}^{n_{in}} \left(p^N_{\theta_i^{in}} + p^E_{\theta_i^{in}} + p^W_{\theta_i^{in}} + p^S_{\theta_i^{in}} \right) \phi_{ij} \right] =$$
$$\sum_{j=1}^{n_{out}} p^N_{\theta_j^{out}} \sum_{i=1}^{n_{in}} \phi_{ij} = \sum_{j=1}^{n_{out}} p^N_{\theta_j^{out}} \phi_j^{out},$$

whereby we have used the fact that the sum of projection coefficients over all cardinal directions is 1 (see property 3 in the definition of p_θ and (4.5)).

To gain more insight into the concept of partial flows, let us consider an example of an intersection that has one incoming and one outgoing road, as shown in Figure 4.4. Hence, we define the incoming flow in NEWS formulation from Figure 4.4:

$$\bar{\phi}^{in} = \begin{pmatrix} \bar{\phi}^{in}_N \\ \bar{\phi}^{in}_E \\ \bar{\phi}^{in}_W \\ \bar{\phi}^{in}_S \end{pmatrix} = \begin{pmatrix} 0 \\ \bar{\phi}_{EN} + \bar{\phi}_{EE} \\ 0 \\ \bar{\phi}_{SN} + \bar{\phi}_{SE} \end{pmatrix}.$$

Thereby, we see that $\bar{\phi}^{in}_N = \bar{\phi}^{in}_W = 0$, since the incoming road has a zero weight with respect to both North and West direction, while it has non-zero weights with South and East directions.

The outgoing road has non-zero weights only with North and East direction, which results into $\bar{\phi}^{in}_S = \bar{\phi}_{SN} + \bar{\phi}_{SE}$ and $\bar{\phi}^{in}_E = \bar{\phi}_{EN} + \bar{\phi}_{EE}$. Hence, the flow on the outgoing road yields:

$$\bar{\phi}^{out} = \begin{pmatrix} \bar{\phi}^{out}_N \\ \bar{\phi}^{out}_E \\ \bar{\phi}^{out}_W \\ \bar{\phi}^{out}_S \end{pmatrix} = \begin{pmatrix} \bar{\phi}_{SN} + \bar{\phi}_{EN} \\ \bar{\phi}_{SE} + \bar{\phi}_{EE} \\ 0 \\ 0 \end{pmatrix}.$$

Also note that in Figure 4.4 there is no flow in the West direction, therefore all the flows containing at least one "W" are zero, e.g., $\bar{\phi}_{NW} = \bar{\phi}_{SW} = 0$, etc.

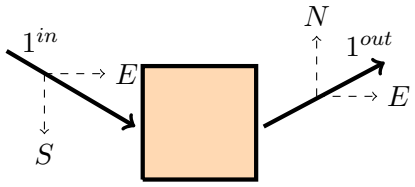

Figure 4.4: Sketch of an intersection with one incoming road 1^{in} and one outgoing road 1^{out}.

4.1.2.3 Turning and supply ratios in NEWS formulation

Similar to the traffic model in road formulation given by (4.5) and (4.4), we would like to define partial flows in the NEWS formulation using the demand-supply concept as in (2.15) and (2.16). For this, we will need to define turning $\bar{\alpha}$ and supply ratios $\bar{\beta}$ in the NEWS formulation. Moreover, we will also have to define the parameters of triangular FD $\bar{v}$, $\bar{\omega}$, $\bar{\rho}_{max}$ in the NEWS formulation to be able to derive the complete model.

Demand $\bar{D} \in \mathbb{R}^{4\times 1}$ and supply $\bar{S} \in \mathbb{R}^{4\times 1}$ functions from (2.17) can be formulated in terms

of NEWS using coefficient matrices P_{in}, P_{out} as in (4.7):

$$\begin{aligned} \bar{D} &= P_{in} \min\{v^{in}\rho^{in}, \phi^{in}_{max}\}, \\ \bar{S} &= P_{out} \min\{\omega^{out}(\rho^{out}_{max} - \rho^{out}), \phi^{out}_{max}\}. \end{aligned} \tag{4.11}$$

Now, without loss of generality, let us consider the partial flow from East to North $\bar{\phi}_{EN}$, which we would like to be able to express using demand and supply as in (4.4):

$$\bar{\phi}_{EN} = \min\{\bar{\alpha}_{EN}\bar{D}_E, \bar{\beta}_{EN}\bar{S}_N\}, \tag{4.12}$$

where $\bar{\alpha}_{EN}$ is the TR from East to North, and $\bar{\beta}_{EN}$ is the SR of the North provided for vehicles arriving from the East, i.e., the same as β_{ij} from (4.3) but in the NEWS formulation.

The coefficients $\bar{\alpha}_{EN}$ and $\bar{\beta}_{EN}$ need to be determined, which can be done using (4.10), in which we substitute (4.4) that yields

$$\bar{\phi}_{EN} = \sum_{i=1}^{n_{in}} \sum_{j=1}^{n_{out}} p^E_{\theta^{in}_i} p^N_{\theta^{out}_j} \min\left\{\alpha_{ij} v^{in}_i \rho^{in}_i,\ \beta_{ij}\omega^{out}_j(\rho^{out}_{max,j} - \rho^{out}_j),\ \alpha_{ij}\phi^{in}_{max,i},\ \beta_{ij}\phi^{out}_{max,j}\right\}.$$

This expression is a sum over minimum functions, which is tedious to handle. We make the following *approximation*: change the order of taking the minimum and the summations. This leads to the minimum over just four arguments as in the demand-supply concept (4.4):

$$\bar{\phi}_{EN} \approx \min\left\{\sum_{j=1}^{n_{out}} p^N_{\theta^{out}_j} \sum_{i=1}^{n_{in}} p^E_{\theta^{in}_i} \alpha_{ij} v^{in}_i \rho^{in}_i, \sum_{j=1}^{n_{out}} p^N_{\theta^{out}_j} \sum_{i=1}^{n_{in}} p^E_{\theta^{in}_i} \beta_{ij}\omega^{out}_j(\rho^{out}_{max,j} - \rho^{out}_j), \dots\right\}.$$

Notice that the difference between putting minimum inside and outside the summation is decreasing as the level of the homogeneity in the congestion of roads increases. This approximation is exact if all roads in the network are in the same traffic regime, i.e., either all roads are in free-flow or congested.

We set the latter expression equal to (4.12) for $\phi = \phi_{max}$, and get the coefficients $\bar{\alpha}_{EN}$ and $\bar{\beta}_{EN}$ that read

$$\bar{\alpha}_{EN} = \frac{\sum_{j=1}^{n_{out}} \left[p^N_{\theta^{out}_j} \sum_{i=1}^{n_{in}} \alpha_{ij} p^E_{\theta^{in}_i} \phi^{in}_{max,i}\right]}{\sum_{i=1}^{n_{in}} p^E_{\theta^{in}_i} \phi^{in}_{max,i}}, \tag{4.13}$$

and

$$\bar{\beta}_{EN} = \frac{\sum_{i=1}^{n_{in}} \left[p^E_{\theta^{in}_i} \sum_{j=1}^{n_{out}} \beta_{ij} p^N_{\theta^{out}_j} \phi^{out}_{max,j}\right]}{\sum_{j=1}^{n_{out}} p^N_{\theta^{out}_j} \phi^{out}_{max,j}}. \tag{4.14}$$

4.1.2.4 FD parameters and densities in NEWS formulation

Consider demand and supply functions in the NEWS formulation. From one side, we can calculate them using the projection matrices P_{in} and P_{out} as in (4.11). From the other side, we would like to be able to calculate demand and supply using a fundamental diagram as in (2.17), which should enable us to describe traffic flow in a unified way for any intersection. Recall that FD parameters depend on a specific road, while another road might already have a different speed limit or capacity.

Thus, we are going to define a unified FD in NEWS formulation such that the FD is defined for each direction separately. This equivalently means that the parameters of FD will all become 4-dimensional vectors or 4×4 diagonal matrices. Let us consider the FD for the North direction, while similar steps should be done for other directions. That is, for $\bar{D}_N$ and $\bar{S}_N$ we would like to find kinematic wave speeds $\bar{v}_N^{in}$ and $\bar{\omega}_N^{out}$ and density transformations $\bar{\rho}_N^{in}$ and $\bar{\rho}_N^{out}$ such that the following relations would hold:

$$\begin{aligned} \bar{D}_N &= \sum_{i=1}^{n_{in}} p_i^N \min\{v_i\rho_i, \phi_{max,i}\} \approx \min\{\bar{v}_N^{in}\bar{\rho}_N^{in}, \bar{\phi}_{max,N}^{in}\}, \\ \bar{S}_N &= \sum_{j=1}^{n_{out}} p_j^N \min\{\omega_j(\rho_{max,j} - \rho_j), \phi_{max,j}\} \approx \min\{\bar{\omega}_N^{out}(\bar{\rho}_{max,N}^{out} - \bar{\rho}_N^{out}), \bar{\phi}_{max,N}^{out}\}. \end{aligned} \tag{4.15}$$

Note that in the case when there are much more than 4 roads, we can use only approximations of the fundamental diagram.

By approximating sum of minimum functions as a minimum of sums and writing the conditions on maximal flows together, we get a system of two equations

$$\begin{aligned} \sum_{i=1}^{n_{in}} p_i^N v_i \rho_{c,i} &= \bar{v}_N^{in}\bar{\rho}_{c,N}^{in}, \\ \sum_{j=1}^{n_{out}} p_j^N \omega_j(\rho_{max,j} - \rho_{c,j}) &= \bar{\omega}_N^{out}(\bar{\rho}_{max,N}^{out} - \bar{\rho}_{c,N}^{out}). \end{aligned} \tag{4.16}$$

System (4.16) is undetermined, since it consists of two equations that have five unknowns $(\bar{v}_N^{in}, \bar{\omega}_N^{out}, \bar{\rho}_{c,N}^{in}, \bar{\rho}_{c,N}^{out}, \bar{\rho}_{max,N}^{out})$.

In general, we get the coordinates of each road, its number of lanes and speed limits as network data. Speed limits are directly related to the kinematic wave speeds v_j, while the maximal density $\rho_{max,j}$ on each road j (either incoming or outgoing) is determined by its number of lanes and the minimal car-to-car distance (we again assume it to be 6 m). Knowing $\rho_{max,j}$ for every road, we can easily obtain the critical density $\rho_{c,j}$ from the shape of the fundamental diagram (recall that we have assumed $\rho_c = \rho_{max}/3$). Negative kinematic wave speeds ω_j can be obtained from the speed limits v_j and critical density $\rho_{c,j}$ using (2.3) as

$$\omega_j = \frac{\rho_{c,j} v_j}{\rho_{max,j} - \rho_{c,j}}.$$

Both incoming and outgoing roads contribute to the vehicle density in some neighborhood of the intersection. Moreover, since we want to have a general model, which is symmetric with respect to incoming and outgoing roads, and in order to define each parameter only once, we assume symmetry $\bar{\rho}_N^{in} = \bar{\rho}_N^{out} = \bar{\rho}_N$, $\bar{v}_N^{in} = \bar{v}_N^{out} = \bar{v}_N$ and $\bar{\omega}_N^{in} = \bar{\omega}_N^{out} = \bar{\omega}_N$. Assume further that densities are transformed into NEWS formulation in the same way as it is done for the flows (4.7), i.e.:

$$\bar{\rho}_N = \sum_{i=1}^{n_{in}} p_i^N \rho_i + \sum_{j=1}^{n_{out}} p_j^N \rho_j, \tag{4.17}$$

which then also holds for maximal $\bar{\rho}_{max,N}$ and critical $\bar{\rho}_{c,N}$ densities. After we have defined all the densities, using symmetry assumption we can express the velocities from (4.16) as

$$\bar{v}_N = \frac{\sum_{i=1}^{n_{in}} p_i^N v_i \rho_{c,i} + \sum_{j=1}^{n_{out}} p_j^N v_j \rho_{c,j}}{\bar{\rho}_{c,N}},$$
$$\bar{\omega}_N = \frac{\sum_{i=1}^{n_{in}} p_i^N \omega_i (\rho_{max,i} - \rho_{c,i}) + \sum_{j=1}^{n_{out}} p_j^N \omega_j (\rho_{max,j} - \rho_{c,j})}{\bar{\rho}_{max,N} - \bar{\rho}_{c,N}}.$$

Recall that all these calculations are not limited to the particular triangular shape of FD, and thus can be performed in the same way for any type of FD as long as it is a concave function of density as it is also assumed in the LWR model (see Remark 4.1). The only thing that would have changed for different FD shapes are formulas for its parameters (**??**), since each FD can have a different set of parameters.

For a better overview, we have summarized all the notations introduced in this and next sections in Appendix A.3.2.

4.1.3 Derivation of the NEWS model

Our main goal here is to derive the macroscopic NEWS model for multi-directional traffic that can describe the evolution of traffic in terms of density (as in case of 1D and 2D LWR). For the moment, we can already describe traffic flow for any intersection in the unified way, which became possible due to the concept of partial flows in the NEWS formulation given by (4.12) with (4.13) and (4.14). The dynamic NEWS model in terms of density will be derived by considering an intersection and its outgoing roads that should be viewed as incoming roads for the neighboring intersections. In the end, we will be able to formulate a valid model for the whole urban area due to a unified description of traffic behavior at any intersection. This unified description will be obtained using the continuation method that was introduced in [110].

4.1.3.1 Continuation

Previously, we considered inflows ϕ^{in} and outflows ϕ^{out} with respect to some intersection. However, for the derivation of the macroscopic continuum model, we consider inflows and outflows with respect to roads that will be denoted by ψ^{in} and ψ^{out} as in Figure 4.5.

Recall that θ is an angle between the road orientation and the East direction. Denote the flow in the direction θ as ψ_θ. Essentially, there are two flows with direction θ: inflow ψ^{in}_θ which is a sum of all flows entering a road with direction θ, and outflow ψ^{out}_θ which is a sum of all flows outgoing from this road. Notice that, in the following, we will deal *only with outgoing roads*. Thus, we skip the superscript in the notation of angle, i.e., $\theta^{out}_j = \theta_j$.

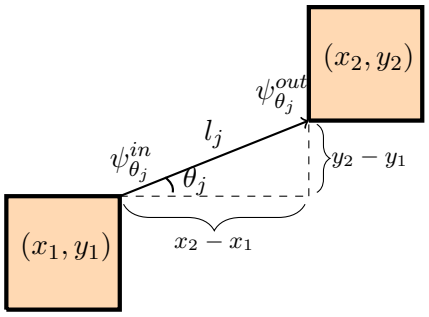

Figure 4.5: Illustration of notations used for derivation of the NEWS model.

Now consider some road j of length l_j that is an outgoing road for the intersection located at (x_1, y_1), see Figure 4.5. The density evolution on road j that is connecting the intersection at (x_1, y_1) and the intersection at (x_2, y_2) is given by

$$\frac{\partial \rho_j}{\partial t} = \frac{1}{l_j}\left(\psi^{in}_{\theta_j}(x_1, y_1) - \psi^{out}_{\theta_j}(x_2, y_2)\right),$$

where $\theta_j = \text{atan}[(y_2 - y_1)/(x_2 - x_1)]$ as in Figure 4.5. Notice that there are no bars here in the notations, since we again refer to the road formulation.

The equation written above depends on two different space points (x_1, y_1) and (x_2, y_2). However, we would like to obtain an equation that is given for a unique point of space. In order to achieve that, we can perform continuation at the beginning of the road (x_1, y_1). In its simplest form, the continuation method corresponds to the first-order term of Taylor expansion in spatial coordinates, which reads

$$\psi^{out}_{\theta_j}(x_2, y_2) \approx \psi^{out}_{\theta_j}(x_1, y_1) + (x_2 - x_1)\frac{\partial \psi^{out}_{\theta_j}}{\partial x} + (y_2 - y_1)\frac{\partial \psi^{out}_{\theta_j}}{\partial y},$$

and assuming this approximation to be an equality, we get the following model

$$\frac{\partial \rho_j}{\partial t} = \frac{1}{l_j}\left(\psi^{in}_{\theta_j}(x_1, y_1) - \psi^{out}_{\theta_j}(x_1, y_1) - (x_2 - x_1)\frac{\partial \psi^{out}_{\theta_j}}{\partial x} - (y_2 - y_1)\frac{\partial \psi^{out}_{\theta_j}}{\partial y}\right),$$

or simply

$$\frac{\partial \rho_j}{\partial t} = \frac{1}{l_j}\left(\psi^{in}_{\theta_j}(x_1, y_1) - \psi^{out}_{\theta_j}(x_1, y_1)\right) - \cos\theta_j \frac{\partial \psi^{out}_{\theta_j}}{\partial x} - \sin\theta_j \frac{\partial \psi^{out}_{\theta_j}}{\partial y}.$$

At the same time, by performing continuation at the end of the road (x_2, y_2) we arrive at

$$\frac{\partial \rho_j}{\partial t} = \frac{1}{l_j}\left(\psi^{in}_{\theta_j}(x_2, y_2) - \psi^{out}_{\theta_j}(x_2, y_2)\right) - \cos\theta_j \frac{\partial \psi^{in}_{\theta_j}}{\partial x} - \sin\theta_j \frac{\partial \psi^{in}_{\theta_j}}{\partial y}.$$

Since the density along the road is assumed to be constant, both continuous models can be used to represent the original one. The first model is defined in terms of the beginning of the road (x_1, y_1) and contains spatial derivatives of $\psi^{out}_{\theta_j}$, whereas the second model is defined in terms of the end of the road (x_2, y_2) and contains spatial derivatives of $\psi^{in}_{\theta_j}$. However, performing continuation not at the end points but somewhere in between can result into a more general form that unifies these two models.

Let us perform continuation of the model for some arbitrary point along the road (x, y) whose coordinates lie between two endpoints (x_1, y_1) and (x_2, y_2):

$$x = x_1\gamma + x_2(1-\gamma), \qquad y = y_1\gamma + y_2(1-\gamma),$$

where $\gamma \in [0, 1]$. Thus, by performing continuation at (x, y), we arrive at

$$\begin{aligned}\frac{\partial \rho_j}{\partial t} = \frac{1}{l_j}\left(\psi^{in}_{\theta_j}(x, y) - \psi^{out}_{\theta_j}(x, y)\right) &- \cos\theta_j \frac{\partial((1-\gamma)\psi^{in}_{\theta_j} + \gamma\psi^{out}_{\theta_j})}{\partial x} \\ &- \sin\theta_j \frac{\partial((1-\gamma)\psi^{in}_{\theta_j} + \gamma\psi^{out}_{\theta_j})}{\partial y}.\end{aligned} \tag{4.18}$$

Now let the vector-flow on road j be

$$\vec{\Psi}_{\theta_j} = \psi_{\theta_j}\begin{pmatrix}\cos\theta_j \\ \sin\theta_j\end{pmatrix}, \quad \text{where} \quad \psi_{\theta_j} = (1-\gamma)\psi^{in}_{\theta_j} + \gamma\psi^{out}_{\theta_j}.$$

Then, the model (4.18) can be rewritten as

$$\frac{\partial \rho_j}{\partial t} = \frac{1}{l_j}\left(\psi^{in}_{\theta_j}(x, y) - \psi^{out}_{\theta_j}(x, y)\right) - \nabla \cdot \vec{\Psi}_{\theta_j}(x, y), \tag{4.19}$$

where ∇ is a nabla operator defined as $\nabla = (\frac{\partial}{\partial x}, \frac{\partial}{\partial y})$.

This model (4.19) predicts the dynamics of the vehicle density at some outgoing road j with direction θ_j. Equation (4.19) has the same form for any intersection located at (x_k, y_k), where $k \in \{1, \ldots, K\}$ is an index used to label intersections in the network. Notice that parameter γ was introduced only for the derivation purposes, it will not explicitly appear in the final model, see details below.

4.1.3.2 The NEWS model

We would like to translate the model given in road formulation (4.19) into NEWS formulation, which allows to describe traffic flow direction at any intersection in a unified way independently of the number of its outgoing roads. Recall that densities in every direction layer are transformed as in (4.17). Let us again consider the North direction for simplicity, while the same steps should be performed for all other directions.

Thus, multiplying the equation (4.19) by $p^N_{\theta_j}$ and taking the summation, we get the model that predicts the evolution of vehicle density in the North direction on outgoing roads of an intersection located at (x_k, y_k) that reads

$$\frac{\partial \bar{\rho}_N}{\partial t} = \sum_{j=1}^{n_{out}} p^N_{\theta_j} \frac{1}{l_j} \left(\psi^{in}_{\theta_j} - \psi^{out}_{\theta_j} \right) - \nabla \cdot \left(\sum_{j=1}^{n_{out}} p^N_{\theta_j} \vec{\Psi}_{\theta_j} \right). \tag{4.20}$$

We cannot further simplify the equation (4.20) towards the NEWS formulation, since the summations contain additional index-dependent coefficients such as $1/l_j$, $\sin\theta_j$ and $\cos\theta_j$ (embedded in $\vec{\Psi}_{\theta_j}$). Let us then approximate the system (4.20) by averaging road lengths l_j such that the mean length of outgoing roads conserves the maximum number of cars:

$$L = \frac{\sum\limits_{j=1}^{n_{out}} \rho_{max,j} l_j}{\sum\limits_{j=1}^{n_{out}} \rho_{max,j}}.$$

Further, we also approximate sine and cosine in (4.20) as

$$\overline{\cos\theta}_N = \frac{\sum\limits_{j=1}^{n_{out}} p^N_{\theta_j} \cos\theta_j \phi_{max,j}}{\sum\limits_{j=1}^{n_{out}} p^N_{\theta_j} \phi_{max,j}}, \qquad \overline{\sin\theta}_N = \frac{\sum\limits_{j=1}^{n_{out}} p^N_{\theta_j} \sin\theta_j \phi_{max,j}}{\sum\limits_{j=1}^{n_{out}} p^N_{\theta_j} \phi_{max,j}}.$$

Substituting these approximations into (4.20), we get

$$\begin{aligned} \frac{\partial \bar{\rho}_N}{\partial t} = {} & \frac{1}{L} \sum_{j=1}^{n_{out}} p^N_{\theta_j} \left(\psi^{in}_{\theta_j} - \psi^{out}_{\theta_j} \right) \\ & - \nabla \cdot \left(\sum_{j=1}^{n_{out}} \left(\frac{\overline{\cos\theta}_N}{\overline{\sin\theta}_N} \right) p^N_{\theta_j} \left((1-\gamma)\psi^{in}_{\theta_j} + \gamma \psi^{out}_{\theta_j} \right) \right), \end{aligned}$$

or simply

$$\frac{\partial \bar{\rho}_N}{\partial t} = \frac{1}{L} \left(\bar{\psi}^{in}_N - \psi^{out}_N \right) - \nabla \cdot \left(\left(\frac{\overline{\cos\theta}_N}{\overline{\sin\theta}_N} \right) \left((1-\gamma)\bar{\psi}^{in}_N + \gamma \bar{\psi}^{out}_N \right) \right), \tag{4.21}$$

where we can further define $\bar{\psi}_N = (1-\gamma)\bar{\psi}^{in}_N + \gamma \bar{\psi}^{out}_N$.

Notice that this model (4.21) is the macroscopic NEWS model, since it does not depend on road index j any more. In some sense, the model (4.21) is defined for any particular space point in the vicinity of an intersection. Therefore, it makes no more sense to have separate notations for flows related to intersections $\bar{\phi}$ and roads $\bar{\psi}$. Thus, for convenience and consistency with other parts of this manuscript, we will again use the notation $\bar{\phi}$ for flows.

The model (4.21) can be further simplified in order to get rid of spatial derivatives over multi-directional flows, since otherwise the PDE can lose hyperbolicity and, moreover, we want to eliminate the parameter γ.

4.1.3.3 Model simplification

The term under the space derivative in (4.21) is $\bar{\phi}_N = (1-\gamma)\bar{\phi}_N^{in} + \gamma\bar{\phi}_N^{out}$. Recall that by (4.8) and (4.9) we can express inflows and outflows at any point as sums over partial flows:

$$\begin{aligned}\bar{\phi}_N^{in} &= \bar{\phi}_{NN} + \bar{\phi}_{EN} + \bar{\phi}_{WN} + \bar{\phi}_{SN},\\ \bar{\phi}_N^{out} &= \bar{\phi}_{NN} + \bar{\phi}_{NE} + \bar{\phi}_{NW} + \bar{\phi}_{NS}.\end{aligned}$$

Therefore, we can insert this definition into $\bar{\phi}_N$ and get

$$\begin{aligned}\bar{\phi}_N = \bar{\phi}_{NN} &+ \left[(1-\gamma)\bar{\phi}_{EN} + \gamma\bar{\phi}_{NE}\right] +\\ &+ \left[(1-\gamma)\bar{\phi}_{WN} + \gamma\bar{\phi}_{NW}\right] + \left[(1-\gamma)\bar{\phi}_{SN} + \gamma\bar{\phi}_{NS}\right].\end{aligned} \tag{4.22}$$

This means that (4.21) requires taking spatial derivatives over multi-directional flows. However, the model (4.21) would be considerably simplified if each term under the spatial derivative could be written only as a function of demand and supply of the corresponding direction, i.e.,

$$\bar{\phi}_N = \min\{\bar{D}_N, \bar{S}_N\}. \tag{4.23}$$

Now we make an assumption that *the network is well-designed in terms of maximal flows*, that is

$$\bar{\alpha}_{NE}\bar{\phi}_{max,N} = \bar{\beta}_{NE}\bar{\phi}_{max,E}. \tag{4.24}$$

Physically, this assumption means that if vehicles move at maximal possible flow before an intersection, they continue to use roads' transportation capacities at maximum after the intersection.

The proof that (4.23) holds under the assumption of a well-designed network (4.24), being rather technical, is shifted to Appendix B.7, where we show that there exists parameter γ such that (4.23) holds. Thus, the transported term under the derivative in (4.21) can be approximated by a standard flow in the demand-supply formulation that depends only on the

density of the same direction. Hence, the full system of equations can be written as

$$\begin{cases} \dfrac{\partial \bar{\rho}_N}{\partial t} = \dfrac{1}{L}\left(\bar{\phi}_N^{in} - \bar{\phi}_N^{out}\right) - \dfrac{\partial(\overline{\cos\theta}_N \bar{\phi}_N)}{\partial x} - \dfrac{\partial(\overline{\sin\theta}_N \bar{\phi}_N)}{\partial y}, \\ \dfrac{\partial \bar{\rho}_E}{\partial t} = \dfrac{1}{L}\left(\bar{\phi}_E^{in} - \bar{\phi}_E^{out}\right) - \dfrac{\partial(\overline{\cos\theta}_E \bar{\phi}_E)}{\partial x} - \dfrac{\partial(\overline{\sin\theta}_E \bar{\phi}_E)}{\partial y}, \\ \dfrac{\partial \bar{\rho}_W}{\partial t} = \dfrac{1}{L}\left(\bar{\phi}_W^{in} - \bar{\phi}_W^{out}\right) - \dfrac{\partial(\overline{\cos\theta}_W \bar{\phi}_W)}{\partial x} - \dfrac{\partial(\overline{\sin\theta}_W \bar{\phi}_W)}{\partial y}, \\ \dfrac{\partial \bar{\rho}_S}{\partial t} = \dfrac{1}{L}\left(\bar{\phi}_S^{in} - \bar{\phi}_S^{out}\right) - \dfrac{\partial(\overline{\cos\theta}_S \bar{\phi}_S)}{\partial x} - \dfrac{\partial(\overline{\sin\theta}_S \bar{\phi}_S)}{\partial y}, \end{cases} \tag{4.25}$$

where the term $\bar{\phi}^{in} - \bar{\phi}^{out}$ is given by

$$\begin{pmatrix} \bar{\phi}_N^{in} - \bar{\phi}_N^{out} \\ \bar{\phi}_E^{in} - \bar{\phi}_E^{out} \\ \bar{\phi}_W^{in} - \bar{\phi}_W^{out} \\ \bar{\phi}_S^{in} - \bar{\phi}_S^{out} \end{pmatrix} = \begin{pmatrix} \bar{\phi}_{EN} + \bar{\phi}_{WN} + \bar{\phi}_{SN} - \bar{\phi}_{NE} - \bar{\phi}_{NW} - \bar{\phi}_{NS} \\ \bar{\phi}_{NE} + \bar{\phi}_{WE} + \bar{\phi}_{SE} - \bar{\phi}_{EN} - \bar{\phi}_{EW} - \bar{\phi}_{ES} \\ \bar{\phi}_{NW} + \bar{\phi}_{EW} + \bar{\phi}_{SW} - \bar{\phi}_{WN} - \bar{\phi}_{WE} - \bar{\phi}_{WS} \\ \bar{\phi}_{NS} + \bar{\phi}_{ES} + \bar{\phi}_{WS} - \bar{\phi}_{SN} - \bar{\phi}_{SE} - \bar{\phi}_{SW} \end{pmatrix},$$

where partial flows between two direction layers are obtained as demand-supply problem, e.g.:

$$\bar{\phi}_{EN} = \min\{\bar{\alpha}_{EN}\bar{D}_E, \bar{\beta}_{EN}\bar{S}_N\}.$$

This system of equations describes the density evolution in the vicinity of one intersection. Thus, the density $\bar{\rho}(x, y, t)$ and the flow $\bar{\phi}(x, y, t)$ are space- and time-dependent functions, whereas all the parameters are constant ($\bar{\alpha}$, $\bar{\beta}$, L, $\bar{v}$, $\bar{\omega}$, $\bar{\rho}_{max}$, $\overline{\cos\theta}$, $\overline{\sin\theta}$).

Notice that the term $\bar{\phi}^{in} - \bar{\phi}^{out}$ is responsible for mixing between different density layers, e.g., $\bar{\phi}_N^{in} = \bar{\phi}_{SN} + \bar{\phi}_{WN} + \bar{\phi}_{EN}$ accounts for vehicles that were moving to the South, West and East, and then turned to the North.

System (4.25) together with a 4-dimensional fundamental diagram (that can be any concave Lipschitz continuous vector function) represents the **NEWS model**, which is one of the main results of this whole chapter. It models the evolution of vehicle density on outgoing roads of an intersection in all cardinal directions: North, East, West and South.

The last step that needs to be taken is to obtain a continuous PDE system describing traffic flow propagation in the *whole network*. This can be done by approximating the entire parameters of system (4.25) over the whole continuum domain. Let us again define a bounded rectangular domain $\Omega \in \mathbb{R}^2 : [x_{min}, x_{max}] \times [y_{min}, y_{max}]$, as it was done for 2D LWR model in Section 3.1.1. The size of Ω is determined by the size of the considered urban network.

First, we calculate $\bar{\alpha}$, $\bar{\beta}$, L, $\bar{v}$, $\bar{\omega}$, $\bar{\rho}_{max}$, $\overline{\cos\theta}$, $\overline{\sin\theta}$ for all K intersections in the network. Then, we apply the inverse distance weighting method described in Section 3.1.3.1 to approximate all these parameters over a continuum plane, e.g., the value of an average road length can be defined $\forall (x, y) \in \Omega$

$$L(x, y) = \frac{\sum_{k=1}^{K} L(x_k, y_k) w_k e^{-\mu\sqrt{(x-x_k)^2+(y-y_k)^2}}}{\sum_{k=1}^{K} w_k e^{-\eta\sqrt{(x-x_k)^2+(y-y_k)^2}}}, \tag{4.26}$$

where μ is a weighting parameter used to denote the sensitivity of the estimated variables to the distance from the intersections (and not roads as it was meant in Section 3.1.3.1). Thus, the influence of the intersection parameter, e.g. $L(x_k, y_k)$, decreases exponentially with the distance to this intersection.

Further, w_k in (4.26) is the weight of intersection k, which can be used to assign larger weights to intersections with important roads. If one wants to emphasize the main transportation arteries of the city (its most used roads), w_k can be set to larger values for particular intersections (i.e., $w_k > 1$). The main arteries are revealed from the historical (TomTom) data (see [42] for Functional Road Classification). Note that the most used roads are not necessarily the roads with largest transportation capacities due to a non-optimal design of a urban network. For example, imagine a road with many lanes that does not connect any important points in a city, and thus it is not used at maximum. At the same time, another road with the same transportation capacity connecting important locations has been used more extensively according to historical data, and thus one can assign larger weights to intersections that are connected to this road directly. Otherwise, setting all $w_k = 1$ assures that pure network infrastructure data are used. Notice that the intersection weights w_k change only the interpolation procedure and not the network and model parameters itself, and it can be calculated as:

$$w_k = \frac{1}{n_{in,k} + n_{out,k}} \sum_{i=1}^{n_{in,k}} w_{q,i} + \sum_{j=1}^{n_{out,k}} w_{q,j}, \qquad \forall k \in \{1, \dots, K\}, \tag{4.27}$$

where w_q are weights of roads based on their importance classes. There are 7 road classes in total, see Figure 4.11. We assign $w_q = 2$ for all roads of classes 1 and 2 (all major roads of high importance), and for any other case (classes from 3 to 7) we set $w_q = 1$.

Thus, we define all the geometrical and FD parameters $\forall (x, y) \in \Omega$ using inverse distance weighting (IDW) as in (4.26). As a result, we obtain a continuous PDE system that looks like (4.25) with time- and space-dependent density $\bar{\rho}(x, y, t)$ and flow $\bar{\phi}(x, y, \bar{\rho})$, while all parameters are obtained using (4.26), which makes them space-dependent functions, i.e., $\bar{\alpha}(x, y)$, $\bar{\beta}(x, y)$, $\bar{v}(x, y)$, etc.

4.1.3.4 Extended model with source and sink terms

In a urban network of finite size there exist roads, through which cars can enter or exit the domain. Such roads are called sources and sinks, respectively. The boundary conditions for the PDE system (4.25) are thus directly determined by these sources and sinks, i.e., upstream and downstream boundary conditions are specified for sources and sinks, respectively. It appears that they can be trivially captured by the NEWS model, which will also allow us to design boundary control for multi-directional urban traffic in Section 4.3. Let us now show how sources are implemented into the model (4.25), while the implementation of sinks can be done in the same way.

We consider some road j, and the exterior vehicles penetrate its entry at flow $\psi_{\theta_j}^{source}$ (we use again ψ for flow, since it is here formulated in terms of roads). We take this additional

flow of vehicles into account by adding it into equation (4.19) for road j, which yields

$$\frac{\partial \rho_j}{\partial t} = \frac{1}{l_j}\left(\psi^{in}_{\theta_j} - \psi^{out}_{\theta_j}\right) - \nabla \cdot \vec{\Psi}_{\theta_j} + \frac{1}{l_j}\psi^{source}_{\theta_j}. \tag{4.28}$$

In general, when we want to specify inflow for some road, we can only propose it in terms of demand function. This is equivalent to the weak boundary conditions, see Section 2.1.5. Then, the amount of flow entering this road depends on its supply, which is in turn determined by the traffic state of this road:

$$\psi^{source}_{\theta_j} = \min\{D^{source}_{\theta_j}, S_{\theta_j}(\rho_j)\}.$$

We can rewrite (4.28) in NEWS formulation by performing the transformations described in Section 4.1.3.2, which leads us to the extended NEWS model (with sinks also included):

$$\begin{cases} \dfrac{\partial \bar\rho_N}{\partial t} = \dfrac{1}{L}\left(\bar\phi^{in}_N - \bar\phi^{out}_N + \bar\phi^{source}_N - \bar\phi^{sink}_N\right) - \dfrac{\partial(\overline{\cos\theta}_N \bar\phi_N)}{\partial x} - \dfrac{\partial(\overline{\sin\theta}_N \bar\phi_N)}{\partial y}, \\ \dfrac{\partial \bar\rho_E}{\partial t} = \dfrac{1}{L}\left(\bar\phi^{in}_E - \bar\phi^{out}_E + \bar\phi^{source}_E - \bar\phi^{sink}_E\right) - \dfrac{\partial(\overline{\cos\theta}_E \bar\phi_E)}{\partial x} - \dfrac{\partial(\overline{\sin\theta}_E \bar\phi_E)}{\partial y}, \\ \dfrac{\partial \bar\rho_W}{\partial t} = \dfrac{1}{L}\left(\bar\phi^{in}_W - \bar\phi^{out}_W + \bar\phi^{source}_W - \bar\phi^{sink}_W\right) - \dfrac{\partial(\overline{\cos\theta}_W \bar\phi_W)}{\partial x} - \dfrac{\partial(\overline{\sin\theta}_W \bar\phi_W)}{\partial y}, \\ \dfrac{\partial \bar\rho_S}{\partial t} = \dfrac{1}{L}\left(\bar\phi^{in}_S - \bar\phi^{out}_S + \bar\phi^{source}_S - \bar\phi^{sink}_S\right) - \dfrac{\partial(\overline{\cos\theta}_S \bar\phi_S)}{\partial x} - \dfrac{\partial(\overline{\sin\theta}_S \bar\phi_S)}{\partial y}, \end{cases} \tag{4.29}$$

where

$$\bar\phi^{source}_N = \min\{\bar D^{source}_N, \bar S_N\}, \qquad \bar\phi^{sink}_N = \min\{\bar D_N, \bar S^{sink}_N\},$$

with

$$\bar D^{source}_N = \sum_{j=1}^{n_{out}} p^N_{\theta_j} D^{source}_{\theta_j}, \qquad \bar S^{sink}_N = \sum_{j=1}^{n_{out}} p^N_{\theta_j} S^{sink}_{\theta_j}.$$

Further, one needs to approximate $\bar D^{source}_N$ and $\bar S^{sink}_N$ in the whole domain, since originally we specify it in terms of roads of the network. In contrast to all other variables obtained by (4.26), the overall number of incoming cars should be conserved. Thus, we choose Gaussian kernel for the approximation of demand and supply functions:

$$\bar D^{source}_N(x,y) = \sum_{k=1}^{K} \bar D^{source}_N(x_k, y_k) G_\sigma(x - x_k, y - y_k),$$

where $G_{d_0}(x,y)$ is a two-dimensional symmetric Gaussian kernel with standard deviation d_0:

$$G_{d_0}(x,y) = \frac{1}{2\pi {d_0}^2} e^{-\frac{1}{2{d_0}^2}(x^2+y^2)},$$

which is very similar to the kernel density estimation (3.8). The difference is that here the function depends on the positions of intersections. Parameter d_0 can be tuned to change the range of influence of demand and supply functions around the intersection. Note that such a choice of $G_{d_0}(x,y)$ provides that its integral over the whole domain equals 1, therefore the

overall incoming demand in (4.29) is the same as in the original network model (4.28) (road formulation).

Notice that from now on, we will consider all the variables and parameters only in terms of NEWS formulation. Therefore, for the remaining part of this thesis, we omit bars everywhere in the notations of NEWS variables keeping in mind that these are 4-dimensional vectors, e.g., density and FD, or 4×4 diagonal matrices, e.g., TR and SR matrices. We keep the overlines only for $\overline{\cos\theta}$ and $\overline{\sin\theta}$, since these do not preserve the sense of cosine and sine functions in NEWS formulation (the sum of their squares is not necessarily equal to 1).

4.1.4 Mathematical properties of NEWS model

Let us now investigate the properties of the NEWS model. For its explicit analysis, we take system (4.25) that does not include any source terms. In this section, we will check whether our system represents a conservation law, then we will discuss the boundedness of its state ρ, and, finally, we will show that the model represents a hyperbolic PDE system.

4.1.4.1 Conservation law

The overall density in the network is the sum over the densities in all four directions, that is

$$\rho = \rho_N + \rho_E + \rho_W + \rho_S.$$

By taking its time derivative we get

$$\frac{\partial \rho}{\partial t} = \frac{\partial \rho_N}{\partial t} + \frac{\partial \rho_E}{\partial t} + \frac{\partial \rho_W}{\partial t} + \frac{\partial \rho_S}{\partial t},$$

and for each of these terms we can substitute the corresponding PDE from our model (4.25). It appears that all the mixing terms $(\phi^{in} - \phi^{out})$ cancel each other, and we simply get

$$\frac{\partial \rho}{\partial t} = -\nabla \cdot \Phi, \tag{4.30}$$

where

$$\Phi = \left(\frac{\overline{\cos\theta}_N}{\overline{\sin\theta}_N}\right)\phi_N + \left(\frac{\overline{\cos\theta}_E}{\overline{\sin\theta}_E}\right)\phi_E + \left(\frac{\overline{\cos\theta}_W}{\overline{\sin\theta}_W}\right)\phi_W + \left(\frac{\overline{\cos\theta}_S}{\overline{\sin\theta}_S}\right)\phi_S,$$

which has a form of a conservation law, where the conserved quantity is the overall density in the network.

4.1.4.2 Boundedness of the state

The boundedness of the density $\rho \in [0, \rho_{max}]$ is not violated in the model given by (4.25), since the terms under the derivatives are resolved using the standard Godunov scheme, i.e., traffic flow in each direction is determined by the minimum between demand and supply, as in

LWR formalism. For example, consider the North direction, then the term under the spatial derivative in (4.25) is just

$$\phi_N = \min\{D_N, S_N\}.$$

Mixing terms with a positive sign (these are ϕ_{SN}, ϕ_{WN} and ϕ_{EN} in the equation for ρ_N) depend on the supply of N, e.g.,

$$\phi_{EN} = \min\{\alpha_{EN} D_E, \beta_{EN} S_N\}.$$

If $\rho_N = \rho_{max,N}$, then

$$S_N = 0 \Rightarrow \phi_{EN} = 0 \Rightarrow \frac{\partial \rho_N}{\partial t} \leq 0,$$

which means that positive terms can not contribute to the increase of density, whenever it has reached $\rho_{max,N}$.

Let us now consider negative mixing terms. These depend on the demand of the North direction, e.g.,

$$\phi_{NE} = \min\{\alpha_{NE} D_N, \beta_{NE} S_E\},$$

which in case of $\rho_N = 0 \Rightarrow D_N = 0$ yields

$$\phi_{NE} = 0 \Rightarrow \frac{\partial \rho_N}{\partial t} \geq 0.$$

This implies that negative terms do not contribute to the decrease of density when it is already zero.

4.1.4.3 Hyperbolicity

Let us now investigate whether the model (4.25) is a hyperbolic PDE (as it is the case for 1D LWR (2.1) but not the general case for multi-directional 2D LWR [102]). Hyperbolicity is a fundamental property determining the behavior of solutions, which also plays an important role in the choice of the corresponding numerical scheme. For example, if we show that the model is a hyperbolic PDE, then we can apply the Godunov scheme for numerical simulation, as it is usually done for hyperbolic models such as 1D LWR.

In contrast to other types of partial differential equations, in a hyperbolic PDE any disturbance made in the initial data travels along the characteristics of the equation with a finite propagation speed. Although the definition of hyperbolicity is fundamentally a qualitative one, there are precise criteria with which one can define whether a partial differential equation is hyperbolic. Thus, equation (4.25) can be written in a following general form:

$$\partial_t \rho + \partial_x \big[F^x(\rho, x, y)\big] + \partial_y \big[F^y(\rho, x, y)\big] = g(\rho, x, y), \tag{4.31}$$

where F^x and F^y are the flow matrices defined from (4.25) as

$$F^x = \begin{bmatrix} \overline{\cos\theta}_N \phi_N & 0 & 0 & 0 \\ 0 & \overline{\cos\theta}_E \phi_E & 0 & 0 \\ 0 & 0 & \overline{\cos\theta}_W \phi_W & 0 \\ 0 & 0 & 0 & \overline{\cos\theta}_S \phi_S \end{bmatrix},$$

and

$$F^y = \begin{bmatrix} \overline{\sin\theta}_N \phi_N & 0 & 0 & 0 \\ 0 & \overline{\sin\theta}_E \phi_E & 0 & 0 \\ 0 & 0 & \overline{\sin\theta}_W \phi_W & 0 \\ 0 & 0 & 0 & \overline{\sin\theta}_S \phi_S \end{bmatrix}.$$

The right-hand side term $g(\rho, x, y)$ from (4.31) corresponds to the vector containing all the mixing terms from (4.25):

$$g(\rho, x, y) = \frac{1}{L} \begin{pmatrix} \phi_{EN} + \phi_{WN} + \phi_{SN} - \phi_{NE} - \phi_{NW} - \phi_{NS} \\ \phi_{NE} + \phi_{WE} + \phi_{SE} - \phi_{EN} - \phi_{EW} - \phi_{ES} \\ \phi_{NW} + \phi_{EW} + \phi_{SW} - \phi_{WN} - \phi_{WE} - \phi_{WS} \\ \phi_{NS} + \phi_{ES} + \phi_{WS} - \phi_{SN} - \phi_{SE} - \phi_{SW} \end{pmatrix}.$$

The spatial derivatives of flow matrices from (4.31) can be written as a chain rule

$$\begin{aligned} \partial_x \big[F^x(\rho, x, y)\big] &= \partial_\rho F^x(\rho, x, y) \cdot \partial_x \rho + \partial_x F^x(\rho, x, y), \quad \text{and} \\ \partial_y \big[F^y(\rho, x, y)\big] &= \partial_\rho F^y(\rho, x, y) \cdot \partial_y \rho + \partial_y F^y(\rho, x, y), \end{aligned}$$

which is further inserted into equation (4.31) that yields

$$\partial_t \rho + \partial_\rho F^x(\rho, x, y) \cdot \partial_x \rho + \partial_\rho F^y(\rho, x, y) \cdot \partial_y \rho = b(\rho, x, y), \tag{4.32}$$

where $b(\rho, x, y) = g(\rho, x, y) - \partial_x F^x(\rho, x, y) - \partial_y F^y(\rho, x, y)$. According to Section 3.1 of [126], the right-hand side part of (4.32) $b(\rho, x, y)$ does not play any significant role for the analysis of the equation. Thus, we simply omit it by setting $b(\rho) = 0$.

Let us further rewrite (4.32) as

$$\partial_t \rho + A^x \partial_x \rho + A^y \partial_y \rho = 0, \tag{4.33}$$

where $A^x = \partial F^x / \partial \rho$ and $A^y = \partial F^y / \partial \rho$ represent matrices of flow derivatives:

$$A^x = \begin{bmatrix} \overline{\cos\theta}_N \frac{\partial \phi_N}{\partial \rho} & 0 & 0 & 0 \\ 0 & \overline{\cos\theta}_E \frac{\partial \phi_E}{\partial \rho} & 0 & 0 \\ 0 & 0 & \overline{\cos\theta}_W \frac{\partial \phi_W}{\partial \rho} & 0 \\ 0 & 0 & 0 & \overline{\cos\theta}_S \frac{\partial \phi_S}{\partial \rho} \end{bmatrix},$$

and

$$A^y = \begin{bmatrix} \overline{\sin\theta}_N \frac{\partial \phi_N}{\partial \rho} & 0 & 0 & 0 \\ 0 & \overline{\sin\theta}_E \frac{\partial \phi_E}{\partial \rho} & 0 & 0 \\ 0 & 0 & \overline{\sin\theta}_W \frac{\partial \phi_W}{\partial \rho} & 0 \\ 0 & 0 & 0 & \overline{\sin\theta}_S \frac{\partial \phi_S}{\partial \rho} \end{bmatrix}.$$

The system (4.33) is symmetrisable hyperbolic, since matrices A^x and A^y are both symmetric. This implies that the system (4.33) is hyperbolic [126], which equivalently means that our model given by (4.25) is a hyperbolic PDE system.

4.1.5 Discussions

In this section, we have rigorously derived a new macroscopic traffic model to predict traffic evolution from the cell transmission model on one intersection. The main challenge thereby was to find a unified approach to describe the direction of traffic flow at intersections that have different number of incoming and outgoing roads and might be oriented arbitrarily. We faced this challenge by introducing the NEWS formulation of traffic in Section 4.1.2, where flow and densities are formulated such if there would exist only four principal directions of traffic: North, East, West and West (which gave the abbreviation NEWS). To enable such a formulation, we introduced projection matrices that use the intersection geometry to determine, in which direction it has more impact. For instance, we classify a road to be oriented towards North-East, if its orientation has non-zero projection weights for North and East directions. From a unified model for one intersection (that can be seen just as a point in space), we moved to the continuation of this model. This is a special technique that helped us to translate an ODE-like model into a PDE-like model. As a result, we could formulate the model (4.25) for vehicle density evolving in 4 directions on outgoing roads in the vicinity of intersections. Then, we applied inverse distance weighting to define the parameters everywhere in a continuum plane that may incorporate any urban network of interest.

While deriving the NEWS model (4.25), we had to introduce several new concepts. The main of them is the concept of partial flows that allowed us to capture the truly multi-directional behaviour of traffic. Thus, the model includes traffic flow that changes its original direction of movement. For example, there is a non-zero flow from the North direction layer to the East, since there might be vehicles that move to the North, and then they reach an intersection and turn to the East. This modeling phenomenon is equivalent to including turning ratio information at intersections in NEWS formulation. Thus, for every intersection we consider 16 origin-destination pairs, as shown in Figure 4.3. One of the major assumptions that were made is that the urban network is well-designed in terms of road capacities. Thus, road capacities must be such that cars do not get blocked when they turn, i.e., high demand to enter roads with large capacities (e.g., highways or major traffic roads) and low demand to enter minor roads.

The NEWS model corresponds to a conservation law, where the conserved quantity is the number of vehicle density in a network. The state of this model was shown to be bounded, and moreover, the NEWS model represents a hyperbolic PDE. In the next Section 4.2, we will validate this model by using synthetic data from microsimulator, as well as by using real data from sensors installed in Grenoble downtown.

4.2 Validation of NEWS model

This section is devoted to validation of the NEWS model that was derived and analyzed in the previous Section 4.1. First, we will discuss the numerical method used to simulate traffic with NEWS model. Then, the similarity measure will be introduced to enable a quantitative

comparison of two density distributions. Further, we will compare the density predicted by the numerical simulation of NEWS model (4.25) with the results predicted by commercial software Aimsun. Finally, we will compare the prediction results with the data obtained from real-life measurements in Grenoble city center.

a) Google satellite view b) Network in Aimsun

Figure 4.6: Selected area in Grenoble downtown.

4.2.1 Numerical scheme

As a network, we take an area located in Grenoble downtown with a total surface of around 1.4×1 km^2, see Figure 4.6a) for the Google satellite view and Figure 4.6b) for the network model in Aimsun of this area. Notice that this is the same area as in Figures 3.13 and 3.18.

For the numerical simulation of (4.25), we use the Godunov scheme in two dimensions. We start by defining a numerical grid in $\Omega \times \mathbb{R}^+$ by setting

- n_x to be number of cells to discretize x dimension,
- n_y to be number of cells to discretize y dimension,
- $\Delta x = (x_{max} - x_{min})/n_x$ to be the space cell size in x dimension,
- $\Delta y = (y_{max} - y_{min})/n_y$ to be the space cell size in y dimension,
- Δt to be the time cell size,
- $(i\Delta x, j\Delta y, k\Delta t)$ for $i \in \{1, \dots, n_x\}$, $j \in \{1, \dots, n_y\}$ and $k \in \mathbb{Z}^+$ to be the grid point.

For the simulation of traffic on this area of Grenoble, we set $n_x = 60$ and $n_y = 60$, i.e., the 2D plane is divided into $n_x \times n_y = 3600$ cells. Similarily to Section 2.1.6, the mesh sizes Δx and Δy and time step Δt are chosen such that they satisfy the Courant-Friedrichs-Lewy condition.

The discrete density vector is then $\rho^k(i,j) = \left(\rho_N^k(i,j), \rho_E^k(i,j), \rho_W^k(i,j), \rho_S^k(i,j)\right)^T$. The density in each direction $s = \{N, E, W, S\}$ is updated $\forall (i,j,k) \in \{1,\dots,n_x\} \times \{1,\dots,n_y\} \times \mathbb{Z}^+$ as

$$\rho_s^{k+1}(i,j) = \rho_s^k(i,j) + \Delta t \Big[E_s^k(i,j) + F_{x,s}^k(i,j) + F_{y,s}^k(i,j) + H_s^k(i,j) \Big],$$

where $E_s^k(i,j)$ corresponds to the mixing term between direction layers

$$\begin{aligned} E_s^k(i,j) = & \frac{1}{L(i,j)} \sum_{\substack{r=1 \\ r \neq s}}^{4} \Big(\min \Big\{ \alpha_{rs}(i,j) D_r^k(i,j), \beta_{rs}(i,j) S_s^k(i,j) \Big\} \\ & - \min \Big\{ \alpha_{sr}(i,j) D_s^k(i,j), \beta_{sr}(i,j) S_r^k(i,j) \Big\} \Big), \end{aligned}$$

and $F_{x,s}^k(i,j)$, $F_{y,s}^k(i,j)$ correspond to derivative terms. The derivative term w.r.t. x dimension can be computed as

$$\begin{aligned} F_{x,s}^k(i,j) = & \frac{\overline{\cos\theta}_s(i,j) + \overline{\cos\theta}_s(i-1,j)}{2\Delta x} \min \Big\{ D_s^k(i-1,j), S_s^k(i,j) \Big\} \\ & - \frac{\overline{\cos\theta}_s(i,j) + \overline{\cos\theta}_s(i+1,j)}{2\Delta x} \min \Big\{ D_s^k(i,j), S_s^k(i+1,j) \Big\}, \end{aligned}$$

while the derivative term w.r.t. y dimension is similarly computed as

$$\begin{aligned} F_{y,s}^k(i,j) = & \frac{\overline{\sin\theta}_s(i,j) + \overline{\sin\theta}_s(i,j-1)}{2\Delta y} \min \Big\{ D_s^k(i,j-1), S_s^k(i,j) \Big\} \\ & - \frac{\overline{\sin\theta}_s(i,j) + \overline{\sin\theta}_s(i,j+1)}{2\Delta y} \min \Big\{ D_s^k(i,j), S_s^k(i,j+1) \Big\}. \end{aligned}$$

Notice that $F_{x,s}^k(i,j)$, $F_{y,s}^k(i,j)$ are obtained using the upwind scheme [34] for $\overline{\cos\theta}_s(i,j) > 0$, $\overline{\sin\theta}_s(i,j) > 0$. The upwind scheme is used to guarantee the correct direction of information propagation in a flow field, which needs to be reversed if $\overline{\cos\theta}_s(i,j) < 0$ for $F_{x,s}^k(i,j)$ and $\overline{\sin\theta}_s(i,j) < 0$ for $F_{y,s}^k(i,j)$.

Finally, $H_s^k(i,j)$ includes source and sink terms, thus it is computed as

$$H_s^k(i,j) = \frac{1}{L(i,j)} \Big(\min \Big\{ D_s^{source,k}(i,j), S_s^k(i,j) \Big\} - \min \Big\{ D_s^k(i,j), S_s^{sink,k}(i,j) \Big\} \Big).$$

4.2.2 Structural similarity measure

In order to enable a quantitative comparison between two density distributions, we use the *structural similarity measure* (SSIM) [151]. This should be understood as an index used to measure the similarity between two images. Thereby, three different image properties are compared: luminance, contrast and structure. In general, the SSIM between two density distributions $\rho_1(i,j)$ (NEWS prediction) and $\rho_2(i,j)$ (reference distribution) $\forall (i,j) \in \{1,\dots,n_x\} \times \{1,\dots,n_y\}$ can be calculated as:

$$SSIM(\rho_1, \rho_2) = \frac{(2\zeta_1\zeta_2 + c)(2\sigma_{12} + c)}{(\zeta_1^2 + \zeta_2^2 + c)(\sigma_1^2 + \sigma_2^2 + c)}, \tag{4.34}$$

where ζ_1 and ζ_2 are the mean values of distributions ρ_1 and ρ_2 over the domain that are computed as:

$$\zeta(\rho) = \frac{1}{n_x}\frac{1}{n_y}\sum_{s=N}^{S}\sum_{i=1}^{n_x}\sum_{j=1}^{n_y}\rho_s(i,j). \tag{4.35}$$

This term is used to compare luminance of two images. Then, σ_1 and σ_2 in (4.34) are the standard deviations of density distributions used to compare the signal contrasts:

$$\sigma(\rho) = \sqrt{\frac{1}{n_x}\frac{1}{n_y}\sum_{i=1}^{n_x}\sum_{j=1}^{n_y}\left(\sum_{s=N}^{S}\rho_s(i,j) - \zeta(\rho)\right)^2},$$

and σ_{12} is the correlation coefficient of two density distributions used to measure the similarity of their structures:

$$\sigma(\rho_1,\rho_2) = \frac{1}{n_x}\frac{1}{n_y}\sum_{i=1}^{n_x}\sum_{j=1}^{n_y}\left(\sum_{s=N}^{S}\rho_{s,1}(i,j) - \zeta_1\right)\left(\sum_{s=N}^{S}\rho_{s,2}(i,j) - \zeta_2\right).$$

Finally, $c > 0$ in (4.34) is a constant that needs to be small, e.g., we take $c = 1 \cdot 10^{-13}$ for the computation. This constant prevents instability, when the denominator is close to zero. The range of SSIM is $[-1, 1]$, where 1 is achieved if two images are identical, whereas -1 means that one image is the inverse of the second image.

The main advantage of using SSIM is that it is a perception-based metric used to detect structural changes in the image, while, for example, the mean square error evaluates only the absolute error rather than the differences in congestion patterns. Thus, even if two density distributions are characterized to have the same number of cars, the SSIM is still able to detect whether congested zones have different shapes.

4.2.3 Model validation with Aimsun

We run a scenario of congestion formation in the selected area of Grenoble downtown (see Figure 4.6). For this, we use microsimulator Aimsun and perform also a numerical simulation of traffic density governed by NEWS model (4.29). For the numerical simulation we deploy the Godunov scheme in two dimensions described in Section 4.2.1. Then, the obtained steady states are compared, as it was done for the comparison of 2D LWR model and MFD-based model with Aimsun in Section 3.1.7. Recall that Aimsun takes network, turning ratios and inflows as input, and produces microsimulations of vehicle trajectories. We then reconstruct the density distribution from vehicle positions in Aimsun and compare it to the state predicted by NEWS model. The density reconstruction is done using KDE method, see Section 3.1.3.2.

In general, we have access to the following network data: (x, y) coordinates of all intersections and its corresponding roads, as well as speed limits and number of lanes for each road. Using these data, we compute the parameters of the fundamental diagram v, ω, ρ_{max} and the intersection parameters α, β, L, $\overline{\cos\theta}$, $\overline{\sin\theta}$ in the NEWS framework for all the intersections

as follows. For each road j in the selected Grenoble area, we read the free-flow velocity v_j from its speed limit data. Then, the maximal density $\rho_{max,j}$ is computed by placing a car every 6 m at every road, and then KDE is used as described in Section 3.1.3.2. Here we assume that each vehicle has influence within $d_0 = 70$ m range around its position, see (3.8). Further, we assume that the critical density $\rho_{c,j} = \rho_{max,j}/3$ everywhere (triangular FD), which allows us also to calculate the negative kinematic wave speed ω_j and the road capacities $\phi_{max,j}$. Then, these parameters are translated into NEWS formulation using the network geometry, see Section 4.1.2.4 for more details.

In order to determine the traffic flow direction, we use turning ratios α_{ij} for each road i towards road j that are estimated as a function of road capacities:

$$\alpha_{ij} = \frac{\phi_{max,j}}{\sum_{q=1}^{n_{out}} \phi_{max,q}}.$$

Then, supply ratios β_{ij} are calculated using (4.3). Both ratios α and β are translated into NEWS formulation as in (4.13) and (4.14). Further, the coordinates of road's both ends are used to determine its length l_j and orientation angle θ_j, from which we then obtain L, $\overline{\cos\theta}$, $\overline{\sin\theta}$ in NEWS formulation as described in Section 4.1.3.2.

Then, all these intersection and FD parameters are approximated for every grid point $(i,j) \in \{1,\dots,n_x\} \times \{1,\dots,n_y\}$ using IDW method, see Section 4.1.3.3. Thereby, we do not deploy intersection weights, i.e., all $w_k = 1$ in (4.26), since here the pure network infrastructure data are used. Weights are assigned to intersections with important roads for the validation with real data in Section 4.2.4. For the results presented here, we choose the weighting parameter $\mu = 20$, which is a relatively low value meaning that only the global trend in the network geometry is reproduced, see Figure 3.1 for more intuition.

First of all, we load the Grenoble network into Aimsun (see Figure 4.6b)), and let vehicles enter through its boundaries by specifying inflows. We choose inflows such that the main stream of vehicles comes from the South of the area. The microsimulations evolve for 2.5 min, and then the state is saved and later used as an initial condition for both Aimsun and numerical simulation of the NEWS model. Afterwards, we continue the microsimulation on Aimsun until we do not perceive any structural changes in the state, which indicates that a steady state has been achieved. The results are saved as vehicle positions at all time instants. Therefore, we use KDE to transform the standard Aimsun data into a density distribution. KDE in 1D is also used to smooth inflows such that they enter the domain in a continuous line rather than at discrete points of space. We set constant inflows in order to let the system converge to a steady state. We then perform a numerical simulation of the NEWS model as described in Section 4.2.1 using the initial conditions from Aimsun.

The results are depicted in Figure 4.7, where the comparison of both density distributions is shown for $t \in [0, 50]$ min. We see that in both cases the distributions look quite similar but not identical, which might be caused by several things. In Aimsun, vehicles are restricted to move only on real physical roads, while more freedom of movement is perceived in a PDE-driven system. Moreover, in Aimsun, turning ratios indicate the probability with which a car

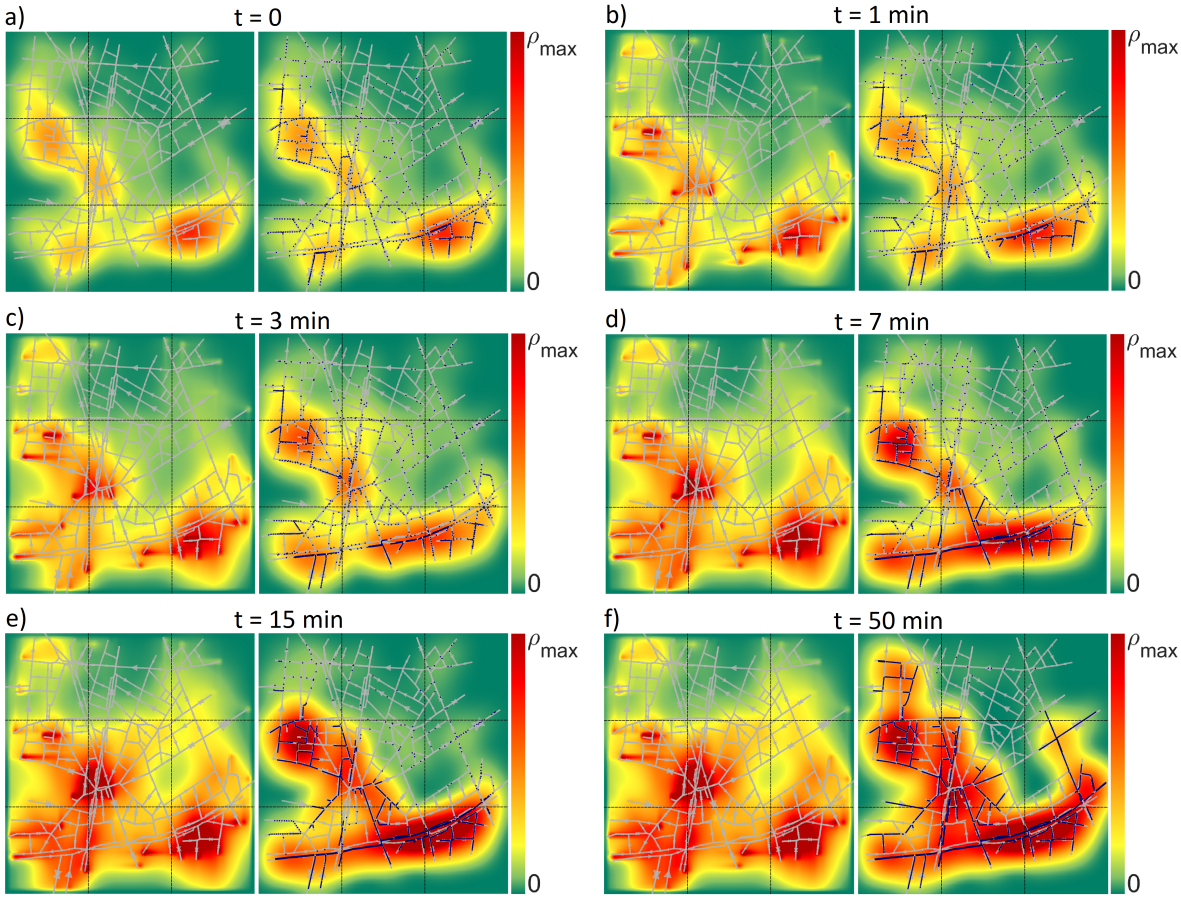

Figure 4.7: Congestion formation in Grenoble downtown for $t \in [0, 50]$ min: numerical simulation of density governed by NEWS model (left plots) and Aimsun (right plots). Weighting parameter: $\mu = 20$. Black dashed lines separate Grenoble in zones used for the calculation of SSIM.

turns to one or another road, whenever it reaches an intersection at some time instant. Thus, TR in Aimsun should be understood as mathematical expectation rather than deterministic values. Hence, it often appears that scenarios in Aimsun, although having the same initial condition and inflows, converge to different density distributions. Vehicles might get stuck in different parts of the city, while this is unlikely to happen during the numerical simulation of NEWS density, where cars move on a continuum space. However, on a global scale traffic regimes seem to be reproduced correctly in most parts of the city.

Let us now compute the structural similarity measure (4.34) to compare two density distributions from Figure 4.7. For that the domain is divided into 9 windows of equal size, as drawn in Figure 4.8a). We do this in order to be able to compare density distributions zone-by-zone. The zones are numbered from top left to bottom right, as shown in Figure 4.8a). The SSIM

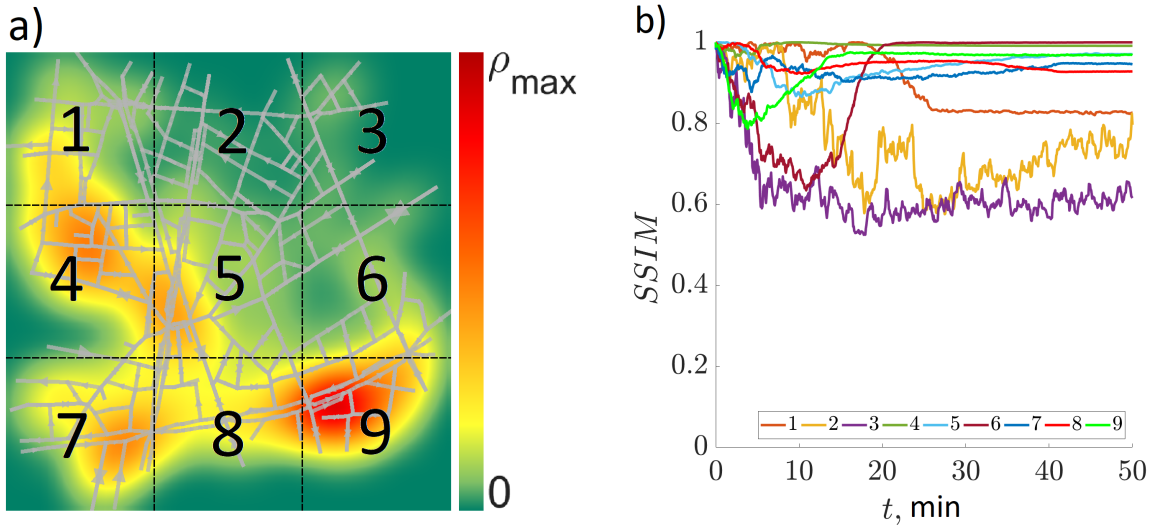

Figure 4.8: a) Zone numbering in Grenoble network, b) structural similarity zone-by-zone: $SSIM_l$ with $l = \{1, \ldots, 9\}$.

of the whole domain is then calculated as the mean value over all zones:

$$\overline{SSIM}(\rho_1, \rho_2) = \frac{\sum_{l=1}^{N} SSIM_l \, \zeta_l(\rho_2)}{\sum_{l=1}^{N} \zeta_l(\rho_2)}, \tag{4.36}$$

where $N = 9$ is the total number of zones in the domain, $SSIM_l$ is referred to zone l each given by (4.34), and $\zeta_l(\rho_2)$ is the average of the density distribution used to assign larger weights to zones that are strongly occupied in the reference distribution (here, ρ_2 is the total density in Aimsun). Thus, the fewer cars a zone has, the smaller is its weight. The weights are assigned in order to avoid giving too much importance to zones that are currently almost empty. Notice that $\zeta_l(\rho_2(t))$ is a time-dependent parameter.

In its original formulation, SSIM values range from -1 to 1. In order to facilitate the interpretation of this index in the context of density comparison, we make its range to be $SSIM \in [0, 1]$ by doing $(SSIM + 1)/2$. Thus, $SSIM = 1$ implies that two distributions are identical, and $SSIM = 0$ means that one distribution is completely the opposite of the second one (inverted image).

The SSIM of corresponding zones in both distributions is depicted as a function of time in Figure 4.8b). It seems that the most problematic zones are the most empty ones that are concentrated in the upper part of the domain (zones 2 and 3), while the best captured zones are the most congested ones (zones 4 and 9). This can be explained by the fact that the main stream of vehicles enters the domain from the South (since this is where the largest inflows are set), where they build the most congested areas. Thus, cars might not have reached the upper part in Aimsun, since they got stuck in the Southern part of the area.

Finally, in order to unable a quantitative comparison of the density in the whole Grenoble

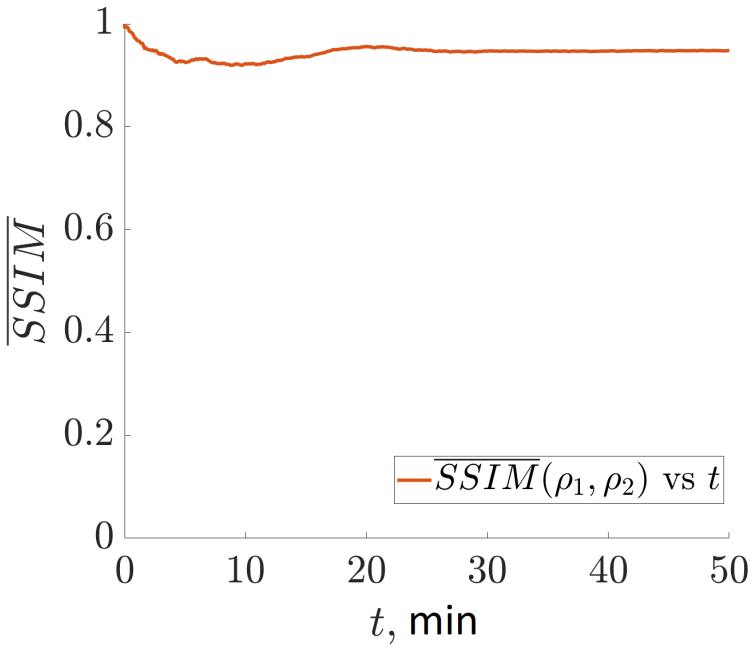

Figure 4.9: Mean value over zones of $\overline{SSIM}$ computed by (4.36) between densities obtained with Aimsun and numerical simulation of NEWS as a function of time.

area, the SSIM is averaged over all zones by using (4.36), and we obtain the result depicted in Figure 4.9. Thereby, we can see that the overall SSIM is approximately equal to 0.9 ($\approx 90\%$ accuracy), which indicates that the congested steady state is close to be reproduced correctly by our model (4.25).

4.2.4 Model validation with real data

For the model validation with real data, we make use of Grenoble Traffic Lab for Urban Networks known as GTL Ville, see `http://gtlville.inrialpes.fr/`. This is an experimental platform for real-time collection of traffic data coming from a network of stationary flow sensors installed in Grenoble downtown, see Figure 4.10. This platform also provides real-time traffic indicators oriented towards the users of the city, traffic operators and researchers [143]. The collected data and computed indicators are available for download at the GTL website.

Moreover, for model validation with real data we use the available information on road importance that is obtained from historical TomTom data, see Figure 4.11 for Functional Road Classification (FRC) of the selected zone in Grenoble. The road classes are used to distinguish major roads that experience heavy traffic from minor roads that are usually related to residential areas and experience only light traffic. The major roads of high importance (highways) belong to class 1, and the class number increases as the road importance decreases (the least important roads are of class 7). These roads classes are used to assign larger weights to important roads (4.27), which is then used for the IDW (4.26) to approximate

a) Fixed sensors b) Bluetooth devices

Figure 4.10: Sensor location in Grenoble downtown: a) fixed flow sensors: R denote radars and L denote induction loops, b) automatic vehicle identifiers using Bluetooth installed at 12 intersections of Grenoble during a measurement campaign lasting one week. These figures are taken from [120].

network parameters.

The maximal densities at every road $\rho_{max,j}$, capacities $\phi_{max,j}$, road lengths l_j and orientations θ_j are the same as described above, since these parameters are defined by the network topology, which remains the same for the real-life experiment. However, the free-flow speed data are now taken from floating car data reported from several vehicles that are equipped with devices such as a GPS navigator. The free-flow speed is estimated as the maximal speed of a vehicle in the absence of other cars, and it starts decreasing as the density of surrounding cars increases. It is worth noting that, in general, the free-flow speed is lower than the corresponding speed limit value, since in reality cars lose their average velocity, e.g., by stopping at traffic lights. Thus, our data indicate that the free-flow speed is approximately equal to $60 - 70\%$ of road's speed limit.

Now let us explain how do we get turning ratios α_{ij}. These data are obtained from automatic vehicle identifiers using Bluetooth devices that were installed at adjacent incoming and outgoing roads of 12 intersections in total, see their location in Figure 4.10b). These identifiers are able to detect vehicles equipped with another Bluetooth device, which enables to assign origin and destination roads of individual vehicles. For the estimation of the remaining turning ratios (since there are more than 12 intersections in total), the information on road importance is used (FRC), and then the optimization problem minimizing the deviation of predicted and actual flows is solved.

Finally, we also get the estimated density values for every road ρ_j for every minute of the 8th of January 2021 from 6 am to 9 pm, as well as inflows and outflows at domain boundaries. Notice that in this scenario inflows are time-dependent functions. Estimation of free-flow speed, turning ratios, vehicle density and boundary flows is described in more details in [119].

Figure 4.11: Functional Road Classification of Grenoble downtown. The image is taken from [120].

In Figure 4.10a) the sensors marked in blue are those giving boundary inflows and red sensors give boundary outflows. Sensors marked in green were used for the validation of state estimation procedure. Notice that the state estimation procedure is not free of error and it does not reconstruct the state exactly, since there are only a limited number of sensors due to economical cost.

In order to get density values all over the continuum plane, i.e., at every point in Grenoble downtown (not only at physical roads), we divide each road into 10 parts, and at the boundary between each part we set a group of vehicles. Thus, there is a known number of vehicles at 10 points of every road. We then assume that all these cars contribute to the global density around $d_0 = 70$ m from its positions using KDE method, see Section 3.1.3.2. We also use KDE for the inflow values, as it was done in the previous example.

The results are depicted in Figure 4.12, where the comparison of two density distributions is shown. Again, we see that in both cases the distributions look quite similar. The first possible reason for these distributions to be non-identical is the probabilistic nature of turning ratios in reality opposed to deterministic nature in numerical simulation. Another reason is that the NEWS model does not include traffic lights, as well as it is not able to capture accidents or the effect of pedestrians crossing a road. Moreover, the NEWS model does not take into account parking lots. Thus, in reality parking vehicles are seen as stationary objects that do not contribute to the traffic flow any more, while in NEWS-driven system these vehicles stay in the domain and create congestions, since the NEWS model is a conservation law.

Another source of mismatch could be induced by data on inflows and outflows. The problem is that the data represent estimated measurements of the flows in the city that we can not enforce in our system, since there is always a demand-supply problem that needs to

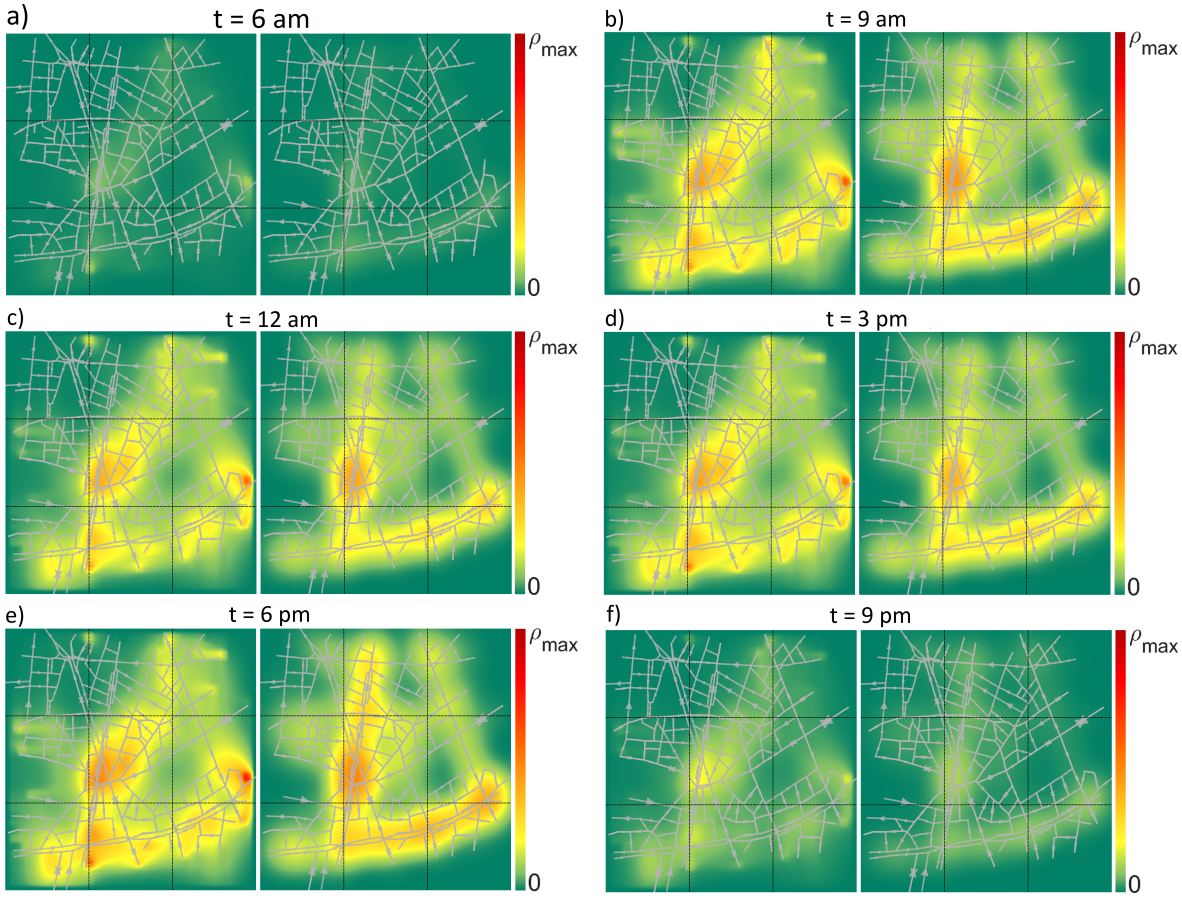

Figure 4.12: Evolution of traffic density in Grenoble downtown on 8th of January, 2021 from $t = 6$ am to $t = 9$ pm: numerical simulation of NEWS model (left plots) and real data (right plots). Weighting parameter $\mu = 20$.

be solved, i.e.,

$$\phi^{source} = \min\{D_{ext}, S(\rho)\}, \quad \phi^{sink} = \min\{D(\rho), S_{ext}\},$$

where ext is used in the subscript to highlight that these functions depend on what happens outside the domain. Thus, the available data are not related to demand and supply at domain boundaries but to actual inflow $\hat{\phi}^{source}$ and outflow $\hat{\phi}^{sink}$ of the system (hats are used to denote the measurement data).

To understand which problems can be provoked by these issues, let us consider some measured outflow $\hat{\phi}^{sink}$, which in turn is also just a result of solving the minimum between demand and supply, i.e.,

$$\hat{\phi}^{sink} = \min\{D(\hat{\rho}), S_{ext}\}, \tag{4.37}$$

where demand $D(\hat{\rho})$ depends on the measured density, which might be something different than the one we get from the numerical simulation of NEWS-driven density.

For the numerical simulation, the best thing we can do with the measured outflow data

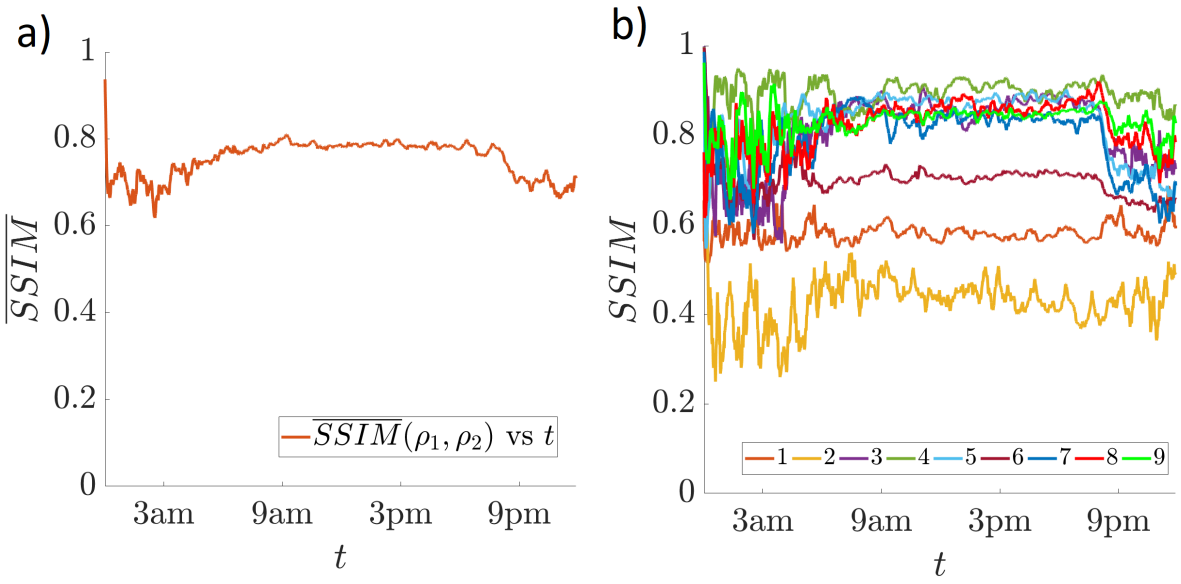

Figure 4.13: a) Mean $\overline{SSIM}$ (4.36) between the density ρ_1 predicted by numerical simulation of NEWS model and the density ρ_2 estimated from real data as a function of time, b) similarity zone-by-zone: $SSIM_l$ with $l = \{1, \ldots, 9\}$. Weighting parameter: $\mu = 20$.

$\hat{\phi}^{sink}$ is to use it as a supply of the external area:

$$\phi^{sink} = \min\{D(\rho), \hat{\phi}^{sink}\}. \tag{4.38}$$

However, it follows from (4.37) that $\hat{\phi}^{sink} \leq S_{ext}$, where the equality holds in case of congested traffic. If the traffic is not congested, then setting the external supply to be equal to measured outflow might lead to blocking vehicles at domain exit instead of letting them come out.

Two distributions are again compared by using the weighted SSIM averaged over 9 zones as in the previous case using (4.36) and (4.34). The result is depicted in Figure 4.13a), while Figure 4.13b) is referred to SSIM for each zone computed using (4.34). Notice that the zone numbering here is preserved the same as in Figure 4.8a). The worst captured zones are 1 and 2 located on the upper part of the city, and the best results are achieved for zones 5, 4 and 8. A possible reason might be the fact that the cars get stuck at the bottom of the city in the real experiment, while they move more freely in a PDE governed system (as in Section 4.2.3). In general, notice that the best results are achieved for the time when the congestion level is the highest, as we can see from Figure 4.13a). This is related to the weighting parameters used for the calculation of SSIM (4.36). Weights tend to introduce more noisiness into computation, when there are only a few cars in the city. Finally, recall that the real-life data are also an approximation, since these densities are obtained by the estimation procedure that is not error-free due to the lack of sensors at every road. On average, the total SSIM is around 0.8 (80% accuracy), which indicates that two density distributions are still quite close.

4.2.5 Reproducibility of the results

It is worth noting that the source code used for model validation is an *open source* project that you can find here: https://github.com/Lyurlik/multidirectional-traffic-model. The README.md file contains all the essential information about the code structure and the data files such that anyone can get use of it for different purposes (e.g., prediction of traffic density for a different urban network). Thus, the results are made to be reproducible.

This code is used to produce two different vehicle density distributions: by running a numerical simulation of NEWS model (4.25), and the other one is the reconstructed density from data obtained from real sensors.

In order to run the code, one needs to have the following files:

Network topology

1. *"../ModelValidation/IntersectionTable.csv"* – contains information about intersections: x and y coordinates of every intersection (columns 1 and 2), its `ID` (column 3) and whether it is a node on border (column 4), which means that this intersection is located at domain boundary through which vehicles may enter (inflows), or exit (outflows);
2. *"../ModelValidation/RoadTable.csv"* – contains information about roads: `ID1` and `ID2` (columns 3 and 4) are the id's of corresponding intersections that the road is connecting, `ID_road` (column 5) is the road's ID, `max_vel` (column 6) is its free-flow limit estimated from real measurements, then we have number of lanes (column 7) and road's length (column 8);
3. *"../ModelValidation/RoadFRC.csv"* – contains information about road importance: column 1 is the road's ID, and column 2 is its importance class from 1 to 7 with roads of class 1 being the most important;
4. *"../ModelValidation/TurnTable.csv"* – contains turning ratios between any pair of roads: `ID1` of incoming road (column 1), `ID2` of outgoing road (column 2) and the turning ratio between these roads (column 5).

Data from real sensors

5. *"../ModelValidation/Timestamp.csv"*– contains time in seconds at which the data are given (unix timestamp), the time step equals to one minute;
6. *"../ModelValidation/Density.csv"* – contains estimated density from real sensors: first number is `road_id` followed by its density (that is assumed to be constant within one road) at all time instants, then the next `road_id` with its density data for each time instant and so on;
7. *"../ModelValidation/AllInflows.csv"* – contains inflow values (in veh/hour) for every road for every time step (one minute). If road is outgoing from intersection that is not on border, then the inflow value is zero;

8. *"../ModelValidation/AllOutflows.csv"* – contains outflow values (in veh/hour) for every road for every time step (one minute). If road is incoming into intersection that is not on border, then the outflow value is zero.

Code structure

The main file of the project is **mainwindow.cpp**: in its constructor we specify the file names to be loaded, simulation starting time (line 27) and simulation step size (line 29). The paths to files containing network and density data are also specified there. We can also change the weighting parameter μ used to approximate parameters for every cell (line 4), and parameter d_0 (line 5) is the standard deviation parameter used for Gaussian kernel estimation.

Other important classes are:

- **UrbanNetwork**, which contains all the network geometry information (this is the place, where all the network files are read). This network is used for both density predictions. In its function *loadRoads*, one needs to specify the minimum distance between the heads of two consequential vehicles, which is then used for the computation of ρ_max (we set it to 6 m).
- **NEWSModel**, which contains translation procedure of all network and intersection parameters into NEWS formulation (function *processIntersections*). After all parameters are defined in NEWS terms, it calls *constructInterpolation* function that approximates these parameters on every grid point in space using their known values at every intersection. Then update is performed, where the Godunov numerical scheme is applied for the state update using NEWS model. There is also a function *getSSIMDiff_mean_weighted* used to compute the weighted SSIM between two densities (4.36).
- **GrenobleData**, where all the data estimated from the real-life experiments are loaded. In function *reconstructDensity*, the density initially given for each road is defined for every cell. Thereby, every road is divided in 10 parts, and density values are presented as points on the border between these parts. Then, Gaussian kernel estimation is used to determine density for every cell in the domain.
- **TrafficSystem**, which implements concurrent threads for a parallel NEWS simulation relative to the main visualization thread.

4.2.6 Discussions

In this section, we demonstrated how the NEWS model predicts the traffic state compared to the ground true results. For this purpose, we deployed the Godunov scheme in 2D to run a numerical simulation of vehicle density governed by NEWS model. The predicted density was then compared to the reference density distribution obtained from two different sources: microsimulator Aimsun (Figure 4.7) that produced vehicle trajectories using synthetic data, and estimated density from data coming from sensors installed in Grenoble downtown (Figure

4.12). These data from real-life measurements are available for download at our experimental platform GTL Ville. To enable a quantitative comparison of vehicle densities, we implemented the measure of structural similarity, which is an index used to reveal to which extent are two images similar.

In both cases, the predicted density looked quite similar to the reference density distribution, i.e., the index revealed at least 80% similarity in both cases. In the first case (NEWS vs Aimsun), the predicted densities are similar to 90%. There are several sources of mismatch. The first one to name is that in Aimsun as well as in a real urban network, vehicles are restricted to move along physical roads, while in a PDE-driven system this is not that strict, since the underlying surface is a 2D continuum plane. Another reason is that, in reality, turning ratios are only expectation values rather than deterministic values as in NEWS model. Thus, the proportion of cars turning to one or another road may be different from the given fixed proportion due to the finite duration of experiment. The NEWS framework assumes also that there are 4 possible directions for traffic at every intersection. If there are at least two roads with different orientation angles θ going approximately in the same direction (e.g., North-East), then the NEWS framework introduces mismatches due to approximations it makes with projection matrices. Another assumption of NEWS relies on optimally designed networks in terms of capacities. This assumption means that the usage of roads is related to its capacities, i.e., more cars tend to turn to highways than to roads of minor importance.

In the second case (NEWS vs real data), we had to deal with some additional problems. The first problem to name is that not all the roads in Grenoble downtown are equipped with sensors due to high economical cost. Thus, the data available for every road come from the estimation procedure that is not free of errors. The second problem to be mentioned is related to boundary flows. Namely, the measured flow data can not be enforced in our NEWS model. They can only be suggested as boundary conditions, which are fulfilled only if the traffic state at the boundary points admits it (demand-supply problem). Finally, we can also name the parking lots as sources of errors. In the real-life experiment, cars stop at parking lots and are not detected by sensors, thus, the reconstructed density does not take them into account. On the contrary, the NEWS model is based on a conservation law. Thus, if vehicles stop at parking lots before exiting the domain, they are counted as obstacles that create congestions.

However, the validation results revealed a good agreement with the prediction. The NEWS model appeared to be a good approximation of multi-directional traffic in urban networks, which was confirmed by real-life measurement data. The code used for model validation is available as an open source project, and the NEWS model can be deployed to predict traffic on any urban network of interest in further research projects. In the next section, we will suggest a boundary control technique used to mitigate congestions in a urban network with multi-directional traffic governed by NEWS model.

4.3 Boundary control for multi-directional traffic

In this section, we design a boundary control law for a multi-directional urban traffic governed by NEWS model. This controller acts such that initially congested traffic achieves the best possible desired equilibrium. This steady state provides congestion mitigation, which equivalently implies throughput maximization of the transportation network. Thus, the control goal here is similar to what has already been done for uni-directional urban traffic in Section 3.4.

Our main contribution here is an extensive analysis of possible desired space-varying profiles that the system can achieve. In this section, we will see that finding an admissible steady state is far from being trivial for multi-directional traffic systems. Moreover, we will also use Lyapunov methods to show the exponential convergence of the traffic state to the desired equilibrium.

4.3.1 NEWS model for congested traffic regime

Let us consider the NEWS model (4.25) for a special case of congested traffic regime. Restricting to one traffic regime allows to considerably simplify the system for analysis, as it was done in Sections 3.4 and 2.2. A congested traffic in some urban area will be controlled from its downstream boundary such that the level of congestion is minimized under the constraint that $\rho(x,y,t) \geq \rho_c(x,y)\ \forall (x,y,t) \in \Omega \times \mathbb{R}^+$ for all 4 directions. Recall that $\Omega \in \mathbb{R}^2 : [x_{min}, x_{max}] \times [y_{min}, y_{max}]$ is a bounded rectangular domain, whose size is determined by the size of the urban area under study.

Without loss of generality, consider a partial flow ϕ_{EN} of vehicles that originate from the North and then turn to the East, as drawn in Figure 4.3. Its value is determined by the minimum of flow demand of the East layer and supply of the North layer, i.e., recall (4.12):

$$\phi_{EN} = \min\{\alpha_{EN} D_E, \beta_{EN} S_N\},$$

with turning and supply rations being given by (4.13), (4.14). Using the definition of demand and supply functions for triangular FD (4.15), we can further rewrite ϕ_{EN} as

$$\phi_{EN} = \min\{\alpha_{EN} v_E \rho_E,\ \alpha_{EN} \phi_{max,E},\ \beta_{EN} \omega_N (\rho_{max,N} - \rho_N),\ \beta_{EN} \phi_{max,N}\}. \tag{4.39}$$

In the congested traffic regime, the minimum in demand-supply problem is always resolved to the benefit of supply. This in turn implies for (4.39) that

$$\phi_{EN} = \beta_{EN} \omega_N (\rho_{max,N} - \rho_N).$$

Using this expression and fixing $\rho_0(x,y) \in [\rho_c(x,y), \rho_{max}(x,y)]\ \ \forall (x,y) \in \Omega$ as initial density distribution condition, we can now introduce the following IBVP for the NEWS model (4.25)

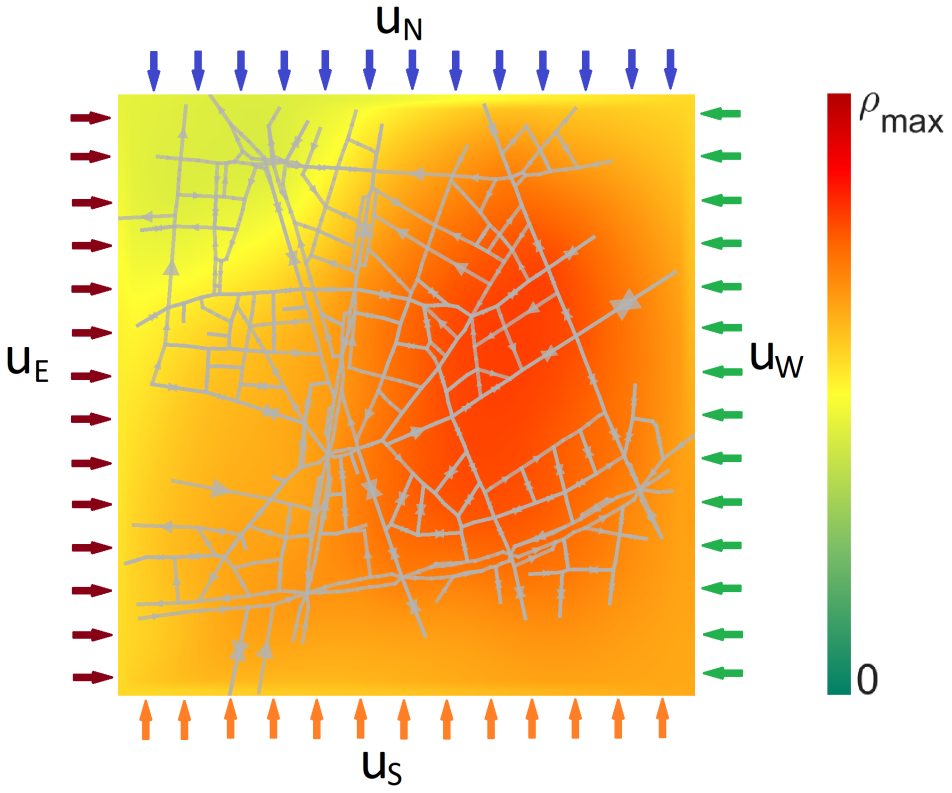

Figure 4.14: Vehicle density in a 2D continuum plane that incorporates Grenoble downtown. Downstream boundaries for control of multi-directional traffic are indicated by colorful arrows: North in blue (u_N), East in dark red (u_E), West in green (u_W) and South in orange (u_S).

that describes the dynamics of congested traffic density on some urban area:

$$\begin{cases} \dfrac{\partial \rho}{\partial t} = \dfrac{1}{L}(I - B)W\,(\rho_{max} - \rho) - \dfrac{\partial [C\,W\,(\rho_{max} - \rho)]}{\partial x} - \dfrac{\partial [S\,W\,(\rho_{max} - \rho)]}{\partial y}, \\ \rho(x, y, t) = u(x, y, t), \quad \forall (x, y) \in \Gamma_{out}, \\ \rho(x, y, 0) = \rho_0(x, y), \end{cases} \tag{4.40}$$

where $\Gamma_{out} \subset \Omega$ represents a set of boundary points (x, y) associated with the domain exit (downstream boundary):

$$\Gamma_{out} = (y_{max}, x_{max}, x_{min}, y_{min})^T.$$

The congested traffic state governed by the NEWS system (4.40) is controlled at the downstream boundary Γ_{out} by specifying the control vector $u = (u_N, u_E, u_W, u_S)^T$. See Figure 4.14, where the arrows are used to denote the boundaries to be activated for control of traffic in each direction.

Finally, C, S, W and B in (4.40) are all 4×4 matrices such that C and S are diagonal

matrices, W is a positive-definite diagonal matrix, and B is a non-negative matrix:

$$C = \begin{bmatrix} \overline{\cos\theta}_N & 0 & 0 & 0 \\ 0 & \overline{\cos\theta}_E & 0 & 0 \\ 0 & 0 & \overline{\cos\theta}_W & 0 \\ 0 & 0 & 0 & \overline{\cos\theta}_S \end{bmatrix}, \qquad S = \begin{bmatrix} \overline{\sin\theta}_N & 0 & 0 & 0 \\ 0 & \overline{\sin\theta}_E & 0 & 0 \\ 0 & 0 & \overline{\sin\theta}_W & 0 \\ 0 & 0 & 0 & \overline{\sin\theta}_S \end{bmatrix},$$

$$W = \begin{bmatrix} \omega_N & 0 & 0 & 0 \\ 0 & \omega_E & 0 & 0 \\ 0 & 0 & \omega_W & 0 \\ 0 & 0 & 0 & \omega_S \end{bmatrix}, \qquad B = \begin{bmatrix} \beta_{NN} & \beta_{NE} & \beta_{NW} & \beta_{NS} \\ \beta_{EN} & \beta_{EE} & \beta_{EW} & \beta_{ES} \\ \beta_{WN} & \beta_{WE} & \beta_{WW} & \beta_{WS} \\ \beta_{SN} & \beta_{SE} & \beta_{SW} & \beta_{SS} \end{bmatrix}.$$

4.3.2 Desired equilibrium

Let the error from the desired equilibrium be denoted by $\tilde{\rho}(x, y, t)$, which is defined as in (1.9). To keep everything simple, the desired space-varying equilibria take values only in the congested regime range, i.e., $\rho_d(x, y) \geq \rho_c(x, y)\ \forall (x, y) \in \Omega$.

The time derivatives of state and error coincide, which in combination with (4.40) yields

$$\frac{\partial \tilde{\rho}}{\partial t} = \frac{1}{L}(I - B)W\,(\rho_{max} - \rho_d - \tilde{\rho}) - \frac{\partial[C\,W\,(\rho_{max} - \rho_d - \tilde{\rho})]}{\partial x} - \frac{\partial[S\,W\,(\rho_{max} - \rho_d - \tilde{\rho})]}{\partial y}. \tag{4.41}$$

Let us also write the dynamics of the desired density that is a time-constant function:

$$\frac{\partial \rho_d}{\partial t} = 0 = \frac{1}{L}(I - B)W\,(\rho_{max} - \rho_d) - \frac{\partial[C\,W\,(\rho_{max} - \rho_d)]}{\partial x} - \frac{\partial[S\,W\,(\rho_{max} - \rho_d)]}{\partial y}. \tag{4.42}$$

If we subtract (4.42) from (4.41), we also obtain the pure error term dynamics:

$$\frac{\partial \tilde{\rho}}{\partial t} = \frac{1}{L}(B - I)W\tilde{\rho} + \frac{\partial[C\,W\tilde{\rho}]}{\partial x} + \frac{\partial[S\,W\tilde{\rho}]}{\partial y}. \tag{4.43}$$

We seek to find a desired density distribution that corresponds to congestion minimization, and then to design a boundary control that stabilizes the traffic state to that desired equilibrium. Thereby, the desired density profile must remain in the congested regime, i.e., $\rho_d(x, y) \geq \rho_c(x, y)\ \ \forall (x, y) \in \Omega$, and its values at the boundaries should be proportional to the maximal densities at the corresponding boundary coordinates, i.e., $\exists \gamma \in [1/3, 1]$ such that

$$\rho_d(x, y) = \gamma \rho_{max}(x, y), \qquad \forall (x, y) \in \Gamma_{out}. \tag{4.44}$$

The range of constant γ is related to the requirement for ρ_d to stay in the congested regime, since with $\gamma = 1/3$ the desired state equals the critical density ρ_c (recall that $\rho_c = 1/3\rho_{max}$ in case of triangular FD). Thus, we need to determine constant γ that provides congestion minimization given (4.44).

Problem 4.1
Find the desired space-varying density $\rho_d(x, y)\ \forall (x, y) \in \Omega$ that corresponds to the state of minimal congestion under the constraints that $\rho_d(x, y) \geq \rho_c(x, y)\ \ \forall (x, y) \in \Omega$, and boundary values being proportional to maximal densities (4.44).

Remark 4.2
Minimizing congestion means finding $\rho_d(x,y) \geq \rho_c(x,y)\ \ \forall (x,y) \in \Omega$ *such that* $\|\rho_d(\cdot) - \rho_c(\cdot)\|_\infty$ *is minimized. The* L_∞ *space norm is defined as in* (1.8).

Remark 4.3
Physically, a proportional relation of density values at the boundaries to the corresponding maximal densities (4.44) *implies that boundaries are filled in a homogeneous way. This might be useful in a situation when vehicles concentrated in a city center tend to leave it simultaneously, e.g., when people drive back home from their offices.*

In order to find a desired profile satisfying Problem 4.1, we need to solve the PDE (4.42) that describes its structural dependence on (x,y). First of all, we need to introduce a change of variables $\hat{\rho}(x,y)\ \ \forall (x,y) \in \Omega$ as

$$\hat{\rho}(x,y) = \rho_{max}(x,y) - \rho_d(x,y), \tag{4.45}$$

which being inserted into (4.42) yields

$$\frac{1}{L}(I - B)W\hat{\rho} = \frac{\partial[C\,W\hat{\rho}]}{\partial x} + \frac{\partial[S\,W\hat{\rho}]}{\partial y}. \tag{4.46}$$

Then, we compute the desired state $\rho_d(x,y)\ \ \forall (x,y) \in \Omega$ by performing the following steps:

1. Initial guess: set the desired density at the downstream boundary Γ_{out} equal to the corresponding critical values, i.e., pick the lowest possible $\gamma = 1/3$, which leads to

$$\hat{\rho}(x,y) = \frac{2}{3}\rho_{max}(x,y), \qquad \forall (x,y) \in \Gamma_{out}.$$

2. Consider the same area in Grenoble city center as in all previous sections, also see Figure 4.6. Define a numerical grid for this area in Ω as in Section 4.2.1 but without discretization of time, since we deal with a time-constant PDE.

3. Discretize the PDE system given by (4.46). For convenience, we consider the PDE for the density in the North direction, and then the same steps should be done for the remaining directions. In accordance with the upwind scheme [34] used to provide the correct direction of information propagation in a flow field, the discretization scheme of $\overline{\cos\theta}_N\omega_N\hat{\rho}_N$ and $\overline{\sin\theta}_N\omega_N\hat{\rho}_N$ depends on the signs of $\overline{\cos\theta}_N$ and $\overline{\sin\theta}_N$, that is $\forall (i,j) \in \{1,\dots,n_x\} \times \{1,\dots,n_y\}$:

$$\overline{\cos\theta}_N(i,j) > 0: \quad \frac{\overline{\cos\theta}_N(i+1,j)\omega_N(i+1,j)\hat{\rho}_N(i+1,j) - \overline{\cos\theta}_N(i,j)\omega_N(i,j)\hat{\rho}_N(i,j)}{\Delta x},$$
$$\overline{\cos\theta}_N(i,j) < 0: \quad \frac{\overline{\cos\theta}_N(i,j)\omega_N(i,j)\hat{\rho}_N(i,j) - \overline{\cos\theta}_N(i-1,j)\omega_N(i-1,j)\hat{\rho}_N(i-1,j)}{\Delta x}.$$

The same can be written for $\overline{\sin\theta}_N$ and for y-direction, for which we fix i and vary j.

Therefore, we can define 4×4 diagonal matrices Q^x, Q^y, R^x and R^y that capture the upwind scheme as

$$\overline{\cos\theta}_N(i,j) > 0 \ :$$
$$Q^x_{NN}(i,j) = \frac{\overline{\cos\theta}_N(i+1,j)\omega_N(i+1,j)}{\Delta x}, \quad R^x_{NN}(i,j) = 0,$$
else :
$$Q^x_{NN}(i,j) = 0, \quad R^x_{NN}(i,j) = -\frac{\overline{\cos\theta}_N(i-1,j)\omega_N(i-1,j)}{\Delta x},$$

and the same can be written for $\overline{\sin\theta}_N$ and y-direction, for which we fix i and vary j.

4. Define also a 4×4 matrix P as:

$$P(i,j) = \frac{1}{L(i,j)}(B(i,j) - \mathbb{I})W(i,j) - \frac{|C(i,j)|W(i,j)}{\Delta x} - \frac{|S(i,j)|W(i,j)}{\Delta y}.$$

Using the definition of matrices P, Q^x, Q^y, R^x and R^y, we can now write the PDE system for $\hat{\rho}$ given by (4.46) in a discretized form that reads $\forall (i,j) \in \{1,\dots,n_x\} \times \{1,\dots,n_y\}$:

$$\begin{aligned} &P(i,j)\hat{\rho}(i,j) + Q^x(i,j)\hat{\rho}(i+1,j) + Q^y(i,j)\hat{\rho}(i,j+1) \\ &+ R^x(i,j)\hat{\rho}(i-1,j) + R^y(i,j)\hat{\rho}(i,j-1) = 0. \end{aligned} \tag{4.47}$$

Notice that $\hat{\rho}(0,j)$, $\hat{\rho}(n_x+1,j)$, $\hat{\rho}(i,0)$, $\hat{\rho}(i,n_y+1)$ take the values from the boundary conditions (ghost cells).

5. System (4.47) is solved using the alternating direction implicit method, which is equivalently known as dimensional splitting, see [114]. At each iteration, first x and then y steps are performed. At each x step, the terms $\hat{\rho}(i,j-1)$ and $\hat{\rho}(i,j+1)$ take fixed values from the previous iteration, while $\hat{\rho}(i-1,j)$ and $\hat{\rho}(i+1,j)$ are fixed for each y step. At x step, our system (4.47) is solved for every j by the block tridiagonal matrix algorithm, while at y step this algorithm is applied for every column i.

6. Thus, we have described the numerical method to obtain a solution $\hat{\rho}$ for the PDE (4.47), which is not necessarily optimal. Since this PDE (4.47) is a linear system, $\alpha\hat{\rho}$ for $\alpha \in [0,1]$ is also its solution. Let us estimate the parameter α^* that provides the optimal equilibrium as in Problem 4.1.

Consider again the desired state ρ_d that is obtained from (4.45) as

$$\rho_d = \rho_{max} - \alpha\hat{\rho}. \tag{4.48}$$

By choosing $\alpha = 0$ we obtain $\rho_d = \rho_{max}$, while by choosing $\alpha = 1$ we achieve $\rho_d = \rho_c$ at the boundaries (see step 1 and use $\rho_c = 1/3\rho_{max}$). This implies that by taking an intermediate value of α, we guarantee the congested traffic regime at the boundaries. Let us calculate α^* that provides for the desired state ρ_d to be as close as possible to ρ_c while staying in the congested regime (see Remark 4.2), for which in general we can write:

$$\frac{\rho_d}{\rho_c} \geq 1 \Rightarrow \frac{\rho_{max} - \alpha\hat{\rho}}{1/3\rho_{max}} \geq 1 \Rightarrow 3 - 3\alpha\frac{\hat{\rho}}{\rho_{max}} \geq 1 \Rightarrow \alpha \leq \frac{2}{3}\frac{\rho_{max}}{\hat{\rho}}, \qquad \forall (x,y) \in \Omega.$$

From the discussion above, it follows that the optimal state is achieved if $\exists(x^*, y^*)$, for which

$$\alpha^* = \min_{\substack{(x,y)\in\Omega \\ s\in\{N,E,W,S\}}} \frac{2}{3}\frac{\rho_{max,s}(x,y)}{\hat{\rho}_s(x,y)}. \tag{4.49}$$

Thus, the optimal desired profile in the whole domain Ω can be obtained from (4.48) for optimal $\alpha = \alpha^*$

$$\rho_d(x,y) = \rho_{max}(x,y) - \alpha^*\hat{\rho}(x,y), \qquad (x,y)\in\Omega, \tag{4.50}$$

with α^* being given by (4.49). To get an expression for the optimal desired profile $\rho_d(x,y)$ at the boundary $\forall(x,y)\in\Gamma_{out}$, we take $\hat{\rho}$ from step 1 and insert it into (4.50), which yields

$$\rho_d(x,y) = \gamma^*\rho_{max}(x,y), \qquad \text{with } \gamma^* = 1 - \frac{2}{3}\alpha^*, \quad \forall(x,y)\in\Gamma_{out}. \tag{4.51}$$

As a result, we have derived the expression for optimal desired equilibrium (4.50) that corresponds to the state of minimal congestion. As we can see, it depends on the solution $\hat{\rho}$ of system (4.47) that can be found numerically using alternation direction implicit method. We could also get an explicit formula for optimal equilibrium at the domain boundary Γ_{out} given by (4.51). This is a useful expression, since it directly determines the boundary control variables $u(x,y)$ from (4.40), see details below.

4.3.3 Boundary control design

After we have analyzed the desired profile corresponding to the state of minimal congestion (see Remark 4.2), let us formulate the boundary control design problem as follows.

Problem 4.2
Find a time-constant boundary controller $u(x,y)$ such that a congested density governed by NEWS system (4.40) converges to the desired space-varying density $\rho_d(x,y)$ given by (4.50) $\forall(x,y)\in\Omega$ as $t\to\infty$.

In order to prove the convergence to the desired profile, we have to assume that the main directions of transportation coincide with the cardinal directions, which for example holds for a Manhattan grid type of traffic networks.

Assumption 4.1
The matrices C and S from (4.40) are constant in space, e.g., they can be defined as:

$$\begin{aligned} &\overline{\cos\theta}_N = 0, \quad ,\overline{\cos\theta}_E = 1 \quad \overline{\cos\theta}_W = -1, \quad \overline{\cos\theta}_S = 0, \\ &\overline{\sin\theta}_N = 1, \quad \overline{\sin\theta}_E = 0, \quad \overline{\sin\theta}_W = 0, \quad \overline{\sin\theta}_S = -1. \end{aligned} \tag{4.52}$$

In general, the further analysis requires these variables to be just constant in space, but we choose (4.52) for simplicity. We also make an assumption on supply ratios:

Assumption 4.2
SR matrix B is constant in space, which in turn implies that every intersection has the same turning ratio pattern.

Let us now show that setting the boundary controller equal to the desired state at the boundary under Assumptions 4.1 and 4.2 provides the exponential convergence of traffic state to the desired equilibrium in the whole domain. This is formalized as follows.

Theorem 4.1
Under Assumptions 4.1 and 4.2, let the boundary controller be defined as

$$u(x,y) = \begin{pmatrix} \rho_{d,N}(x, y_{max}) \\ \rho_{d,E}(x_{max}, y) \\ \rho_{d,W}(x_{min}, y) \\ \rho_{d,S}(x, y_{min}) \end{pmatrix}, \quad \forall (x,y) \in \Gamma_{out}, \tag{4.53}$$

then $\exists K, k > 0$ such that

$$\|\rho(t) - \rho_d\|^2_{L^2} \leqslant e^{-kt} K \|\rho(0) - \rho_d\|^2_{L^2},$$

i.e., the state $\rho(x,y,t)$ exponentially converges to the desired equilibrium $\rho_d(x,y)$ $\forall (x,y) \in \Omega$ as $t \to \infty$.

Remark 4.4
Although for simplicity of the proof we assumed a regular Manhattan grid structure (Assumption 4.1), the feedforward boundary controller (4.53) can be applied to a more general network, as will be shown on a numerical example, for which we take the network of Grenoble downtown.

Proof of Theorem 4.1. Let us first analyze matrix $B - I$. Its non-diagonal elements are positive, and its diagonal elements are negative. Moreover, $B - I$ has one eigenvalue equal to zero and all others are negative, as it is shown in Appendix B.8. Therefore, $B - I$ is a negative singular M-matrix with one zero eigenvalue. Thus, there exists a positive-definite diagonal 4×4 matrix D such that

$$D(B - I) + (B^T - I)D \leqslant 0. \tag{4.54}$$

Let us also introduce a diagonal 4×4 matrix composed by exponential functions as follows:

$$E = \begin{bmatrix} e^y & 0 & 0 & 0 \\ 0 & e^x & 0 & 0 \\ 0 & 0 & e^{-x} & 0 \\ 0 & 0 & 0 & e^{-y} \end{bmatrix}.$$

This matrix is used as weights in each direction that helps achieving exponential convergence. We define the following Lyapunov function candidate:

$$\begin{aligned} V = \int_{x_{min}}^{x_{max}} \int_{y_{min}}^{y_{max}} \tilde{\rho}^T W D E \tilde{\rho} \, dy dx = \int_{x_{min}}^{x_{max}} \int_{y_{min}}^{y_{max}} (\tilde{\rho}_N^2 \omega_N D_N e^y \\ + \tilde{\rho}_E^2 \omega_E D_E e^x + \tilde{\rho}_W^2 \omega_W D_W e^{-x} + \tilde{\rho}_S^2 \omega_S D_S e^{-y}) \, dy dx, \end{aligned} \tag{4.55}$$

where D_N, D_S, D_W and D_E are the diagonal elements of matrix D.

The function (4.55) is obviously positive-definite, since matrix $WDE > 0$. Let us now take its time derivative, which yields

$$\dot{V} = \int_{x_{min}}^{x_{max}} \int_{y_{min}}^{y_{max}} 2\frac{\partial \tilde{\rho}^T}{\partial t} WDE\tilde{\rho}\, dydx, \tag{4.56}$$

where the error dynamics $\partial\tilde{\rho}/\partial t$ should be taken from (4.43), which allows us to further expand (4.56) as:

$$\begin{aligned}\dot{V} = &\int_{x_{min}}^{x_{max}} \int_{y_{min}}^{y_{max}} \frac{1}{L}(W\tilde{\rho})^T \left(DE(B-I) + (B^T - I)DE\right) W\tilde{\rho}\, dydx \\ &+ 2\int_{x_{min}}^{x_{max}} \int_{y_{min}}^{y_{max}} (W\tilde{\rho})^T DE \left(\frac{\partial[C\,W\tilde{\rho}]}{\partial x} + \frac{\partial[S\,W\tilde{\rho}]}{\partial y}\right) dydx.\end{aligned} \tag{4.57}$$

Let us now denote the first term of (4.57) as $\dot{V}_1$ and the second term as $\dot{V}_2$. The term $\dot{V}_1$ is negative due to (4.54) and the fact that matrix E is non-negative, i.e.,

$$\dot{V}_1 = \int_{x_{min}}^{x_{max}} \int_{y_{min}}^{y_{max}} \frac{1}{L}(W\tilde{\rho})^T \left(DE(B-I) + (B^T - I)DE\right) W\tilde{\rho}\, dydx < 0.$$

We further consider $\dot{V}_2$ by inserting the values of matrices C and S (4.52) from Assumption 4.1

$$\begin{aligned}\dot{V}_2 \;=\; 2\int_{x_{min}}^{x_{max}} \int_{y_{min}}^{y_{max}} \Big(&\omega_E\tilde{\rho}_E D_E e^x \frac{\partial(\omega_E\tilde{\rho}_E)}{\partial x} - \omega_W\tilde{\rho}_W D_W e^{-x}\frac{\partial(\omega_W\tilde{\rho}_W)}{\partial x} \\ &+ \omega_N\tilde{\rho}_N D_N e^y \frac{\partial(\omega_N\tilde{\rho}_N)}{\partial y} - \omega_S\tilde{\rho}_S D_S e^{-y}\frac{\partial(\omega_S\tilde{\rho}_S)}{\partial y}\Big) dydx.\end{aligned}$$

This expression is then integrated by parts, which yields:

$$\begin{aligned}\dot{V}_2 = &\int_{y_{min}}^{y_{max}} \Big[e^{-x}(\sqrt{D_W}\omega_W\tilde{\rho}_W)^2 - e^{x}(\sqrt{D_E}\omega_E\tilde{\rho}_E)^2\Big]_{x=x_{min}} dy \\ &+ \int_{y_{min}}^{y_{max}} \Big[e^{x}(\sqrt{D_E}\omega_E\tilde{\rho}_E)^2 - e^{-x}(\sqrt{D_W}\omega_W\tilde{\rho}_W)^2\Big]_{x=x_{max}} dy \\ &+ \int_{x_{min}}^{x_{max}} \Big[e^{-y}(\sqrt{D_S}\omega_S\tilde{\rho}_S)^2 - e^{y}(\sqrt{D_N}\omega_N\tilde{\rho}_N)^2\Big]_{y=y_{min}} dx \\ &+ \int_{x_{min}}^{x_{max}} \Big[e^{y}(\sqrt{D_N}\omega_N\tilde{\rho}_N)^2 - e^{-y}(\sqrt{D_S}\omega_S\tilde{\rho}_S)^2\Big]_{y=y_{max}} dx \\ &- \int_{x_{min}}^{x_{max}}\int_{y_{min}}^{y_{max}} \Big(e^{x}D_E(\omega_E\tilde{\rho}_E)^2 + e^{-x}D_W(\omega_W\tilde{\rho}_W)^2 \\ &\qquad + e^{y}D_N(\omega_N\tilde{\rho}_N)^2 + e^{-y}D_S(\omega_S\tilde{\rho}_S)^2\Big)dydx.\end{aligned} \tag{4.58}$$

By setting the boundary controller $u(x,y)$ as in (4.53), we achieve that $\forall t \in \mathbb{R}^+$

$$\begin{aligned}&\tilde{\rho}_N(x, y_{max}, t) = 0, \quad \tilde{\rho}_S(x, y_{min}, t) = 0, \quad \forall x \in [x_{min}, x_{max}], \\ &\tilde{\rho}_W(x_{min}, y, t) = 0, \quad \tilde{\rho}_E(x_{max}, y, t) = 0, \quad \forall y \in [y_{min}, y_{max}],\end{aligned} \tag{4.59}$$

and one ensures that the first four integrals in (4.58) go to zero. The last term in (4.58) can be bounded as follows

$$\begin{aligned}&\int_{x_{min}}^{x_{max}}\int_{y_{min}}^{y_{max}} \Big(e^{x}D_E(\omega_E\tilde{\rho}_E)^2 + e^{-x}D_W(\omega_W\tilde{\rho}_W)^2 \\ &+ e^{y}D_N(\omega_N\tilde{\rho}_N)^2 + e^{-y}D_S(\omega_S\tilde{\rho}_S)^2\Big)dydx \\ &\leq - \min_{\substack{(x,y)\in\Omega \\ q\in\{N,S,W,E\}}} \omega_q(x,y) \int_{x_{min}}^{x_{max}}\int_{y_{min}}^{y_{max}} \Big(e^{x}D_E\omega_E\tilde{\rho}_E^2 \\ &+ e^{-x}D_W\omega_W\tilde{\rho}_W^2 + e^{y}D_N\omega_N\tilde{\rho}_N^2 + e^{-y}D_S\omega_S\tilde{\rho}_S^2\Big)dydx,\end{aligned} \tag{4.60}$$

where we have used the fact that the kinematic wave speed is positive by definition, i.e., $\omega > 0$.

The integral on the right-hand side of (4.60) coincides with the Lyapunov function (4.55). This means that by inserting (4.59) into (4.58) and also by using the bound from (4.60), we can write

$$\dot{V} = \dot{V}_1 + \dot{V}_2 \leq \dot{V}_2 \leq -kV,$$

where $k \in \mathbb{R}^+$ is a positive constant

$$k = \min_{\substack{(x,y)\in\Omega \\ q\in\{N,E,W,S\}}} \omega_q(x,y).$$

One can also prove that the state $\tilde{\rho}$ converges to zero in L_2 norm exponentially. Indeed, note that the Lyapunov function V from (4.55) defines an equivalent norm on the density space:

$$m \left\|\tilde{\rho}\right\|_{L^2}^2 \leqslant V \leqslant M \left\|\tilde{\rho}\right\|_{L^2}^2$$

with

$$m = \min_{\substack{(x,y)\in\Omega \\ q\in\{N,E,W,S\}}} \omega_q(x,y) D_q E_q(x,y),$$

$$M = \max_{\substack{(x,y)\in\Omega \\ q\in\{N,E,W,S\}}} \omega_q(x,y) D_q E_q(x,y).$$

By the exponential convergence of the Lyapunov function we have

$$V(t) \leqslant e^{-kt} V(0),$$

therefore $\forall (x,y) \in \Omega$

$$\left\|\tilde{\rho}(t)\right\|_{L^2}^2 \leqslant e^{-kt} \frac{M}{m} \left\|\tilde{\rho}(0)\right\|_{L^2}^2 .$$

□

Remark 4.5
Assumption 4.2 on space-independent B can be relaxed, if it is possible to find such a matrix D that satisfies inequality (4.54), and whose elements $D_E(y)$ and $D_W(y)$ may depend on y, while $D_N(x)$ and $D_S(x)$ may depend on x.

4.3.4 Numerical example

Finally, we demonstrate how a boundary control given by (4.53) works in practice using a selected area Grenoble downtown with a total surface of around 1.4×1 km^2, which is the same area as in all previous sections of this chapter, e.g., see Figure 4.6. For the numerical simulation of traffic density evolution governed by NEWS system (4.40) in the congested regime, we again deploy the Godunov scheme in 2D as described in 4.2.1. The downstream boundary conditions in (4.40) are set to the desired optimal density as in (4.53), while the upstream boundary conditions are initialised with the maximal possible flow as in Section 3.4.3, where the control of congested uni-directional traffic was considered. We will thus demonstrate how the boundary controller (4.53) performs for congestion mitigation purposes given the initial state

$$\rho_0(x,y) = \rho_{max}(x,y), \qquad \forall (x,y) \in \Omega.$$

The results of control performance on a congested traffic in Grenoble downtown are shown in Figure 4.15. The continuous approximation of FD and network parameters using IDW method (4.26) was done with a low weighting parameter $\mu = 5$, such that only the global trend of motion is reproduced.

Figure 4.15a) illustrates the initial vehicle density that indicates the state of a traffic jam. The optimal desired equilibrium profile ρ_d obtained by following all the steps in Section

4.3.2 is illustrated in Figure 4.15b). Recall that the desired state corresponds to congestion minimization under the constraints formulated in Problem 4.1. The desired state is found by first solving the PDE for $\hat{\rho}$ given by (4.47) and then using (4.50), where we use $\alpha^* = 0.51$ that was obtained using (4.49). Further, we show the impact of boundary controller (4.53) on the congested traffic state after $t = 5$ min, $t = 20$ min and $t = 50$ min in Figures 4.15c), 4.15d) and 4.15e), respectively. We can see that the controlled state at $t = 50$ min is identical to the desired equilibrium from Figure 4.15b).

We could quantitatively measure the similarity between two density distributions by deploying the mean SSIM (denoted by $\overline{SSIM}$), see Section 4.2.2 and (4.36). Thereby, the Grenoble area was again divided into 9 zones to compute SSIM using (4.36). Notice that SSIM as a function of time is shown in Figure 4.15f), where range of SSIM is preserved as in its original formulation, i.e., $\overline{SSIM} \in [-1, 1]$. Thus, after $t = 50$ min of boundary control action, SSIM approaches 1, which implies that two density distributions in Figures 4.15e) and 4.15b) are identical.

4.4 Chapter conclusions

In this chapter, we suggested our own way to deal with multi-directional traffic evolving on urban networks of arbitrary size. Multi-directional traffic is much more close to represent urban traffic in realistic situations compared to 2D LWR approach considered in the previous Chapter 3. The global idea was to derive a PDE model that captures the traffic behaviour evolving in a urban network in any direction with flow crossings.

We started elaborating a modeling approach for multi-directional traffic by considering a traffic flow model at one intersection based on the classical CTM. Each intersection is characterized by a certain number of incoming and outgoing roads that may be arbitrarily oriented in space. Thus, the traffic flow model has a different number of parameters to tune for each individual intersection. As a network may consist of thousands of intersections, we had to find a unified approach to describe traffic at intersections regardless of their individual parameters. Thereby, we assumed that the dynamics of multi-directional traffic can be represented by only 4 direction layers: North, East, West and South. This led to the formulation of NEWS framework that deploys geometry-based projection matrices to map the traffic flow along any road into the nearest cardinal directions. The projection weights vary continuously with road's orientation angle. For instance, if a road goes exactly to the North, the projection weight for the North direction is equal to 1 (maximal possible angle), while it is equal to 0.5 if the road is oriented perfectly towards North-East or North-West. We have also introduced the concept of partial flows to capture various origin-destination patterns at intersections. For instance, ϕ_{NE} is the flow of vehicles that were moving along a road oriented to the North, and then at intersection turned to the road oriented to the East direction.

Thus, we were able to obtain a traffic flow model that predicts the rate of change of vehicle accumulation at intersection in a unified way. However, since our goal was the derivation of a traffic model on a macroscopic scale, we wanted to formulate the traffic state in terms of

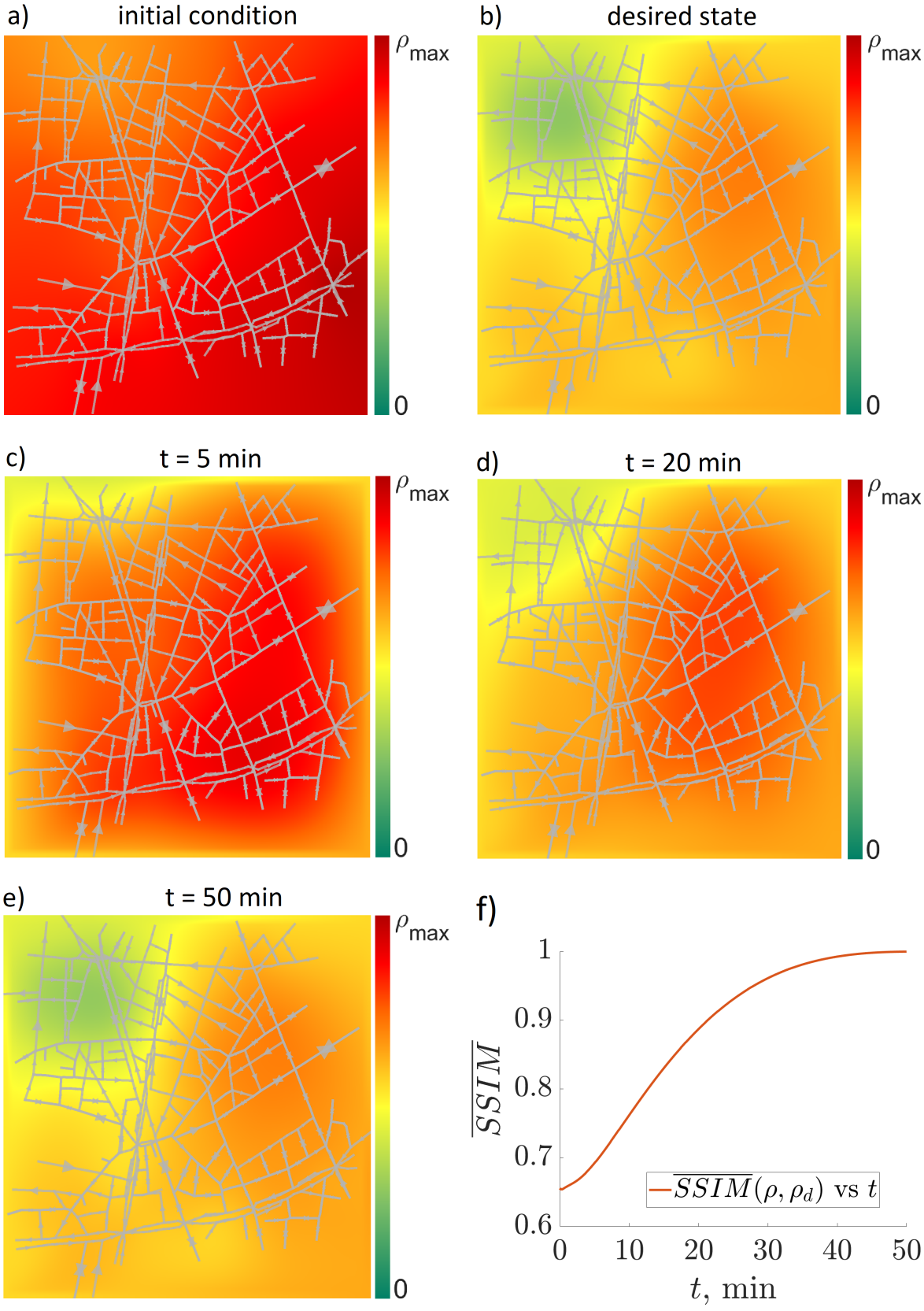

Figure 4.15: Boundary control of congested traffic in Grenoble downtown: a) initial congested state ρ_0, b) desired equilibrium ρ_d; controlled state after: c) $t = 5$ min, d) $t = 20$ min, e) $t = 50$ min; d) $\overline{SSIM}$ between the state and the desired density as a function of time.

density. Therefore, we also applied the continuation method to be able to define the model predicting the evolution of vehicle density in the vicinity of an intersection. This method was used to turn an ODE into a PDE, which allowed us to obtain a macroscopic continuum model for one intersection. Since every intersection was described in a unified way, we finally applied the inverse distance weighting to define all the intersection parameters for every point in a continuum plane. The derivation of the NEWS model was done analytically using only one assumption on network structure. Namely, urban networks under consideration must be well-designed in terms of maximal flows, i.e., if vehicles move at maximal flow before an intersection, they continue using the road capacity at maximum after the turn.

As a result, in Section 4.1, we derived the NEWS model (4.29) that predicts the evolution of traffic in four cardinal directions. The propagation of traffic flow in each direction is driven by the demand-supply concept that uses a fundamental diagram. Moreover, vehicles moving in some layer can switch to another layer, i.e., there is a mixing between different layers, which is an important aspect due to its physical ubiquity.

The mathematical properties of the NEWS model have also been analyzed. The PDE system was shown to be hyperbolic for any parameter set, as it is often the case for conservation law based traffic models. Being able to classify a model as a hyperbolic PDE significantly simplifies the analysis for future tasks such as explicit control design or steady state estimation, since a lot of analytical results have already been elaborated for this type of systems. It was also shown that the model represents a conservation law with traffic density being the conserved quantity. Moreover, it was shown that its state is bounded, which is a realistic assumption for traffic modeling, since vehicles can not be located infinitely dense.

The model prediction results have been validated in Section (4.2) using microsimulation Aimsun, and experimental platform GTL Ville that provides real-time data from a network of real sensors installed in Grenoble downtown. The validation results revealed that the density distribution predicted by NEWS model stays in a good agreement with the reference density, i.e., 90% of similarity with Aimsun and 80% similarity with the real-life experiment. Although the validation results proved a high prediction quality with the NEWS model, it is however not completely error-free, since it is based on several assumptions that do not necessarily hold for a general traffic situation in reality. The model validation with real data was made to be an open source project such that the results are reproducible and can be used for future studies.

In the last Section 4.3 of this chapter, the NEWS model has been investigated from the control perspective, whereby we restricted to the congested traffic regime for simplicity. We have analyzed the class of admissible desired equilibria that must satisfy a certain system of PDEs. We have posed and solved the problem of finding an equilibrium state that corresponds to the state of congestion minimization in a urban network under the constraint that its range must remain in the congested regime. Further, we proved the exponential convergence of a congested state controlled from the boundary to this desired equilibrium using Lyapunov methods. Thereby, for the proof, we had to assume several restrictive assumptions such as Manhattan grid like topology of underlying urban networks, and similar turning ratio patterns at intersections. These assumptions were introduced only to simplify the proof and are not

necessarily real restrictions needed to provide the functionality of the suggested controller, which was shown in a numerical example. Finally, we again used the same area in Grenoble downtown as in Section 4.2 to demonstrate the performance of the derived feedforward boundary controller with the help of a numerical example. It was shown that the controller acts such that the traffic density converges to the desired optimal equilibrium in finite time, which is related to the hyperbolic nature of NEWS PDE.

An appealing direction for future studies might be finding equilibria profiles that admit mixed traffic regimes. Another possible extension may include elaborating a boundary controller under the constraint that the activation boundary is a set of points on real roads rather than a continuous line, as it is assumed to be in a PDE-driven model. More research perspectives are given in Chapter Conclusions and Perspectives.

Conclusions and Perspectives

Summary of contributions

This thesis was devoted to traffic control on urban networks. Thereby, we have used the macroscopic modeling approach that enables characterizing traffic as a fluido-dynamic system, and its state is described in terms of vehicle density. This is a beneficial form to analyze traffic on large-scale networks, since it allows us to consider traffic as a single dynamic object rather than a collection of vehicles. By considering traffic on a macroscopic scale, the model-based control design becomes scalable and easy to validate even for arbitrarily large urban networks. We were mainly interested in predicting congestion formations in large transportation networks and in dissolving them through the boundary control, i.e., by setting appropriate on- and off-ramps. Reaching such a goal implies taking a big step towards the development of intelligent transportation networks. In this work, we proceeded towards the global goal of traffic control on any urban network step-by-step. First, traffic on single roads was considered and analyzed for control. Then, we looked at traffic on urban networks with a preferred direction of motion. Finally, we developed our own approach to modeling traffic with any direction of movement. Let us summarize the main contributions that have been achieved at each of these stages.

Traffic control on roads

We considered traffic evolving on single roads of finite lengths using the LWR approach in Chapter 2. The goal of this chapter was to design a boundary control law that acts such that any desired space- and time-varying vehicle density profile is tracked for asymptotic time. To be admissible, the desired vehicle density must be governed by the LWR PDE as well. A space- and time-dependent desired state can be seen as a generalization of any desired state. Stabilization of traffic to some desired equilibrium is just a special case of trajectory tracking, and can be achieved by applying the same control law. Also notice that non-stationary profiles are more frequent in real traffic situations.

There are however two major difficulties that arise for LWR-driven traffic control design. The first difficulty is that there are no classical solutions to the LWR PDE due to the non-linearity of the fundamental diagram even for a smooth initial datum. Characteristic lines propagate with different speeds, and whenever they cross, the discontinuities in the solution arise. This requires considering solutions in the weak sense, and the unique solution is the one that satisfies the Lax entropy condition. Thus, treating discontinuities is a tedious procedure that gets even more complicated, if we design control to track some trajectory that also does not exist in the classical sense.

The second difficulty is that considering traffic governed by LWR PDE on finite roads requires to include boundary conditions into the consideration. One needs to consider these

conditions also in the weak sense, since in general they can not be imposed for all time, which equivalently means that the demand-supply problem needs to be solved. This triggers a general problem, when the boundary conditions need to be designed for traffic control. We can not even analyze how the system evolves under the effect of control in a straightforward way, since the controller may not be accepted by the system.

Thus, we first considered a more simple case by restricting only to congested traffic in Section 2.2. Considering traffic only in the congested regime considerably facilitates the structure of the traffic system that becomes linear, as well as boundary conditions can be imposed in a strong sense. We also added a general unknown in-domain disturbance to the system. This was done to capture the unmeasured influence of vehicles that come from minor roads and aggravate congestion. Thus, we designed the optimal boundary controller that acts to minimize the deviation from the desired trajectory while attenuating disturbance. The deviation is minimized in sense of L_2 norm if the boundary controller from Theorem 2.1 is applied. We also achieved the minimization of the deviation in sense of L_∞ norm by applying the boundary control law from Theorem 2.2. When it comes to practical applications, the minimization norm should be chosen based on the available knowledge of the disturbance source, i.e., L_2 norm should be minimized if the unmeasured flow of vehicles originates from many minor roads, while we choose the L_∞ minimization if the disturbance is related to a stream of vehicles originating from a single major road. In both cases, the designed controllers have feedback parts used to attenuate the disturbance. Although the controllers are optimal, in general, the in-domain disturbance can not be completely rejected by acting only from the boundary due to a finite propagation speed of information, which is a general property of hyperbolic systems. The material of Section 2.2 was published in [137].

In Section 2.3, we extended this result by considering the full LWR system (without disturbance), for which no classical solutions exist. The traffic state as well as the desired trajectory are governed by the LWR PDE, which implies that they can be in different traffic regimes. Solving a boundary control task for such a system is a much more general result, since real-life traffic usually builds non-trivial density patterns, e.g., it can be partially in the free-flow traffic regime and partially congested. We could solve this problem by considering the LWR system in Hamilton-Jacobi formulation that represents its integral (cumulative) form. This formulation enabled us to obtain a continuous solution to the LWR system explicitly for large enough time. It was possible due to a convenient shape of the triangular fundamental diagram. The solution to the LWR system in H-J formulation was then used to analyze the boundary conditions in terms of control restrictive functions. The cumulative H-J formulation thus enabled us to estimate the time periods during which the road boundaries can not accept the proposed controller values. The main result of this section is the boundary control law with feedback term in Theorem 2.3, and we can also say that it is *the main result of the whole Chapter 2*. We have shown that even with time periods during which no control can be imposed, the system exponentially converges to the desired trajectory in Hamilton-Jacobi formulation. This result implies that under this control law, the number of vehicles on the controlled traffic road converges to the desired number of vehicles pointwise. This also means that the vehicle density converges to the desired trajectory in the integral sense over arbitrarily small intervals. Thus, we suggested a general approach to solve any control task for LWR-

driven mixed-regime traffic on a single road by acting only from the road boundary, and it was published in [133].

Uni-directional traffic on networks

After the boundary control problem for a general traffic state was solved for a single road, we were seeking to find a holistic approach to solve any control tasks for urban traffic in Chapter 3. This was done within the same modeling approach but in two dimensions, i.e., we used the 2D LWR model to predict the evolution of traffic on a urban network by approximating it as a 2D continuum plane. Namely, traffic is again seen as a fluid that propagates along a 2D plane that is a rectangular domain whose size is determined by the size of the underlying network that represents a set of roads and intersections. The network infrastructure is incorporated as an explicit space-dependency of the fundamental diagram that captures various speed limits and transportation capacities along the roads of urban network. The FD parameters are approximated everywhere in the continuum, and its values are mostly influenced by the parameters of the closest roads. The direction of traffic flow propagation is determined by the direction field that depends on the network geometry. The structure of the model implies that the integral lines of the direction field do not cross. Moreover, to be well-defined on a continuum plane, we can apply this model only to urban networks that contain no loops. These two requirements (no crossing lines and no loops) makes this model applicable only to uni-directional networks, i.e., there must be a preferred direction of motion. This restriction makes it difficult to use this model for a general multi-directional traffic. However, the 2D LWR model can be useful in a variety of situations. For example, many people driving simultaneously to the business district (e.g., at 9 am on a weekday) create a uni-directional traffic pattern.

The second space dimension makes it difficult to analyze the 2D LWR model in its original form for the control design. For example, it was not clear which boundary point should be actuated such that some area inside the domain is affected. In Section 3.2, we elaborated a technique that turns this 2D model into a parametrized system of 1D LWR equations with an explicitly space-dependent FD. This technique is the main contribution of Chapter 3. It is based on the curvilinear coordinate transformation that scales and rotates the space such that it is then treated as a continuum, in which traffic propagates along straight lines (as in Figure 3.7). Thus, the 2D LWR model was rewritten in new coordinates (3.34), and it is seen as a continuum plane composed of inhomogeneous roads. The big advantage of this system is that we could apply similar control techniques as in the previous chapter but handling the explicit space-dependency of FD and an additional space parameter.

In Section 3.3, we discussed the equilibria that can be achieved in urban networks given inflows and network structure (published in [135]). Then, this result was used in Section 3.4 to obtain the optimal equilibrium state corresponding to congestion mitigation. Thereby, we considered a simplistic case of traffic being only in the congested regime. The boundary controller is given in Theorem 3.1, and it was shown that it is able to drive congested urban traffic to an equilibrium of maximal throughput (published in [138]). Next, in Section 3.5, we solved the problem of boundary control design for mixed-regime urban traffic such that

it tracks any desired space- and time-dependent trajectory. This is the same problem as considered for 1D case, and thus it could also be solved using the H-J formulation. This was however more technically involved and not that straightforward due to the space-dependency of the Hamiltonian. The designed boundary controller is presented in Theorem 3.2. This result is a general solution to the boundary control problem for any urban network that has a preferred direction of motion that can achieve any time- and space-dependent profile governed by the 2D LWR model.

Finally, in Section 3.6, control was designed in a different way than in all the preceding parts. Namely, we demonstrated the ability to control urban traffic using the variable speed limit applied continuously in space and time (in-domain controller). The VSL controller given in Theorem 3.3 is able to drive urban traffic to any desired equilibrium. The difference with respect to the previous boundary control result is that this desired equilibrium is not even restricted to satisfy the conservation law equation. This is possible, since the controller is designed such that the closed-loop system loses the conservation law structure, i.e., it feedback linearizes the system. Thus, the desired equilibrium is bounded only by the maximal density that is determined by the network structure. It was shown that the controller is smooth in space for some special dependencies of FD on VSL in Theorem 3.4. Then we also designed an equilibrium that provides that the system is used at its maximal theoretical throughput by the maximal possible number of drivers. The material presented in Sections 3.5 and 3.6 was sent for a publication [132].

Multi-directional traffic on networks

In Chapter 4, we addressed the main limitation of the previous results that have been developed only for uni-directional traffic. A new model for traffic with multiple directions was introduced in Section 4.1. This model is explicitly derived from the demand-supply concept for one intersection. Since a urban network usually contains much more than one intersection, we had to develop a new framework that can describe traffic in a unified way for all intersections. The main difficulty was introduced by the fact that every intersection may have an arbitrary number of incoming and outgoing roads.

We suggested to introduce a projection matrix that assigns weights to every road with respect to 4 cardinal directions, which are North, East, West and South (NEWS). Thus, every intersection is approximated as if it would have 4 incoming and 4 outgoing roads in each direction, i.e., 16 pairs of origin-destination flows can be defined. This enabled us to formulate a traffic flow model at every intersection in a unique way such that it predicts the rate of change in the number of vehicles at intersection given inflows and outflows in NEWS formulation. Further, the continuation method was applied to translate this ODE model into a PDE that describes the evolution of vehicle density in the vicinity of an intersection. This was done, since our goal was to derive a macroscopic continuous model, as in the previous chapters but allowing any possible direction. Thus, we obtained a unique model that describes the evolution of density in 4 direction layers at every intersection in the same way. Using approximation methods, we defined also the parameters of FD everywhere in the continuum.

Therefore, we obtained the NEWS model (4.25) that is the main contribution of Chapter 4. It consists of mixing and transportation terms. The mixing term is responsible for modeling of inter-layer traffic flow, which is an essential phenomenon that allows to capture turning ratios correctly. The transportation term describes the spatial propagation of traffic flow in each direction layer that depends only on demand and supply functions of the corresponding direction.

In Section 4.1.4, the properties of this new model have been studied. It was shown that this model represents a conservation law. Its state is always positive and bounded by the traffic jam density that is determined by the network topology. Then, we also showed that this model corresponds to a hyperbolic partial differential equation for any possible parameter set. Being able to classify a traffic model as a hyperbolic conservation law allows to consider the properties of its solution in the same way as it is done for other hyperbolic conservation laws such as 1D LWR, as well as the same finite difference approximation method can be applied for numerical simulations.

The ability to consistently predict traffic evolution on large-scale networks using the NEWS model was validated in Section 4.2. First, we used synthetic traffic data obtained by running a congestion formation scenario on a commercial microsimulator Aimsun. It predicts the trajectories of individual vehicles given some network with defined road and intersection parameters as well as the inflow rate. The same scenario and parameters were taken for the numerical simulation of traffic with NEWS-driven dynamics. The results were compared using the structural similarity index that is a perception-based measure of similarity between two images (density distributions). The index revealed 90% of similarity meaning that the NEWS model is able to predict the evolution of traffic with the accuracy of 90%. The main factor explaining that two distributions are not identical is a pure continuous nature of the NEWS model, which does not strictly prohibit cars to move outside of real roads.

Then, the NEWS prediction results were also validated with real data obtained from the experimental platform GTL Ville (Grenoble Traffic Lab) that collects traffic data from a set of real sensors installed in Grenoble downtown. These data are related to inflows and outflows at stationary points, turning ratios were obtained with Bluetooth devices, and TomTom data provide velocities. It is important to note that due to economic cost sensors are not installed at every road. The rest of the traffic state in Grenoble downtown was reconstructed using heuristic algorithms. Thus, the NEWS traffic density was compared to the traffic density reconstructed from real measurements, and the similarity index revealed 80% of similarity. The results are presented in Figure 4.12, which is the major contribution of Section 4.2 (and one of the main contributions of this whole chapter). An additional source of distribution mismatch comes through the disability to enforce the same inflow and outflow data as in the real-life experiment due to the demand-supply problem. The derivation of NEWS model and its validation with synthetic and real data was sent for a publication [136].

Finally, we analyzed the NEWS model for the case of multi-directional traffic in the congested regime, and designed a boundary control law to manage this traffic in Section 4.2 (sent for a publication [134]). The control goal thereby was again to drive the system to the best equilibrium proving the maximal throughput under the constraint that mathematically traffic

could still be described by the NEWS system in congested traffic regime. The most non-trivial thing was to analyze admissible equilibria, for which some PDEs had to be solved. The designed boundary controller is presented in Theorem 4.1. For its proof, we had to assume a Manhattan grid structure of network and a similar supply ratio pattern at every intersection, which are however not necessarily real restrictions that need to hold in order to achieve the convergence to the desired state with the boundary controller.

Perspectives and extensions

Based on the results of this PhD thesis, I see a plenty of appealing directions for the future research. The following open questions seem to be the most relevant ones:

- In this thesis, traffic was described in a quite simplistic way, since LWR model represents the most simple macroscopic model of traffic. In general, it is well known that LWR modeling approach has several drawbacks, since it does not take many important phenomena such as bounded acceleration or capacity drop due to the transition from free-flow to congested traffic regime. Moreover, a possible way to refine the description of traffic is to take into account different driver classes based on their velocity (fast and slow). Thus, one could investigate the boundary control problem to track a desired space- and time-varying profile using a more sophisticated modeling approach that addresses limitations of LWR model (higher-order and multi-class models).

- The 2D LWR model is restricted to describe traffic on networks that have a preferred direction of motion, which is not realistic for general traffic. A similar problem was encountered for MFD-based models. Recall that MFD becomes ill-defined in zones with heterogeneously congested roads, and partitioning algorithms had to be developed to divide a network into homogeneously congested zones. Thus, as a promising extension of research on macroscopic urban traffic modeling, one could develop partitioning algorithms that would divide a urban network into zones that have a preferred direction of motion.

- In both Chapters 3 and 4, the boundary controllers were designed for traffic evolving on a continuum rectangular domain that approximates the underlying urban network. As a result, we obtained control laws defined on a continuum line, which is not directly interpretable physically. It would be thus interesting to investigate this problem and to develop a method to map the boundary controllers defined on continuous lines into actuators that are set on specific points or intervals on real roads.

- In Chapter 4 the NEWS model was derived. This model is a system of only four PDEs that is able to predict the evolution of multi-directional traffic on urban networks quite accurately (which was confirmed with experimental data). It is important for future studies to rigorously characterize the mathematical properties of its solutions. Moreover, the last Section 4.3 presented the first control result for traffic governed by the NEWS

model, however for a simplified case of congested traffic. It would be thus appealing to extend this result to capture mixed-regime traffic.

Appendix A: List of symbols

A.1 Traffic on one road

$\rho(x,t)$	one-dimensional vehicle density	veh/m
$\phi(x,t)$	one-dimensional vehicle flow	veh/s
$\rho_d(x,t)$	desired vehicle density trajectory	veh/m
$\tilde{\rho}(x,t)$	deviation of the state from the desired density	veh/m
$\Phi(\rho)$	flux function (constant parameters)	veh/s
$D(\rho)$	demand function	veh/s
$S(\rho)$	supply function	veh/s
$\rho_{in}(t)$	proposed density at the upstream boundary	veh/m
$\rho_{out}(t)$	proposed density at the downstream boundary	veh/m
$\rho_0(x)$	initial density at $t = 0$	veh/m
$\phi_{in}(t)$	inflow to the road stretch	veh/s
$\phi_{out}(t)$	outflow from the road stretch	veh/s
v, ω	kinematic wave speeds in triangular FD (constant)	m/s
ρ_c	critical density (constant)	veh/m
ρ_{max}	maximal density (constant)	veh/m
ϕ_{max}	road capacity (constant)	veh/s
L	road length (constant)	m
t_{ctr}	minimal controllability time	s
$M_{\mathrm{Ini}}(x)$	initial cumulative vehicle number at $t = 0$	veh
$M_{\mathrm{Up}}(t)$	cumulative vehicle number at road entry $x = 0$	veh
$M_{\mathrm{Down}}(t)$	cumulative vehicle number at road exit $x = L$	veh

A.2 Uni-directional traffic on a 2D plane

Variable	Meaning	Units
$\rho(x,y,t)$	two-dimensional vehicle density	veh/m^2
$\vec{\Phi}(x,y,\rho)$	flux vector function	veh/(s·m)
$\Phi(x,y,\rho)$	flux magnitude (space-varying parameters)	veh/(s·m)
$\vec{d_\theta}(x,y)$	direction field set by network geometry	-
Ω	bounded continuum domain that approximates network	m
∇	two-dimensional nabla operator	1/m
$\rho_0(x,y)$	initial density at $t=0$	veh/m^2
$v(x,y)$, $\omega(x,y)$	kinematic wave speeds (triangular FD)	m/s
$v_{max}(x,y)$	maximal free-way kinematic wave speed (Greenshields FD)	m/s
$\rho_c(x,y)$	critical density	veh/m^2
$\rho_{max}(x,y)$	maximal density	veh/m^2
$\phi_{max}(x,y)$	road capacity	veh/(s·m)
μ	weighting parameter for continuous approximation	1/m
(ξ,η)	curvilinear spatial coordinates	m
$\alpha(\xi,\eta)$, $\beta(\xi,\eta)$	scaling factors used to preserve the metric in (ξ,η)-space	-
$\rho_{max}(\xi,\eta)$	maximal density in (ξ,η)-space	veh/m^2
$\phi_{max}(\xi,\eta)$	road capacity in (ξ,η)-space	veh/(s·m)
$v(\xi,\eta)$, $\omega(\xi,\eta)$	kinematic wave speeds in (ξ,η)-space (triangular FD)	m/s
$v_{max}(\xi,\eta)$	maximal free-way kinematic wave speed in (ξ,η)-space (Greenshields FD)	m/s
$D(\rho_{in}(\eta))$	demand at the upstream boundary of η-line	veh/(s·m)
$S(\rho_{out}(\eta))$	supply at the downstream boundary of η-line	veh/(s·m)
$\phi_{max}^{min}(\eta)$	capacity at the strongest bottleneck along the η-line	-
$t_{ctr}(\eta)$	minimal controllability time for η-line	s

A.3 Multi-directional traffic on a 2D plane

A.3.1 Road formulation

Variable	Meaning	Units
$\rho(x, y, t)$	vehicle density	veh/m
$\Phi(x, y, \rho)$	flow function	veh/s
$v(x, y)$	kinematic wave speed in free-flow regime	m/s
$\omega(x, y)$	kinematic wave speed in congested regime	m/s
$\rho_c(x, y)$	critical vehicle density	veh/m
$\phi_{max}(x, y)$	flow capacity	veh/s
$D(\rho)$	demand function	veh/s
$S(\rho)$	supply function	veh/s
ϕ_i^{in}	inflow to intersection from road i	veh/s
ϕ_j^{out}	outflow from intersection to road j	veh/s
ψ_j^{in}	inflow into road j	veh/s
ψ_j^{out}	outflow from road j	veh/s
n_{in}	number of incoming roads for intersection	-
n_{out}	number of outgoing roads from intersection	-
ϕ_{ij}	flow from road i to road j	veh/s
α_{ij}	turning ratio from road i to road j	-
β_{ij}	supply coefficient of road j for the flow from road i	-
D_{ij}	flow demand of road i to enter road j	veh/s
S_{ij}	supply of road j for flow coming from road i	veh/s
θ_i	angle that road i builds with the East direction	rad
l_i	length of road i	m

A.3.2 The NEWS formulation

Variable	Meaning	Units
$p_\theta^N, p_\theta^E, p_\theta^W, p_\theta^S$	projection coefficients w.r.t. corresponding directions	-
$P_{in} \in \mathbb{R}^{4\times n_{in}}$	projection matrix for incoming roads into NEWS	-
$P_{out} \in \mathbb{R}^{4\times n_{out}}$	projection matrix for outgoing roads into NEWS	-
$\bar{\rho}(x,y,t)$	4-dim density vector	veh/m
$\bar{\Phi}(x,y,\bar{\rho})$	4-dim flow function	veh/s
$\bar{\rho}_{max}(x,y)$	4-dim maximal density	veh/m
$\bar{v}(x,y)$, $\bar{\omega}(x,y)$	4-dim kinematic wave speeds	m/s
$\bar{\rho}_c(x,y)$	4-dim critical density	veh/m
$\bar{\phi}_{max}(x,y)$	4-dim flow capacity	veh/s
$\bar{D}(x,y,\bar{\rho})$	4-dim demand function	veh/s
$\bar{S}(x,y,\bar{\rho})$	4-dim supply function	veh/s
$\bar{\phi}_N^{in}(x,y)$	inflow into intersection in the North direction	veh/s
$\bar{\phi}_N^{out}(x,y)$	outflow from intersection in the North direction	veh/s
$\bar{\phi}_{NE}(x,y)$	partial flow from North to East wrt intersection	veh/s
$\bar{\psi}_N^{in}(x,y)$	inflow into outgoing road in the North direction	veh/s
$\bar{\psi}_N^{out}(x,y)$	outflow from outgoing road in the North direction	veh/s
$\bar{\psi}_{NE}(x,y)$	partial flow from North to East wrt outgoing roads	veh/s
$\bar{\alpha}_{EN}(x,y)$	turning ratio from East to North layer	-
$\bar{\beta}_{EN}(x,y)$	supply of East layer for the flow from the North	-
$\overline{\cos\theta}(x,y)$, $\overline{\sin\theta}(x,y)$	average direction parameters of intersection	-
$L(x,y)$	average length of outgoing roads of intersection	m

Appendix B: Analysis of traffic systems

B.1 Method of characteristics for a system with disturbance

Here we provide the details on how to obtain a solution $\tilde{\rho}(x,t)$ to a transport equation with a disturbance term (2.37). Since in this case we are dealing with a linear system (2.37), we can apply the method of characteristics to find its solution $\tilde{\rho}(x,t)\ \forall (x,t) \in [0,L] \times \mathbb{R}^+$. According to the method of characteristics, finding a solution is equivalent to finding an integral surface S such that the coefficient vector field $V = (1, -\omega, \delta(x))$ is tangent at each point for any curve $\Gamma \in S$ [46].

Let us introduce a variable s used for the parametrization of Γ. Thus, we need to find a curve $\Gamma = (x(s), y(s), z(s)) \in \mathbb{R}^3$ such that the following system of ODEs is satisfied:

$$\begin{cases} \dfrac{dx}{ds} = -\omega, \\ \dfrac{dt}{ds} = 1, \\ \dfrac{dz}{ds} = \delta(x(s)). \end{cases}$$

By eliminating s from the first two ODEs, we obtain the projection of the characteristic curve in (x,t)-plane : $t - \frac{L-x}{\omega} = \text{const}$. Note that we consider only $t \geq \frac{L-x}{\omega}$, since the control action has a finite propagation time $t_{ctr} = \frac{L}{\omega}$.

Now let us estimate $\tilde{\rho}(x,t)$ from the third ODE. For this, we need to parametrize the line passing through two points (x,t) and $(L, t - \frac{L-x}{\omega})$: in the first variable it is $x(y) = y$ as y varies from x to L, and in the second variable it is $t(y) = (t - \frac{(y-x)}{\omega})$. If z has to be on the integral curve, then $z(y) = \tilde{\rho}(y, t - \frac{(y-x)}{\omega})$. Therefore, the third ODE becomes

$$-\omega \frac{dz}{dy} = \delta(y).$$

Integration from L to x of both sides yields

$$\frac{1}{\omega} \int_x^L \delta(y) dy = \tilde{\rho}(x,t) - \tilde{\rho}(L, t - \frac{L-x}{\omega}).$$

Notice that we need to perform similar steps in order to obtain a solution $\tilde{\rho}(x,t)$ for $t < \frac{L-x}{\omega}$. In this case, the projection of the characteristic curve in (x,t)-plane is $x+\omega t = \text{const}$.

B.2 Solution of a Hamilton-Jacobi system

Here we explicitly derive the analytic solution of a H-J problem as in (2.25) for the special case of Hamiltonian being a triangular FD. In this case, the convex transform (2.30) of a triangular FD (2.2) yields

$$L(v') = \phi_{max} - \rho_c v', \qquad \forall v' \in [-\omega, v], \tag{B.1}$$

and it is illustrated in Figure 2.5.

In order to obtain a unique solution $M(x,t)\ \forall (x,t) \in [0,L] \times \mathbb{R}^+$ for the case of triangular FD, we should explicitly calculate "solution candidates" $M_{\text{Up}}(x,t)$, $M_{\text{Down}}(x,t)$ and $M_{\text{Ini}}(x,t)$, and then extract the minimum of these functions as in (2.34).

B.2.1 Upstream boundary condition

The function $M_{\text{Up}}(x,t)$ denotes the solution of the Lax-Hopf formula (2.32) that originates from the upstream boundary $x = 0$ at time $t - T$ given the initial cost $M_{\text{Up}}(T-t)$ (a more detailed explanation is given in 2.1.8).

By looking at the value condition function c defined in (2.26), we establish that the initial cost in (2.33) is given by $c(x - Tv', t - T) = M_{\text{Up}}(t - T)$. The equality to zero of the first argument of function c is achieved for $T = \frac{x}{v'}$, where $v' \in [-\omega, v]$. Since T can only be positive by definition, the minimal value of the time interval should be $T_{min} = \frac{x}{v}$. Using (B.1), this results into the following infimum problem:

$$M_{\text{Up}}(x,t) = \inf_{T \in [\frac{x}{v}, +\infty]} (M_{\text{Up}}(t-T) + T\phi_{max}) - x\rho_c.$$

Using the expression for the upstream boundary condition (2.27), the infimum problem reads

$$M_{\text{Up}}(x,t) = \inf_{T \in [\frac{x}{v}, +\infty]} \left(\int_0^{t-T} \phi_{in}(\tau) d\tau + T\phi_{max} \right) + \int_0^L \rho_0(s) ds - x\rho_c,$$

which by using $T\phi_{max} = \int_{t-T}^{T} \phi_{max} d\tau$ can be rewritten as

$$M_{\text{Up}}(x,t) = \inf_{T \in [\frac{x}{v}, +\infty]} \left(\int_{t-T}^{t} (\phi_{max} - \phi_{in}(\tau))\, d\tau \right) + \int_0^L \rho_0(s) ds + \int_0^t \phi_{in}(\tau) d\tau - x\rho_c.$$

The infimum is achieved for $T = T_{min} = \frac{x}{v}$, i.e., the correct solution is related to the path along which the vehicle has the maximal velocity. Substituting $T = T_{min}$, we get $\forall x \in [0, L]$

$$\begin{aligned} t < \frac{x}{v} : \quad & M_{\text{Up}}(x,t) = +\infty, \\ t \geq \frac{x}{v} : \quad & M_{\text{Up}}(x,t) = \int_0^{t-\frac{x}{v}} \phi_{in}(\tau)\, d\tau + \int_0^{L} \rho_0(s)\, ds, \end{aligned} \tag{B.2}$$

where for $t < x/v$ the value of $M_{\text{Up}}(x,t)$ is undefined, thus, we set it to infinity.

B.2.2 Downstream boundary condition

Further, we need to calculate $M_{\text{Down}}(x,t)$, which is related to the downstream boundary $x = L$. The space argument in the value condition function now becomes $x - Tv' = L \Rightarrow T = \frac{x-L}{v'}$ with $v' \in [-\omega, v]$. Thus, the smallest value of the time interval should be $T_{min} = \frac{x-L}{-\omega}$. The calculation is done performing the same steps as for $M_{\text{Up}}(x,t)$, and we obtain $\forall x \in [0, L]$

$$\begin{aligned} t < \frac{L-x}{\omega} : \quad & M_{\text{Down}}(x,t) = +\infty, \\ t \geq \frac{L-x}{\omega} : \quad & M_{\text{Down}}(x,t) = \int_0^{t-\frac{L-x}{\omega}} \phi_{out}(\tau)\, d\tau + \rho_{max}(L-x). \end{aligned} \tag{B.3}$$

B.2.3 Initial condition

Finally, we calculate the function $M_{\text{Ini}}(x,t)$ determined by the vehicle with known label at $t = 0$ (2.29). The equality to zero of the time argument in the value condition function is provided by $T = t$. This yields

$$M_{\text{Ini}}(x,t) = \inf_{v' \in [-\omega, v]} \left(M_{\text{Ini}}(x - tv') - t\rho_c v' \right) + t\phi_{max}.$$

Using the definition of $M_{\text{Ini}}(x)$ from (2.29), we obtain

$$M_{\text{Ini}}(x,t) = \inf_{v' \in [-\omega, v]} \left(\int_{x-tv'}^{L} \rho_0(s)\, ds - t\rho_c v' \right) + t\phi_{max}.$$

We decompose the integral as

$$\int_{x-tv'}^{L} \rho_0(s)\, ds = \int_{x}^{L} \rho_0(s)\, ds + \int_{x-tv'}^{x} \rho_0(s)\, ds,$$

and the second term as $-t\rho_c v' = \int_{x-tv'}^{x} -\rho_c \, ds$, which leads us to

$$M_{\text{Ini}}(x,t) = \int_{x}^{L} \rho_0(s)\, ds + t\phi_{max} + \inf_{v' \in [-\omega, v]} \left(\int_{x-tv'}^{x} (\rho_0(s) - \rho_c)\, ds \right).$$

We define $y = x - tv'$ and take the infimum over y:

$$M_{\text{Ini}}(x,t) = \int_{x}^{L} \rho_0(s)\, ds + t\phi_{max} + \inf_{y \in [x-tv, x+t\omega]} \left(\int_{y}^{x} (\rho_0(s) - \rho_c)\, ds \right).$$

Note that the space coordinates should not lie outside the road stretch, i.e., we must provide that $x \in [0, L]$, which is achieved in four possible cases:

$$\begin{aligned}
&t < \min\left\{\frac{x}{v}, \frac{L-x}{\omega}\right\} : \quad M_{\text{Ini}}(x,t) = H(x,t) + \inf_{y \in [x-tv, x+t\omega]} \left(\int_{y}^{x} (\rho_0(s) - \rho_c)\, ds \right), \\
&t \in \left[\frac{L-x}{\omega}, \frac{x}{v}\right) : \quad M_{\text{Ini}}(x,t) = H(x,t) + \inf_{y \in [x-tv, L]} \left(\int_{y}^{x} (\rho_0(s) - \rho_c)\, ds \right), \\
&t \in \left[\frac{x}{v}, \frac{L-x}{\omega}\right) : \quad M_{\text{Ini}}(x,t) = H(x,t) + \inf_{y \in [0, x+t\omega]} \left(\int_{y}^{x} (\rho_0(s) - \rho_c)\, ds \right), \\
&t \geq \max\left\{\frac{x}{v}, \frac{L-x}{\omega}\right\} : \quad M_{\text{Ini}}(x,t) = H(x,t) + \inf_{y \in [0, L]} \left(\int_{y}^{x} (\rho_0(s) - \rho_c)\, ds \right), \\
&\text{with} \quad H(x,t) = \int_{x}^{L} \rho_0(s)\, ds + t\phi_{max}.
\end{aligned} \tag{B.4}$$

In general, the infimum value is related to the number of crossings of critical density, and it cannot be exactly calculated for a general case unless additional assumptions on initial conditions are imposed.

B.2.4 Unique solution

In order to obtain the unique solution to H-J system (2.25), we need to find the minimum of (B.2), (B.3) and (B.4) as in (2.34). Thus, depending on the values of t, the explicit solution

to H-J system (2.25) can be divided into four different cases $\forall x \in [0, L]$ (see a) - d) below).

a) $t < \min\left\{\frac{x}{v}, \frac{L-x}{\omega}\right\}$:

$$M(x,t) = H(x,t) + \inf_{y\in[x-tv,x+t\omega]} \left(\int_y^x (\rho_0(s) - \rho_c)\, ds \right),$$

b) $t \in \left[\frac{L-x}{\omega}, \frac{x}{v}\right)$:

$$M(x,t) = \min\left\{ H(x,t) + \inf_{y\in[x-tv,L]} \left(\int_y^x (\rho_0(s) - \rho_c)\, ds \right), \int_0^{t-\frac{L-x}{\omega}} \phi_{out}(\tau)\, d\tau + \rho_{max}(L-x) \right\},$$

c) $t \in \left[\frac{x}{v}, \frac{L-x}{\omega}\right)$:

$$M(x,t) = \min\left\{ H(x,t) + \inf_{y\in[0,x+t\omega]} \left(\int_y^x (\rho_0(s) - \rho_c)\, ds \right), \int_0^{t-\frac{x}{v}} \phi_{in}(\tau)\, d\tau + \int_0^L \rho_0(s) ds \right\}, \tag{B.5}$$

d) $t \geq \max\left\{\frac{x}{v}, \frac{L-x}{\omega}\right\}$:

$$M(x,t) = \min\left\{ H(x,t) + \inf_{y\in[0,L]} \left(\int_y^x (\rho_0(s) - \rho_c)\, ds \right), \int_0^{t-\frac{x}{v}} \phi_{in}(\tau) d\tau + \int_0^L \rho_0(s)\, ds, \int_0^{t-\frac{L-x}{\omega}} \phi_{out}(\tau)\, d\tau + \rho_{max}(L-x) \right\},$$

with $H(x,t) = \int_x^L \rho_0(s)\, ds + t\phi_{max}$.

As already mentioned above, in all the cases a) - d) the information on crossings of the critical value by the initial density is required in order to solve the infimum problem.

B.3 H-J solution for large time

The solution to the Hamilton-Jacobi system is given by (B.5), which is divided into four different cases depending on the value of time t. Let us determine the solution for large time,

which is then used for the analysis of the traffic system behaviour for $t \to \infty$. Notice that the solution candidate $M_{\text{Ini}}(x,t)$ associated with the initial condition given by (B.4) is the most "confusing" term, since it contains an unresolved infimum problem. However, the only time-depending term in (B.4) is $t\phi_{max}$, thus $dM_{\text{Ini}}/dt = \phi_{max}$. Taking the time derivative for other terms yields $dM_{\text{Up}}/dt = \phi_{in}(t - x/v)$ and $dM_{\text{Down}}/dt = \phi_{out}(t - (L-x)/\omega)$. By the capacity constraint $\phi(\rho(\cdot,\cdot)) \leq \phi_{max}$, we establish that the term M_{Ini} grows faster than the others (or in some special cases equally fast).

B.3.1 Time when initial conditions leave the system

Let us estimate the minimal time t_{min}, after which the initial condition does not affect the solution of a H-J system (2.25), i.e., $\forall (x,t) \in [0,L] \times [t_{min}, +\infty)$: $M_{\text{Ini}}(x,t) \geq M_{\text{Up}}(x,t)$ or $M_{\text{Ini}}(x,t) \geq M_{\text{Down}}(x,t)$. Let us first establish the earliest time, for which $M_{\text{Ini}}(x,t) \geq M_{\text{Up}}(x,t)$, then we will do the same for $M_{\text{Down}}(x,t)$, and then the final value will be the minimum of two cases.

Thus, using $M_{\text{Up}}(x,t)$ from (B.2) and $M_{\text{Ini}}(x,t)$ from (B.4) with $t\phi_{max} = \int_0^{t-\frac{x}{v}} \phi_{max}\, d\tau + \frac{x}{v}\phi_{max}$, we can write $\forall (x,t) \in [0,L] \times \left[\max\left\{\frac{x}{v}, \frac{L-x}{\omega}\right\}, +\infty\right)$ that

$$\begin{aligned} M_{\text{Ini}}(x,t) - M_{\text{Up}}(x,t) = &\int_0^{t-\frac{x}{v}} (\phi_{max} - \phi_{in}(\tau))\, d\tau + \frac{x}{v}\phi_{max} \\ &- \int_0^x \rho_0(s)\, ds + \inf_{y\in[0,L]} \int_y^x (\rho_0(s) - \rho_c)\, ds. \end{aligned} \tag{B.6}$$

Let us use the following bounds

$$\frac{x}{v}\phi_{max} \geq 0, \quad -\int_0^x \rho_0(s) ds \geq -L\rho_{max}, \quad \text{and} \quad \inf_{y\in[0,L]} \left(\int_y^x (\rho_0(s) - \rho_c)\, ds \right) \geq -L\rho_c,$$

which are then inserted into (B.6), and we get the following lower bound

$$M_{\text{Ini}}(x,t) - M_{\text{Up}}(x,t) \geq \int_0^{t-\frac{x}{v}} (\phi_{max} - \phi_{in}(\tau))\, d\tau - L\left(\rho_{max} + \rho_c\right). \tag{B.7}$$

Further, using Assumption 2.2 we can make another lower bound:

$$\int_0^{t-\frac{x}{v}} (\phi_{max} - \phi_{in}(\tau))\, d\tau \geq \left\lfloor \frac{t - \frac{x}{v}}{T} \right\rfloor \varepsilon,$$

where $\varepsilon > 0$ and $T = \min\left\{\frac{L}{v}, \frac{L}{\omega}\right\}$. This enables us to provide a further lower bound of (B.7):

$$M_{\text{Ini}}(x,t) - M_{\text{Up}}(x,t) \geq \left\lfloor \frac{t - \frac{L}{v}}{T} \right\rfloor \varepsilon - L\left(\rho_{max} + \rho_c\right). \tag{B.8}$$

Finally, we use (B.8) to determine the lowest t, for which the term $M_{\text{Ini}}(x,t) - M_{\text{Up}}(x,t)$ becomes non-negative $\forall x \in [0, L]$:

$$t \geq \frac{L}{v} + \left\lceil \frac{L}{\varepsilon}\left(\rho_{max} + \rho_c\right) \right\rceil \min\left\{\frac{L}{v}, \frac{L}{\omega}\right\}. \tag{B.9}$$

Following the same steps, we obtain that $M_{\text{Ini}}(x,t) - M_{\text{Down}}(x,t) \geq 0$ for all such t that are not smaller than

$$t \geq \frac{L}{\omega} + \left\lceil \frac{L}{\varepsilon}\left(\rho_{max} + \rho_c\right) \right\rceil \min\left\{\frac{L}{v}, \frac{L}{\omega}\right\}. \tag{B.10}$$

The earliest time after which we can neglect the effect of the initial condition on the solution is thus the minimum of (B.9) and (B.10):

$$t_{min} = \min\left\{\frac{L}{v}, \frac{L}{\omega}\right\}\left(1 + \left\lceil \frac{L}{\varepsilon}\left(\rho_{max} + \rho_c\right) \right\rceil\right). \tag{B.11}$$

B.3.2 H-J solution for $t \geq t_{min}$

Thus, we have estimated the minimal time t_{min} (B.11) needed for the initial conditions to leave the system. Thus, in the H-J solution given by (B.5), the term M_{Ini} can be excluded from the minimum operator $\forall t \in [t_{min}, +\infty)$:

$$M(x,t) = \min\left\{ \int_0^{t-\frac{x}{v}} \phi_{in}(\tau)\, d\tau + \int_0^{L} \rho_0(s)\, ds,\ \int_0^{t-\frac{L-x}{\omega}} \phi_{out}(\tau)\, d\tau + \rho_{max}(L-x) \right\},$$

which is the solution of the Hamilton-Jacobi system for all $t \geq t_{min}$. This expression can be used to study the asymptotic behavior of systems governed by H-J PDEs with a triangular FD being their Hamiltonian.

B.4 Necessary conditions for tracking desired state

In accordance with Problem 2.3, we should find $u_{in}(t)$ and $u_{out}(t)$ $\forall t \in \mathbb{R}^+$ such that the equality of $M(x,t)$ and $M_d(x,t)$ up to some constant M_0 is guaranteed $\forall x \in [0, L]$ as $t \to \infty$. For the equality of two minimum functions (2.60) and (2.61), it is sufficient to provide the

equality of their arguments, thus, $\forall\,(x,t) \in [0,L] \times [t_{min}, +\infty)$ we get

$$\begin{aligned} \int_0^{t-\frac{x}{v}} \phi_{in_d}(\tau)\,d\tau + \int_0^{L} \rho_{d_0}(s)\,ds + M_0 &= \int_0^{t-\frac{x}{v}} \phi_{in}(\tau)\,d\tau + \int_0^{L} \rho_0(s)\,ds, \\ \int_0^{t-\frac{L-x}{\omega}} \phi_{out_d}(\tau)\,d\tau + \rho_{max}(L-x) + M_0 &= \int_0^{t-\frac{L-x}{\omega}} \phi_{out}(\tau)\,d\tau + \rho_{max}(L-x). \end{aligned} \tag{B.12}$$

Firstly, by taking the time derivative of (B.12), we see that in the steady-state $\phi_{in}(t) \equiv \phi_{in_d}(t)$ and $\phi_{out}(t) \equiv \phi_{out_d}(t)$.

Secondly, by expressing M_0 from both parts of (B.12), we obtain the necessary condition (2.66) to track ρ_d.

B.5 Solution of a H-J PDE with space-dependent Hamiltonian

Here we consider the initial boundary value problem in Hamilton-Jacobi formulation given by (3.41) for a traffic system evolving on a large urban network. This problem contains an explicit space-dependency in the fundamental diagram that captures the network infrastructure. We find its solution explicitly for the case of space-dependent triangular FD using the variational principle (3.47).

In the following, we will skip writing η in the arguments to make the notations less heavy. Let us here assume that we solve the H-J PDE explicitly for each line of constant η. The Legendre transform (2.30) of the triangular FD is

$$L(\xi, v') = \phi_{max}(\xi) - \rho_c(\xi)v' \quad \forall v' \in [-\omega(\xi), v(\xi)]. \tag{B.13}$$

We need to calculate the viability episolutions $M_{\mathrm{Up}}(\xi,t)$, $M_{\mathrm{Down}}(\xi,t)$ and $M_{\mathrm{Ini}}(\xi,t)$ associated with given value conditions $M_{\mathrm{Up}}(t)$, $M_{\mathrm{Down}}(t)$ and $M_{\mathrm{Ini}}(\xi)$, respectively, using (3.43), (3.44), (3.45) and (3.47). Notice that these viability episolutions are equivalent to "solution candidates" that were discussed in Section 2.1.8. Finally, the unique solution of (3.41) corresponds to the minimum of three functions:

$$M(\xi,t) = \min\left\{M_{\mathrm{Up}}(\xi,t), M_{\mathrm{Down}}(\xi,t), M_{\mathrm{Ini}}(\xi,t)\right\}, \tag{B.14}$$

which is similar to (2.34) but in (ξ,η)-space.

Notice that, in the following, we will consider only solutions for large enough time

$$t \geq \max\left\{\int_{\xi_{min}}^{\xi_{max}} \frac{1}{v(\hat{\xi})} d\hat{\xi}, \int_{\xi_{min}}^{\xi_{max}} \frac{1}{\omega\hat{\xi})} d\hat{\xi}\right\}. \tag{B.15}$$

B.5.1 Upstream boundary condition

The solution candidate $M_{\mathrm{Up}}(\xi,t)$ is related to the cumulative vehicle number originating from the upstream boundary ξ_{min} at initial time.

From the definition of the value condition function (3.42), we get $c(\hat{\xi}(0),t-T)=M_{\mathrm{Up}}(t-T)$ in (3.47). The upstream boundary condition is assigned to the upstream boundary ξ_{min}, which implies the following start and end points of the observer trajectory that starts traveling from the upstream boundary with non-constant speed $v'(\tau)$:

$$\hat{\xi}(0)=\xi_{min},\quad \hat{\xi}(t)=\xi_{min}+\int_0^t v'(\tau)\,d\tau,\quad \text{where}\quad v'(\tau)\in\left[-\omega\left(\hat{\xi}(\tau)\right),v\left(\hat{\xi}(\tau)\right)\right]. \tag{B.16}$$

Using (B.13) and (3.47), we formulate the following problem associated to the solution that originates from this boundary:

$$M_{\mathrm{Up}}(\xi,t)=\inf_{(T,v')\in S_{\mathrm{Up}}}\left(M_{\mathrm{Up}}(t-T)+\int_0^T\phi_{max}\left(\hat{\xi}(\tau)\right)\,d\tau-\int_0^T\rho_c(\hat{\xi}(\tau))v'(\tau)\,d\tau\right),$$

where the infimum is taken over domain S_{Up} that is defined exactly as in (3.48) but with $\left(\hat{\xi}(0),t-T\right)\in\mathrm{Dom}(c_{\mathrm{Up}})$, where $c_{\mathrm{Up}}=M_{\mathrm{Up}}(t)$ as in (3.42).

With the expression for the upstream boundary condition (3.43), the infimum problem can be rewritten as

$$\begin{aligned}M_{\mathrm{Up}}(\xi,t)=\inf_{(T,v')\in S_{\mathrm{Up}}}\Bigg(&\int_0^{t-T}\phi_{in}(\tau)\,d\tau+\int_{\xi_{min}}^{\xi_{max}}\rho_0(\hat{\xi})\,d\hat{\xi}+\\&\int_0^T\phi_{max}\left(\hat{\xi}(\tau)\right)\,d\tau-\int_0^T\rho_c\left(\hat{\xi}(\tau)\right)v'(\tau)\,d\tau\Bigg).\end{aligned} \tag{B.17}$$

Now let us consider in more details the last term $\int_0^T\rho_c\left(\hat{\xi}(\tau)\right)v'(\tau)d\tau$. By definition $d\hat{\xi}=v'(\tau)d\tau$, which allows us to perform the following change of variables:

$$\int_0^T\rho_c\left(\hat{\xi}(\tau)\right)v'(\tau)\,d\tau=\int_{\xi_{min}}^{\xi}\rho_c(\hat{\xi})\,d\hat{\xi}=:R_c(\xi), \tag{B.18}$$

where $R_c(\xi)$ is a new variable that denotes the cumulative critical density. Further, we can decompose the integrals in (B.17) as

$$\int_0^{t-T}\phi_{in}(\tau)d\tau+\int_0^T\phi_{max}(\hat{\xi}(\tau))d\tau=\int_0^t\phi_{in}(\tau)d\tau+\int_0^T\left(\phi_{max}(\hat{\xi}(\tau))-\phi_{in}(t-T+\tau)\right)d\tau. \tag{B.19}$$

Thus, using (B.18) and (B.19) we can rewrite (B.17) as

$$M_{\mathrm{Up}}(\xi,t) = \inf_{(T,v')\in S_{\mathrm{Up}}} \left(\int_0^T \left(\phi_{max}(\hat{\xi}(\tau)) - \phi_{in}(t-T+\tau) \right) d\tau \right) + \int_0^t \phi_{in}(\tau)\, d\tau + \int_{\xi_{min}}^{\xi_{max}} \rho_0(\hat{\xi})\, d\hat{\xi} - R_c(\xi). \tag{B.20}$$

From Assumption 3.1 on the restrictions for inflows and outflows, we have $\phi_{in}(t) \leq \phi_{max}(\xi)\ \forall(\xi,t) \in [\xi_{min},\xi_{max}] \times \mathbb{R}^+$, which means that the first integral in (B.20) is always positive. Hence, the infimum in (B.20) is achieved, when the traveling time T is minimized. This implies that the solution is assigned to a traveler that moves with the maximal speed at each space point, i.e., (B.16) becomes

$$\hat{\xi}(t) = \xi_{min} + \int_0^t v(\hat{\xi}(\tau))\, d\tau, \tag{B.21}$$

where v is the maximal kinematic wave speed. Thus, in the infimum, T is the solution to (B.21) for $t = T$:

$$\frac{\partial \xi}{\partial T} = v(T) \ \Rightarrow\ \frac{\partial T}{\partial \xi} = \frac{1}{v(\xi)} \ \Rightarrow\ T_v(\xi) = \int_{\xi_{min}}^{\xi} \frac{1}{v(\hat{\xi})} d\hat{\xi}. \tag{B.22}$$

With (B.22), the viability solution related to the upstream boundary yields for (B.17)

$$M_{\mathrm{Up}}(\xi,t) = \int_0^{T_v(\xi)} \phi_{max}(\hat{\xi}(\tau))\, d\tau + \int_0^{t-T_v(\xi)} \phi_{in}(\tau)\, d\tau + \int_{\xi_{min}}^{\xi_{max}} \rho_0(\hat{\xi})\, d\hat{\xi} - R_c(\xi). \tag{B.23}$$

We rewrite the first term on the right-hand side of (B.23) as

$$\int_0^{T_v(\xi)} \phi_{max}(\hat{\xi}(\tau))\, d\tau = \int_0^{T_v(\xi)} \rho_c(\hat{\xi}(\tau)) v(\hat{\xi}(\tau))\, d\tau.$$

Using (B.21), we can perform the change of variables in the latter integral as

$$\int_0^{T_v(\xi)} \rho_c(\hat{\xi}(\tau)) v(\hat{\xi}(\tau))\, d\tau = \int_{\xi_{min}}^{\xi} \rho_c(\hat{\xi}(\tau))\, d\hat{\xi} = R_c(\xi).$$

With this result, two $R_c(\xi)$ terms with opposite signs in (B.23) cancel each other, and we obtain the solution associated with the upstream boundary

$$M_{\mathrm{Up}}(\xi,t) = \int_0^{t-T(\xi)} \phi_{in}(\tau)\, d\tau + \int_{\xi_{min}}^{\xi_{max}} \rho_0(\hat{\xi})\, d\hat{\xi}. \tag{B.24}$$

B.5.2 Downstream boundary condition

As the second step, we need to obtain the solution $M_{\text{Down}}(\xi, t)$ that is related to the downstream boundary ξ_{max}. Notice that viable evolutions related to this boundary are characterized by the following start and end points of traveling:

$$\hat{\xi}(0) = \xi_{max}, \quad \hat{\xi}(t) = \xi_{max} + \int_0^t v'(\tau)\, d\tau, \quad \text{where} \quad v'(\tau) \in \left[-\omega\left(\hat{\xi}(\tau)\right), v\left(\hat{\xi}(\tau)\right)\right]. \tag{B.25}$$

As in the previous case, we use the expression for the downstream boundary condition $M_{\text{Down}}(t)$ from (3.44) and the result from (B.19), and write the following infimum problem

$$\begin{aligned} M_{\text{Down}}(\xi, t) = \inf_{(T, v') \in S_{\text{Down}}} \Bigg(& \int_0^T \left(\phi_{max}(\hat{\xi}(\tau)) - \phi_{out}(t - T + \tau)\right) d\tau \\ & - \int_0^T \rho_c(\hat{\xi}(\tau)) v'(\tau)\, d\tau \Bigg) + \int_0^t \phi_{out}(\tau)\, d\tau, \end{aligned} \tag{B.26}$$

where the infimum is now taken over domain S_{Down} defined as in (3.48) with $\left(\hat{\xi}(0), t - T\right) \in \text{Dom}(c_{\text{Down}})$, where $c_{\text{Down}} = M_{\text{Down}}(t)$ as in (2.26).

Again using Assumption 3.1, we obtain that the infimum is achieved for the minimal traveling time interval T, which corresponds to:

$$T_\omega(\xi) = \int_\xi^{\xi_{max}} \frac{1}{\omega(\hat{\xi})} d\hat{\xi} \quad \text{and} \quad v' = -\omega. \tag{B.27}$$

We use (B.27) and $\phi_{max} = \rho_c v$ to solve the infimum problem (B.26), which yields:

$$M_{\text{Down}}(\xi, t) = \int_0^{t - T_\omega(\xi)} \phi_{out}(\tau)\, d\tau + \int_0^{T_\omega(\xi)} \rho_c(\hat{\xi}(\tau)) v(\hat{\xi}(\tau))\, d\tau + \int_0^{T_\omega(\xi)} \rho_c(\hat{\xi}(\tau)) \omega(\hat{\xi}(\tau))\, d\tau. \tag{B.28}$$

From definition of the critical density for triangular FD (2.3) we get

$$\rho_c = \frac{\rho_{max}\omega}{v + \omega} \Rightarrow \rho_{max}\omega = \rho_c(v + \omega),$$

which is then inserted into (B.28):

$$M_{\text{Down}}(\xi, t) = \int_0^{t - T_\omega(\xi)} \phi_{out}(\tau)\, d\tau + \int_0^{T_\omega(\xi)} \rho_{max}(\hat{\xi}(\tau)) \omega(\hat{\xi}(\tau))\, d\tau.$$

Finally, we perform the change of variables

$$\int_0^{T_\omega(\xi)} \rho_{max}(\hat{\xi}(\tau)) \omega(\hat{\xi}(\tau))\, d\tau = \int_\xi^{\xi_{max}} \rho_{max}(\hat{\xi})\, d\hat{\xi},$$

and thus obtain the solution associated with the downstream boundary:

$$M_{\text{Down}}(\xi,t) = \int_0^{t-T_\omega(\xi)} \phi_{out}(\tau)d\tau + \int_\xi^{\xi_{max}} \rho_{max}(\hat{\xi})\, d\hat{\xi}. \tag{B.29}$$

B.5.3 Initial condition

As the third step, we need to calculate $M_{\text{Ini}}(\xi,t)$ that is related to the vehicle with known label at initial time that follows the path of viable evolution (see (2.29)).

We can already establish that $T = t$, since the viability evolution starts its path at initial time. Thus, using the variational principle (3.47) with initial condition given by (3.45), we can state the infimum problem as

$$M_{\text{Ini}}(\xi,t) = \inf_{v'\in S_{\text{Ini}}} \left(\int_{\hat{\xi}_0}^{\xi_{max}} \rho_0(\hat{\xi})\, d\hat{\xi} + \int_0^t \phi_{max}(\hat{\xi}(\tau))\, d\hat{\xi} - \int_0^t \rho_c(\hat{\xi}(\tau))v'(\tau)\, d\tau \right), \tag{B.30}$$

where domain S_{Ini} is defined as in (3.48) for $T = t$:

$$\begin{aligned} S_{\text{Ini}} = \Big\{ v' \;\Big|\; & v'(\cdot) \in L^1(0,t),\;\; \dot{\hat{\xi}}(\tau) = v'(\tau), \\ & \hat{\xi}(t) = \xi,\;\; v'(\tau) \in \left[-\omega\left(\hat{\xi}(\tau)\right), v\left(\hat{\xi}(\tau)\right) \right], \\ & \hat{\xi}(0) \in [\xi_{min}, \xi_{max}] \Big\}. \end{aligned} \tag{B.31}$$

In the first term of the right-hand side of (B.30), the integral runs from $\hat{\xi}_0$ used to define the coordinate from which the viable evolution starts its path at initial time:

$$\hat{\xi}(0) = \hat{\xi}_0, \quad \hat{\xi}(t) = \hat{\xi}_0 + \int_0^t v'(\tau)\, d\tau, \quad \text{where} \quad v'(\tau) \in \left[-\omega\left(\hat{\xi}(\tau)\right), v\left(\hat{\xi}(\tau)\right) \right]. \tag{B.32}$$

Again we use the change of variables such that $v'(\tau)d\tau = d\hat{\xi}$ and rewrite (B.30) as

$$M_{\text{Ini}}(\xi,t) = \inf_{v'\in S_{\text{Ini}}} \left(\int_{\hat{\xi}_0}^{\xi_{max}} \rho_0(\hat{\xi})\, d\hat{\xi} - \int_{\hat{\xi}_0}^{\xi} \rho_c(\hat{\xi})\, d\hat{\xi} + \int_0^t \phi_{max}(\hat{\xi}(\tau))\, d\hat{\xi} \right). \tag{B.33}$$

We can not further simplify (B.33), unless some specific information about the initial conditions is known. However, we can estimate the lower bound of (B.33) term by term:

$$M_{\text{Ini}}(\xi,t) \geq 0 - \int_{\xi_{min}}^{\xi_{max}} \rho_c(\hat{\xi})\, d\hat{\xi} + \int_0^t \phi_{max}^{min}\, d\tau, \tag{B.34}$$

where ϕ_{max}^{min} is the capacity at the strongest bottleneck along the η-line defined in (3.51).

As already mentioned above, the unique solution (B.14) is the minimum of three functions. In the following section, we will show that starting from some time t_{min}, the initial conditions will have left the system and thus can be excluded from the minimum operator.

B.5.4 Time when initial conditions leave the system

Here we aim to estimate the minimal time $t_{min}(\eta)$ such that $\forall(\xi,\eta,t) \in \bar{\Omega} \times [t_{min}(\eta), +\infty)$: $M_{\text{Ini}}(\xi,\eta,t) \geq M_{\text{Up}}(\xi,\eta,t)$ or $M_{\text{Ini}}(\xi,\eta,t) \geq M_{\text{Down}}(\xi,\eta,t)$. This was already done for the 1D case in Appendix B.3.1. However, now this minimal time is different for each η-line. Therefore, we will again write the dependence on η in the notations to gain more clarity.

First of all, we will estimate the time after which $M_{\text{Ini}}(\xi,\eta,t) \geq M_{\text{Up}}(\xi,\eta,t)$, then we do the same for $M_{\text{Ini}}(\xi,\eta,t) \geq M_{\text{Down}}(\xi,\eta,t)$. Finally, $t_{min}(\eta)$ is found as the smallest value of these two results.

We combine the result for $M_{\text{Up}}(\xi,\eta,t)$ (B.24) with the lower bound for $M_{\text{Ini}}(\xi,\eta,t)$ (B.34), and write

$$\begin{aligned} M_{\text{Ini}}(\xi,\eta,t) - M_{\text{Up}}(\xi,\eta,t) \geq &- \int_{\xi_{min}(\eta)}^{\xi_{max}(\eta)} \rho_c(\hat{\xi},\eta)\, d\hat{\xi} - \int_{\xi_{min}(\eta)}^{\xi_{max}(\eta)} \rho_0(\hat{\xi},\eta)\, d\hat{\xi} \\ &+ \int_0^{t-T_v(\xi,\eta)} \left(\phi_{max}^{min}(\eta) - \phi_{in}(\eta,\tau)\right)\, d\tau + \int_0^{T_v(\xi,\eta)} \phi_{max}^{min}(\eta)\, d\tau. \end{aligned} \tag{B.35}$$

Now let us estimate the lower bounds for the terms from (B.35) as

$$\int_0^{T_v(\xi,\eta)} \phi_{max}^{min}(\eta)\, d\tau \geq 0 \quad \text{and} \quad - \int_{\xi_{min}(\eta)}^{\xi_{max}(\eta)} \rho_0(\hat{\xi},\eta)\, d\hat{\xi} \geq - \int_{\xi_{min}(\eta)}^{\xi_{max}(\eta)} \rho_{max}(\hat{\xi},\eta)\, d\hat{\xi}.$$

which yields

$$\begin{aligned} M_{\text{Ini}}(\xi,\eta,t) - M_{\text{Up}}(\xi,\eta,t) \geq &- \int_{\xi_{min}(\eta)}^{\xi_{max}(\eta)} \left(\rho_{max}(\hat{\xi},\eta) + \rho_c(\hat{\xi},\eta)\right)\, d\hat{\xi} \\ &+ \int_0^{t-T_v(\xi,\eta)} \left(\phi_{max}^{min}(\eta) - \phi_{in}(\eta,\tau)\right)\, d\tau. \end{aligned} \tag{B.36}$$

Using Assumption 3.1, we are able to estimate the following lower bound for the second term on the right-hand side of (B.36):

$$\int_0^{t-T_v(\xi,\eta)} \left(\phi_{max}^{min}(\eta) - \phi_{in}(\eta,\tau)\right)\, d\tau \geq \left\lfloor \frac{t - T_v(\xi,\eta)}{t_{ctr}(\eta)} \right\rfloor \epsilon,$$

with $\epsilon > 0$, and $t_{ctr}(\eta)$ is the minimal controllability time defined in (3.74), which can be used to rewrite (B.36) as

$$M_{\mathrm{Ini}}(\xi,\eta,t) - M_{\mathrm{Up}}(\xi,\eta,t) \geq \left\lfloor \frac{t - T_v(\xi_{max}(\eta))}{t_{ctr}(\eta)} \right\rfloor \epsilon - \int\limits_{\xi_{min}(\eta)}^{\xi_{max}(\eta)} \Big(\rho_{max}(\hat{\xi},\eta) + \rho_c(\hat{\xi},\eta)\Big)\, d\hat{\xi}. \quad \text{(B.37)}$$

Now we can determine the minimal time, after which the right-hand side of (B.37) is non-negative:

$$t(\eta) \geq \int\limits_{\xi_{min}(\eta)}^{\xi_{max}(\eta)} \frac{1}{v(\hat{\xi},\eta)} d\hat{\xi} + \left\lceil \frac{1}{\epsilon} \int\limits_{\xi_{min}(\eta)}^{\xi_{max}(\eta)} \Big(\rho_{max}(\hat{\xi},\eta) + \rho_c(\hat{\xi},\eta)\Big)\, d\hat{\xi} \right\rceil t_{ctr}(\eta). \quad \text{(B.38)}$$

Afterwards, the same steps are performed to obtain the minimal time, after which $M_{\mathrm{Ini}}(\xi,\eta,t) - M_{\mathrm{Down}}(\xi,\eta,t) \geq 0$ holds:

$$t(\eta) \geq \int\limits_{\xi_{min}(\eta)}^{\xi_{max}(\eta)} \frac{1}{\omega(\hat{\xi},\eta)} d\hat{\xi} + \left\lceil \frac{1}{\epsilon} \int\limits_{\xi_{min}(\eta)}^{\xi_{max}(\eta)} \Big(\rho_{max}(\hat{\xi},\eta) + \rho_c(\hat{\xi},\eta)\Big)\, d\hat{\xi} \right\rceil t_{ctr}(\eta). \quad \text{(B.39)}$$

Then, $t_{min}(\eta)$ is the minimum between (B.38) and (B.39) $\forall \eta \in [\eta_{min}, \eta_{max}]$:

$$t_{min}(\eta) = t_{ctr}(\eta) \left(1 + \left\lceil \frac{1}{\epsilon} \int\limits_{\xi_{min}(\eta)}^{\xi_{max}(\eta)} \Big(\rho_{max}(\hat{\xi},\eta) + \rho_c(\hat{\xi},\eta)\Big)\, d\hat{\xi} \right\rceil \right). \quad \text{(B.40)}$$

Finally, we define the time when initial conditions will leave the system as a whole as t_{min}, which is not dependent on η. Therefore, it should be computed as the maximum possible value of all $t_{min}(\eta)$ for particular η:

$$t_{min} = \max_{\eta \in [\eta_{min}, \eta_{max}]} t_{min}(\eta). \quad \text{(B.41)}$$

B.5.5 Unique solution

The final solution $M(\xi,\eta,t)$ of the H-J system (3.41) can finally be found as a minimum of solutions associated with the upstream (B.24) and downstream (B.29) boundary conditions $\forall t \in [t_{min}, +\infty)$, thus, the effect of initial conditions is negligible:

$$M(\xi,\eta,t) = \min \left\{ \int\limits_{0}^{t - T_v(\xi,\eta)} \phi_{in}(\eta,\tau)\, d\tau + \int\limits_{\xi_{min}(\eta)}^{\xi_{max}(\eta)} \rho_0(\hat{\xi},\eta)\, d\hat{\xi}, \right.$$
$$\left. \int\limits_{0}^{t - T_\omega(\xi,\eta)} \phi_{out}(\eta,\tau) d\tau + \int\limits_{\xi}^{\xi_{max}(\eta)} \rho_{max}(\hat{\xi},\eta)\, d\hat{\xi} \right\}.$$

B.6 Differences in the proofs of Theorems 2.3 and 3.2

Due to the space-dependency in the fundamental diagram in 2D system (3.34), the proof of Theorem 3.2 will be different from the proof of Theorem 2.3. In particular, it must be modified by taking the following differences into account:

1. Space intervals for a 1D road of length L vary as a function of line number η, i.e., $[0, L] \to [\xi_{min}(\eta), \xi_{max}(\eta)]$. This implies that $\frac{L}{v} \to T_v(\xi_{max}(\eta), \eta)$ and $\frac{L}{\omega} \to T_\omega(\xi_{min}(\eta), \eta)$, where $T_v(\xi_{max}(\eta), \eta)$ and $T_\omega(\xi_{min}(\eta), \eta)$ should be taken from (3.76) for $\xi = \xi_{max}(\eta)$ and $\xi = \xi_{min}(\eta)$, respectively.

2. Every occurrence of $L\rho_{max}$ should be substituted by the integral $\int_{\xi_{min}(\eta)}^{\xi_{max}(\eta)} \rho_{max}(\hat{\xi}, \eta)\, d\hat{\xi}$.

3. Equation (2.77) in the proof of Theorem 2.3 should be rewritten as:

$$\begin{aligned} g_{in}(\eta, t) = 0 \quad &\Rightarrow \quad R(\eta, t') \geq \int_{\xi_{min}(\eta)}^{\xi_{max}(\eta)} \rho_c(\hat{\xi}, \eta)\, d\hat{\xi}, \quad \forall t' \in [t - T_\omega(\xi_{min}(\eta), \eta), t]\,, \\ g_{out}(\eta, t) = 0 \quad &\Rightarrow \quad R(\eta, t') \leq \int_{\xi_{min}(\eta)}^{\xi_{max}(\eta)} \rho_c(\hat{\xi}, \eta)\, d\hat{\xi}, \quad \forall t' \in [t - T_v(\xi_{max}(\eta), \eta), t]\,. \end{aligned} \tag{B.42}$$

   We obtain (B.42) by using the following upper bound:

$$\begin{aligned} \int_{t - T_\omega(\xi_{min}(\eta), \eta)}^{t'} \phi_{out}(\eta, \tau)\, d\tau + \int_{t'}^{t} \phi_{in}(\eta, \tau) d\tau &\leq T_\omega(\xi_{min}(\eta), \eta)\, \phi_{max}^{min}(\eta) \\ &\leq \int_{\xi_{min}(\eta)}^{\xi_{max}(\eta)} \frac{\phi_{max}(\hat{\xi}, \eta)}{\omega(\hat{\xi}, \eta)}\, d\hat{\xi} = \int_{\xi_{min}(\eta)}^{\xi_{max}(\eta)} \Big(\rho_{max}(\hat{\xi}, \eta) - \rho_c(\hat{\xi}, \eta)\Big)\, d\hat{\xi}. \end{aligned}$$

B.7 Proof that $\bar{\phi}_N = \min\{\bar{D}_N, \bar{S}_N\}$

Here we prove that the flow in some direction (here North) can be written as a function of demand and supply of the same direction:

$$\bar{\phi}_N = \min\{\bar{D}_N, \bar{S}_N\},$$

which allows to simplify the model (4.21). Thus, here we seek to prove that equation (4.23) holds. The main assumption that needs to be made thereby is that the urban network is well-designed in terms of maximal flows, see (4.24).

Let us consider the term $(1-\gamma)\bar{\phi}_{EN} + \gamma\bar{\phi}_{NE}$ from (4.22). Using the definition of partial flows (4.12), we can write

$$\bar{\phi}_{EN} = \min\{\bar{\alpha}_{EN}\bar{D}_E, \bar{\beta}_{EN}\bar{S}_N\}, \qquad \bar{\phi}_{NE} = \min\{\bar{\alpha}_{NE}\bar{D}_N, \bar{\beta}_{NE}\bar{S}_E\}.$$

Recall that by definition of the demand-supply formulation, if $\bar{D}_E < \bar{\phi}_{max,E}$, then $\bar{S}_E = \bar{\phi}_{max,E}$ and vice versa, see Figure 2.3. The same holds for $\bar{D}_N$ and $\bar{S}_N$. To simplify the notations, let us denote $Q(\gamma) = (1-\gamma)\bar{\phi}_{EN} + \gamma\bar{\phi}_{NE}$. We will prove that there always exists γ such that $Q(\gamma) = \min\{\bar{\alpha}_{NE}\bar{D}_N, \bar{\beta}_{EN}\bar{S}_N\}$. In total, there are six different cases to consider for partial flows $\bar{\phi}_{EN}$ and $\bar{\phi}_{NE}$:

1. $\bar{\alpha}_{EN}\bar{D}_E < \bar{\beta}_{EN}\bar{S}_N$ and $\bar{\alpha}_{NE}\bar{D}_N > \bar{\beta}_{NE}\bar{S}_E$. From the first inequality we obtain

   $$\bar{\alpha}_{EN}\bar{D}_E < \bar{\beta}_{EN}\bar{S}_N \leq \bar{\beta}_{EN}\bar{\phi}_{max,N} = \bar{\alpha}_{EN}\bar{\phi}_{max,E},$$

   where the last equality comes for the assumption that the network is well-designed (4.24). Thus, we get that

   $$\bar{D}_E < \bar{\phi}_{max,E}.$$

   From the other side, if we consider the second inequality, we get

   $$\bar{\beta}_{NE}\bar{S}_E < \bar{\alpha}_{NE}\bar{D}_N \leq \bar{\alpha}_{NE}\bar{\phi}_{max,E} \Rightarrow \bar{S}_E < \bar{\phi}_{max,E}.$$

   According to the demand-supply formulation, it is however not possible that $\bar{D}_E < \bar{\phi}_{max,E}$ and $\bar{S}_E < \bar{\phi}_{max,E}$ hold at the same time. Thus, this case can be excluded from consideration.

2. $\bar{\alpha}_{EN}\bar{D}_E > \bar{\beta}_{EN}\bar{S}_N$ and $\bar{\alpha}_{NE}\bar{D}_N < \bar{\beta}_{NE}\bar{S}_E$. This case is also impossible, since from the first inequality we get $\bar{S}_N < \bar{\phi}_{max,N}$ and from the second inequality we get $\bar{D}_N < \bar{\phi}_{max,N}$, which violates the demand-supply formulation.

3. $\bar{\alpha}_{NE}\bar{D}_N \leq \bar{\beta}_{NE}\bar{S}_E$ and $\bar{\alpha}_{NE}\bar{D}_N \leq \bar{\beta}_{EN}\bar{S}_N$. In this case taking $\gamma = 1$ results into

   $$Q(1) = \bar{\phi}_{NE} = \min\{\bar{\alpha}_{NE}\bar{D}_N, \bar{\beta}_{NE}\bar{S}_E\} = \bar{\alpha}_{NE}\bar{D}_N,$$

   which in combination with the second inequality yields

   $$Q(1) = \min\{\bar{\alpha}_{NE}\bar{D}_N, \bar{\beta}_{EN}\bar{S}_N\},$$

   which is the desired property achieved with $\gamma = 1$ (demand and supply refer to the same direction).

4. $\bar{\alpha}_{EN}\bar{D}_E \leq \bar{\beta}_{EN}\bar{S}_N$, $\bar{\alpha}_{NE}\bar{D}_N \leq \bar{\beta}_{NE}\bar{S}_E$ and $\bar{\alpha}_{NE}\bar{D}_N > \bar{\beta}_{EN}\bar{S}_N$.

   From the first inequality for $\gamma = 0$ we obtain

   $$Q(0) = \bar{\phi}_{EN} = \min\{\bar{\alpha}_{EN}\bar{D}_E, \bar{\beta}_{EN}\bar{S}_N\} = \bar{\alpha}_{EN}\bar{D}_E \leq \bar{\beta}_{EN}\bar{S}_N.$$

From the second inequality for $\gamma = 1$ we obtain

$$Q(1) = \bar{\phi}_{NE} = \min\{\bar{\alpha}_{NE}\bar{D}_N, \bar{\beta}_{NE}\bar{S}_E\} = \bar{\alpha}_{NE}\bar{D}_N,$$

and from the third inequality we get

$$Q(1) > \bar{\beta}_{EN}\bar{S}_N.$$

Combining these results all together, we show the desired property:

$$\begin{cases} Q(0) \le \bar{\beta}_{EN}\bar{S}_N, \\ Q(1) > \bar{\beta}_{EN}\bar{S}_N, \end{cases} \Rightarrow \exists\gamma \in [0,1) : \; Q(\gamma) = \bar{\beta}_{EN}\bar{S}_N = \min\{\bar{\alpha}_{NE}\bar{D}_N, \bar{\beta}_{EN}\bar{S}_N\}.$$

5. $\bar{\alpha}_{EN}\bar{D}_E \le \bar{\beta}_{EN}\bar{S}_N$, $\bar{\alpha}_{NE}\bar{D}_N \le \bar{\beta}_{NE}\bar{S}_E$ and $\bar{\alpha}_{NE}\bar{D}_N \le \bar{\beta}_{EN}\bar{S}_N$. The analysis here is the same as in case (3): we take $\gamma = 1$, which results into $Q(1) = \min\{\bar{\alpha}_{NE}\bar{D}_N, \bar{\beta}_{NE}\bar{S}_N\}$.

6. $\bar{\alpha}_{EN}\bar{D}_E \ge \bar{\beta}_{EN}\bar{S}_N$, $\bar{\alpha}_{NE}\bar{D}_N \ge \bar{\beta}_{NE}\bar{S}_E$ and $\bar{\alpha}_{NE}\bar{D}_N > \bar{\beta}_{EN}\bar{S}_N$. Here we should proceed as we did in case (4): taking $\gamma = 0$ results into $Q(0) = \bar{\beta}_{EN}\bar{S}_N$. Further, by the second condition we obtain $Q(1) \le \bar{\alpha}_{NE}\bar{D}_N$. Therefore, there exists $\gamma \in [0,1]$ such that $Q(\gamma) = \min\{\bar{\alpha}_{NE}\bar{D}_N, \bar{\beta}_{EN}\bar{S}_N\}$.

Hence, if we assume that γ can be manipulated independently for every pairwise flow, we can summarize the discussion above in the formula: $(1-\gamma)\bar{\phi}_{EN} + \gamma\bar{\phi}_{NE} = \min\{\bar{\alpha}_{NE}\bar{D}_N, \bar{\beta}_{EN}\bar{S}_N\}$. This leads to the following transformation of (4.22):

$$\begin{aligned}\bar{\phi}_N = \bar{\phi}_{NN} &+ \min\{\bar{\alpha}_{NS}\bar{D}_N, \bar{\beta}_{SN}\bar{S}_N\} + \\ &+ \min\{\bar{\alpha}_{NW}\bar{D}_N, \bar{\beta}_{WN}\bar{S}_N\} + \min\{\bar{\alpha}_{NE}\bar{D}_N, \bar{\beta}_{EN}\bar{S}_N\}.\end{aligned}$$

Finally, using the approximation by replacing the sum of minima with the minimum of sums, we can write

$$\begin{aligned}\bar{\phi}_N = \min\{&\bar{\alpha}_{NN}\bar{D}_N + \bar{\alpha}_{NS}\bar{D}_N + \bar{\alpha}_{NW}\bar{D}_N + \bar{\alpha}_{NE}\bar{D}_N, \\ &\bar{\beta}_{NN}\bar{S}_N + \bar{\beta}_{SN}\bar{S}_N + \bar{\beta}_{WN}\bar{S}_N + \bar{\beta}_{EN}\bar{S}_N\} = \min\{\bar{D}_N, \bar{S}_N\},\end{aligned}$$

which is exactly the property we wanted to prove (4.23).

B.8 Eigenvalues of matrix $B - I$

Let us now analyze eigenvalues of matrix $B - I$, where B is the SR matrix from (4.40). To simplify the notations, we introduce $\bar{B} = B - I$ that reads

$$\bar{B} = \begin{bmatrix} \beta_{NN} - 1 & \beta_{NE} & \beta_{NW} & \beta_{NS} \\ \beta_{EN} & \beta_{EE} - 1 & \beta_{EW} & \beta_{ES} \\ \beta_{WN} & \beta_{WE} & \beta_{WW} - 1 & \beta_{WS} \\ \beta_{SN} & \beta_{SE} & \beta_{SW} & \beta_{SS} - 1 \end{bmatrix}. \tag{B.43}$$

By Gershgorin circle theorem, every eigenvalue of $\bar{B}$ lies within at least one of the Gershgorin discs $d(\bar{b}_{ii}, R_i)$, where d is a closed disc centered at $\bar{b}_{ii}$ with radius $R_i = \sum_{j \neq i} |\bar{b}_{ji}|$.

Consider the first row of matrix $\bar{B}$ given by (B.43). The Gershgorin disc is centred at $\beta_{NN} - 1$, and its radius is $R_1 = \beta_{NE} + \beta_{NW} + \beta_{NS} = 1 - \beta_{NN}$. The remaining rows of matrix $\bar{B}$ can be analyzed in exactly the same way. Due to the Gershgorin theorem, in general, every result looks similar to

$$|\lambda - (\beta_{NN} - 1)| \leq (1 - \beta_{NN}),$$

which implies that $\mathrm{Re}\lambda(\bar{B}) \leq 0 \ \forall \lambda(\bar{B})$ and if $\mathrm{Re}\lambda(\bar{B}) = 0$, then $\lambda(\bar{B}) = 0$.

Let us consider $\lambda(\bar{B}) = 0$ with x being the corresponding eigenvector:

$$x^T \bar{B} = 0 = x^T \lambda(\bar{B}).$$

Using the definition of matrix $\bar{B}$, we further get

$$x^T (B - \mathbb{I}) = 0 \Rightarrow x^T B = x^T.$$

Thus, it follows that x is also the eigenvector of matrix B associated with the eigenvalue $\lambda(B) = 1$.

Note that matrix B is a positive matrix, i.e., $\beta_{ij} > 0$ for $1 \leq i, j \leq 4$ (assume we have no zero turning ratios). Then, by Perron-Frobenius theorem, $\lambda(B) = 1$ is a Perron root (since all columns of B sum to 1), and thus it is a simple root. It follows that all the eigenvalues of matrix $\bar{B} = B - \mathbb{I}$ are strictly negative and only one eigenvalue is zero.

Bibliography

[1] Ole Morten Aamo. "Disturbance rejection in 2×2 linear hyperbolic systems." In: *IEEE Transactions on Automatic Control* 58.5 (2013), pp. 1095–1106 (cit. on p. 26).

[2] Mohamed Abdel-Aty, Jeremy Dilmore, and Albinder Dhindsa. "Evaluation of variable speed limits for real-time freeway safety improvement." In: *Accident Analysis and Prevention* 38.2 (2006), pp. 335–345 (cit. on p. 4).

[3] K. Aboudolas and N. Geroliminis. "Perimeter and boundary flow control in multi-reservoir heterogeneous networks." In: *Transportation Research Part B: Methodological* 55 (2013), pp. 265–281 (cit. on pp. 6, 71, 74).

[4] R. Aghamohammadi and J. A. Laval. "A Continuum Model for Cities Based on the Macroscopic Fundamental Diagram: a Semi-Lagrangian Solution Method." In: *Transportation Research Procedia* 38 (2019), pp. 380–400 (cit. on p. 6).

[5] R. Aghamohammadi and J. A. Laval. "Dynamic traffic assignment using the macroscopic fundamental diagram: A Review of vehicular and pedestrian flow models." In: *Transportation Research Part B: Methodological* 137 (2020), pp. 99–118 (cit. on pp. 5, 6).

[6] Henrik Anfinsen and Ole Morten Aamo. "Disturbance rejection in the interior domain of linear 2×2 hyperbolic systems." In: *IEEE Transactions on Automatic Control* 60.1 (2015), pp. 186–191 (cit. on p. 26).

[7] Henrik Anfinsen and Ole Morten Aamo. "Model Reference Adaptive Control of 2×2 Coupled Linear Hyperbolic PDEs." In: *IEEE Transactions on Automatic Control* 63.8 (2018), pp. 2405–2420 (cit. on p. 26).

[8] Rainer Ansorge. "What does the entropy condition mean in traffic flow theory?" In: *Transportation Research Part B* 24.2 (1990), pp. 133–143 (cit. on pp. 2, 16).

[9] George B. Arfken and Hans J. Weber. *Mathematical Methods for Physicists*. Vol. 67. Forth Edition. Americal Journal of Physics, 1999 (cit. on p. 78).

[10] J.-P. Aubin, A. Bayen, and P. Saint-Pierre. "Dirichlet problems for some Hamilton-Jacobi equations with inequality constraints." In: *SIAM J. Control Optim.* 47.5 (2008), pp. 2348 –2380 (cit. on p. 25).

[11] J.-P. Aubin, A. Bayen, and P. Saint-Pierre. *Viability Theory: New Directions*. Springer, Paris, 2011 (cit. on pp. 21, 22, 98).

[12] A. Aw and M. Rascle. "Resurrection of "second order models" of traffic flow?" In: *SIAM J. Appl. Math.* 60.3 (2000), pp. 916 –938 (cit. on p. 2).

[13] C. Bardos, A. Y. Leroux, and J. C. Nedelec. "First order quasilinear equations with boundary conditions." In: *Communications in Partial Differential Equations* 4.9 (1979), pp. 1017–1034. eprint: https://doi.org/10.1080/03605307908820117 (cit. on p. 17).

[14] G. Bastin et al. "Exponential boundary feedback stabilization of a shock steady state for the inviscid Burgers equation." In: *Math. Mod. Meth. Appl. Sci.* 29.2 (2019), pp. 271 –316 (cit. on pp. 4, 41).

[15] Alexandre M. Bayen, Robin L. Raffard, and Claire J. Tomlin. "Network Congestion Alleviation Using Adjoint Hybrid Control: Application to Highways." In: *Hybrid Systems: Computation and Control*. Ed. by Rajeev Alur and George J. Pappas. Berlin, Heidelberg: Springer Berlin Heidelberg, 2004, pp. 95–110 (cit. on p. 4).

[16] Nikolaos Bekiaris-Liberis and Rafael Vazquez. "Nonlinear bilateral output-feedback control for a class of viscous Hamilton–Jacobi PDEs." In: *Automatica* 101 (2019), pp. 223–231 (cit. on p. 41).

[17] Richard Bellman and George Adomian. "Dynamic Programming and Partial Differential Equations." In: *Partial Differential Equations: New Methods for Their Treatment and Solution*. Dordrecht: Springer Netherlands, 1985, pp. 28–35 (cit. on p. 25).

[18] S. Benzoni-Gavage and R. M. Colombo. "An n-populations model for traffic flow." In: *Eur. J. Appl. Math.* 14.5 (2003), pp. 587 –612 (cit. on p. 2).

[19] Sébastien Blandin, Xavier Litrico, and Alexandre Bayen. "Boundary stabilization of the inviscid Burgers equation using a Lyapunov method." In: *49th IEEE Conference on Decision and Control (CDC)*. 2010, pp. 1705–1712 (cit. on p. 4).

[20] Sébastien Blandin et al. "Regularity and Lyapunov Stabilization of Weak Entropy Solutions to Scalar Conservation Laws." In: *IEEE Transactions on Automatic Control* 62.4 (2017), pp. 1620–1635 (cit. on pp. 4, 26, 41).

[21] A. Bressan. *Hyperbolic systems of conservation laws*. Vol. 20. Graduate Studies in Mathematics. Oxford Lecture Series in Mathematics and its Applications, 2000 (cit. on p. 2).

[22] Raimund Bürger et al. "Difference schemes, entropy solutions, and speedup impulse for an inhomogeneous kinematic traffic flow model." In: *Networks & Heterogeneous Media* 3.1 (2008), pp. 1–41 (cit. on pp. 80, 81).

[23] Rodrigo Castelan Carlson, Ioannis Papamichail, and Markos Papageorgiou. "Local Feedback-Based Mainstream Traffic Flow Control on Motorways Using Variable Speed Limits." In: *IEEE Transactions on Intelligent Transportation Systems* 12.4 (2011), pp. 1261–1276 (cit. on p. 4).

[24] Rodrigo Castelan Carlson et al. "Optimal Motorway Traffic Flow Control Involving Variable Speed Limits and Ramp Metering." In: *Transportation Science* 44.2 (2010), pp. 238–253 (cit. on p. 106).

[25] Jose M. del Castillo. "Three new models for the flow–density relationship: derivation and testing for freeway and urban data." In: *Transportmetrica* 8.6 (2012), pp. 443–465. eprint: https://doi.org/10.1080/18128602.2011.556680 (cit. on p. 15).

[26] Yacine Chitour and Benedetto Piccoli. "Traffic circles and timing of traffic lights for cars flow." In: *Discrete and Continuous Dynamical Systems - B* 5.3 (2005), pp. 599–630 (cit. on p. 5).

[27] Christian G. Claudel and Alexandre M. Bayen. "Lax–Hopf Based Incorporation of Internal Boundary Conditions Into Hamilton-Jacobi Equation. Part II: Computational Methods." In: *IEEE Transactions on Automatic Control* 55.5 (2010), pp. 1158–1174 (cit. on p. 3).

[28] Christian G. Claudel and Alexandre M. Bayen. "Lax–Hopf Based Incorporation of Internal Boundary Conditions Into Hamilton–Jacobi Equation. Part I: Theory." In: *IEEE Transactions on Automatic Control* 55.5 (2010), pp. 1142–1157 (cit. on pp. 3, 23).

[29] G. M. Coclite, M. Garavello, and B. Piccoli. "Traffic Flow on a Road Network." In: *SIAM J. Math. Anal.* 36.6 (2005), pp. 1862–1886 (cit. on p. 5).

[30] R. M. Colombo. "Wave Front Tracking in Systems of Conservation Laws." In: *Applications of Mathememathics* 49.6 (2004), pp. 501–537 (cit. on p. 3).

[31] J. M. Coron et al. "Local exponential H_2 stabilization of a 2×2 quasilinear hyperbolic system using backstepping." In: *SIAM J. Control Optim.* 51.3 (2013), pp. 2005–2035 (cit. on p. 4).

[32] Jean-Michel Coron, Brigitte d'Andrea Novel, and Georges Bastin. "A Strict Lyapunov Function for Boundary Control of Hyperbolic Systems of Conservation Laws." In: *IEEE Transactions on Automatic Control* 52.1 (2007), pp. 2–11 (cit. on p. 4).

[33] R. Courant, K. Friedrichs, and H. Lewy. "On the Partial Difference Equations of Mathematical Physics." In: *IBM Journal of Research and Development* 11.2 (1967), pp. 215–234 (cit. on pp. 19, 82).

[34] R. Courant, E. Isaacson, and M. Rees. "On the Solution of Nonlinear Hyperbolic Differential Equations by Finite Differences." In: *Communications on Pure and Applied Math.* 5 (1952), pp. 243–255 (cit. on pp. 145, 161).

[35] Carlos F. Daganzo. "A behavioral theory of multi-lane traffic flow. Part I: Long homogeneous freeway sections." In: *Transportation Research Part B: Methodological* 36.2 (2002), pp. 131–158 (cit. on p. 2).

[36] Carlos F. Daganzo. "A variational formulation of kinematic waves: basic theory and complex boundary conditions." In: *Transportation Research Part B: Methodological* 39.2 (2005), pp. 187–196 (cit. on pp. 3, 23).

[37] Carlos F. Daganzo. "On the variational theory of traffic flow: Well-posedness, duality and applications." In: *Netw. Heter. Med.* 1 (2006), pp. 601–619 (cit. on pp. 3, 24).

[38] Carlos F. Daganzo. "The cell transmission model: A dynamic representation of highway traffic consistent with the hydrodynamic theory." In: *Transportation Research Part B: Methodological* 28.4 (1994), pp. 269–287 (cit. on pp. 1, 3, 14, 122).

[39] Carlos F. Daganzo. "The cell transmission model, part ii: network traffic." In: *Transportation Research Part B: Methodological* 29.2 (1995), pp. 79–93 (cit. on pp. 3, 5, 123, 124).

[40] Carlos F. Daganzo and Nikolas Geroliminis. "An analytical approximation for the macroscopic fundamental diagram of urban traffic." In: *Transportation Research Part B: Methodological* 42 (2008), pp. 771–781 (cit. on pp. 5, 63).

[41] Carlos F. Daganzo, Wei-Hua Lin, and J. M. Del Castillo. "A simple physical principle for the simulation of freeways with special lanes and priority vehicles." In: *Transportation Research Part B: Methodological* 31.2 (1997), pp. 103–125 (cit. on p. 2).

[42] Antonino D'Andrea et al. "A functional road classification with data mining techniques." In: *Transport* 29.4 (2014), pp. 419–430. eprint: https://doi.org/10.3846/16484142.2014.984329 (cit. on p. 138).

[43] Carlotta Donadello and Vincent Perrollaz. "Exact controllability to trajectories for entropy solutions to scalar conservation laws in several space dimensions." In: *Comptes Rendus Mathematique* 357.3 (2019), pp. 263–271 (cit. on p. 4).

[44] Anya Désilles. "Viability approach to Hamilton-Jacobi-Moskowitz problem involving variable regulation parameters." In: *Networks & Heterogeneous Media* 8.3 (2013), pp. 707–726 (cit. on p. 98).

[45] Jie Du et al. "Revisiting Jiang's dynamic continuum model for urban cities." In: *Transportation Research Part B: Methodological* 56 (2013), pp. 96–119 (cit. on p. 6).

[46] Lawrence C. Evans. *Partial differential equations*. Vol. 19. Graduate Studies in Mathematics. American Mathematical Society, Providence, RI, 1998, pp. xviii+662 (cit. on pp. 2, 15, 29, 185).

[47] Shimao Fan. *Data-fitted generic second order macroscopic traffic flow models*. PhD Thesis. Temple University, 2013 (cit. on p. 68).

[48] Shimao Fan, Michael Herty, and Benjamin Seibold. "Comparative model accuracy of a data-fitted generalized Aw-Rascle-Zhang model." In: *arXiv preprint arXiv:1310.8219* 3 (2013) (cit. on p. 68).

[49] José Ramón D. Frejo et al. "Hybrid model predictive control for freeway traffic using discrete speed limit signals." In: *Transportation Research Part C: Emerging Technologies* 46 (2014), pp. 309–325 (cit. on p. 4).

[50] M. Garavello and B. Piccoli. *Traffic Flow on Networks. Conservation Laws Models*. MO, USA: AIMS Series on Applied Mathematics, Springfield, 2006 (cit. on p. 5).

[51] Mauro Garavello and Benedetto Piccoli. "Conservation laws on complex networks." In: *Annales de l'Institut Henri Poincaré C, Analyse non linéaire* 26.5 (2009), pp. 1925–1951 (cit. on p. 5).

[52] Y. E. Ge and Xizhao Zhou. "An alternative definition of dynamic user optimum on signalised road networks." In: *Journal of Advanced Transportation* 46.3 (2012), pp. 236–253 (cit. on p. 5).

[53] Niklas Geroliminis and Carlos F. Daganzo. "Existence of urban-scale macroscopic fundamental diagrams: Some experimental findings." In: *Transportation Research Part B: Methodological* 42 (2008), pp. 756–770 (cit. on pp. 5, 63).

[54] Nikolas Geroliminis, Jack Haddad, and Mohsen Ramezani. "Optimal Perimeter Control for Two Urban Regions With Macroscopic Fundamental Diagrams: A Model Predictive Approach." In: *IEEE Transactions on Intelligent Transportation Systems* 14.1 (2013), pp. 348–359 (cit. on p. 6).

[55] Nikolas Geroliminis and Jie Sun. "Properties of a well-defined macroscopic fundamental diagram for urban traffic." In: *Transportation Research Part B: Methodological* 45.3 (2011), pp. 605–617 (cit. on p. 6).

[56] S. K. Godunov. "A difference method for numerical calculation of discontinuous solutions of the equations of hydrodynamics." In: *Matematicheskii Sbornik* 47.3 (1959), pp. 271–306 (cit. on pp. 3, 19).

[57] J. M. Greenberg, A. Klar, and M. Rascle. "Congestion on multilane highways." In: *SIAM J. Appl. Math.* 63.3 (2003), pp. 818–833 (cit. on p. 2).

[58] B. D. Greenshields et al. "A study of traffic capacity." In: *Highway Research Board proceedings* 1935 (1935) (cit. on pp. 1, 14, 63).

[59] B. D. Greenshields et al. "The photographic method of studying traffic behavior." In: *Highway Research Board proceedings* 13 (1934), pp. 382–399 (cit. on p. 1).

[60] M. Gugat et al. "Optimal control for traffic flow networks." In: *J. Optim. Th. Applic.* 26.3 (2005), pp. 589–616 (cit. on pp. 4, 5).

[61] Jack Haddad. "Robust Constrained Control of Uncertain Macroscopic Fundamental Diagram Networks." In: *Transportation Research Procedia* 7 (2015). 21st International Symposium on Transportation and Traffic Theory Kobe, Japan, 5-7 August, 2015, pp. 669–688 (cit. on p. 6).

[62] Jack Haddad and Nikolas Geroliminis. "On the stability of traffic perimeter control in two-region urban cities." In: *Transportation Research Part B: Methodological* 46.9 (2012), pp. 1159–1176 (cit. on p. 5).

[63] M. Hajiahmadi et al. "Optimal dynamic route guidance: A model predictive approach using the macroscopic fundamental diagram." In: *16th International IEEE Conference on Intelligent Transportation Systems (ITSC 2013)*. 2013, pp. 1022–1028 (cit. on pp. 6, 63).

[64] Dirk Helbing. "A fluid dynamic model for the movement of pedestrians." In: *arXiv preprint cond-mat/9805213* (1998) (cit. on p. 65).

[65] V. Henn. "A Wave-Based Resolution Scheme for the Hydrodynamic LWR Traffic Flow Model." In: *Traffic and Granular Flow '03*. Ed. by Serge P. Hoogendoorn et al. Berlin, Heidelberg: Springer Berlin Heidelberg, 2005, pp. 105–124 (cit. on p. 3).

[66] R. Herman and I. Prigogine. "A two-fluid approach to town traffic." In: *Science* 204 (1979), pp. 148–151 (cit. on p. 5).

[67] Flurin S. Hänseler et al. "A dynamic network loading model for anisotropic and congested pedestrian flows." In: *Transportation Research Part B: Methodological* 95 (2017), pp. 149–168 (cit. on p. 6).

[68] H. W. Ho and S. C. Wong. "Two-dimensional Continuum Modeling Approach to Transportation Problems." In: *Journal of Transportation Systems Engineering and Information Technology* 6.6 (2006), pp. 53–68 (cit. on p. 5).

[69] H. Holden and N. H. Risebro. "A Mathematical Model of Traffic Flow on a Network of Unidirectional Roads." In: *SIAM J. Math. Anal.* 26.4 (1995), pp. 999–1017 (cit. on p. 5).

[70] H. Holden and N. H. Risebro. *Front tracking for hyperbolic conservation laws*. Vol. 152. Springer-Verlag, New York: Applied Mathematical Sciences, 2002 (cit. on p. 2).

[71] R. L. Hughes. "A continuum theory for the flow of pedestrians." In: *Transportation Research Part B: Methodological* 36.6 (2002), pp. 507–535 (cit. on pp. 6, 65).

[72] D. Jacquet, M. Krstic, and C.C. de Wit. "Optimal control of scalar one-dimensional conservation laws." In: *2006 American Control Conference*. 2006, 6 pp.– (cit. on p. 4).

[73] Yan-Qun Jiang, Pei-Jie Ma, and Shu-Guang Zhou. "Macroscopic modeling approach to estimate traffic-related emissions in urban areas." In: *Transportation Research Part D: Transport and Environment* 60 (2018). Special Issue on Traffic Modeling for Low-Emission Transport, pp. 41–55 (cit. on p. 6).

[74] Yanqun Jiang et al. "A dynamic traffic assignment model for a continuum transportation system." In: *Transportation Research Part B: Methodological* 45.2 (2011), pp. 343–363 (cit. on p. 6).

[75] Wen-Long Jin. "A kinematic wave theory of lane-changing traffic flow." In: *Transportation Research Part B: Methodological* 44.8 (2010), pp. 1001–1021 (cit. on p. 2).

[76] K. T. Joseph and G. D. Veerappa Godwa. "Explicit formula for the solution of convex conservation laws with boundary condition." In: *Duke Mathematical Journal* 62.2 (1991), pp. 401–416 (cit. on pp. 3, 22).

[77] K. T. Joseph and G. D. Veerappa Godwa. "Solution of convex conservation laws in a strip." In: *Proc. of the Indian Academy of Sciences-Mathematical Sciences* 102.1 (1992), pp. 29–47 (cit. on p. 3).

[78] Iasson Karafyllis and Markos Papageorgiou. "Feedback control of scalar conservation laws with application to density control in freeways by means of variable speed limits." In: *Automatica* 105 (2019), pp. 228–236 (cit. on pp. 105, 106, 109).

[79] Long Kejun et al. "Model predictive control for variable speed limit in freeway work zone." In: *2008 27th Chinese Control Conference*. 2008, pp. 488–493 (cit. on p. 4).

[80] E. Kometani and T. Sasaki. "Dynamic behaviour of traffic with a non-linear spacing-speed relationship." In: *Proceedings of the Symposium on Theory of Traffic Flow, Research Laboratories, General Motors, New York*. 1959, pp. 105–109 (cit. on p. 1).

[81] S. N. Kruzhkov. "First order quasilinear equations in several independent variables." In: *Matematicheskii Sbornik* 123.2 (1970), pp. 228–255 (cit. on p. 64).

[82] Jorge A. Laval and Felipe Castrillón. "Stochastic approximations for the macroscopic fundamental diagram of urban networks." In: *Transportation Research Part B: Methodological* 81 (2015). ISTTT 21 for the year 2015, pp. 904–916 (cit. on p. 5).

[83] P. D. Lax. "Nonlinear hyperbolic equations." In: *Comm. Pure Appl. Math.* 6 (1953), pp. 231–258 (cit. on pp. 2, 16).

[84] J. P. Lebacque. "A Two Phase Extension of the LWR Model Based on the Boundedness of Traffic Acceleration." In: *Taylor, M.A.P. (Ed.) Transportation and Traffic Theory in the 21st Century, Emerald Group Publishing Limited, Bingley* (2002), pp. 697–718 (cit. on p. 2).

[85] J. P. Lebacque. "First-order macroscopic traffic flow models: Intersection modeling, network modeling." In: *16th International Symposium on Transportation and Traffic Theory*. 2005 (cit. on p. 18).

[86] J. P. Lebacque. "The godunov scheme and what it means for first order traffic flow models." In: *Proceedings of the ISTTT Conference*. 2005 (cit. on p. 18).

[87] L. Leclercq et al. "Macroscopic traffic dynamics with heterogeneous route patterns." In: *Transportation Research Part C: Emerging Technologies* 59 (2015), pp. 292–307 (cit. on pp. 6, 63).

[88] Ludovic Leclercq. "A New Numerical Scheme for Bounding Acceleration in the LWR Model." In: *4th IMA International Conference on Mathematics in Transport, London, UK*. 2007, pp. 279–292 (cit. on p. 2).

[89] R. J. LeVeque. *Numerical Methods for Conservation Laws*. Basel, Switzerland: Birkhauser Verlag, 1990 (cit. on pp. 3, 4).

[90] David Levinson and Lei Zhang. "Ramp meters on trial: Evidence from the Twin Cities metering holiday." In: *Transportation Research Part A: Policy and Practice* 40.10 (2006), pp. 810–828 (cit. on p. 4).

[91] Michael Z. F. Li. "A Generic Characterization of Equilibrium Speed-Flow Curves." In: *Transportation Science* 42.2 (2008), pp. 220–235. eprint: https://doi.org/10.1287/trsc.1070.0201 (cit. on pp. 1, 15).

[92] Tatsien Li. *Controllability and Observability for Quasilinear Hyperbolic Systems*. Vol. 3. American Institute of Mathematical Sciences and Higher Education Press, Springfield, Beijing: AIMS Series on Applied Mathematics, 2010 (cit. on p. 4).

[93] Yanning Li, Edward Canepa, and Christian Claudel. "Optimal Control of Scalar Conservation Laws Using Linear/Quadratic Programming: Application to Transportation Networks." In: *IEEE Transactions on Control of Network Systems* 1.1 (2014), pp. 28–39 (cit. on p. 41).

[94] Yanning Li, Edward Canepa, and Christian Claudel. "Optimal traffic control in highway transportation networks using linear programming." In: *2014 European Control Conference (ECC)*. 2014, pp. 2880–2887 (cit. on p. 41).

[95] Zhibin Li et al. "Development of a Control Strategy of Variable Speed Limits to Reduce Rear-End Collision Risks Near Freeway Recurrent Bottlenecks." In: *IEEE Transactions on Intelligent Transportation Systems* 15.2 (2014), pp. 866–877 (cit. on p. 4).

[96] J. M. Lighthill and G. Whitham. "On kinematic waves, II: A theory of traffic flow on long crowded roads." In: *Proc. R. Soc. Lond. A* 229 (1955), pp. 317–345 (cit. on pp. 2, 13).

[97] Z. Y. Lin et al. "A predictive continuum dynamic user-optimal model for a polycentric urban city." In: *Transportmetrica B: Transport Dynamics* 5.3 (2017), pp. 228–247 (cit. on p. 6).

[98] J.-L. Lions. "Controlabilite Exacte, Perturbations et Stabilisation de Systemes Distribues. Tome 1." In: *RMA* 8 (1988) (cit. on p. 4).

[99] Yadong Lu et al. "Explicit construction of entropy solutions for the Lighthill–Whitham–Richards traffic flow model with a piecewise quadratic flow–density relationship." In: *Transportation Research Part B: Methodological* 42.4 (2008), pp. 355–372 (cit. on p. 3).

[100] Pierre-Emmanuel Mazaré et al. "Analytical and grid-free solutions to the Lighthill–Whitham–Richards traffic flow model." In: *Transportation Research Part B: Methodological* 45.10 (2011), pp. 1727–1748 (cit. on p. 3).

[101] Stéphane Mollier. *Two-dimensional macroscopic models for large scale traffic networks.* University Grenoble Alpes: PhD Thesis, 2020 (cit. on p. 67).

[102] Stéphane Mollier, Maria Laura Delle Monache, and Carlos Canudas-de-Wit. "A step towards a multidirectional 2D model for large scale traffic networks." In: *TRB 2019 - 98th Annual Meeting Transportation Research Board, Washington D.C., USA*. Jan. 2019, pp. 1–7 (cit. on pp. 6, 141).

[103] Stéphane Mollier et al. "Two-dimensional macroscopic model for large scale traffic networks." In: *Transportation Research Part B: Methodological* 122 (2019), pp. 309 –326 (cit. on pp. 6, 63, 66, 68, 73).

[104] Karl Moskowitz. "Discussion of freeway level of service as influenced by volume and capacity characteristics by dr drew and cj keese." In: *Proc. Highway Research Record.* Vol. 99. 1965, pp. 43–44 (cit. on p. 21).

[105] Ajith Muralidharan and Roberto Horowitz. "Computationally efficient model predictive control of freeway networks." In: *Transportation Research Part C: Emerging Technologies* 58 (2015). Special Issue: Advanced Road Traffic Control, pp. 532–553 (cit. on p. 4).

[106] G.F. Newell. "A simplified theory of kinematic waves in highway traffic, part I: General theory." In: *Transportation Research Part B: Methodological* 27.4 (1993), pp. 281–287 (cit. on pp. 2, 21).

[107] G.F. Newell. "A simplified theory of kinematic waves in highway traffic, part II: Queueing at freeway bottlenecks." In: *Transportation Research Part B: Methodological* 27.4 (1993), pp. 289–303 (cit. on pp. 2, 21).

[108] G.F. Newell. "A simplified theory of kinematic waves in highway traffic, part III: Multi-destination flows." In: *Transportation Research Part B: Methodological* 27.4 (1993), pp. 305–313 (cit. on pp. 2, 21).

[109] G.F. Newell. "Nonlinear Effects in the Dynamics of Car Following." In: *Operations Research* 9.2 (1961) (cit. on p. 2).

[110] Denis Nikitin, Carlos Canudas de Wit, and Paolo Frasca. "A Continuation Method for Large-Scale Modeling and Control: from ODEs to PDE, a Round Trip." In: *arXiv:2101.10060* (2021) (cit. on pp. 122, 132).

[111] M. Papageorgiou, H. Hadj-Salem, and J. Blosseville. "ALINEA: a local feedback control law for on-ramp metering." In: *Transp. Res. Rec.* 1320 (1991), pp. 58–64 (cit. on p. 5).

[112] M. Papageorgiou et al. "Review of road traffic control strategies." In: *Proceedings of the IEEE* 91.12 (2003), pp. 2043–2067 (cit. on p. 5).

[113] Markos Papageorgiou, Elias Kosmatopoulos, and Ioannis Papamichail. "Effects of Variable Speed Limits on Motorway Traffic Flow." In: *Transportation Research Record* 2047.1 (2008), pp. 37–48. eprint: https://doi.org/10.3141/2047-05 (cit. on pp. 4, 5).

[114] D. W. Peaceman and H. H. Rachford Jr. "The numerical solution of parabolic and elliptic differential equations." In: *Journal of the Society for Industrial and Applied Mathematics* 3.1 (1955), pp. 28–41 (cit. on p. 162).

[115] Vincent Perrollaz. "Exact Controllability of Scalar Conservation Laws with an Additional Control in the Context of Entropy Solutions." In: *SIAM J. Control Optim.* 50.4 (2012), pp. 2025–2045 (cit. on p. 4).

[116] L. A. Pipes. "An Operational Analysis of Traffic Dynamics." In: *Journal of Applied Physics* 24.3 (1953), pp. 274–281 (cit. on p. 1).

[117] Christophe Prieur, Joseph Winkin, and Georges Bastin. "Robust boundary control of systems of conservation laws." In: *Mathematics of Control, Signals, and Systems* 20.2 (2008), pp. 173–197 (cit. on p. 26).

[118] P. Richards. "Shock waves on the highway." In: *Operations Research* 47.1 (1956), pp. 42–51 (cit. on pp. 2, 13).

[119] M. Rodriguez-Vega, C. Canudas-de-Wit, and H. Fourati. "Urban network traffic state estimation using a data-based approach." In: *CTS 2021 - 16th IFAC Symposium on Control in Transportation Systems, Lille, France*. June 2021 (cit. on p. 151).

[120] Martin Rodriguez-Vega. *Optimal sensor placement and density estimation in large-scale traffic networks*. University Grenoble Alpes: PhD Thesis, 2021 (cit. on pp. 151, 152).

[121] Fabio Della Rossa, Carlo D'Angelo, and Alfio Quarteroni. "A distributed model of traffic flows on extended regions." In: *Networks & Heterogeneous Media* 5.3 (2010), pp. 525–544 (cit. on p. 6).

[122] David L. Russell. "Controllability and Stabilizability Theory for Linear Partial Differential Equations: Recent Progress and Open Questions." In: *SIAM Review* 20.4 (1978), pp. 639–739 (cit. on p. 4).

[123] Mohammadreza Saeedmanesh and Nikolas Geroliminis. "Dynamic clustering and propagation of congestion in heterogeneously congested urban traffic networks." In: *Transportation Research Procedia* 23 (2017). Papers Selected for the 22nd International Symposium on Transportation and Traffic Theory Chicago, Illinois, USA, 24-26 July, 2017., pp. 962–979 (cit. on p. 6).

[124] J. M. Torné Santos, D. M. Rosas Diaz, and F. Soriguera Marti. "Evaluation of speed limit management on c-32 highway access to barcelona." In: *Proc. 90th Annu. Meeting Transp. Res. Board*. 2011, p. 2397 (cit. on p. 4).

[125] David Schrank, Bill Eisele, and Tim Lomax. *Urban Mobility Report 2019* (cit. on p. 3).

[126] D. Serre. *Systems of Conservation Laws I: Hyperbolicities, Entropies, Shock Waves*. Cambridge: Cambridge University Press, 1999 (cit. on pp. 16, 142).

[127] Michele D. Simoni and Christian G. Claudel. "A Fast Lax–Hopf Algorithm to Solve the Lighthill–Whitham–Richards Traffic Flow Model on Networks." In: *Transportation Science* 54.6 (2020) (cit. on p. 3).

[128] R. J. Smeed. "The road capacity of city centers." In: *Traffic Engineering and Control* 8 (1966), pp. 455–458 (cit. on p. 5).

[129] Issam S. Strub and Alexandre M. Bayen. "Weak formulation of boundary conditions for scalar conservation laws: An application to highway traffic modelling." In: *International Journal of Robust and Nonlinear Control* 16.16 (2006), pp. 733–748. arXiv: arXiv:1505.02595v1 (cit. on pp. 18, 42).

[130] Shuxia Tang and Miroslav Krstic. "Sliding mode control to the stabilization of a linear 2×2 hyperbolic system with boundary input disturbance." In: *Proceedings of the American Control Conference*. American Automatic Control Council, 2014, pp. 1027–1032 (cit. on p. 26).

[131] J. M. Thomson. "Speeds and flows of traffic in Central London: 2. Speed-flow relations." In: *Traffic Engineering and Control* 8 (1967), pp. 721–725 (cit. on p. 5).

[132] Liudmila Tumash, Carlos Canudas de Wit, and Maria Laura Delle Monache. "Boundary and VSL Control for Large-Scale Urban Traffic Networks." In: *Submitted to IEEE Transactions on Automatic Control* (2020) (cit. on pp. 7, 8, 176).

[133] Liudmila Tumash, Carlos Canudas de Wit, and Maria Laura Delle Monache. "Boundary Control Design for Traffic with Nonlinear Dynamics." In: *IEEE Transactions on Automatic Control (early access)* (2022) (cit. on pp. 7, 175).

[134] Liudmila Tumash, Carlos Canudas de Wit, and Maria Laura Delle Monache. "Boundary Control for Multi-Directional Traffic on Urban Networks." In: *Submitted to 2021 IEEE 60th Conference on Decision and Control (CDC), December 2021, Austin, Texas, USA* (2021) (cit. on pp. 8, 177).

[135] Liudmila Tumash, Carlos Canudas de Wit, and Maria Laura Delle Monache. "Equilibrium manifolds in 2D fluid traffic models." In: *IFAC 2020 – 21st IFAC World Congress 2020, July 2020, Berlin, Germany*. 2020 (cit. on pp. 8, 175).

[136] Liudmila Tumash, Carlos Canudas de Wit, and Maria Laura Delle Monache. "Multi-Directional Continuous Traffic Model For Large-Scale Urban Networks." In: *Submitted to Transportation Research Part B: Methodological* (2021) (cit. on pp. 8, 177).

[137] Liudmila Tumash, Carlos Canudas de Wit, and Maria Laura Delle Monache. "Robust tracking control design for fluid traffic dynamics." In: *2019 IEEE 58th Conference on Decision and Control (CDC), December 2019, Nice, France*. 2020 (cit. on pp. 7, 174).

[138] Liudmila Tumash, Carlos Canudas de Wit, and Maria Laura Delle Monache. "Topology-based control design for congested areas in urban networks." In: *2020 IEEE 23rd International Conference on Intelligent Transportation Systems (ITSC), September 2020, Rhodes, Greece*. 2020 (cit. on pp. 8, 175).

[139] Stefan Ulbrich. "A Sensitivity and Adjoint Calculus for Discontinuous Solutions of Hyperbolic Conservation Laws with Source Terms." In: *SIAM Journal on Control and Optimization* 41.3 (2002), pp. 740–797 (cit. on p. 4).

[140] Femke van Wageningen-Kessels et al. "Genealogy of traffic flow models." In: *EURO Journal on Transportation and Logistics* 4.4 (2015), pp. 445–473 (cit. on p. 1).

[141] Suyash C. Vishnoi and Christian G. Claudel. "Variable Speed Limit and Ramp Metering Control of Highway Networks Using Lax-Hopf Method: A Mixed Integer Linear Programming Approach." In: *IEEE Transactions on Intelligent Transportation Systems* (2021), pp. 1–16 (cit. on pp. 5, 41).

[142] J. C. Williams, H. S. Mahmassani, and R. Herman. "Urban traffic network flow models." In: *Transportation Research Record* 1112.4 (1987), pp. 78–88 (cit. on pp. 5, 63).

[143] Carlos Canudas de Wit et al. "Grenoble Traffic Lab: An Experimental Platform for Advanced Traffic Monitoring and Forecasting [Applications of Control]." In: *IEEE Control Systems Magazine* 35.3 (2015), pp. 23–39 (cit. on pp. 36, 150).

[144] G. C. K. Wong and S. C. Wong. "A multi-class traffic flow model – an extension of LWR model with heterogeneous drivers." In: *Transportation Research Part A: Policy and Practice* 36.9 (2002), pp. 827–841 (cit. on p. 2).

[145] S. C. Wong and G. C. K. Wong. "An analytical shock-fitting algorithm for LWR kinematic wave model embedded with linear speed–density relationship." In: *Transportation Research Part B: Methodological* 36.8 (2002), pp. 683–706 (cit. on p. 3).

[146] Chun-Xiu Wu et al. "Steady-state traffic flow on a ring road with up- and down-slopes." In: *Physica A: Statistical Mechanics and its Applications* 403 (2014), pp. 85–93 (cit. on pp. 80, 85–87).

[147] Huan Yu and Miroslav Krstic. "Traffic congestion control for Aw–Rascle–Zhang model." In: *Automatica* 100 (2019), pp. 38–51 (cit. on p. 31).

[148] Lei Zhang and David Levinson. "Ramp metering and freeway bottleneck capacity." In: *Transportation Research Part A: Policy and Practice* 44.4 (2010), pp. 218–235 (cit. on p. 4).

[149] Peng Zhang and Ru-Xun Liu. "Hyperbolic conservation laws with space-dependent flux: I. Characteristics theory and Riemann problem." In: *Journal of Computational and Applied Mathematics* 156.1 (2003), pp. 1–21 (cit. on pp. 85, 87).

[150] Yihang Zhang and Petros A. Ioannou. "Combined Variable Speed Limit and Lane Change Control for Truck-Dominant Highway Segment." In: *2015 IEEE 18th International Conference on Intelligent Transportation Systems*. 2015, pp. 1163–1168 (cit. on p. 4).

[151] Zhou Wang et al. "Image quality assessment: from error visibility to structural similarity." In: *IEEE Transactions on Image Processing* 13.4 (June 2004), pp. 600–612 (cit. on p. 145).

[152] A. K. Ziliaskopoulos et al. "Large-scale dynamic traffic assignment: implementation issues and computational analysis." In: *Journal of Transportation Engineering* 130.5 (2004), pp. 585–593 (cit. on p. 5).

[153] Yue Zu, Ran Dai, and Jing Dong. "Convex optimization for energy-efficient traffic control." In: *2016 IEEE 55th Conference on Decision and Control (CDC)*. 2016, pp. 6759–6764 (cit. on p. 41).